

JOURNAL OF

CHROMATOGRAPHY A

INCLUDING ELECTROPHORESIS AND OTHER SEPARATION METHODS

EDITORS

U.A.Th. Brinkman (Amsterdam)
 R.W. Giese (Boston, MA)
 J.K. Haken (Kensington, N.S.W.)
 L.R. Snyder (Orinda, CA)
 S. Terabe (Hyogo)

EDITORS, SYMPOSIUM VOLUMES,
 E. Heftmann (Orinda, CA), Z. Deyl (Prague)

EDITORIAL BOARD

D.W. Armstrong (Rolla, MO)
 W.A. Aue (Halifax)
 P. Bocek (Brno)
 A.A. Boulton (Saskatoon)
 P.W. Carr (Minneapolis, MN)
 N.H.C. Cooke (San Ramon, CA)
 V.A. Davankov (Moscow)
 G.J. de Jong (Weesp)
 Z. Deyl (Prague)
 S. Dilli (Kensington, N.S.W.)
 Z. El Rassi (Stillwater, OK)
 H. Engelhardt (Saarbrücken)
 F. Erni (Basle)
 M.B. Evans (Hatfield)
 J.L. Glajch (N. Billerica, MA)
 G.A. Guiochon (Knoxville, TN)
 P.R. Haddad (Hobart, Tasmania)
 I.M. Hais (Hradec Králové)
 W.S. Hancock (Palo Alto, CA)
 S. Hjertén (Uppsala)
 S. Honda (Higashi-Osaka)
 Cs. Horváth (New Haven, CT)
 J.F.K. Huber (Vienna)
 K.-P. Hupe (Waldbronn)
 J. Janák (Brno)
 P. Jandera (Pardubice)
 B.L. Karger (Boston, MA)
 J.J. Kirkland (Newport, DE)
 E. sz. Kováts (Lausanne)
 K. Macek (Prague)
 A.J.P. Martin (Cambridge)
 L.W. McLaughlin (Chestnut Hill, MA)
 E.D. Morgan (Keele)
 J.D. Pearson (Kalamazoo, MI)
 H. Poppe (Amsterdam)
 F.E. Regnier (West Lafayette, IN)
 P.G. Righetti (Milan)
 P. Schoenmakers (Amsterdam)
 R. Schwarzenbach (Dübendorf)
 R.E. Shoup (West Lafayette, IN)
 R.P. Singhal (Wichita, KS)
 A.M. Siouffi (Marseille)
 D.J. Strydom (Boston, MA)
 N. Tanaka (Kyoto)
 K.K. Unger (Mainz)
 R. Verpoorte (Leiden)
 Gy. Vigh (College Station, TX)
 J.T. Watson (East Lansing, MI)
 B.D. Westerlund (Uppsala)

EDITORS, BIBLIOGRAPHY SECTION

Z. Deyl (Prague), J. Janák (Brno), V. Schwarz (Prague)

ELSEVIER

JOURNAL OF CHROMATOGRAPHY A

INCLUDING ELECTROPHORESIS AND OTHER SEPARATION METHODS

Scope. The *Journal of Chromatography A* publishes papers on all aspects of **chromatography, electrophoresis** and related methods. Contributions consist mainly of research papers dealing with chromatographic theory, instrumental developments and their applications. In the *Symposium volumes*, which are under separate editorship, proceedings of symposia on chromatography, electrophoresis and related methods are published. *Journal of Chromatography B: Biomedical Applications*—This journal, which is under separate editorship, deals with the following aspects: developments in and applications of chromatographic and electrophoretic techniques related to clinical diagnosis or alterations during medical treatment; screening and profiling of body fluids or tissues related to the analysis of active substances and to metabolic disorders; drug level monitoring and pharmacokinetic studies; clinical toxicology; forensic medicine; veterinary medicine; occupational medicine; results from basic medical research with direct consequences in clinical practice.

Submission of Papers. The preferred medium of submission is on disk with accompanying manuscript (see *Electronic manuscripts* in the Instructions to Authors, which can be obtained from the publisher, Elsevier Science B.V., P.O. Box 330, 1000 AH Amsterdam, Netherlands). Manuscripts (in English; *four* copies are required) should be submitted to: Editorial Office of *Journal of Chromatography A*, P.O. Box 681, 1000 AR Amsterdam, Netherlands, Telefax (+31-20) 5862 304, or to: The Editor of *Journal of Chromatography B: Biomedical Applications*, P.O. Box 681, 1000 AR Amsterdam, Netherlands. Review articles are invited or proposed in writing to the Editors who welcome suggestions for subjects. An outline of the proposed review should first be forwarded to the Editors for preliminary discussion prior to preparation. Submission of an article is understood to imply that the article is original and unpublished and is not being considered for publication elsewhere. For copyright regulations, see below.

Publication information. *Journal of Chromatography A* (ISSN 0021-9673): for 1994 Vols. 652–682 are scheduled for publication. *Journal of Chromatography B: Biomedical Applications* (ISSN 0378-4347): for 1994 Vols. 652–662 are scheduled for publication. Subscription prices for *Journal of Chromatography A*, *Journal of Chromatography B: Biomedical Applications* or a combined subscription are available upon request from the publisher. Subscriptions are accepted on a prepaid basis only and are entered on a calendar year basis. Issues are sent by surface mail except to the following countries where air delivery via SAL is ensured: Argentina, Australia, Brazil, Canada, China, Hong Kong, India, Israel, Japan, Malaysia, Mexico, New Zealand, Pakistan, Singapore, South Africa, South Korea, Taiwan, Thailand, USA. For all other countries airmail rates are available upon request. Claims for missing issues must be made within six months of our publication (mailing) date. Please address all your requests regarding orders and subscription queries to: Elsevier Science B.V., Journal Department, P.O. Box 211, 1000 AE Amsterdam, Netherlands. Tel.: (+31-20) 5803 642; Fax: (+31-20) 5803 598. Customers in the USA and Canada wishing information on this and other Elsevier journals, please contact Journal Information Center, Elsevier Science Inc., 655 Avenue of the Americas, New York, NY 10010, USA, Tel. (+1-212) 633 3750, Telefax (+1-212) 633 3764.

Abstracts/Contents Lists published in Analytical Abstracts, Biochemical Abstracts, Biological Abstracts, Chemical Abstracts, Chemical Titles, Chromatography Abstracts, Current Awareness in Biological Sciences (CABS), Current Contents/Life Sciences, Current Contents/Physical, Chemical & Earth Sciences, Deep-Sea Research/Part B: Oceanographic Literature Review, Excerpta Medica, Index Medicus, Mass Spectrometry Bulletin, PASCAL-CNRS, Referativnyi Zhurnal, Research Alert and Science Citation Index.

US Mailing Notice. *Journal of Chromatography A* (ISSN 0021-9673) is published weekly (total 52 issues) by Elsevier Science B.V., (Sara Burgerhartstraat 25, P.O. Box 211, 1000 AE Amsterdam, Netherlands). Annual subscription price in the USA US\$ 4994.00 (US\$ price valid in North, Central and South America only) including air speed delivery. Second class postage paid at Jamaica, NY 11431. **USA POSTMASTERS:** Send address changes to *Journal of Chromatography A*, Publications Expediting, Inc., 200 Meacham Avenue, Elmont, NY 11003. Airfreight and mailing in the USA by Publications Expediting.

See inside back cover for Publication Schedule, Information for Authors and information on Advertisements.

© 1994 ELSEVIER SCIENCE B.V. All rights reserved.

0021-9673/94/\$07.00

No part of this publication may be reproduced, stored in a retrieval system or transmitted in any form or by any means, electronic, mechanical, photocopying, recording or otherwise, without the prior written permission of the publisher, Elsevier Science B.V., Copyright and Permissions Department, P.O. Box 521, 1000 AM Amsterdam, Netherlands.

Upon acceptance of an article by the journal, the author(s) will be asked to transfer copyright of the article to the publisher. The transfer will ensure the widest possible dissemination of information.

Special regulations for readers in the USA—This journal has been registered with the Copyright Clearance Center, Inc. Consent is given for copying of articles for personal or internal use, or for the personal use of specific clients. This consent is given on the condition that the copier pays through the Center the per-copy fee stated in the code on the first page of each article for copying beyond that permitted by Sections 107 or 108 of the US Copyright Law. The appropriate fee should be forwarded with a copy of the first page of the article to the Copyright Clearance Center, Inc., 27 Congress Street, Salem, MA 01970, USA. If no code appears in an article, the author has not given broad consent to copy and permission to copy must be obtained directly from the author. The fee indicated on the first page of an article in this issue will apply retroactively to all articles published in the journal, regardless of the year of publication. This consent does not extend to other kinds of copying, such as for general distribution, resale, advertising and promotion purposes, or for creating new collective works. Special written permission must be obtained from the publisher for such copying.

No responsibility is assumed by the Publisher for any injury and/or damage to persons or property as a matter of products liability, negligence or otherwise, or from any use or operation of any methods, products, instructions or ideas contained in the materials herein. Because of rapid advances in the medical sciences, the Publisher recommends that independent verification of diagnoses and drug dosages should be made.

Although all advertising material is expected to conform to ethical (medical) standards, inclusion in this publication does not constitute a guarantee or endorsement of the quality or value of such product or of the claims made of it by its manufacturer.

Ⓢ The paper used in this publication meets the requirements of ANSI/NISO Z39.48-1992 (Permanence of Paper).

Printed in the Netherlands

CONTENTS

(Abstracts/Contents Lists published in Analytical Abstracts, Biochemical Abstracts, Biological Abstracts, Chemical Abstracts, Chemical Titles, Chromatography Abstracts, Current Awareness in Biological Sciences (CABS), Current Contents/Life Sciences, Current Contents/Physical, Chemical & Earth Sciences, Deep-Sea Research/Part B: Oceanographic Literature Review, Excerpta Medica, Index Medicus, Mass Spectrometry Bulletin, PASCAL-CNRS, Referativnyi Zhurnal, Research Alert and Science Citation Index)

Publisher's note V

REGULAR PAPERS

Column Liquid Chromatography

- Frontal analysis of protein adsorption on a membrane adsorber
by A. Shiosaki, M. Goto and T. Hirose (Kumamoto, Japan) (Received 25 May 1994) 1
- High-performance protein separations with novel strong ion exchangers
by J. Horvath (Fullerton, CA, USA), E. Boschetti and L. Guerrier (Villeneuve la Garenne, France) and N. Cooke (Fullerton, CA, USA) (Received 30 May 1994) 11
- Enantiomer separation by high-performance liquid chromatography on polysiloxane-based chiral stationary phases
by M. Schleimer (Tübingen, Germany) W.H. Pirkle (Urbana, IL, USA) and V. Schurig (Tübingen, Germany) (Received 3 May 1994) 23
- Axially dissymmetric bianthracene-based chiral stationary phase for the high-performance liquid chromatographic separation of enantiomers
by S. Oi, H. Ono, H. Tanaka, M. Shijo and S. Miyano (Sendai, Japan) (Received 29 March 1994) 35
- Role of hydroxyl groups in chiral recognition of cannabinoids by carbamated amylose
by S. Abu-Lafi, M. Sterin and S. Levin (Jerusalem, Israel) (Received 1 June 1994) 47
- Preliminary computer simulation for fine tuning of the high-performance liquid chromatography of some phenolic acids
by T.H. Dzido and H.D. Smolarz (Lublin, Poland) (Received 19 May 1994) 59
- Purification of recombinant human granulocyte-macrophage colony-stimulating factor from the inclusion bodies produced by transformed *Escherichia coli* cells
by M. Belew (Uppsala, Sweden), Y. Zhou (Beijing, China), S. Wang (Hebei, China) and L.-E. Nyström and J.-C. Janson (Uppsala, Sweden) (Received 31 May 1994) 67
- Limited enzymatic digestion for the determination of the quantities of minor diastereomeric impurities in preparations of RMP-7, a peptide containing a reduced peptide bond
by J.A. Straub, A. Akiyama, P. Parmar and G.F. Musso (Cambridge, MA, USA) (Received 31 May 1994) 85
- Complete purification of tRNA, charged or modified with hydrophobic groups, by reversed-phase high-performance liquid chromatography on a C₄/C₁₈ column system
by J.R. Mesters, E.L.H. Vorstenbosch, A.J. de Boer and B. Kraal (Leiden, Netherlands) (Received 26 May 1994) 93
- Determination of copper(II) chlorophyllin by reversed-phase high-performance liquid chromatography
by H. Inoue, H. Yamashita, K. Furuya, Y. Nonomura and N. Yoshioka, (Yokohama, Japan) and S. Li (Beijing, China) (Received 14 June 1994) 99
- Comparison of isocratic and gradient elution reversed-phase behaviour of high-molecular-mass polystyrenes in dichloromethane and acetonitrile
by R.A. Shalliker and P.E. Kavanagh (Waurin Ponds, Australia) and I.M. Russell (Belmont, Australia) (Received 27 May 1994) 105

Gas Chromatography

- Determination of reactive hydrocarbons by capillary gas chromatography with the reduction gas detector
by X.-L. Cao, C.N. Hewitt and K.S. Waterhouse (Lancaster, UK) (Received 3 May 1994) 115
- Retention of halocarbons on a hexafluoropropylene epoxide-modified graphitized carbon black. II. Ethane-based compounds
by T.J. Bruno and M. Caciari (Boulder, CO, USA) (Received 16 May 1994) 123

(Continued overleaf)

Contents (continued)

- Combined solvent extraction–mass spectrometry determination of free phenol traces in poly(vinyl chloride) products
by J. Vilaplana, J. López and A. Jiménez (Alicante, Spain) (Received 7 June 1994) 133

Supercritical Fluid Chromatography and Extraction

- Direct and indirect approaches to enantiomeric separation of benzodiazepines using micro column techniques
by S.R. Almquist and P. Petersson (Uppsala, Sweden), W. Walther (Basle, Switzerland) and K.E. Markides
(Uppsala, Sweden) (Received 8 June 1994) 139

- Supercritical fluid extraction using a new restrictor design
by F. Mellor (Darmstadt, Germany) and U. Just and Th. Strumpf (Berlin, Germany) (Received 7 June 1994) 147

Electrophoresis

- UV detection in capillary zone electrophoresis. Peaks or dips – that is the question
by J.L. Beckers (Eindhoven, Netherlands) (Received 27 May 1994) 153

- Spectrophotometric determination of ionization constants by capillary zone electrophoresis
by J.A. Cleveland, Jr. and C.L. Martin (Indianapolis, IN, USA) and S.J. Gluck (Midland, MI, USA) (Received
11 May 1994) 167

- Identification of tryptophan and tyrosine residues in peptides separated by capillary electrophoresis by their second-
derivative spectra using diode-array detection
by R. Grimm, A. Graf and D.N. Heiger (Waldbronn, Germany) (Received 8 June 1994) 173

- Protein microheterogeneity and crystal habits: the case of epidermal growth factor receptor isoforms as isolated in a
multicompartment electrolyzer with isoelectric membranes
by W. Weber (Hamburg, Germany), E. Wenisch (Milan, Italy and Vienna, Austria), N. Günther, U. Marnitz and C.
Betzel (Hamburg, Germany) and P.G. Righetti (Milan, Italy) (Received 25 May 1994) 181

SHORT COMMUNICATIONS

Column Liquid Chromatography

- Antibody against branched epitope as an affinity ligand to separate the parent protein
by Z.J. Yao, M.C.C. Kao, K.C. Loh and M.C.M. Chung (Singapore, Singapore) (Received 9 June 1994) 190

- Determination of purine bases and nucleosides by conventional and microbore high-performance liquid chromatography and
gas chromatography with an ion-trap detector
by P. Šimek, A. Jegorov and F. Dusbábek (České Budějovice, Czech Republic) (Received 20 June 1994) 195

- Size-exclusion chromatography of nylons in methylene chloride–dichloroacetic acid
by T.H. Mourey and T.G. Bryan (Rochester, NY, USA) (Received 12 April 1994) 201

Electrophoresis

- Determination of trace impurities of peptides and alkaloids by capillary electrophoresis–ion spray mass spectrometry
by F.Y.L. Hsieh, J. Cai and J. Henion (Ithaca, NY, USA) (Received 15 June 1994) 206

BOOK REVIEW

- Practical High-Performance Liquid Chromatography (by V.R. Meyer), reviewed by H. Engelhardt (Saarbrücken, Germany) 212

JOURNAL OF CHROMATOGRAPHY A

VOL. 679 (1994)

JOURNAL OF CHROMATOGRAPHY A

INCLUDING ELECTROPHORESIS AND OTHER SEPARATION METHODS

EDITORS

U.A.Th. BRINKMAN (Amsterdam), R.W. GIESE (Boston, MA), J.K. HAKEN (Kensington, N.S.W.),
L.R. SNYDER (Orinda, CA), S. TERABE (Hyogo)

EDITORS, SYMPOSIUM VOLUMES

E. HEFTMANN (Orinda, CA), Z. DEYL (Prague)

EDITORIAL BOARD

D.W. Armstrong (Rolla, MO), W.A. Aue (Halifax), P. Boček (Brno), A.A. Boulton (Saskatoon), P.W. Carr (Minneapolis, MN), N.H.C. Cooke (San Ramon, CA), V.A. Davankov (Moscow), G.J. de Jong (Weesp), Z. Deyl (Prague), S. Dilli (Kensington, N.S.W.), Z. El Rassi (Stillwater, OK), H. Engelhardt (Saarbrücken), F. Erni (Basle), M.B. Evans (Hatfield), J.L. Glajch (N. Billerica, MA), G.A. Guiochon (Knoxville, TN), P.R. Haddad (Hobart, Tasmania), I.M. Hais (Hradec Králové), W.S. Hancock (Palo Alto, CA), S. Hjertén (Uppsala), S. Honda (Higashi-Osaka), Cs. Horváth (New Haven, CT), J.F.K. Huber (Vienna), K.-P. Hupe (Waldbronn), J. Janák (Brno), P. Jandera (Pardubice), B.L. Karger (Boston, MA), J.J. Kirkland (Newport, DE), E. sz. Kováts (Lausanne), K. Macek (Prague), A.J.P. Martin (Cambridge), L.W. McLaughlin (Chestnut Hill, MA), E.D. Morgan (Keele), J.D. Pearson (Kalamazoo, MI), H. Poppe (Amsterdam), F.E. Regnier (West Lafayette, IN), P.G. Righetti (Milan), P. Schoenmakers (Amsterdam), R. Schwarzenbach (Dübendorf), R.E. Shoup (West Lafayette, IN), R.P. Singhal (Wichita, KS), A.M. Siouffi (Marseille), D.J. Strydom (Boston, MA), N. Tanaka (Kyoto), K.K. Unger (Mainz), R. Verpoorte (Leiden), Gy. Vigh (College Station, TX), J.T. Watson (East Lansing, MI), B.D. Westerlund (Uppsala)

EDITORS, BIBLIOGRAPHY SECTION

Z. Deyl (Prague), J. Janák (Brno), V. Schwarz (Prague)



ELSEVIER

Amsterdam – Lausanne – New York – Oxford – Shannon – Tokyo

J. Chromatogr. A, Vol. 679 (1994)

© 1994 ELSEVIER SCIENCE B.V. All rights reserved.

0021-9673/94/\$07.00

No part of this publication may be reproduced, stored in a retrieval system or transmitted in any form or by any means, electronic, mechanical, photocopying, recording or otherwise, without the prior written permission of the publisher, Elsevier Science B.V., Copyright and Permissions Department, P.O. Box 521, 1000 AM Amsterdam, Netherlands.

Upon acceptance of an article by the journal, the author(s) will be asked to transfer copyright of the article to the publisher. The transfer will ensure the widest possible dissemination of information.

Special regulations for readers in the USA – This journal has been registered with the Copyright Clearance Center, Inc. Consent is given for copying of articles for personal or internal use, or for the personal use of specific clients. This consent is given on the condition that the copier pays through the Center the per-copy fee stated in the code on the first page of each article for copying beyond that permitted by Sections 107 or 108 of the US Copyright Law. The appropriate fee should be forwarded with a copy of the first page of the article to the Copyright Clearance Center, Inc., 27 Congress Street, Salem, MA 01970, USA. If no code appears in an article, the author has not given broad consent to copy and permission to copy must be obtained directly from the author. The fee indicated on the first page of an article in this issue will apply retroactively to all articles published in the journal, regardless of the year of publication. This consent does not extend to other kinds of copying, such as for general distribution, resale, advertising and promotion purposes, or for creating new collective works. Special written permission must be obtained from the publisher for such copying.

No responsibility is assumed by the Publisher for any injury and/or damage to persons or property as a matter of products liability, negligence or otherwise, or from any use or operation of any methods, products, instructions or ideas contained in the materials herein. Because of rapid advances in the medical sciences, the Publisher recommends that independent verification of diagnoses and drug dosages should be made.

Although all advertising material is expected to conform to ethical (medical) standards, inclusion in this publication does not constitute a guarantee or endorsement of the quality or value of such product or of the claims made of it by its manufacturer.

Ⓢ The paper used in this publication meets the requirements of ANSI/NISO Z39.48-1992 (Permanence of Paper).

Printed in the Netherlands



ELSEVIER

Journal of Chromatography A, 679 (1994) V

JOURNAL OF
CHROMATOGRAPHY A

Publisher's note

We are pleased to announce that Professor Shigeru Terabe of the Himeji Institute of Technology, Hyogo, Japan has accepted our invitation to join the team of Editors of the Journal of Chromatography A, as from September 1st, 1994.

Professor Terabe's main research interests include the development of high-resolution separation methods with special emphasis on capillary electrophoresis including electrokinetic chromatography.

We are certain that Professor Terabe will maintain and add to the existing reputation of the Journal. We wish him every success and much personal satisfaction in this position.

Frontal analysis of protein adsorption on a membrane adsorber

Ayahito Shiosaki, Motonobu Goto*, Tsutomu Hirose

Department of Applied Chemistry, Kumamoto University, Kumamoto 860, Japan

First received 18 March 1994; revised manuscript received 25 May 1994

Abstract

The adsorption behaviour of two kinds of proteins, myoglobin and ovalbumin, with a membrane adsorber, DEAE MemSep 1000 (Millipore), was studied in comparison with a bead-based packed-bed adsorber, DEAE Sephacel (Pharmacia-LKB), by means of frontal analysis. Adsorption isotherms were obtained by integrating the breakthrough curves for various feed concentrations. Adsorption isotherms were expressed by the Langmuir equation and the adsorption capacity for the membrane adsorber was smaller than that for the packed-bed adsorber. The breakthrough curves of myoglobin for the membrane adsorber were independent of the flow-rate, but those of ovalbumin were affected by the flow-rate. Abnormal behaviour was observed for the adsorption of ovalbumin on a membrane adsorber. With the packed-bed adsorber, the breakthrough curves for both proteins were significantly affected by the flow-rate. A mathematical model for the membrane adsorber involving axial dispersion and adsorption kinetics was derived. The model simulated the breakthrough curves for myoglobin well. Axial dispersion was dominant for the membrane adsorber whereas intraparticle diffusion was dominant for the packed-bed adsorber.

1. Introduction

Downstream processes such as extraction, concentration, separation and purification are key techniques for the production of biological macromolecules such as enzymes, proteins and antibodies. Especially separation and purification play an important role in downstream treatment processing for biochemistry and biotechnology [1]. Considerable efforts have been devoted to the optimization of conventional methods and

the development of new methods based on new principles in order to increase the productivity of separation and purification processes.

Liquid column chromatography is one of the most popular techniques for protein separation and purification and has been widely used in various fields of biotechnology from HPLC analysis to industrial-scale processes, because it is possible to purify proteins without losing their biological activity and to operate with simple equipment under mild conditions. Conventional bead-based packed-bed operation in column chromatography is carried out by pumping the feed solution to the packed bed containing porous particles. Packed-bed operation is not

* Corresponding author.

necessarily the most suitable method for dealing with a large amount of dilute protein solution. Efficient adsorption can be realized when the breakthrough curve is steep with a high flow-rate resulting from a large overall adsorption rate which includes adsorbate–adsorbent association kinetics and mass transfer. The overall adsorption rate of protein is generally slow because of the large mass transfer resistance. With large porous particles, diffusion pathways for the proteins are relatively long and therefore low flow-rates are required to suppress kinetic effects. This causes long cycle times and inefficient operation in terms of operation time. On the other hand, efficient utilization of the adsorber can be attained when smaller particles of adsorbent are used because the dynamic adsorption capacity increases owing to the steep breakthrough. However, smaller particles make it difficult to operate at higher flow-rates owing to the high pressure drop [2], resulting in lower productivity. Therefore, an alternative technique to the packed-bed operation has been developed for preparative operation.

A membrane adsorber has been used to bypass these fundamental limitations of the packed-bed adsorber [2–5]. The ligands are immobilized on the surface of the membrane pores. The pores are designed to be large enough to permit convective flow. The overall adsorption rate may be large and steep breakthrough is expected because it is not affected by diffusion due to the convection through the pores of the membrane. Thus, mass transfer and pressure drop limitations could be minimized. Therefore, it is possible to operate at lower pressure drops, higher flow-rates and short cycle times. The membrane adsorber may allow the rapid processing of large volumes of feed stream and may be suitable for the separation and purification of large amounts of dilute protein solutions.

Membrane modules reported in the literature are classified into two types, stacked flat-sheet membranes or hollow fibre membranes. Brandt et al. [2] prepared an affinity membrane in a stacked membrane module. They demonstrated

the efficient isolation of fibrinogen an immunoglobulin G with gelatin- and protein A-containing membranes. Liu and Fried [6] measured breakthrough curves of lysozyme through a stacked affinity membrane of cellulose–Cibacron Blue. Kim et al. [7] prepared a hollow fibre affinity membrane. The adsorption and elution behaviour of bovine γ -globulin with an affinity membrane containing hydrophobic amino acids as ligands was studied. These experimental studies revealed that the breakthrough curves were not influenced by the flow-rate. Hence diffusion resistance of a solute can be eliminated by convective flow through pores in the membrane.

Models of membrane adsorbers have been studied with regard to breakthrough analysis. A mathematical model including axial diffusion and adsorption kinetics was developed by Suen and Etzel [3], and was subsequently extended to multi-component systems [4]. Liu and Fried [6] developed a model including radial diffusion in addition to axial diffusion.

The membrane adsorber might suffer from heterogeneity of the membrane, that is, variation of the pore-size distribution, membrane thickness distribution, porosity distribution, etc., because of the short pathway in the flow direction. Suen and Etzel [3], Liu and Fried [6] and Goto and Hirose [8] have pointed out that the effect of heterogeneity is significant for a membrane adsorber.

The objective of this study was to investigate the adsorption behaviour of proteins with a membrane adsorber in comparison with a packed-bed adsorber. Two kinds of proteins, myoglobin and ovalbumin, were used as adsorbates. Breakthrough curves for each adsorber were measured and adsorption isotherms were obtained by integrating the breakthrough curves. The breakthrough curves and adsorption isotherms for the membrane adsorber were compared with those for the packed-bed adsorber. Mathematical models for each adsorber were derived and compared with the experimental results.

2. Model equations for breakthrough curve calculation

2.1. Model for a packed-bed adsorber

The breakthrough curves for a packed-bed adsorber may be described by the following model, containing rate processes of intraparticle and external film mass transfer resistance, axial dispersion and local adsorption kinetics. Some of these rate processes may cause broadening of the breakthrough curve.

The mass balance over a section of adsorber is expressed as

$$\begin{aligned} \varepsilon \cdot \frac{\partial c}{\partial t} + \varepsilon v \cdot \frac{\partial c}{\partial z} \\ = \varepsilon D \cdot \frac{\partial^2 c}{\partial z^2} - (1 - \varepsilon) a_p k_f (c - c_i|_{r=r_0}) \end{aligned} \quad (1)$$

where c and c_i are the concentration in interparticle void space and in the pore of particle, respectively, and D and k_f denote axial dispersion coefficient and external film mass transfer coefficient, respectively. A mass balance within a particle is given by

$$\varepsilon_i \cdot \frac{\partial c_i}{\partial t} = D_e \cdot \frac{1}{r^2} \cdot \frac{\partial}{\partial r} \left(r^2 \cdot \frac{\partial c_i}{\partial r} \right) - \frac{\partial q}{\partial t} \quad (2)$$

where D_e and q are intraparticle effective diffusivity and the amount adsorbed, respectively. The association rate between adsorbate and adsorbent may be expressed by second order in the forward direction and first order in the reverse direction [9]:

$$\frac{\partial q}{\partial t} = k_a c_i (q_\infty - q) - k_d q \quad (3)$$

where k_a , k_d and q_∞ are adsorption and desorption rate constants and maximum adsorption capacity, respectively. Eq. 3 is the rate equation which reduces to the Langmuir isotherm at equilibrium.

The initial and boundary conditions are

$$D_e \cdot \frac{\partial c_i}{\partial r} \Big|_{r=r_0} = k_f (c - c_i|_{r=r_0}) \quad \text{at } r = r_0 \quad (4)$$

$$\frac{\partial c_i}{\partial r} \Big|_{r=0} = 0 \quad \text{at } r = 0 \quad (5)$$

$$c = q = c_i = 0 \quad \text{at } z \geq 0, t = 0 \quad (6)$$

$$\varepsilon v c - \varepsilon D \cdot \frac{\partial c}{\partial z} = \varepsilon v c_0 \quad \text{at } z = 0, t > 0 \quad (7)$$

$$\frac{\partial c}{\partial z} = 0 \quad \text{at } z = L, t > 0 \quad (8)$$

where c_0 is the feed concentration of protein for step input.

Using the linear driving force (LDF) approximation [10], Eqs. 1–8 reduce to

$$\varepsilon \frac{\partial c}{\partial t} + \varepsilon v \cdot \frac{\partial c}{\partial z} = \varepsilon D \cdot \frac{\partial^2 c}{\partial z^2} - (1 - \varepsilon) a_p k_p (c - \bar{c}_i) \quad (9)$$

$$\varepsilon_i \cdot \frac{\partial \bar{c}_i}{\partial t} = a_p k_p (c - \bar{c}_i) - \frac{\partial \bar{q}}{\partial t} \quad (10)$$

$$\frac{\partial \bar{q}}{\partial t} = k_a \bar{c}_i (q_\infty - \bar{q}) - k_d \bar{q} \quad (11)$$

$$c = \bar{q} = \bar{c}_i = 0 \quad \text{at } z \geq 0, t = 0 \quad (12)$$

$$\varepsilon v c - \varepsilon D \cdot \frac{\partial c}{\partial z} = \varepsilon v c_0 \quad \text{at } z = 0, t > 0 \quad (13)$$

$$\frac{\partial c}{\partial z} = 0 \quad \text{at } z = L, t > 0 \quad (14)$$

where $Bi = k_f r_0 / D_e$ and $a_p = 3 / r_0$. The overall mass transfer coefficient, k_p , is given by $k_p = k_f / (1 + Bi/5)$, where intraparticle diffusion and external mass transfer effects are combined. \bar{c}_i and \bar{q} are average values of c_i and q , respectively.

Eqs. 9–14 were solved numerically using the finite-difference method for the simulation of breakthrough curves for a packed-bed adsorber.

2.2. Model for a membrane adsorber

In a membrane adsorber, intraparticle and external mass transfer resistance may be negligible because of convection through the pores of the membrane. Therefore, the model for the membrane adsorber is derived by excluding the terms of these mass transfer resistance from the

above model for the packed-bed adsorber. The resulting rate processes contain only axial dispersion and adsorption kinetics. The model equations derived are identical with the model of Suen and Etzel [3].

$$\varepsilon \cdot \frac{\partial c}{\partial t} + \varepsilon v \cdot \frac{\partial c}{\partial z} = \varepsilon D \cdot \frac{\partial^2 c}{\partial z^2} - (1 - \varepsilon) \frac{\partial q}{\partial t} \quad (15)$$

$$\frac{\partial q}{\partial t} = k_a c (q_\infty - q) - k_d q \quad (16)$$

Liu and Fried [6] developed a model involving both radial dispersion and axial dispersion. As radial dispersion is less important than axial dispersion, it is neglected here. Eqs. 15 and 16, with initial and boundary conditions, Eqs. 6–8, were solved numerically by using the finite-difference method based on Crank–Nicholson's differencing scheme for the simulation of breakthrough curve for a membrane adsorber.

2.3. Calculation of breakthrough curve

The equations for the packed-bed and the membrane adsorbers were solved on a PC to simulate the adsorption processes.

The values of the maximum adsorption capacity q_∞ and equilibrium constant $K_d (=k_d/k_a)$ were determined from the experimental adsorption isotherms. Kinetic parameters involved in the model equations, overall mass transfer coefficient k_p , axial Peclet number $Pe (=vL/D)$ and adsorption rate constant k_a , were evaluated by fitting with the experimental breakthrough curves in the following procedure.

For the packed-bed adsorber, it was assumed as an initial guess that the value of Pe was 80, which corresponds to a particle Peclet number $vd_p/D = 0.5$ [11], and the value of k_a was infinite (or sufficiently large). Then k_p was determined by fitting the experimental data for the highest flow-rate, because broadening of the curve may be controlled by intraparticle diffusion for higher flow-rates. Theoretical curves for other flow-rates were calculated using the same parameters. If the calculated curve with those parameters did not agree with the experimental data for lower flow-rates, the calculations were repeated with

modified parameters of Pe or k_a until they agreed with the experimental data.

In the case of the membrane adsorber, it was assumed as an initial guess that k_a was infinite (or sufficiently large) and axial dispersion caused the broadening of the breakthrough curve. The value of Pe was determined in the same way as for the packed-bed adsorber. If the calculated curve did not agree with the experimental curve for the entire flow-rate range, the value of k_a was decreased.

3. Experimental

Adsorption breakthrough curves were measured at 277 K for two kinds of anion exchanger: (a) an adsorber consisting of a stack of membrane, DEAE MemSep 1000 (Millipore), and (b) an adsorber packed with spherical beads, DEAE Sephacel (Pharmacia–LKB). The physical properties of the adsorbers are summarized in Table 1. Both adsorbers had the same volume. The membrane adsorber consisted of a multi-layer microporous membrane assembled within the housing as shown in Fig. 1.

Myoglobin (horse heart; Sigma) and ovalbumin (Sigma) were used as adsorbates. The molecular mass and isoelectric point for myoglobin are 17 800 and 7.3, respectively, and those for ovalbumin are 46 000 and 4.6, respectively.

The breakthrough curves for these adsorbers were measured using the following procedure. First, the adsorber was equilibrated with 0.02 M Tris buffer solution. The pH of the buffer solution was adjusted with HCl to 9.3 and 8.0 for myoglobin and ovalbumin, respectively. The protein dissolved in the buffer solution was pumped to the adsorber until the available capacity of the adsorber was exhausted and the adsorbate concentration in the effluent of the adsorber approached the feed concentration. The effluent concentration was continuously monitored with a UV–Vis spectrophotometer at 533 and 280 nm for myoglobin and ovalbumin, respectively. The adsorbed protein was eluted with an eluent consisting of the buffer solution containing 1 M NaCl. The adsorber was finally

Table 1
Properties of adsorbers

Parameter	DEAE MemSep 1000 membrane adsorber	DEAE Sephacel packed-bed adsorber
Matrix	Cellulose	Cellulose
Pore size (m)	$1.2 \cdot 10^{-6}$	-
Porosity	0.8	-
Average particle diameter (m)	-	$1.0 \cdot 10^{-4}$
Column diameter (m)	$1.8 \cdot 10^{-2}$	$1.04 \cdot 10^{-2}$
Column height (m)	$5.0 \cdot 10^{-3}$	$16 \cdot 10^{-3}$
Bed volume (m ³)	$1.4 \cdot 10^{-6}$	$1.4 \cdot 10^{-6}$

equilibrated with the buffer solution for the next measurement.

4. Results and discussion

Fig. 2 shows adsorption isotherms of myoglobin and ovalbumin for the membrane adsorber, DEAE MemSep 1000, and Fig. 3 those for the packed-bed adsorber, DEAE Sephacel. The adsorption isotherms were obtained by integrating breakthrough curves measured at various feed concentrations at a flow-rate of $1.67 \cdot 10^{-8}$ m³/s. The total adsorption capacity is generally independent of the flow-rate. As will be discussed later, the adsorption capacity for ovalbumin on the membrane adsorber depended on the flow-rate.

Each adsorption isotherm was expressed by a

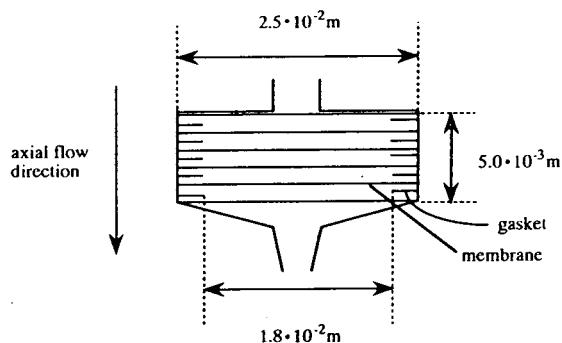


Fig. 1. Schematic diagram of a stack of membranes (DEAE MemSep 1000).

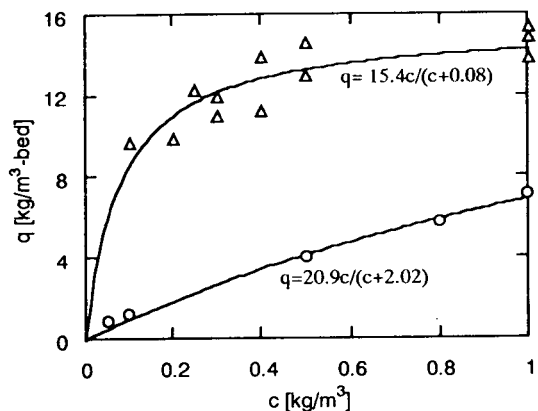


Fig. 2. Adsorption isotherms of (○) myoglobin and (△) ovalbumin for the DEAE MemSep 1000 membrane adsorber.

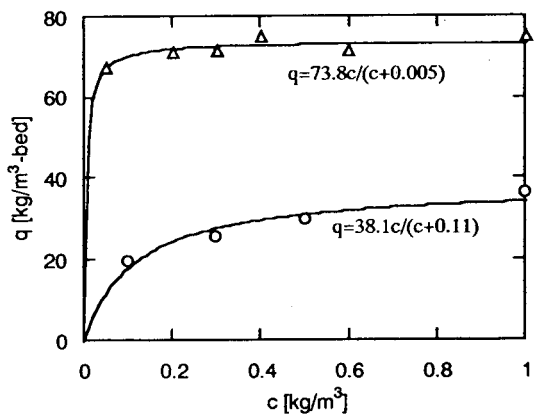


Fig. 3. Adsorption isotherms of (○) myoglobin and (△) ovalbumin for the DEAE Sephacel packed-bed adsorber.

Langmuir equation. The Langmuir constants, q_∞ and K_a , were determined by the least-squares method. The Langmuir equation is also shown in Figs. 2 and 3. Being compared on a mass basis of the adsorbate per unit volume of the adsorber, the amount adsorbed for the membrane adsorber was smaller than that for the packed-bed adsorber. The amount of myoglobin adsorbed was smaller than that of ovalbumin.

The effects of flow-rate on the breakthrough curve of myoglobin and ovalbumin for the membrane adsorber are shown in Fig. 4a and b, respectively. The theoretical breakthrough

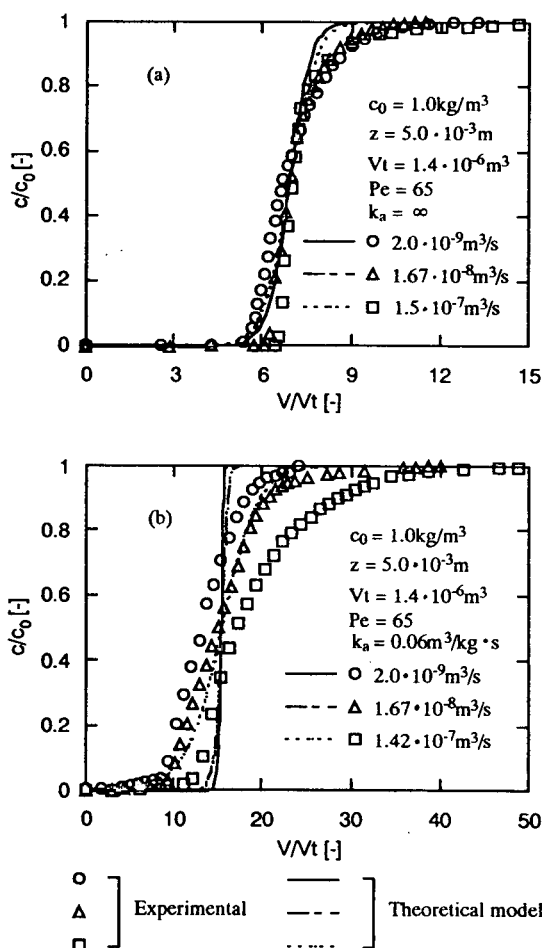


Fig. 4. Effect of flow-rate on the experimental and theoretical breakthrough curves of (a) myoglobin and (b) ovalbumin for the DEAE MemSep 1000 membrane adsorber.

curves calculated by the model are also shown. The ordinate and abscissa are the ratio of effluent concentration to feed concentration and the ratio of effluent volume to bed volume, respectively. The adsorption breakthrough curves of myoglobin were steeper than those of ovalbumin. They were independent of flow-rate because of convection through the pores of the membrane, resulting in negligible diffusion resistance. The mathematical model for myoglobin nearly agreed with the experimental data when the value of Pe was 65 with an infinite value of k_a . On the other hand, the breakthrough curves of ovalbumin depended on flow-rate, especially for the highest flow-rate. The theoretical curves did not agree with the experimental data with any parameters. The dependence of the adsorption capacity on the flow-rate could not be represented by the model.

Fig. 5 shows the effect of flow-rate on the adsorbed amount calculated by integration of the curves after complete breakthrough. The data are plotted as amount adsorbed per unit bed volume against volumetric flow-rate. A larger amount of ovalbumin was adsorbed as the flow-rate increased. This abnormal behaviour cannot be explained by conventional adsorption theory. Kim et al. [7] stated the possibility of a flow-rate effect on adsorption for a membrane adsorber. The deformation of protein by shear stress might

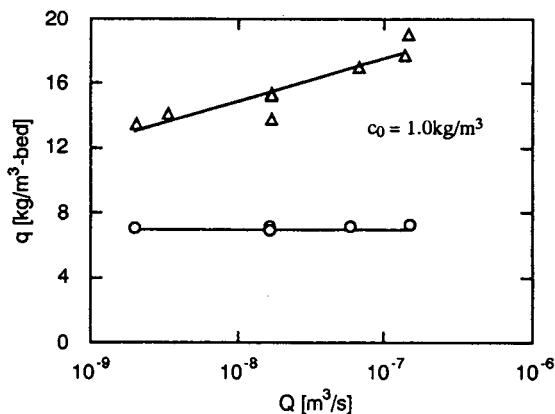


Fig. 5. Effect of flow-rate on the amounts adsorbed of (○) myoglobin and (△) ovalbumin for the DEAE MemSep 1000 membrane adsorber.

affect the adsorption. An effect of flow-rate on adsorption capacity was not observed for bovine γ -globulin on a phenylalanine- or tryptophan-containing membrane system under their experimental conditions. Skidmore et al. [12] observed that bovine serum albumin (BSA) had a higher adsorption capacity for a packed bed than expected from the adsorption isotherm obtained in stirred-tank experiments. This behaviour was not observed for lysozyme. They explained that this was due to multi-layer binding of BSA resulting from the formation of dimers. The dimer formation could be promoted by the flow which brings fresh BSA solution to the adsorbed protein. Therefore, the greater amount adsorbed at higher flow-rates observed in this work might be explained by multi-layer binding of ovalbumin molecules to molecules that are already adsorbed or dimerization of molecules or the influence of protein deformation due to the shear stress of the convective flow in the pores.

Heterogeneities of the membrane such as porosity distribution, thickness distribution and non-uniform flow through the membrane may exist [3,6,8]. Suen and Etzel [3] calculated the breakthrough curves when the membrane thickness and porosity had variations of 10%. They pointed out that even relatively small variations degrade the membrane performance [3]. The model containing these effects may also explain the broadening of the breakthrough curve of ovalbumin for higher flow-rates in the case of the membrane adsorber. When a larger number of membrane sheets are stacked, the influence of heterogeneity of the membrane may become less important.

Another important factor leading to broadening of curves may be non-ideality in the membrane module which includes non-uniform and uneven distribution of flow, leakage along the side of the membranes, variation of space between membranes and dead space in the housing. As mentioned by Liu and Fried [6], this effect is significant in membrane adsorbers.

The effects of flow-rate on the breakthrough curve of both proteins for the packed-bed adsorber are shown in Fig. 6a and b. The breakthrough curves of both proteins were signifi-

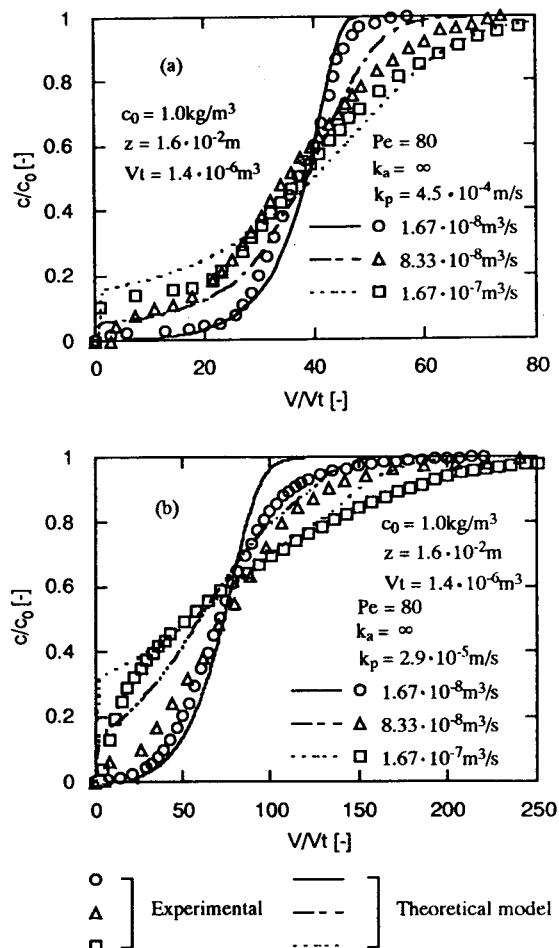


Fig. 6. Effect of flow-rate on the experimental and theoretical breakthrough curves of (a) myoglobin and (b) ovalbumin for the DEAE Sephacel packed-bed adsorber.

cantly affected by the flow-rate. This indicates the influence of the intraparticle diffusion resistance. The breakthrough curves of myoglobin were steeper than those of ovalbumin, mainly because the adsorption capacity of myoglobin is lower than that of ovalbumin and the diffusivity of myoglobin is larger than that of ovalbumin owing to the difference in molecular mass. The abnormal behaviour of ovalbumin observed for the membrane adsorber was not observed for the packed-bed adsorber. The difference between the membrane adsorber and the packed-bed adsorber is the transport mechanism within the

Table 2
Parameters used in the calculation of mathematical models for packed-bed and membrane adsorbers

Protein	Parameter	Packed-bed adsorber	Membrane adsorber
Myoglobin	Pe	65	80
	$k_a(\text{m}^3/\text{kg}\cdot\text{s})$	∞	∞
	$k_p(\text{m/s})$	$4.5 \cdot 10^{-4}$	–
Ovalbumin	Pe	65	80
	$k_a(\text{m}^3/\text{kg}\cdot\text{s})$	∞	0.06
	$k_p(\text{m/s})$	$2.9 \cdot 10^{-5}$	–

adsorbent. The adsorbate molecule is transported to the adsorption site by diffusion for the packed-bed adsorber, whereas it is transported directly by the convective flow for the membrane adsorber. Therefore, liquid flow in the void space of particles does not affect on the adsorption behaviour within the particles. The breakthrough curves were simulated well by the model for the entire flow-rate range.

Table 2 summarizes the parameters estimated by fitting with experimental data. Although the modelling was not successful for the ovalbumin–membrane system, the parameters for the system are listed. In this work, association kinetics between adsorbate and adsorbent were not dominant because the association mechanism was ion exchange in the membrane used here. However, the association between solute and ligand for affinity adsorption may be slower and more important for the membrane adsorber owing to the absence of mass transfer resistance.

5. Conclusions

The breakthrough curves for the membrane adsorber were compared with those for the packed-bed adsorber. The amount adsorbed for the membrane adsorber was smaller than that for the packed-bed adsorber based on a unit volume of the adsorber. The breakthrough curves for the membrane adsorber were steeper than those for the packed-bed adsorber owing to convection through the pores of the membrane, leading to negligible diffusion resistance. For the packed-bed adsorber, the breakthrough curves were

significantly affected by the flow-rate because of intraparticle diffusion resistance.

The breakthrough curves of myoglobin for the membrane were steeper than those of ovalbumin and independent of flow-rate; however, those of ovalbumin were affected by flow-rate. The mathematical model simulated well for myoglobin but not for ovalbumin.

Symbols

a_p	specific surface area (m^{-1})
Bi	$= k_f r_0 / D_e$; Biot number
c	concentration in fluid phase (kg/m^3)
c_0	feed concentration (kg/m^3)
c_i	concentration in fluid phase in pore (kg/m^3)
\bar{c}_i	average value of c_i (kg/m^3)
D	axial dispersion coefficient (m^2/s)
D_e	intraparticle effective diffusivity (m^2/s)
k_a	adsorption rate constant ($\text{m}^3/\text{kg}\cdot\text{s}$)
k_d	desorption rate constant (s^{-1})
k_f	external film mass transfer coefficient (m/s)
k_p	overall mass transfer coefficient (m/s)
K_d	desorption equilibrium constant (kg/m^3)
L	column height (m)
Pe	$= vL/D$; Peclet number
q	amount adsorbed (kg/m^3)
q_∞	adsorption capacity (kg/m^3)
\bar{q}	average value of q (kg/m^3)
Q	volumetric flow-rate (m^3/s)
r	radial coordinate in a particle (m)
r_0	radius of a particle (m)
t	time (s)
v	interstitial velocity (m/s)
V	effluent volume (m^3)

V_t bed volume (m^3)
 z axial distance (m)
 ε bed voidage or membrane porosity
 ε_i porosity of a particle

Acknowledgement

This work was supported by a Grant-Aid for Scientific Research (No. 05750693) from the Ministry of Education, Science and Culture, Japan.

References

- [1] S. Yamamoto and Y. Sano, *J. Chromatogr.*, 597 (1992) 173.
- [2] S. Brandt, R.A. Goffe, S.B. Kessler, J.L. O'Conner and S.E. Zale, *Bio/Technology*, 6 (1988) 779.
- [3] S.Y. Suen and M.R. Etzel, *Chem. Eng. Sci.*, 47 (1992) 1355.
- [4] S.Y. Suen, M. Caracotsios and M.R. Etzel, *Chem. Eng. Sci.*, 48 (1993) 1801.
- [5] K.G. Briefs and M.R. Kula, *Chem. Eng. Sci.*, 47 (1992) 141.
- [6] H.-C. Liu and J.R. Fried, *AIChE J.*, 40 (1994) 40.
- [7] M. Kim, K. Saito, S. Furusaki, T. Sato, T. Sugo and I. Ishigaki, *J. Chromatogr.*, 585 (1991) 45.
- [8] M. Goto and T. Hirose, *J. Chem. Eng. Jpn.* 26 (1993) 523.
- [9] F.H. Arnold and H.W. Blanch, *J. Chromatogr.*, 355 (1986) 13.
- [10] M. Goto, J.M. Smith and B.J. McCoy, *Chem. Eng. Sci.*, 45 (1990) 443.
- [11] O. Levenspiel, *Chemical Reaction Engineering*, Wiley, New York, 2nd ed., 1972.
- [12] C.L. Skidmore, B.J. Horstmann and H.A. Chase, *J. Chromatogr.*, 498 (1990) 113.

High-performance protein separations with novel strong ion exchangers

Judit Horvath^{a,*}, Egisto Boschetti^b, Luc Guerrier^b, Nelson Cooke^a

^aBeckman Instruments Inc., 2500 Harbor Boulevard, Fullerton, CA 92634, USA

^bBioSeptra S.A., 35 Avenue Jean Jaurès, 92395 Villeneuve la Garenne Cedex, France

First received 4 March 1994; revised manuscript received 30 May 1994

Abstract

In this paper, properties of new ion exchangers specifically designed for protein separations are reported. These sorbents are constituted of two main parts: a rigid, porous polystyrene–silica composite material which forms a rigid skeleton and a soft hydrogel bringing strong ionic groups. The later is regularly distributed inside the pores of the skeleton. Characterization of these materials was performed by measuring dynamic sorption capacity, resolving power, separation efficiency and protein recovery. These studies were done using various known proteins and protein mixtures. Some comparisons have been made with commercially available ion exchangers also designed for protein separations.

1. Introduction

High-performance ion-exchange liquid chromatography is a powerful method for separation and purification of biopolymers. Various types of stationary phases were developed based on surface modified silica, polysaccharides and synthetic hydrophilic resins. The stationary phases vary in charge, functionality and pore diameter. Besides the surface chemistry, the pore structure is one of the most important characteristics of a stationary phase, since it determines the surface area of the support as well as the intraparticle solute transport.

Micropellicular [1,2] and non-porous station-

ary phases [3–5] are designed to achieve very fast and very efficient separations of biopolymers. The main advantage of these stationary phases is the rapid mass transfer between the stationary phase and the solutes. By eliminating the pores, the “stagnant mobile phase mass transfer” which is the main cause of the band spreading in the case of porous supports is diminished. The limitation of these phases is the small surface area and the low column permeability due to the small, non-porous spherical particles.

At present the majority of available products are the well-known conventional porous diffusive stationary phases. The size of the pores (100–1000 Å) is large enough to let the biopolymers diffuse rapidly to access to ionic sites [6]. With this pore size these stationary phases have significantly larger surface area and thus considera-

* Corresponding author. Present address: Dionex Corporation, 1228 Titan Way, P.O. Box 3603, Sunnyvale, CA 94088, USA.

bly higher capacity compared to the micropellicular and non-porous phases. However, the slow mass transfer between the pores and the analytes results in peak broadening and in a significantly slower separation process.

In 1990 new, so-called perfusive chromatographic media were introduced [7]. These separation media are constituted of particles with 6000–8000-Å pores transecting the particles, the surface area being increased by the presence of 500–1500-Å interconnecting pores. As a result of the interconnected “throughpores” the particle can be operated in perfusion mode: when the rate of the solute transport due to convective flow inside the particles is greater than the rate of diffusive transport due to concentration gradients [7]. At low flow rates solutes enter the particle through a combination of convective and diffusive transport, but at high flow (Peclet number > 1) convection dominates. Due to convective transport, mass transfer rates are described as high compared to conventional diffusive stationary phases; this gives numerous application advantages to this type stationary phases [7,8]. D.D. Frey et al. [9] studied the effect of intraparticle convection on separations of biomolecules. They concluded that perfusive particles have performance advantages over particles with standard sized pores, mainly for applications that do not require high resolving power to accomplish fast separations. Besides the speed of the separation, another consequence of the very large porous, perfusive structure is the smaller surface area, which results in significant decrease of loading capacity compared to conventional diffusive stationary phases.

More recently a new chromatographic packing material was introduced based on a new hybrid concept [10–12]. A classical, soft tridimensional gel network is used as a protein sorbent; the high capacity of this kind of material was described more than 20 years ago [13]. This gel is not appropriate for high-performance liquid chromatography, due to its softness. In the so-called HyperD particles the gel is surrounded by a polystyrene–silica composite material giving it the necessary physical hardness for use in HPLC

columns. The soft hydrogel can possess chemical functions or ligands appropriate for protein separations. Adsorption–desorption mechanisms are not different from classical hydrogels and necessitate the diffusion of macromolecules inside the gel where the requisite interactions occur and not in the interface between the rigid material and the hydrophilic polymer [14].

In this work main ion-exchange properties are studied with various proteins using the new ion-exchange material known under the trade name of HyperD (see below). We also compared the results to conventional diffusive and perfusive materials. Results shown deal with 10- μ m spherical particles for micropreparative high-performance separations.

2. Experimental

2.1. Columns and stationary phases

The Q and S HyperD ion-exchange stationary phase (10 μ m particle size) was supplied by BioSeptra, France. The stationary phase was packed into Pharmacia's HR 5/5 column system (5 \times 50 mm glass column, with adjustable column top) using the following packing procedure. First, 2 ml of slurry (50% dry material content) was homogenized and filled into an empty reservoir. Then, the slurry was pushed into the empty column, with a Beckman HPLC pump (#126) using inverse flow (against gravity) to obtain a maximum of 950 p.s.i. (1 p.s.i. = 6894.76 Pa) pressure drop on the column. The packing liquid for the Q material was 20% MeOH, 1 M NaCl and 50 mM Tris-HCl at pH 8.62. The packing buffer for the S material was 20% MeOH, 1 M NaCl, 50 mM Na Acetate at pH 4.50. The flow was maintained for 20 min.

Mono Q and Mono S columns (50 \times 5 mm) were purchased from Pharmacia LKB, (Piscataway, NJ, USA). The column configurations and particle size (10 μ m) were identical with the Q and S HyperD columns.

Poros Q/H, Poros S/H and Poros HS/H columns were purchased from PerSeptive Bio-

Systems (Cambridge, MA, USA). The 10- μm particles were prepacked into 50 \times 4.6 mm I.D. polyether ether ketone (PEEK) columns.

For recovery, capacity and some gradient studies Resource Q (30 \times 6.4 mm) 15 μm column from Pharmacia, and the Poros Q II/P (50 \times 4.6 mm PEEK) 20 μm column from PerSeptive BioSystems were also used. Due to the different particle sizes of these two last sorbents (15 and 20 μm , respectively, compared to 10 μm) results of the efficiency, resolution, and separation studies are not presented in this report.

2.2. Instruments

The Beckman (Fullerton, CA, USA) System Gold HPLC system was used throughout this study. The system consisted of a Programmable Solvent Module 126, Programmable Detector Module 166, and Autosampler 507 equipped with loops ranging in size from 25 to 1000 μl . For capacity measurements we used the 50 ml glass superloop from Pharmacia LKB.

The data was collected using an IBM PS/2 Model 56SX computer and evaluated using the System Gold Data system.

For recovery studies we used a Beckman Model DU-7 Spectrophotometer to measure UV absorbance.

2.3. Chemicals

All salts and solvents were HPLC grade. The buffers were filtered through a 0.45- μm filter and degassed before use.

All standard proteins [such as ribonuclease A (RNASE A), ovalbumin (OVA), α -chymotrypsinogen A (α -Chym A), β -lactoglobulin (β -Lact), cytochrome *c* (Cyt C), myoglobin (Myo), lysozyme (Lys), human transferrin (aTRS), human albumin (hA)] were purchased in purified form from Sigma (St. Louis, MO, USA).

$\beta\omega$ -E. Coli extracts were prepared by Dr. Craig Adams (Beckman Instruments, Fullerton, CA, USA) and used without further treatment.

3. Results and discussion

3.1. Q ion exchangers

Isocratic elution of proteins

For preliminary testing, the efficiency was measured under isocratic conditions when flow rate and sample load were varied. Bovine serum albumin (BSA) was used as a test protein under non-retaining conditions for all columns. The lack of retention limits the practical importance of these experiments; however, they are very useful for the comparison of various stationary phases regarding their differences in intraparticle solute transport. The plate numbers were determined from three consecutive injections using the Beckman System Gold software. The data varied less than 1%. At relatively low flow rates the Q HyperD column initially showed a good efficiency. As the flow rate increases, efficiency progressively deteriorated beyond a linear velocity of 360 cm/h (Fig. 1) The Poros Q/H column demonstrated very good reduced plate height values also, which were substantially unchanged up to 550 cm/h linear velocity used in this study. The high efficiency of the Q HyperD column is attributed to the high diffusive permeability of the hydrogel [10,13] and the low level of peak broadening. However, the phenomena of non-equilibrium diffusion rate showed some degree of flow rate dependency.

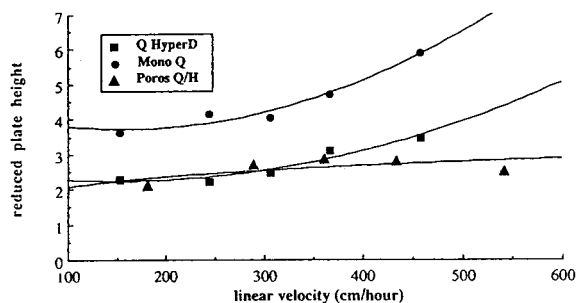


Fig. 1. Reduced plate height versus linear velocity relationship with 10- μm Q ion exchangers. 80 μg (40 μl) bovine serum albumin was injected under non-retaining conditions: 0.4 M NaCl in 50 mM Tris-HCl pH = 8.6 buffer. Detection at 280 nm.

Although some loss of efficiency can be measured at higher flow rates with the Q HyperD column, the flow range where this deterioration starts is close to the maximum operating flow rate due to back-pressure limitation. The conventional diffusive Mono Q column showed the lowest efficiency among the three columns we studied, which decreased much more with increasing flow rates. Here we need to emphasize that the diffusive Mono Q and Q HyperD do not have the speed capability of the perfusive Poros Q column. The pressure limit on the Q HyperD column is 1200 p.s.i. and on the Mono Q column 750 p.s.i. The Poros Q has superior stability: up to 2500 p.s.i. Due to pressure limitations, the maximum flow rates we could use in our comparison did not reach the perfusion limit for the Poros Q column, so all three columns were operated under diffusive conditions.

Fig. 2 shows the relationship between the column efficiency and protein load for the three columns. To determine efficiency we made three consecutive injections and used System Gold software to evaluate the chromatograms. The data varied less than 1%. Q HyperD and Poros Q possess very similar efficiency at the flow rate used (1 ml/min), Mono Q shows somewhat lower plate numbers. As expected, efficiency decreases slightly with increasing protein load for all the columns studied.

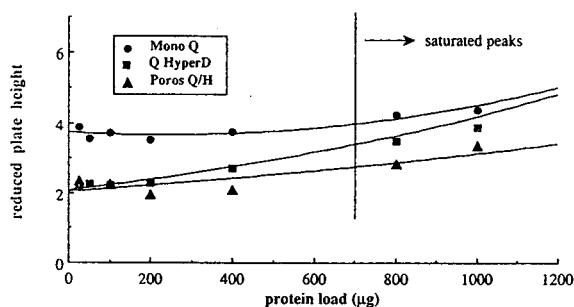


Fig. 2. Reduced plate height versus protein load relationship with 10- μ m Q ion exchangers. Various amounts of bovine serum albumin were injected in 500 μ l injection volume under non-retaining conditions: 1 ml/min 0.4 M NaCl in 50 mM Tris-HCl pH = 8.6 buffer. Detection at 280 nm.

Protein recovery

To measure and compare the protein recovery with various columns, the peak collection method was used. Since the capacities of the columns investigated differ greatly, the amount of BSA injected was 2% of the sorption capacity of each column. Thus, the relative sample load (injected amount compared to the capacity) on each column was similar and gave an effective comparison. The adsorbed BSA was eluted with 1 M NaCl in 50 mM Tris-HCl pH 8.62 buffer, and the recovered BSA was determined by measuring the BSA concentration in the collected samples using UV spectrophotometry. BSA recovery was 67% with Q HyperD and of similar order for MONO Q (73%) and Poros Q/H (70%).

After injection and elution of the protein sample the columns were washed with successive gradient runs (three times) and with 0.1 M sodium hydroxide injection. There was practically no protein elution during these runs. The recovery measurement was repeated three times on each column and the results varied less than 5%. On the basis of these findings, unrecovered BSA is considered here as sample impurity, worse with BSA and much better in the case of cytochrome *c* which we used for S ion exchangers (see below).

Capacity studies

One of the most important characteristics of a preparative HPLC column is its sorption capacity. It determines the highest applicable sample load and thus the productivity of the phase in protein purification. Naturally the dynamic capacity gives even more information about the column: how the capacity will be affected by increasing velocities.

To measure dynamic capacities of the three columns the frontal analysis method was used (5 mg/ml BSA solution). Breakthrough curves were measured at various linear velocities. 50% breakthrough point was taken for calculations to determine capacity; however, 10% breakthrough data for the Q HyperD column are also shown.

Under the experimental conditions studied Q HyperD showed a capacity of about 200 mg/ml

for BSA at 80 cm/h. At 900 cm/h the capacity decreased 25% to 150 mg/ml. At 10% breakthrough, the capacity difference was of about 30 mg/ml corresponding to 20%. Mono Q, Poros Q and Resource Q showed significantly lower capacities: 80, 25 and 70 mg/ml, respectively, at 80 cm/h. Increase in linear velocity resulted in capacity decrease for Mono Q and Resource Q. The sorption capacity of Poros Q remained constant over the entire range of linear velocity studied (Fig. 3).

Gradient elution of protein mixtures

To compare the chromatographic performance of the columns, standard protein samples were used under identical chromatographic conditions. Under these conditions the same reduced linear velocity was adopted for each column (linear velocity was adjusted according to particle size), the gradient length was adjusted to the column length, and the gradient volume was corrected for the dead volume of each individual column. The basis for the adjustments described above was the following equation [15]:

$$b = \frac{t_o}{t_G} \log \frac{k_a}{k_b} \quad (1)$$

where b = gradient steepness parameter, $t_o = V_m /$

F , V_m = dead volume (total volume of the mobile phase inside the column), F = flow rate (ml/min), t_G = gradient duration time (min), k_a and k_b = capacity factor of the solute with A and B eluent (for given gradient solvents $\log k_a/k_b$ is constant).

Standard conditions chosen for Q HyperD were: $F = 1$ ml/min, $t_G = 20$ min, and 0–100% B concentration change during the gradient run. The value of $\log k_a/k_b$ for Q HyperD was calculated from these data and from the measured dead volume. To make the adjustments described above, as a rough estimate, $\log k_a/k_b$ was considered to be the same for each column.

Using these data as well as the measured dead volumes and the constant linear velocity, the t_G values for the other columns were calculated using Eq. 1. The calculated and applied gradient conditions for all the Q columns are summarized in Table 1.

The buffers were identical for all columns; the gradients were run from 0–0.4 M salt as described in Fig. 4 where chromatographic separations are shown.

Q HyperD showed a complete separation of the five components of this mixture with the tendency also to separate the two forms of transferrin. Q HyperD, Mono Q and Resource

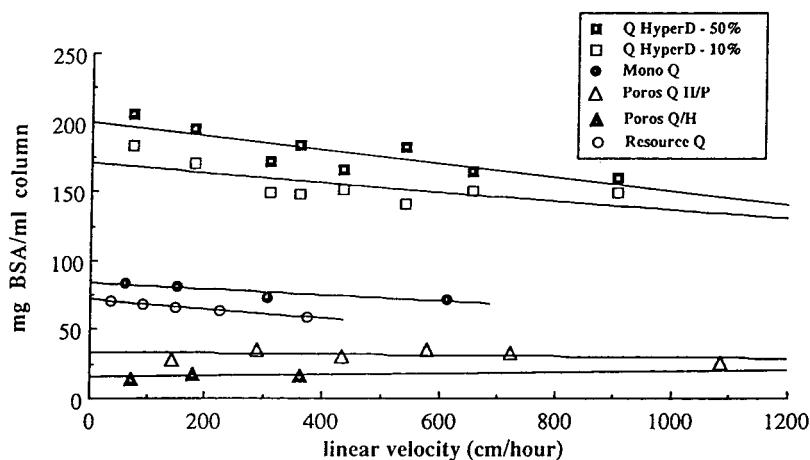


Fig. 3. Dynamic capacity of various Q columns. Method: frontal chromatography of 5 mg/ml bovine serum albumin solution, 50 mM Tris-HCl pH = 8.2 buffer; detection, 290 nm, 50% breakthrough.

Table 1
Established gradient conditions for Q ion-exchange columns

Column	Particle size (μm)	Column size (mm)	V_m (ml)	Linear velocity (cm/h)	Flow rate (ml/min)	t_G (min)
Q HyperD	10	50 × 5	0.87	306	1	20
Mono Q	10	50 × 5	0.89	306	1	20.5
Poros Q/H	10	50 × 4.6	0.66	306	0.85	17.8
ResourceQ	15	30 × 6.4	0.84	204	1.09	17.7

Q showed similar selectivity, the last peak (hA) eluted at around 75% of buffer B concentration. In Poros Q/H proteins were eluted more rapidly probably as a consequence of the weaker ion-exchange groups than the other Q columns: the last peak (hA) eluted at about 50% buffer B.

However, using 0.2 M NaCl buffer B instead of the 0.4 M NaCl, the separation for this column became similar to the separation obtained with Q HyperD and Mono Q columns using 0.4 M NaCl. The Resource Q column resulted in broader peaks than the other Q columns, which

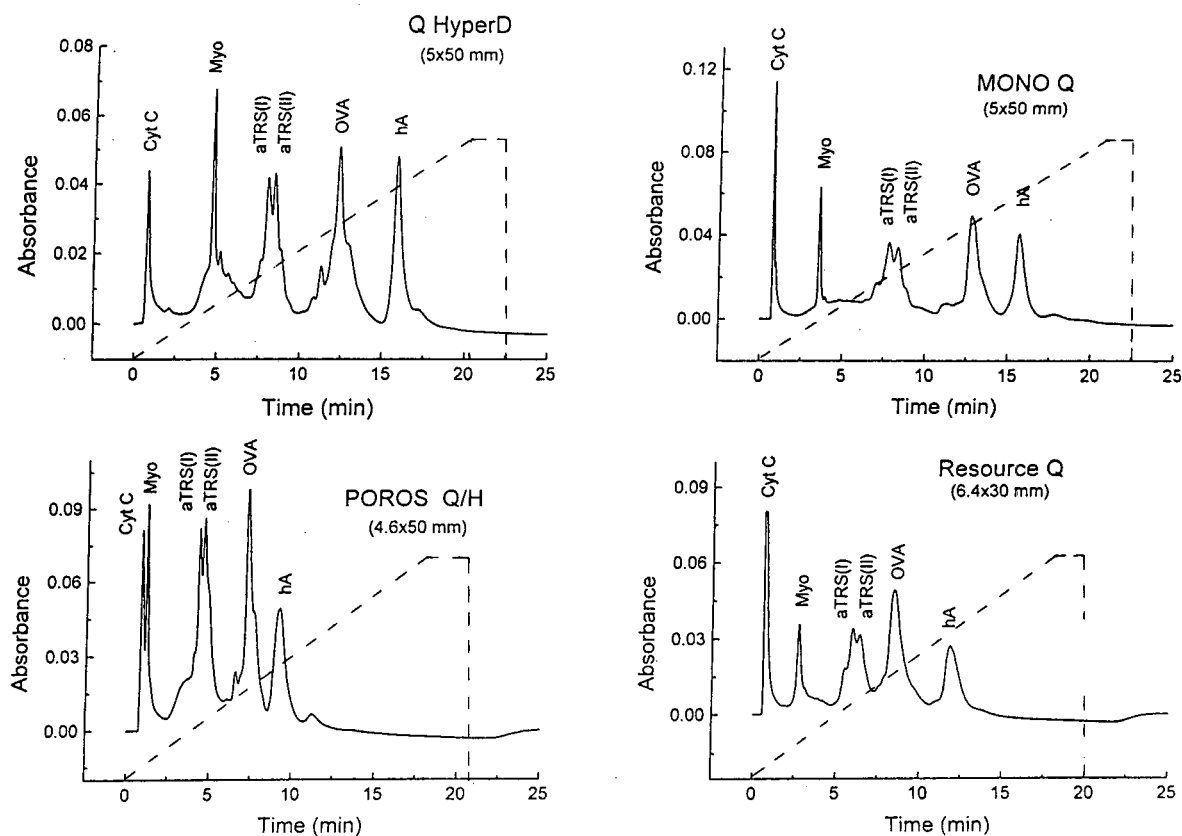


Fig. 4. Separation of 5 standard proteins with gradient elution using various Q columns. Gradient conditions (flow rate and duration time) are described in Table 1. Buffer A, 50 mM Tris-HCl pH = 8.6; buffer B, 0.4 M NaCl in 50 mM Tris-HCl pH = 8.6; detection at 280 nm, total injected protein amount was 297.5 μg in 50 μl .

was understandable considering the particle size differences ($15\ \mu\text{m}$ compared to $10\ \mu\text{m}$). As a summary of these experiments, it can be concluded that in the flow rate range we studied ($0\text{--}1.5\ \text{ml/min}$), no dramatic difference in separation power and selectivity between the columns existed when they were used for the separation of clean, standard proteins under individually adjusted gradient conditions.

Besides testing the columns for standard protein separation, a separation of a crude extract of $\beta\text{-}\omega$ E. Coli was tried, with the $10\text{-}\mu\text{m}$ Q sorbents only. Fig. 5 shows the results obtained using the same, standard gradient conditions. Under standard condition the best resolution by the number of peaks and the best peak width was gotten with the Q HyperD column. Mono Q showed little resolution of the last two main

peaks and a low number of peaks were obtained using the Poros Q column. Under adjusted gradient conditions Q HyperD again showed good resolution and efficiency in comparison to the other two columns. The separation performance with Q HyperD was practically independent of the sample load up to $5\ \text{mg}$ (2% of the capacity) sample injection. Mono Q performance was strongly dependent on the injected sample amount (up to 2% of the capacity was injected); Poros Q gave very similar separations with increasing sample load and separation speed.

3.2. S ion exchangers

Protein recovery study

To measure and compare the protein recovery of S HyperD, cytochrome *c* was used as a model

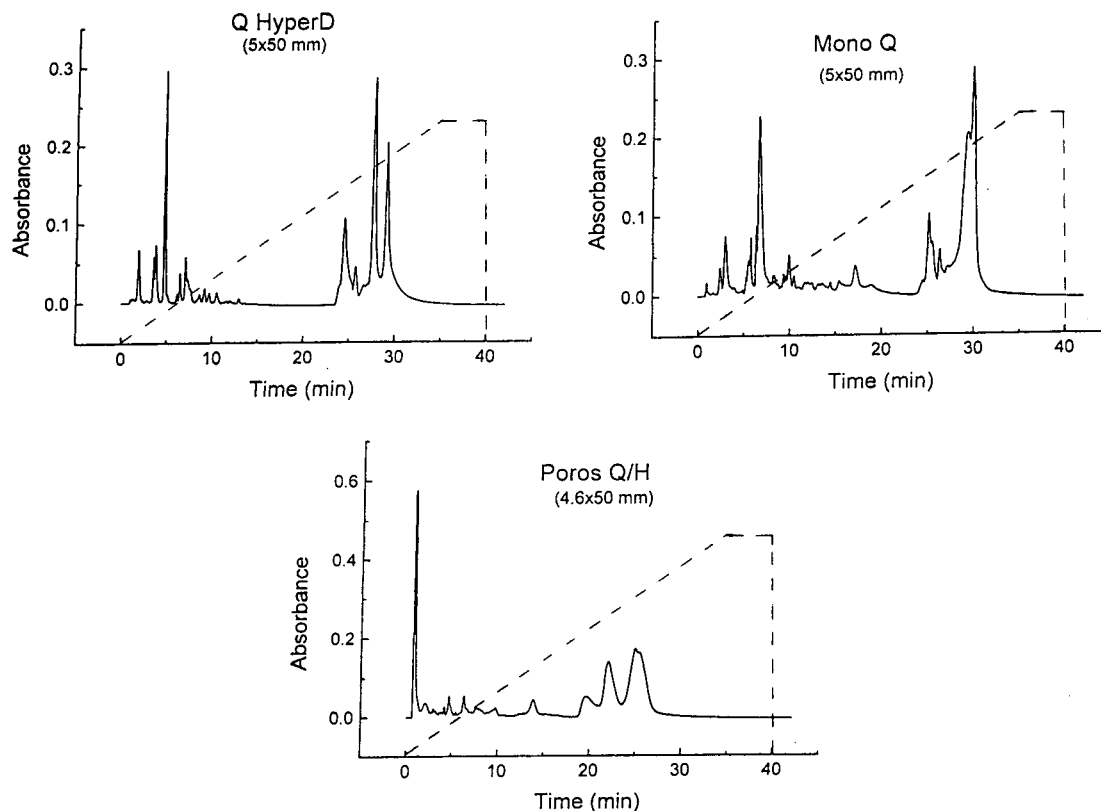


Fig. 5. Separation of $\beta\text{-}\omega$ -E. Coli extract on Q sorbents using the same gradient conditions for all columns. Conditions: $1\ \text{ml/min}$ flow, $35\ \text{min}$ $0\text{--}1\ \text{M}$ NaCl in $50\ \text{mM}$ Tris-HCl $\text{pH} = 8.6$ buffer; detection at $280\ \text{nm}$; injection volume, $30\ \mu\text{l}$; total injected amount $150\ \mu\text{g}$.

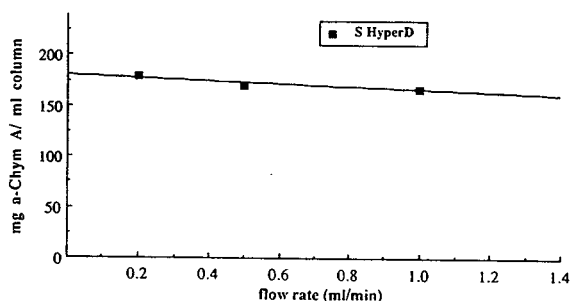


Fig. 6. Dynamic capacity study of S HyperD column. Method: frontal chromatography of 8 mg/ml α -chymotrypsinogen A solution; 50 mM Na acetate pH=4.5 buffer; detection, 290 nm, 50% breakthrough.

protein. The injected amount was 2% of the capacity of the column. The elution buffer was 2 M NaCl in 50 mM Na acetate pH 4.5 buffer, and the concentration of Cyt C was determined by UV spectrophotometry. The protein recovery was found close to 86%. For Mono S, Poros S/H and Poros HS/H capacity results under the same experimental conditions were 80%, 85% and 80%, respectively. The recovery measurement was repeated three times on each column; the results were in a range of less than 6%.

Dynamic capacity

8 mg/ml α -Chymotrypsinogen A solution was used in frontal analysis to measure the capacity of the S HyperD at various flow rates. Fig. 6 shows that the capacity decreases very slowly as a function of flow rate. The measured capacity data of S HyperD compared to the other S columns' capacities as specified by the manufac-

turers in their operating instructions is summarized in Table 2.

Gradient elution of protein mixtures

Mixtures of purified, standard proteins were used to test the columns' performance in gradient elution. Identical gradient conditions were defined as described above; adjustments of buffers and buffer concentrations were also made to obtain the best separation for each protein mixture. It was found that, for complex mixtures (6 proteins), formate buffer permitted better separations than acetate buffer. Preliminary studies gave evidence that the selectivities of the packings studied were rather different. Since the effect of sample load and speed of the separation on resolution was to be measured, the adjustment of final salt concentration during the gradient run was necessary to get approximately the same retention time for the last protein peak with all sorbents. Nevertheless, the absolute resolution values should be interpreted very carefully because of the major differences in surface chemistry. Rather than making a quantitative evaluation based on specific values, all elements of qualitative and quantitative performance of the various columns should be taken into consideration.

Resolution-protein load study

For this study a two-protein mixture was chosen (cytochrome *c* and β -lactoglobulin). The resolutions obtained for this protein mixture were influenced not only by the ion-exchange performance of each packing material and the

Table 2
Comparison of capacity data of various S ion exchangers

Column	Capacity (mg/ml column)	Experimental conditions
S HyperD	160	α -Chymotrypsinogen A; 50 mM Na acetate pH 4.5
Mono S	20–50 ^a	Not available ^a
Poros S/H	20 ^a	Lysozyme; pH 6.2 ^a
Poros HS/H	60 ^a	Lysozyme; pH 6.2 ^a

^a From manufacturer's specifications (operating instructions)

Table 3
Established gradient conditions for S ion-exchange columns

Column	Column size (mm)	V_m (ml)	Linear velocity (cm/h)	Flow rate (ml/min)	t_G (min)	Final concentration (M)
S HyperD	50 × 5	0.87	382.8	1.25	18.8	1.08
Mono S	50 × 5	0.85	382.8	1.25	18.4	0.45
Poros S/H	50 × 4.6	0.65	382.8	1.06	16.6	1.23
Poros HS	50 × 4.6	0.59	382.8	1.06	15.0	0.75

particle size, but also by the indirect influence of the polymer structures. The working conditions used are summarized in Table 3. The runs were repeated three times at every load, and System Gold was used to evaluate the chromatograms. The relative standard deviation was less than 1%. Fig. 7 shows the result of the experiment: the resolution of S HyperD at low protein loading is close to the resolution of Mono S. When protein loading increased up to 600 μg , resolution diminished by 30 to 50% for Poros S/H and HS/H and by about 15% for Mono S while it remained constant for S HyperD.

Nevertheless, we need to state again that the actual resolution values are strongly dependent on the sample–column combination selected, due to the very different selectivities.

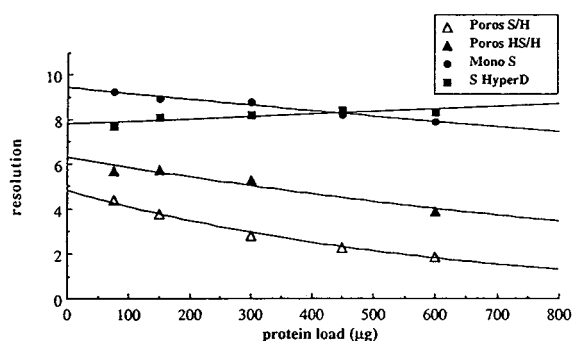


Fig. 7. Effect of the protein load on resolution in gradient elution. Various amounts of cytochrome *c* and β -lactoglobulin were separated using optimized gradient conditions to get similar retention time for the second peak. The exact conditions are summarized in Table 3. Detection, 280 nm; buffer A, 50 mM Na acetate pH = 4.5; buffer B, 1.5 M NaCl in A buffer.

Resolution–speed study

The effect of flow rate on resolution was also investigated while keeping the applied gradient volume constant with steeper gradient profile. The flow rates were chosen to be the original, standard flow (see Table 3) multiplied by 0.33, 0.5, 0.67, 1 and 1.2, termed “speed factor”. The applied flow rates and gradient duration times for each of the columns are summarized in Table 4. The maximum flow rate we could use was 1.5 ml/min, determined by the pressure limit of Mono S and S HyperD columns. Resolution was determined using System Gold software from three consecutive injections. The result varied less than 1%. The measured resolution was plotted as a function of the speed factor (Fig. 8), which is the same for each individual column. S HyperD shows decreasing resolution with increasing speed as well as Mono S. Nevertheless, its resolution for this particular protein mixture remains higher than the Poros S/H and Poros HS/H columns’ resolution at the maximum speed tested. The two Poros columns showed no resolution decrease versus flow rate as theory on perfusion predicts [7].

Separation of a mixture of 6 proteins

To study and compare the resolving power of the columns, the same mixture of 6 proteins was used for all columns with the normalized gradient conditions described above (same linear velocity and dead volume correction). The final salt concentration was chosen in such a way that the elution time of the last protein would be similar. Fig. 9 shows chromatographic separations obtained. S HyperD gave better resolution

Table 4
Gradient conditions used in speed–resolution study of S ion exchangers

Column	Speed factor									
	0.33		0.50		0.67		1.00		1.20	
	Flow	t_G	Flow	t_G	Flow	t_G	Flow	t_G	Flow	t_G
S HyperD	0.41	57.3	0.625	37.6	0.84	27.9	1.25	18.8	1.5	15.7
Mono S	0.41	56.1	0.625	36.8	0.84	27.4	1.25	18.4	1.5	15.3
Poros S/H	0.35	50.3	0.53	33.2	0.71	24.8	1.06	16.6	1.27	13.9
Poros HS	0.35	45.4	0.53	30	0.71	22.4	1.06	15	1.27	12.5

Flow measured in ml/min; t_G in min.

for this sample compared to the other packing materials; with the Poros columns 4 or 5 peaks were separated against 6 for S HyperD. It was also interesting that the elution order of Cyt C and Lys was inverse with Mono S compared to S HyperD; lysozyme possesses a higher isoelectric point than cytochrome *c* (about 11 versus 9.5) and should normally be more retained by strong cation exchangers.

Once again, the influence of the sorbent polymer modified the selectivity to a certain extent which increased the difficulties of interpretation.

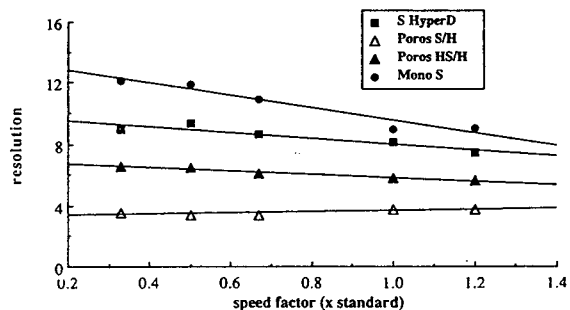


Fig. 8. Effect of the separation speed on the resolution in gradient elution. 150 μ g of cytochrome *c* and β -lactoglobulin were separated using optimized gradient conditions to get similar retention time for the second peak. The speed factor is the number the original flow rate (Table 3.) was multiplied with. The gradient conditions used (flow rate, gradient duration) are summarized in Table 4. The final salt concentrations are summarized in Table 3. Buffer A, 50 mM Na acetate pH = 4.5; buffer B, 1.5 M NaCl in A buffer; detection, 280 nm.

So, regardless of the adjustments we made to establish comparable gradient conditions, results could easily be different for another sample mixture.

4. Conclusions

A performance study of a new ion-exchange packing material (commercially available under the trade name of HyperD) was performed. The results were compared to the most well-known existing packings such as Mono, Resource and Poros columns.

It was found that the HyperD ion exchangers have very high capacity and excellent resolution. The presence of the hydrophilic and permeable ionic gel in the HyperD particles yielded capacities which were improved compared to the conventional porous stationary phases [10,12]. Slightly decreasing resolution and capacity with increasing flow rates are limitations linked to mass transfer issues in the presence of high linear velocities with macromolecules when compared to convection based separations. However, capacity and resolution are high enough, that even when using the column at its maximum, pressure-limited flow rate, both resolution and capacity are the best among the columns studied. Even though the column does not have the flow rate independent performance and the speed capability of the perfusive columns (Poros), the high capacity of HyperD phases enables high

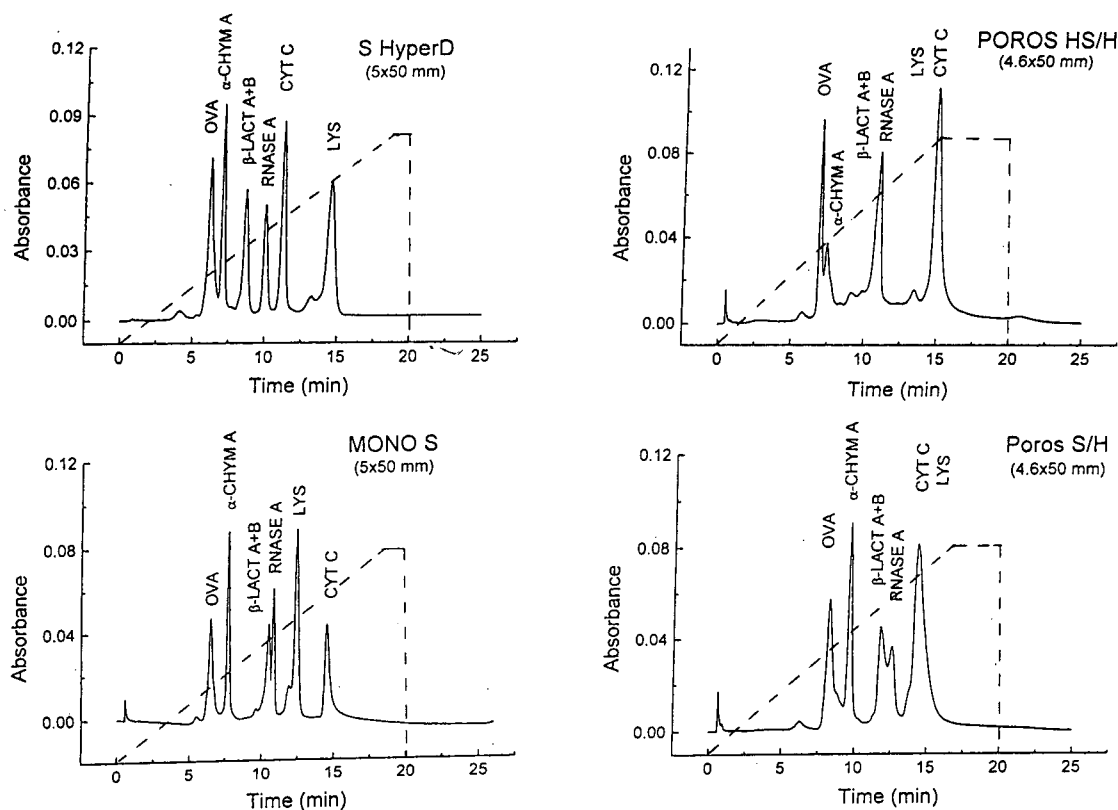


Fig. 9. Gradient separation of 6 standard proteins with S ion exchangers. Normalized gradient conditions were used. Starting buffer, 20 mM Na formate pH = 4.00; injection, 285 μ g total; detection, 280 nm; linear velocity, 382.8 cm/h for all columns. The individual gradients were: S HyperD, 1.25 ml/min 18.8 min (0–0.75 M LiCl); Mono S, 1.25 ml/min 18.4 min (0–1.35 M LiCl); Poros S/H, 1.06 ml/min 16.6 min (0–0.34 M LiCl); Poros HS/H, 1.06 ml/min 15 min (0–1.2 M LiCl).

sample load onto the column. High capacity combined with high resolution and efficiency makes HyperD media very attractive for most separation, purification and isolation problems.

It should also be mentioned that HyperD stationary phases designed primarily for preparative purposes could be appropriate for scaling up the separations. With a larger particle diameter and the same chemistry as the 10- μ m support a particular separation could be transferred easily from analytical and semipreparative to preparative scale.

To summarize the situation of chromatographic packing materials existing today, it can be stated that for the most efficient, fast separation of small amount of samples, non-porous and

micropellicular stationary phases are the most suitable [1–4]. When efficiency and resolution can be sacrificed to gain speed for the separation of relatively small sample amounts convective stationary phases can be recommended [9]. When resolution is more important than the speed of the separation, and the sample amount is relatively small, conventional diffusive stationary phases are suitable [9]. For separations where the sample amount varies from analytical to semi-preparative scale, and especially when future large scale separation is planned, hyperdiffusive stationary phases (HyperD) seem to be the best choice for the chromatographer because it preserves good efficiency and resolution power.

Acknowledgements

The authors wish to acknowledge Dr. Steve Kessler for his stimulating discussions. We further thank Dr. Robert R. Kerr for reviewing the manuscript before submission.

References

- [1] K. Kalghatgi and Cs. Horváth, *J. Chromatogr.*, 398 (1987) 335.
- [2] K. Kalghatgi and Cs. Horváth, in Wittmann-Liebold (Editor), *Methods in Protein Sequence Analysis, Proceedings of the 7th International Conference, Berlin, July 3–8, 1988*, Springer, Berlin, 1989, pp. 248–255.
- [3] Y-F. Maa and Cs. Horváth, *J. Chromatogr.*, 445 (1988) 71.
- [4] Y-F. Maa, S-C. Lin, Cs. Horváth, U-C. Yang and D.M. Crothers, *J. Chromatogr.*, 508 (1990) 61.
- [5] J.K. Duncan, A.J. Chen and C.J. Siebert, *J. Chromatogr.*, 397 (1987) 3.
- [6] M.P. Nowlan and K.M. Gooding, in Mant and Hodges (Editors), *HPLC of Peptides and Proteins: Separation, Analysis and Conformation*, CRC Press, Boca Raton, FL, 1991.
- [7] N.B. Afeyan, N.F. Gordon, I. Mazsaroff, L. Varady and S.P. Fulton, Y.B. Yang and F.E. Regnier, *J. Chromatogr.*, 519 (1990) 1.
- [8] N.B. Afeyan, S.P. Fulton and F.E. Regnier, *J. Chromatogr.*, 544 (1991) 267.
- [9] D.D. Frey, E. Schweinheim and Cs. Horváth, *Biotechnol. Prog.*, 9 (1993) 273.
- [10] E. Boschetti, P. Girot, L. Guerrier, B. André, *Ann. Pharm. Fr.*, 51 (1993) 299.
- [11] A. DePalma., *Genetic Eng. News*, January 1, 1993.
- [12] E. Boschetti, *J. Chromatogr.*, 658 (1994) 207.
- [13] C. Male, *Methods Med. Res.*, 12 (1970) 221.
- [14] S. Kessler, unpublished data.
- [15] L.R. Snyder and J.J. Kirkland, *Introduction to Modern Liquid Chromatography*, John Wiley and Sons, New York, NY, 2nd ed., 1979.

Enantiomer separation by high-performance liquid chromatography on polysiloxane-based chiral stationary phases

Michael Schleimer^{a,1}, William H. Pirkle^{b,*}, Volker Schurig^a

^a*Institut für Organische Chemie der Universität, Auf der Morgenstelle 18, 7400 Tübingen, Germany*

^b*School of Chemical Sciences, University of Illinois, Urbana, IL 61801-3731, USA*

First received 28 February 1994; revised manuscript received 3 May 1994

Abstract

The synthesis of two polysiloxane-based chiral stationary phases (CSPs) derived from a π -acidic N-(3,5-dinitrobenzoyl)- β -amino acid (JEM-1) and a π -basic N-(1-naphthyl)-leucine selector is described as is their systematical comparison with the corresponding “brush”-type CSPs. The enantioselectivity of the polysiloxane-based CSPs is higher under both normal- and reversed-phase conditions. In the normal-phase mode, the greater enantioselectivity stems from smaller retention factors for the least retained enantiomers, presumably because of a reduction of analyte interactions with the support silanols owing to effective shielding of the surface by the polymer. The retention factors of the second-eluted enantiomers are shifted to higher values on the π -basic CSP and to lower values on the π -acidic CSP. The latter CSP shows but a small increase in enantioselectivity relative to the corresponding “brush”-type CSP having a comparable selector loading. The silanophilic interactions can be further reduced by end-capping with hexamethyldisilazane (HMDS). When lower amounts of polar modifier are used, the resolution of the polymeric CSPs approaches that of the corresponding brush-type CSP. Under reversed-phase conditions enantioselectivity is reduced but not to the extent generally found for brush-type CSPs. The presence of the non-polar polymeric backbone can introduce hydrophobic interactions which may alter enantioselectivity. It would seem advantageous to use dimethylpolysiloxanes having a high selector concentration in order to reduce the extent of any non-chiral contribution by the polysiloxane backbone to analyte retention while enhancing the favorable chiral recognition properties of the polymer.

1. Introduction

During the past decade the development of non-volatile, non-leachable polysiloxane-based chiral stationary phases (CSPs) has proven to be of importance in the separation of enantiomers

by gas chromatography (GC). The linkage of chiral molecules to silicones having the potential for cross-linking and/or immobilization leads to gum-like CSPs with low volatility and high physical and chemical stability, all favorable properties for coatings of porous (e.g. silica gel) or non-porous (e.g. glass or fused-silica capillaries) support surfaces. Since the introduction of Chirasil-Val [1,2] into capillary GC, many similar chiral polysiloxanes have been prepared mainly for applications in GC [3,4].

* Corresponding author.

¹ Present address: Marion Merrell Dow et Cie., 16 Rue d'Ankara, 67080 Strasbourg, France.

The spectrum of possible applications in GC was greatly extended by the attachment of permethylated β -cyclodextrin [5] or metal complexes [6] to a polysiloxane backbone. The capability for cross-linking and simultaneous attachment to the support surface enables chiral polysiloxanes to be used for enantiomer separation by supercritical fluid chromatography (SFC) [7–9], LC [10], and, more recently, by electrochromatography using Chirasil-Dex coated capillaries [11]. The synthesis of polysiloxanes containing chiral selectors such as 3,5-dinitrobenzoyl (DNB)-phenylglycine, naphthylalanine and naphthylethylamine and their subsequent coating onto silica gel or into fused-silica capillaries for enantiomer separation by HPLC and SFC was reported about five years ago by Ruffing et al. [10]. However, such CSPs have not yet found much application in the field of enantiomer separation even though such CSPs potentially could provide some advantages relative to the conventional method of silanization of surface silanols with monomeric chiral silicon derivatives. These advantages can be summarized as follows: (i) The preparation of the CSP can be carried out externally under controlled conditions. This allows characterization by spectroscopic or other methods before coating. (ii) The loading of the selector, which is randomly distributed along the polymer chains, can easily be varied either during synthesis of the CSP or by using different film thickness of the coating. (iii) The homogeneous, non-leachable films thus created largely suppress mixed retention mechanisms which might arise from residual silanol groups on the surface of the support.

In this paper, we report on our investigations upon the use of CSPs based on dimethylpolysiloxanes, analogous to those previously introduced by Ruffing et al. [10]. The synthesis of two polysiloxane-anchored chiral selectors, a π -acidic and a π -basic one is described and their behavior in HPLC is compared to the corresponding “brush”-type CSP (which was obtained by the silanization of surface Si-OH of silica gel).

2. Experimental

2.1. Instrumentation

Chromatography was performed using an Anspec-Bischoff Model 2200 isocratic HPLC pump, equipped with a Rheodyne 7125 injector (20 ml) and a Milton Roy LDC UV Monitor D fixed-wavelength (254 nm) detector. The columns were immersed in a constant-temperature bath to regulate temperatures. Integration was carried out with a Hewlett-Packard 3394A recording integrator, using tri-*tert*-butylbenzene (normal phase) and sodium iodide (reversed phase) as void volume markers.

2.2. Materials

Polymethylhydrosiloxane (PMHS), china clay and hexachloroplatinic acid were purchased from Aldrich (Milwaukee, WI, USA). All other silicon containing reagents were obtained from Petrarch Systems (Bristol, MA, USA). The silica, spherical Rexchrom 5 μ m, 300 Å was from Regis (Morton Grove, IL, USA). The ω -olefinated chiral selectors were prepared according to literature [12,13]. All solutes were available from prior studies.

2.3. Synthesis of a dimethylpolysiloxane containing 20% hydromethylsiloxane units

Under an atmosphere of nitrogen 10.0 g (4 mmol polymer, 166 mmol Si-H) of PMHS and 49.2 g (166 mmol) octamethylcyclotetrasiloxane were mixed with 0.7 g of china clay by vigorous stirring. Then 1 ml of concentrated sulfuric acid was added and the mixture held at 70°C for 20 h. After cooling the mixture, the china clay was removed by suction through a frit, which was accelerated by diluting with 150 ml of diethyl ether. The solution was washed with water, the organic layer dried over sodium sulfate, filtered and evaporated. The resulting polymer then was submitted to vacuum (10^{-4} Torr; 1 Torr = 133.322 Pa) at 120°C, yielding 45.6 g (77%) of a

clear viscous fluid. ^1H NMR indicates that the ratio of dimethylsiloxane to methylhydrosiloxane units is 3.8:1 and alkaline hydrolysis shows 2.8 mmol Si–H per gram of pre-polymer.

2.4. General procedure for the synthesis of polysiloxane based CSPs

A 500-mg amount (1.4 mmol Si–H) of the pre-polymer and 1.05 mmol of the selector were dissolved in 40 ml of dry toluene under an atmosphere of nitrogen. The solution was heated to 70°C (for CSP **1P**, and to reflux for CSP **2P**) and half of a solution of ca. 0.2 mg of $\text{H}_2\text{PtCl}_6 \cdot 6\text{H}_2\text{O}$ in 10–15 ml dry tetrahydrofuran was added under nitrogen. After 1 h, the second half of the solution was added and heating was continued for 20 h (for CSP **1P** temperature was reduced to 50°C). The progress of the reaction was monitored by evaporating small aliquots of the solution to dryness and examining them by IR and ^1H NMR spectroscopy. The absence of olefinic protons and the loss of Si–H signals from the ^1H NMR and IR spectra indicate complete reaction of the olefinic selector. This leaves ca. 0.2 mmol g^{-1} Si–H in the resulting chiral polymer.

2.5. Synthesis of a chiral polysiloxane derived from (2R,3R)-undecenyl-N-3.5-dinitrobenzoyl-3-amino-3-phenyl-2-(1,1-dimethylethyl)propanoate (JEM-1) (CSP **1P**)

Following the general procedure, 570 mg (1.05 mmol) of the JEM-1 selector was treated with 500 mg (1.4 mmol Si–H) of the pre-polymer at 70°C. After 2 h, the reaction temperature was lowered to 55°C and reaction was continued for 18 h. After evaporation of the toluene at 30°C the resulting dark yellow polymer was washed with several 10-ml portions of anhydrous methanol which were removed by decantation. Residual methanol was evaporated at 30°C in vacuo (10^{-3} Torr) yielding 1.04 g of CSP **1P**, which was directly used for the coating procedure. Found: 47.07% C, 7.64% H, 3.38% N (calculated: 48.14% C, 7.64% H, 3.66% N).

2.6. Synthesis of a chiral polysiloxane derived from N-(1-naphthyl)-leucine undecenyl ester (N1N-leucine) (CSP **2P**)

Preparation was carried out analogous using 550 mg (1.54 mmol Si–H) of the prepolymer and 470 mg (1.17 mmol) of the N1N-leucine derived selector, which were refluxed for 20 h. After evaporation of the toluene at 30°C the resulting brown polymer was washed with several 10-ml portions of anhydrous methanol, which were removed by decantation. Residual methanol was evaporated at 30°C in vacuo (10^{-3} Torr) yielding 1.0 g of CSP **2P**, which was directly used for the coating procedure. Found: 50.10% C, 9.00% H, 1.39% N (calculated: 50.98% C, 8.66% H, 1.41% N).

2.7. Immobilization of the chiral polymers onto silica gel

A 1.0-g amount of the polymeric CSP **1P** or **2P** was diluted in 20 ml methylene chloride and 4.0 g of silica gel (5 mm, 300 Å), freshly dried by azeotropic distillation with benzene using a Dean–Stark trap) was added. The resulting slurry was sonicated for not more than 10 min after which the solvent was slowly evaporated. Finally, the coated silica gel was heated to 120°C under reduced pressure (10^{-4} Torr) for 24 h. Before packing of the silica gel into a 250 × 4.6 mm I.D. column by conventional methods, it was washed with methylene chloride and methanol (200 ml each), to remove all soluble material (40–100 mg) from the support. As the surface area of the employed silica gel is $100 \text{ m}^2 \text{ g}^{-1}$, the film thickness can be calculated to be somewhat less than 2.5 μm , assuming that the density of the CSPs is 1 g cm^{-3} .

3. Results and discussion

Chiral recognition processes in chromatography are influenced not only by the non-racemic selector chosen but also by the local environment of the selector. The nature of the underlying

support, the manner in which the selector is attached, the absence or presence of extraneous polar (or non-polar) sites at which additional interactions occur with either the analyte or the selector, and the spacing between the chiral sites of the CSP also influence the chromatographic behavior of a given pair of enantiomers.

The aim of this study was to investigate the differences in enantioselectivity and efficiency of CSPs due to variations in the mode of attachment of the selector to the support. For this purpose chiral selectors of demonstrated utility in “brush”-type CSPs, the π -acidic JEM-1 selector (CSP 1) and the π -basic N1N-leucine derived selector (CSP 2), were incorporated into polysiloxanes via hydrosilylation [13] of the olefinic precursors, yielding the polymeric CSPs 1P and 2P (cf. Fig. 1).

In this way, the selectors are randomly distributed along the polymer chains. After coating the polymer onto silica gel, it is subsequently cross-linked/immobilized by heating. This results in

non-leachable CSPs. As pointed out previously by Ruffing et al. [10], the ratio of platinum catalyst (needed for the hydrosilylation step) to the number of Si–H left after this reaction plays an important role in the thermally induced cross-linking and surface bonding. Immobilization and the extent of cross-linking then is controlled by the number of Si–H left after the hydrosilylation step. In analogy to the preparation of other CSPs [5,6] the amount of platinum catalyst needed for hydrosilylation of the JEM-1 or N1N-leucine derived selectors can be reduced to about 0.2 mg per mmol of olefin by raising the temperature and employing aromatic hydrocarbons as solvents. The amount of polymer bonded to the silica gel can be calculated from microanalysis data (see Table 1). It is well known that polymeric stationary phases cannot compete with the high speed of mass transfer found in “brush”-type phases [14] (cf. also the resolution R_s in Table 4). This effect, in conjunction with the adsorption/desorption kinetics of the desired

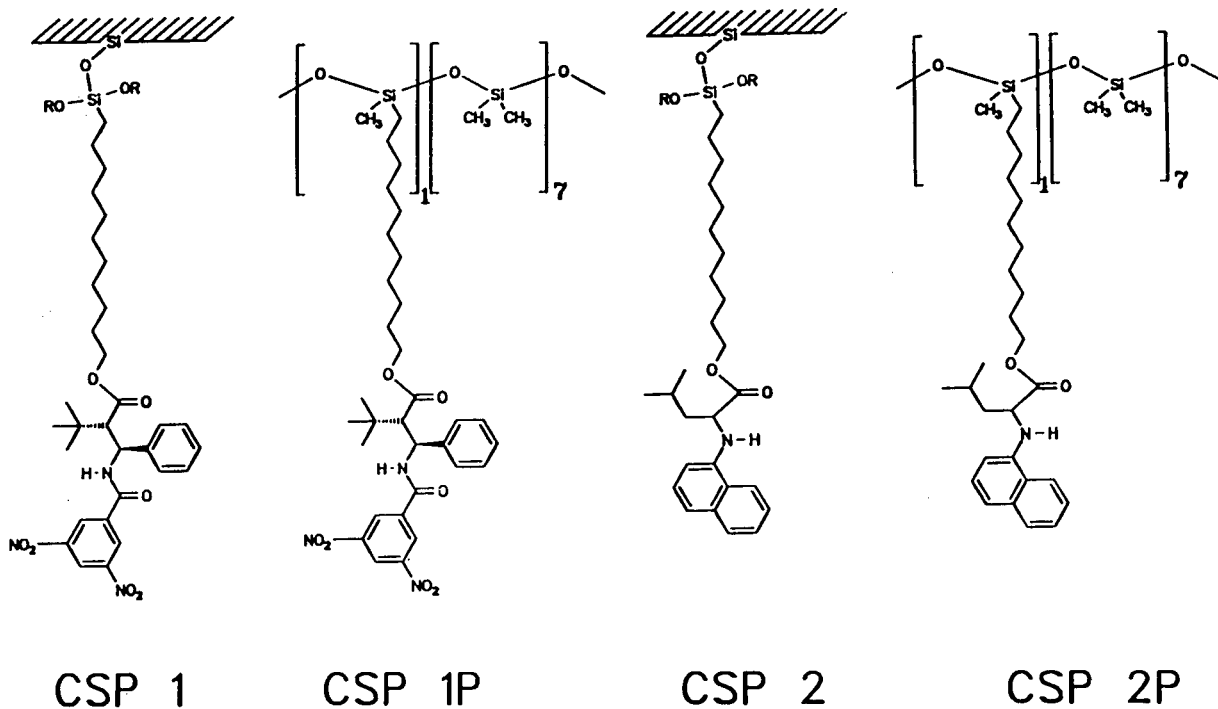


Fig. 1. Structures of “brush”-type CSPs 1 and 2 and their polysiloxane-based analogues CSPs 1P and 2P.

Table 1
Elemental analysis data for silica coated with CSP 1P and CSP 2P

CSP	Coating (%), mg/100 mg SiO ₂	Found			Calculated, mmol/g SiO ₂	
		% C	% H	% N	by C	by N
1P	25	10.00	1.62	0.84	0.181	0.199
2P	25	10.56	1.84	0.29	0.209	0.207

diastereomeric interaction leads to large C terms in the Van Deemter height equivalent to a theoretical plate (HETP) vs. flow-rate curves. This was assumed to be caused principally by the cross-linking of the polymer [15]. The upper branch of the Van Deemter curves, measured for the least-retained enantiomer of the 3,5-dimethylanilide derivative of ibuprofen on CSP 1 and CSP 1P, are depicted for different mobile phase systems in Fig. 2. Interestingly, the relatively large loss in efficiency observed at higher flow-rates in mobile phase system 1 (*n*-hexane–2-propanol, 80:20; compare curve B₁ with A₁), can nearly be compensated by reducing the amount of the polar modifier (system 3: *n*-hexane–2-propanol, 95:5; compare curve B₃ with A₁) thus producing similar efficiency at comparable retention factors. This makes a proper choice of the modifier concentration very important for enantiomer separations on polymeric CSPs since resolution can be affected much more strongly than it is found for the corresponding

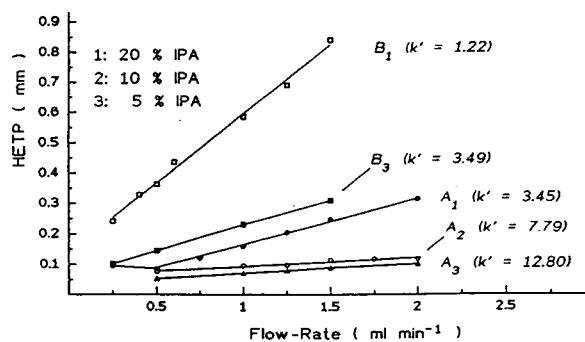
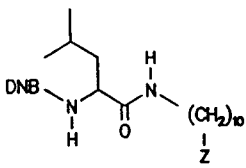


Fig. 2. HETP versus flow-rate for the least-retained enantiomer of the 3,5-dimethylanilide of ibuprofen on CSP 1 (curves A) and CSP 1P (curves B) at different concentrations of 2-propanol (IPA) in *n*-hexane.

“brush”-type CSPs. It is assumed that the lower concentration of the polar modifier affords greater swelling of the polysiloxanes with consequently improved mass transfer characteristics.

The retention and enantioselectivity shown are affected by a number of variables, e.g. the concentration of the selector and the length of the spacer, the film thickness of the polysiloxane, the porosity of the support, the number of residual surface silanols, the mobile phase employed, and the overall polarity of the analyte as determined by polar substituents both near or remote from the stereogenic center(s). This leads to a variety of interactions between the analyte and the stationary phase, not all of which are easily specified [16]. Under normal-phase conditions, silanophilic or other polar interactions which occur in addition to those involved in the chiral recognition process may reduce the observed separation factor by producing unwanted retention [17]. In order to evaluate the extent to which residual surface silanols on the support have been shielded by the polymeric backbone, solutes with remote polar functions in addition to those required for chiral recognition (cf. Table 2) were injected before and after hexamethyldisilazane (HMDS) treatment [18] of CSP 2P. The chromatographic behavior of these analytes was compared to their behavior on a HMDS-endcapped column containing CSP 2. The data indicate that a number of silanols are still accessible after the polysiloxane coating and show that endcapping is advantageous, especially so for those solutes having one or more acidic hydrogen bond donor sites. The endcapping procedure also reduces the C term slightly, as can be seen from Fig. 3 for both enantiomers of the 3,5-dinitrophenylcarbamate of 1-phenylethanol be-

Table 2
The influence of additional polar groups

Analyte	CSP 2, encapped ^a			CSP 2P						
	k'_1	k'_2	α	Not encapped			Encapped ^a			
				k'_1	k'_2	α	k'_1	k'_2	α	
										
Z = H	1.11	26.56	23.9	0.13	6.33	48.7	0.19	7.63	40.2	
Z = CON(ethyl) ₂	2.92	68.38	21.7	0.18	7.05	39.8	0.17	6.73	39.0	
Z = CONH(<i>n</i> -butyl)	2.39	51.19	21.7	0.15	5.40	35.1	0.12	4.65	37.5	
Z = CONH ₂	—	—	—	0.37	11.72	31.7	0.14	7.12	50.8	

^a By purging the column slowly with a solution of 10 ml HMDS in 40 ml dry methylene chloride.

fore (“NOT”) and after HMDS treatment (“HMDS”).

The chromatographic behavior of the polymer-coated columns was evaluated by comparing the retention factors obtained on CSP 2 at different loadings of the silica gel (5 μm , 100 Å) with the values obtained on CSP 2P, coated onto 5 μm , 300 Å silica gel. Representative results for five solutes, all chromatographed under the same normal-phase conditions, are given in Table 3. As expected for the brush-type CSPs (columns A–C), a linear relationship between the retention factors, k' , and the selector loading was

found. Column D, coated with CSP 2P at a selector loading comparable to column A, always gives less retention for the first-eluted enantiomer but more retention for the second-eluted enantiomer. Hence, CSP 2P affords higher enantioselectivities than even heavily loaded type 2 “brush”-type CSPs (columns B and C). Coated also onto 5 μm , 300 Å silica gel, CSP 1P shows significantly reduced retention factors of both enantiomers as can be seen from Table 4. The corresponding separation factors, α , under normal-phase conditions are found to be only slightly higher than those shown by CSP 1, bonded to

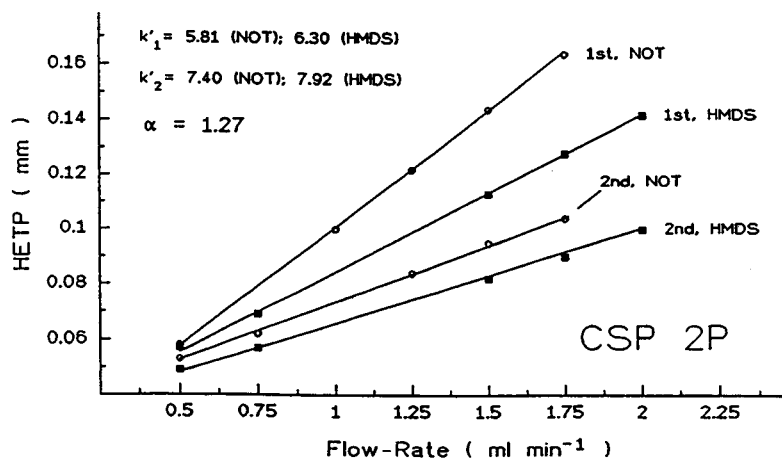


Fig. 3. HETP versus flow rate for the enantiomers of the 3,5-dinitrophenylcarbamate of 1-phenylethanol on CSP 2P before (NOT) and after treatment with hexamethyldisilazane (HMDS). Mobile phase: 2% (v/v) IPA in *n*-hexane.

Table 3
Comparison of “brush”-type (CSP 2) with different loadings to a polymer (CSP 2P)-coated column (D)

Analyte	Parameter	Column ^a			
		A	B	C	D
N-3,5-Dinitrobenzoyl-leucine- <i>n</i> -butylamide	k'_1	0.46	1.19	0.96	0.29
	k'_2	7.90	30.84	21.67	11.11
	α	17.1	26.0	22.7	38.5
N-3,5-Dinitrobenzoyl-phenylalanine- <i>n</i> -butylamide	k'_1	0.72	2.27	1.62	0.54
	k'_2	6.34	25.53	33.78	15.56
	α	8.7	11.2	20.8	30.3
Most retained		L	L	L	L
N-3,5-Dinitrobenzoyl-alanine- <i>n</i> -butylamide	k'_1	0.69	1.63	1.20	0.34
	k'_2	6.42	29.55	18.71	8.31
	α	9.4	18.1	15.5	24.2
N-3,5-Dinitrobenzoyl-leucine-methyl ester	k'_1	0.95	2.54	1.99	0.91
	k'_2	7.02	29.31	20.99	13.08
	α	7.4	11.5	10.5	14.4
N-3,5-Dinitrobenzoyl-phenylalanine-methyl ester	k'_1	1.58	5.12	3.94	1.49
	k'_2	8.65	48.21	33.00	16.30
	α	5.5	9.4	8.4	10.9
Most retained		L	L	L	L

Temperature 22°C; *n*-hexane–2-propanol (80:20, v/v); flow-rate 2 ml min⁻¹.

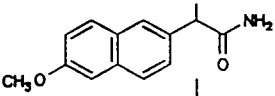
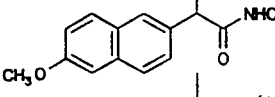
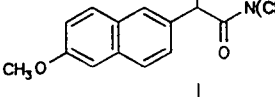
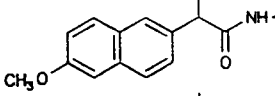
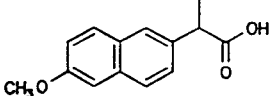
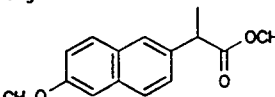
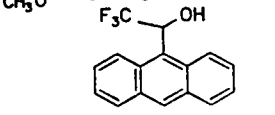
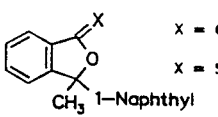
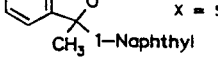
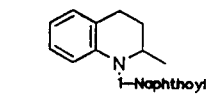
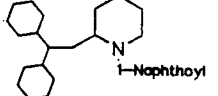
^a Columns: A = low loading, 0.22 mmol g⁻¹ (by C), 0.20 mmol g⁻¹ (by N); B = high loading, 0.32 mmol g⁻¹ (by C), 0.31 mmol g⁻¹ (by N); C = commercially available, 0.27 mmol g⁻¹; D = polymer, 0.21 mmol g⁻¹ (both by C and by N).

5 μm , 100 Å silica gel. The lower retention afforded by the polymeric CSPs is partly due to the larger pore size silica gel (300 Å instead of 100 Å) employed for these columns. This material was chosen not only because there are fewer surface silanols, but also to reduce adsorption, especially of small molecules, into the pores. It is important to note that owing to the lower surface area of the 5 μm 300 Å silica gel (100 m² g⁻¹) the same film thickness is already possible at half of the amount of polymer needed for 5 μm 100 Å silica gel (200 m² g⁻¹). Fig. 4 shows a chromatogram obtained of an N-(1-naphthoyl) derivative of a heterocyclic amine on CSP 1P. A flow-rate of 2 ml min⁻¹ afforded an observed efficiency of about 2500 effective plates for the 250 × 4.6 mm column, a value which can be increased through use of lower mobile phase velocities. The enantiomer separation of the methyl ester of N-(3,5-DNB)-leucine on CSP 2P

(Fig. 5) shows that bandshapes can often easily be improved by increasing the analysis temperature.

Another interesting aspect of polymeric CSPs is their application in reversed-phase systems. The selectors, which are able to form highly selective hydrogen bonds to the analytes, are now part of a non-polar polysiloxane and should be less solvated by the polar mobile phase additives, thus leading to a somewhat greater enantioselectivity than is found with “brush”-type CSPs under reversed-phase conditions. Besides the usual “polar effects” which account for chiral recognition, there are also hydrophobic interactions. In some instances, these can influence enantioselectivity when an alkyl substituent of one enantiomer selectively intercalates between the hydrocarbon spacers connecting the selectors to the polysiloxane backbone [19]. In polysiloxane-based CSPs, silanophobic

Table 4
Comparison of “brush”-type CSP 1 with polymer-coated CSP 1P

Analyte	CSP 1				CSP 1P			
	k'_1	k'_2	α	R_s^a	k'_1	k'_2	α	R_s^a
	—	—	—	—	11.33	16.50	1.4	2.1
	73.31	141.10	1.9	6.9	31.46	60.78	1.9	5.0
	14.84	37.51	2.5	7.2	5.76	16.55	2.9	6.9
	11.34	30.13	2.6	8.9	4.46	11.73	2.6	8.4
	—	—	— ^b	—	—	—	—	— ^b
	2.00	2.33	1.2	1.0	0.91	1.11	1.2	1.0
	1.72	2.24	1.3	2.0	0.83	1.06	1.3	1.0
	15.55	34.83	2.2	5.5	6.58	15.99	2.4	6.6
	2.33	5.81	2.5	4.1	0.96	2.56	2.6	3.5
	14.04	31.49	2.2	6.9	5.99	14.42	2.4	5.6
	15.25	28.75	1.9	5.0	4.19	8.22	2.0	3.2

Temperature 22°C; hexane–2-propanol (95:5, v/v); flow-rate 2 ml min⁻¹.

^a $R_s = 2\Delta t / [w_{\text{base}}(1) + w_{\text{base}}(2)]$, where t = retention time and w = peak width.

^b The separation of underivatized Naproxen is only marginal under these conditions. An improved mobile phase system will be discussed elsewhere.

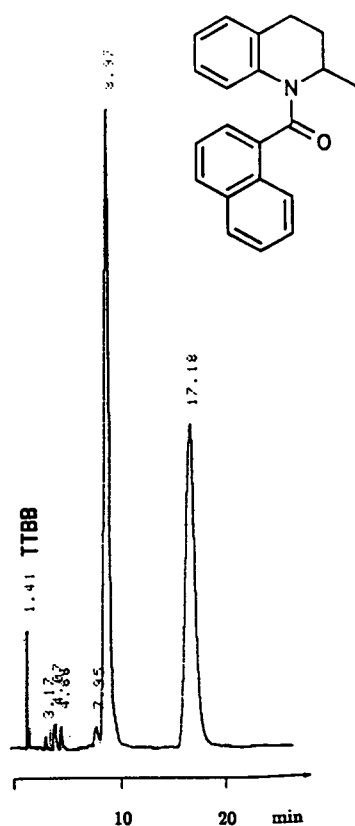


Fig. 4. Enantiomer separation of *N*-(1-naphthoyl)-1,2,3,4-tetrahydro-5,6-benzo- α -picoline on CSP **1P**. Conditions: 1% (v/v) methanol in *n*-hexane at 2.0 ml min⁻¹, 250 \times 4.6 mm column endcapped with HMDS; 22°C; UV 254 nm. TTBB = tri-*tert*-butylbenzene.

interactions caused by the presence of alkyl groups in the polysiloxane backbone are superimposed upon the prior effects. These interactions may be enantioselective since they take place in a chiral environment. However, they may also lower enantioselectivity by causing additional retention. It is therefore instructive to examine homologous series of racemates in order to evaluate the non-polar contributions to retention and enantioselectivity under reversed-phase conditions. Some of the racemates tested are depicted in general form in Fig. 6 as 3, 4, 5 and 6.

When chromatographed with normal phases on CSPs **2** and **2P**, type 3 analytes show the expected decrease in retention with an increase

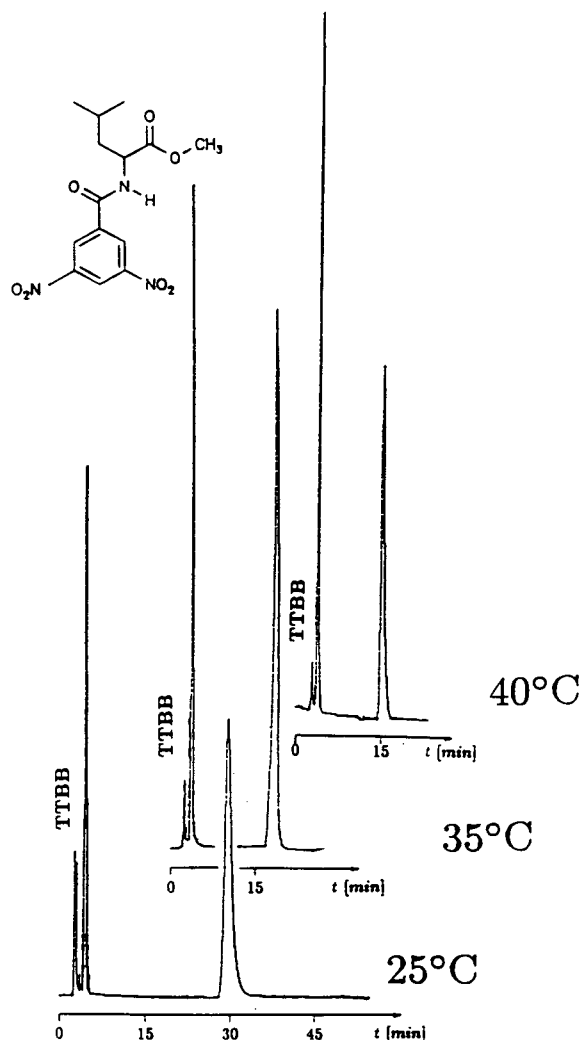


Fig. 5. Enantiomer separation of *N*-(3,5-DNB)-leucine methyl ester on CSP **2P** at different temperatures. Conditions: 20% (v/v) IPA in *n*-hexane at 1.0 ml min⁻¹, 250 \times 4.6 mm column endcapped with HMDS; UV 254 nm.

in the number of methylene units (n), whereas the inverse occurs under reversed-phase conditions. The effect of the value of n on the magnitude of the separation factor, α , is shown for these analytes in Fig. 7. The generally observed reduction in enantioselectivity when going from normal to reversed phases is less pronounced on the polysiloxane-based CSPs than for the “brush”-type counterparts as pointed out before. The contribution of non-polar interac-

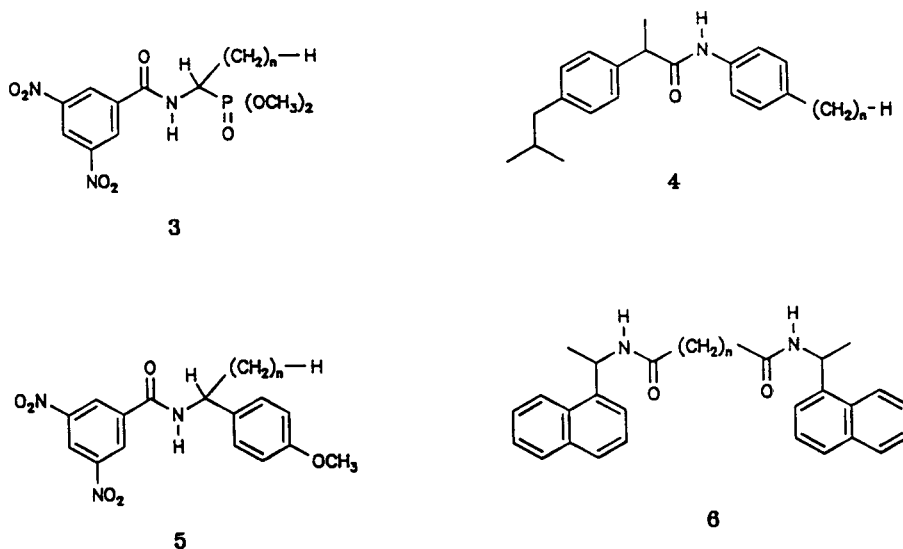


Fig. 6. General structures for the racemates tested.

tions to the enantioselectivity of CSP **2P** towards N-DNB- α -aminoalkylphosphonates is higher than is found on the corresponding CSP **2** as evidenced by the greater slope of the relevant plot in Fig. 7. Here, the more retained enantiomers experience the greater hydrophobic bonding owing to selective intercalation of their alkyl substituents between adjacent strands of bonded phase. The reversed-phase behavior of other analytes on CSP **1P** is shown in Fig. 8. The reversed-phase behavior of CSP **1P** for different

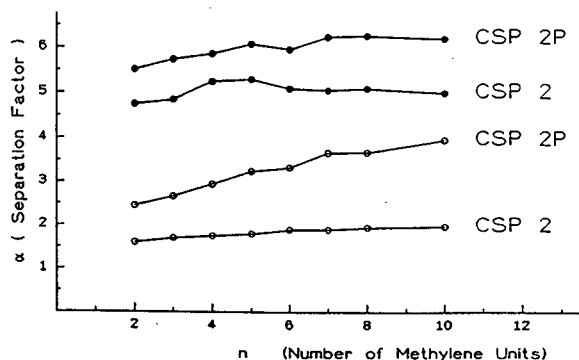


Fig. 7. Separation factor α versus number of methylene units (n) for N-3,5-DNB α -aminoalkylphosphonates (analyte type 3) on CSPs **2** and **2P** in normal and reversed mobile phases. \bullet = *n*-Hexane–2-propanol (80:20); \circ = methanol–water (80:20).

analytes is shown in Fig. 8 (type 4), Fig. 9 (type 5) and Fig. 10 (type 6). Note from Figs. 7–9 that both retention and enantioselectivity increase as the length of the alkyl substituent increases. Eventually however, enantioselectivity no longer increases. This seems to occur when the length of the intercalated alkyl substituent is approximately the same as the length of the tether which connects the selector to the silica. Alkyl substituents longer than this presumably begin to encounter the polysiloxane backbone and/or the silica support. The resulting steric interactions

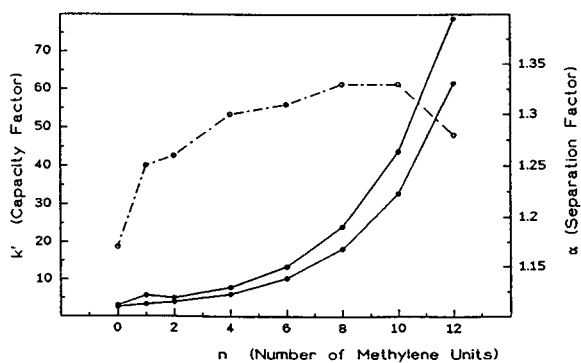


Fig. 8. Retention factor k' (\bullet) and separation factor α (\circ) versus number of methylene units (n) for *p*-alkylanilides of ibuprofen (analyte type 4) on CSP **1P** in reversed mobile phase (acetonitrile–water, 70:30; flow-rate 2 ml min⁻¹).

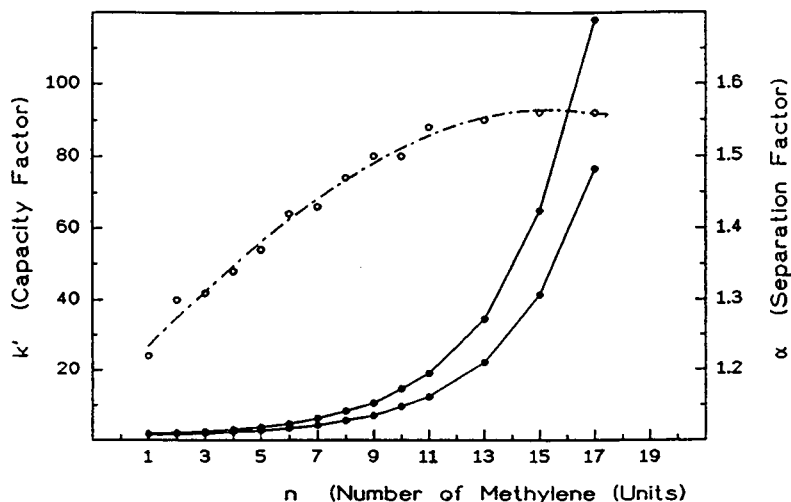


Fig. 9. Retention factor k' (●) and separation factor α (○) versus number of methylene units (n) for N-3,5-DNB-1-(*p*-methoxyphenyl)-aminoalkanes (analyte type 5) on CSP 1P in reversed mobile phase (acetonitrile–water, 70:30; flow-rate 2 ml min^{-1}).

offset any additional hydrophobic bonding which would normally accrue to the more retained enantiomer as the alkyl substituent is lengthened. Similar behavioral trends have been noted for brush-type CSPs. This would seem to suggest that the neighboring selector strands are spatially oriented in similar fashions for both

types of CSPs. It is not intuitively obvious that this should necessarily be the case. Further studies of the effects of film thickness, selector concentration, and selector structure are needed to better understand whether this apparent similarity in spatial orientation is pervasive or occasional. Fig. 9 provides another example of the

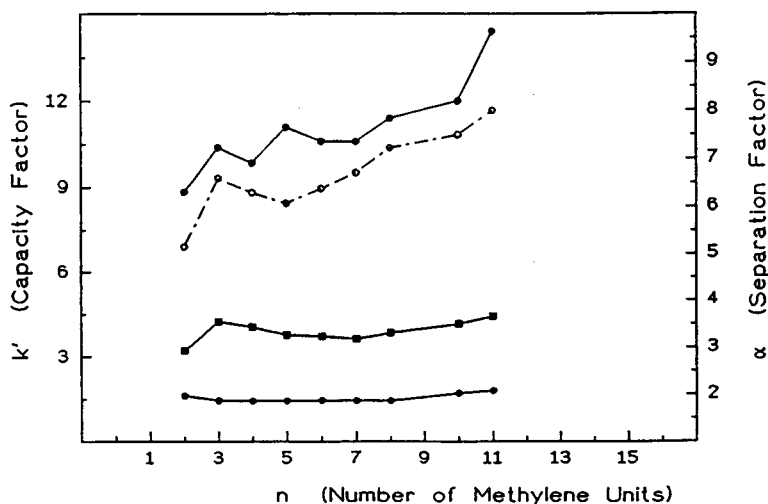


Fig. 10. Retention factor k' (● = $k'_{D,L}$; ■ = k'_{meso}) and separation factor α (○) versus number of methylene units (n) for bis-amides of dicarboxylic acids and α -(1-naphthyl) ethylamine (analyte type 6) on CSP 1P in reversed mobile phase (methanol, flow-rate 2 ml min^{-1}).

resolution of π -acidic enantiomers on a π -acidic CSP.

The plots shown in Fig. 10 demonstrate that both ends of the type 6 bis-amide analytes are capable of simultaneously bonding to neighboring strands of the bonded phase and that the retention (and consequently the enantioselectivity) of the more retained enantiomer is strongly affected by the number of methylene groups connecting the two amide units together. Although the mobile phase is methanol, the retentions of the less retained enantiomers and of the *meso*-diastereomers are but little affected by the number of connecting methylene units.

It has been shown that the enantioselectivity of a chiral selector may be increased by incorporating modest concentrations of the chiral selector into a polysiloxane. It seems to be advantageous to coat relatively thin films of a polysiloxane containing a high concentration of the selector onto the silica gel. This appears to reduce the contributions of the polymeric backbone to reversed-phase retention without losing the desirable properties of the polysiloxane. Because these polysiloxanes are anchored to the silica support, they are likely to be sufficiently robust as to make them useful as CSPs for both analytical- and preparative-scale separation of enantiomers using supercritical fluids as mobile phases in addition to the more traditional liquid mobile phases.

Acknowledgements

This work was supported by funds from the National Science Foundation, from the Deutsche Forschungsgemeinschaft, from Fonds der chemischen Industrie and from Eli Lilly and Company.

References

- [1] H. Frank, G.J. Nicholson and E. Bayer, *J. Chromatogr. Sci.*, 15 (1977) 174.
- [2] H. Frank, *J. High Resolut. Chromatogr. Chromatogr. Commun.*, 11 (1988) 787.
- [3] Y. Dobashi, K. Nakamura, T. Saeki, M. Matsuo, S. Hara and A. Dobashi, *J. Org. Chem.*, 56 (1991) 3299.
- [4] S.G. Allenmark, in R.A. Chalmers and M. Masson (Editors), *Chromatographic Enantioseparation*, Ellis Horwood, Chichester, 1988, p. 79ff.
- [5] V. Schurig, D. Schmalzing, U. Mühleck, M. Jung, M. Schleimer, P. Mussche, C. Duvekot and J. Buyten, *J. High Resolut. Chromatogr.*, 13 (1990) 713.
- [6] M. Schleimer and V. Schurig, *J. Chromatogr.*, 638 (1993) 85.
- [7] V. Schurig, D. Schmalzing and M. Schleimer, *Angew. Chem., Int. Ed. Engl.*, 8 (1991) 30.
- [8] Z. Juvancz and K.E. Markides, *LC·GC*, 5 (1992) 44.
- [9] M. Schleimer and V. Schurig, in B. Wencławiak (Editor), *Analysis with Supercritical Fluids*, Springer, Berlin, 1992, p. 134.
- [10] F.J. Ruffing, J.A. Lux, W. Roeder and G. Schomburg, *Chromatographia*, 26 (1988) 19.
- [11] S. Mayer and V. Schurig, *J. High Resolut. Chromatogr.*, 15 (1992) 129.
- [12] W.H. Pirkle and J.E. McCune, *J. Chromatogr.*, 471 (1989) 271.
- [13] W.H. Pirkle and J.A. Burke, *Chirality*, 1 (1989) 57.
- [14] H. Figge, A. Deege, J. Köhler and G. Schomburg, *J. Chromatogr.*, 351 (1986) 393.
- [15] H. Engelhardt, H. Löw, W. Eberhardt and M. Mauss, *Chromatographia*, 27 (1989) 535.
- [16] W.H. Pirkle and C.J. Welch, *J. Liq. Chromatogr.*, 14 (1991) 2027.
- [17] W.H. Pirkle and C.J. Welch, *J. Chromatogr.*, 589 (1992) 45.
- [18] W.H. Pirkle and R.S. Readnour, *Chromatographia*, 31 (1991) 129.
- [19] W.H. Pirkle, J.P. Chang and J.A. Burke, *J. Chromatogr.*, 598 (1992) 1.

Axially dissymmetric bianthracene-based chiral stationary phase for the high-performance liquid chromatographic separation of enantiomers

Shuichi Oi, Hiroyuki Ono, Hideyuki Tanaka, Masayuki Shijo, Sotaro Miyano*

Department of Biochemistry and Engineering, Faculty of Engineering, Tohoku University, Aramaki-Aoba, Aoba-ku, Sendai 980-77, Japan

Received 29 March 1994

Abstract

Enantiomerically pure (a*R*)-1,1'-bianthracene-2,2'-dicarboxylic acid is prepared and bonded to a 3-aminopropylsilanized silica via an amide linkage to afford a novel chiral stationary phase (CSP 2) for high-performance liquid chromatographic separation of enantiomers. The performance of CSP 2 is compared with that of the previously prepared binaphthalene-based CSP (CSP 1), which was obtained by bonding axially dissymmetric (a*S*)-1,1'-binaphthalene-2,2'-dicarboxylic acid to the silica. As is expected from the chiral discrimination mechanism proposed for CSP 1, in which simultaneous π -donor-acceptor interaction and dipole-stacking interaction between the CSP and the analytes play a critical role for the separation of enantiomers, CSP 2 shows a greatly improved performance as compared with CSP 1 in the separation of a wide range of enantiomeric amino acids, amines, alcohols and carboxylic acids as the 3,5-dinitrophenyl derivatives.

1. Introduction

It is well known that the chiral discrimination ability of a selector molecule mostly determines the performance of a so-called "brush-type" chiral stationary phase (CSP) for the high-performance liquid chromatographic (HPLC) separation of enantiomers [1–3]. In this context, introduction of an axially dissymmetric 1,1'-binaphthalene skeleton into the CSP is of potential interest, considering the fact that the remarkable chiral-discriminating ability of the atropisomeric 1,1'-binaphthalenes has been the subject of intense studies in the last two decades;

highly efficient asymmetric syntheses and/or chiral recognitions have been achieved by the use of this class of optically active molecules [4,5]. In fact, Sogah et al. [6] succeeded as early as 1975 in a complete resolution of amine and amino ester salts by a chiral binaphthalene-crown ether bonded to silica gel, though subsequent applications of atropisomeric biaryls to the CSPs have been quite limited [7–10].

We have previously reported the preparation of a CSP for the HPLC separation of enantiomers by bonding axially dissymmetric (a*S*)-1,1'-binaphthalene-2,2'-dicarboxylic acid [(a*S*)-1] to a 3-aminopropylsilanized silica gel via an amide linkage (CSP 1) (Fig. 1), which efficiently discriminates a wide variety of enantiomeric C-

* Corresponding author.

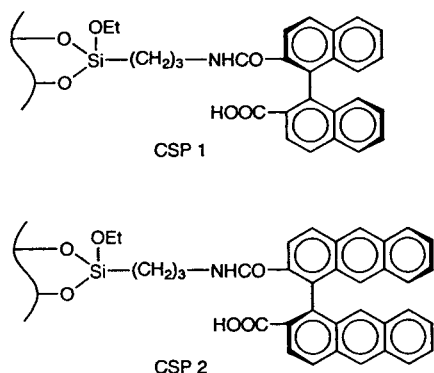


Fig. 1. Axially disymmetric binaphthalene- (CSP 1) and bianthracene-based CSP (CSP 2).

centrochiral analytes as the 3,5-dinitrophenyl derivatives as well as axially chiral 1,1'-biaryls bearing polar substituents on the 2,2'-positions [11]. A simplified chiral discrimination model depicted in Fig. 2 nicely explains the relevant chromatographic behaviours of 3,5-dinitrophenylcarbamates derived from enantiomeric alcohols. It has been supposed that only the approach of the analyte from the upper side of the horizontal naphthalene plane is stereo-differentiating, because it allows π -donor-acceptor interaction between the π -basic naphthalene plane of the CSP and the π -acidic 3,5-dinitrophenyl ring of the analyte to cooperate with

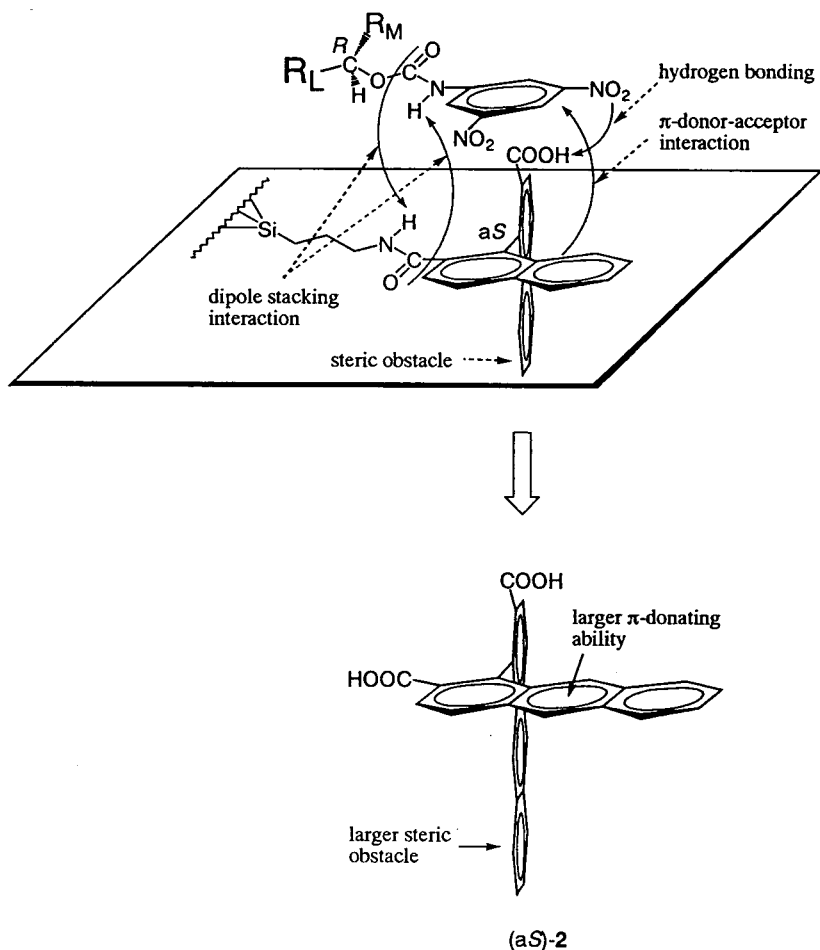


Fig. 2. Chiral discrimination model for binaphthalene-based selector of CSP 1 and an extension to bianthracene-based selector.

the dipole-stacking interaction between the two amide linkages of the CSP and analyte to determine the stability of the adsorbates by virtue of the stereochemistry of the alcohol moieties (Fig. 2). Thus, 3,5-dinitrophenylcarbamates from (*R*)-alcohols are more retained than those from (*S*)-counterparts on CSP 1 bearing (a*S*)-binaphthalene axis. Validity of the chiral discrimination model has been substantiated by ¹H NMR studies of a solubilized model compound of the CSP and analytes as well as the elution behaviours of a wide range of structurally related analytes on CSP 1 [12].

The model strongly tempted us to replace the binaphthalene moiety of CSP 1 by a bianthracene skeleton, because the anthracene nuclei should not only be a far better π -donor but also make a bulkier steric hinge to suppress the non-stereoselective approach of the analytes to the CSP than the naphthalene rings (Fig. 2). Soundness of the hypothesis has partially been proved in a preliminary communication in which the separations of the 3,5-dinitrophenyl-derivatized alcohols were significantly improved by the use of a bianthracene-based CSP (CSP 2) (Fig. 1) [13]. Herein we report the full details of the preparation and performance of CSP 2, showing that it exhibits a greatly improved chiral selectivity as compared with CSP 1 and discriminates a variety of analytes which include amino acids, amines, alcohols and carboxylic acids as the 3,5-dinitrophenyl derivatives and biaryls bearing polar substituents on the 2,2'-positions.

2. Experimental

2.1. General

LC was performed using a Shimadzu LC-6A or a JASCO Trirotor-III apparatus equipped with a Shimadzu SPD-6A or a JASCO Uvidec-100-III ultraviolet detector (254 nm), respectively. A stainless-steel column (250 mm \times 4.6 mm I.D.) was slurry packed with the packing material described below using conventional techniques.

IR spectra were measured on a Shimadzu IR-

460 grating spectrophotometer. Optical rotations were recorded on a Union PM-101 automatic digital polarimeter in a 1-cm cell. Melting points were measured on a Yamato MP-21 apparatus and are uncorrected. Microanalyses were carried out in the Microanalytical Laboratory of the Institute for Chemical Reaction Science, Tohoku University.

2.2. Materials

The preparation of 3-aminopropylsilanized silica gel (Tosoh silica gel base, spherical 5- μ m particles, microsphere diameter, 100 Å) (found: C, 8.10; H, 2.07; N, 1.42%; calculated: 1.01 mmol-NH₂/g gel based on N) was described before [11]. Reagent-grade commercial materials were used as purchased unless otherwise noted. A sample of 2,2'-dimethyl-1,1'-bianthraquinone (**3**) was generously provided by Mitsui Toatsu Chemicals. Solvents used for HPLC were distilled before use.

2.3. Preparation of enantiomerically pure (*aR*)-1,1'-bianthracene-2,2'-dicarboxylic acid [(*aR*)-**2**]

The preparation of enantiomerically pure (*aR*)-**2** was performed according to the procedures reported by Bell and Waring [14] with a slight modification.

2,2'-Bis(dibromomethyl)-1,1'-bianthraquinone (**4**)

Crude bianthraquinone **3** was purified by the method of Ulich and Waldron [15]. A 15.0-g amount of crude **3** was dissolved in concentrated H₂SO₄ (45 ml), to which 13 ml of nitrobenzene were added. To the mechanically stirred solution 15 ml of water were slowly added. During the addition, the temperature of the mixture raised to ca. 100°C. After standing overnight at room temperature, the mixture was filtered and the precipitate was washed with 80% H₂SO₄, and the remaining nitrobenzene was removed by steam distillation. The mixture was filtered and the solid was washed with water and dried in vacuo to give a purified sample, 13.5 g; m.p. > 310°C.

Bromination of **3** was carried out in a 300-ml four-necked flask fitted with a mechanical stirrer, a reflux condenser topped with a gas-absorption trap, a thermometer and a dropping funnel. To a mechanically stirred solution of the purified **3** (12.0 g, 27.2 mmol) in nitrobenzene (75 ml) kept at higher than 170°C was added dropwise a bromine solution (26 g) in nitrobenzene (25 ml) during 6 h, and then the reaction was continued for another 2 h. After the reaction mixture had been cooled to ambient temperature, the resulting yellow precipitate was recovered by filtration, washed with nitrobenzene and then with diethyl ether and dried in vacuo to give bis(di-bromomethyl)bianthraquinone **4**, 15.8 g (77% yield), m.p. > 300°C; IR (KBr) (cm⁻¹), 3100, 1670, 1580, 1500, 1320, 1280, 990, 930, 714, 638.

1,1'-Bianthraquinone-2,2'-dicarboxylic acid (5)

In a 300-ml three-necked flask equipped with a mechanical stirrer, a reflux condenser and a thermometer, were placed concentrated H₂SO₄ (120 ml), anhydrous boric acid (18 g) and **4** (15.0 g, 19.8 mmol). The mixture was stirred at 120–130°C for 5 h. The cooled mixture was slowly added to an ice-water (250 ml), and a brown precipitate was recovered by filtration, washed with water and dried in vacuo to give 2,2'-bisformyl-1,1'-bianthraquinone. This material was used without further purification for the next step by dissolving in hot acetic acid (90 ml). To the stirred solution kept at 60°C was added portion wise CrO₃ (15.0 g, 0.15 mol) during 1 h. The mixture was heated at reflux for 5 h, and then poured into water (300 ml). The precipitated crude diacid **5** was worked up as usual, which included filtration, washing with water free from chromium ions, dissolving in NaOH solution, decoloration with Norite, hot filtration and regeneration of the free acid by addition of concentrated HCl solution. The resulting precipitate was filtered and dried in vacuo to give 4.95 g of **5** (yield 50%), m.p. > 300°C (browned at 285–290°C); IR (KBr) (cm⁻¹), 3600–2500 (br), 1700, 1690, 1580, 1300, 1260, 970, 930, 860, 790, 710. Analysis: found, C 71.43, H 2.96%; calculated for C₃₀H₁₄O₈, C 71.72, H 2.81%.

Racemic 1,1'-bianthracene-2,2'-dicarboxylic acid (2)

To a 500-ml two-necked round-bottomed flask equipped with a mechanical stirrer and a reflux condenser, were placed zinc dust (10 g, 150 mg-atom) and 2 M HCl (20 ml). After the mixture was stirred for several minutes, the inside of the flask was purged with nitrogen and supernatant liquid was removed by decantation. The zinc was further washed with 1 M NaOH (20 ml) and the liquid was again removed by decantation. To the residue were added **5** (4.50 g, 8.96 mmol) and 28% ammonium hydroxide solution (130 ml). The mixture was heated under gentle reflux for 4 h. During the time course the red reaction mixture turned to yellow. At this point, another 180 ml of water were added and reflux was continued for 0.5 h. The mixture was filtered hot. Addition of concentrated HCl to the filtrate caused precipitation of yellow gel. This was filtered, washed with water and dried in vacuo. The dry material was crushed in a mortar and crystallized twice from glacial acetic acid to give **2** as a hairy yellow precipitate, 3.60 g (yield 91%); m.p. 300–305°C. Crystallization from *o*-dichlorobenzene gave pure **2** as yellow prisms, m.p. 305–307°C; IR (KBr) (cm⁻¹), 3600–2500 (br), 1690, 1340, 890, 740, 475. Analysis: found, C 81.43, H 4.10; calculated for C₃₀H₁₈O₄, C 81.68, H 4.32.

Optical resolution of racemic 2

Racemic **2** (3.0 g, 6.8 mmol) was suspended in 120 ml of ethanol and heated at reflux. To the mixture were added 5.0 g of quinidine (15.4 mmol) at once. The suspension disappeared at one time, but soon precipitation began. The mixture was refluxed for another 0.5 h and cooled to room temperature. The precipitate was filtered and again suspended in 50 ml of ethanol and refluxed for 0.5 h. The cool mixture was filtered and dried in vacuo to give a sample of (*aR*)-**2**-quinidine salt, 3.20 g (yield 45%); [α]₅₄₆²⁵ –516° (c 0.52, CHCl₃). The salt was boiled in 80 ml of 1% NaOH solution for 1 h and filtered. The filtrate was made acidic by addition of 6 M HCl, and the resulting precipitate was taken into ethyl acetate. Evaporation of the solvent gave

(aR)-2 as a yellow powder, 1.23 g [yield 86%, based on (aR)-2]; m.p. 257–259°C (acetic acid) (lit. [14], m.p. 253–255°C), $[\alpha]_{546}^{26} -457^\circ$ (c 0.80, acetone) (lit. [14], $[\alpha]_{546}^{26} -440^\circ$ (c 0.80, acetone)). A sample of the optically active diacid was treated with diazomethane to give the dimethyl ester, the enantiomeric homogeneity of which was confirmed by HPLC on N-(3,5-dinitrobenzoyl)phenylglycine-based CSP (Pirkle column).

2.4. Preparation of the CSPs

Binaphthalene-based CSP 1 was that used in the previous studies, which was prepared by bonding (aS)-1,1'-binaphthalene-2,2'-dicarboxylic acid to the above mentioned 3-aminopropylsilylated silica gel; 0.47 mmol binaphthalene unit/g gel [11].

Bianthracene-based CSP 2

A mixture of the 3-aminopropylsilylated silica gel (3.00 g), (aR)-2 (0.92 g, 2.08 mmol) and N-ethoxycarbonyl-2-ethoxy-1,2-dihydroquinoline (EEDQ) (1.03 g) in DMF (30 ml) was irradiated with ultrasound under a nitrogen atmosphere in the water-bath of an ultrasound laboratory cleaner (35 W, 41 kHz) which was maintained at 20°C. After 8 h irradiation, the modified silica gel was filtered, washed successively with tetrahydrofuran, methanol, acetone and diethyl ether, and dried in vacuo to give 3.44 g of CSP 2. Analysis: found, C 16.67, H 1.81%, N 1.51%; calculated, 0.29 mmol bianthracene unit/g gel based on C.

2.5. Preparation of the derivatized enantiomeric analytes

Alcohols (R^1R^2CH-OH) used for derivatization to **8l**, **m**, **n**, **u**, **v**, **y** and **z** were prepared according to the general procedure by using the Grignard method from alkyl bromide (R^1-Br) and aldehyde (R^2-CHO) [16] and those [$R^1R^2CH(CH_2)_n-OH$] to **10a–c** were prepared by the reduction of the corresponding carboxylic acids [$R^1R^2CH(CH_2)_{n-1}-COOH$] with $LiAlH_4$ [12]. Carboxylic acids ($R^1R^2CH-COOH$) used

for derivatization to **11d–h**, **j**, **m–p** and **12a** were prepared via the carboxylation of the corresponding Grignard reagents by treatment with dry ice according to the conventional methods [12]. Parent carboxylic acids **11c** [17] and **11l** [18] were resolved to optically active forms by use of quinine and (S)-(+)-phenylethylamine, respectively, for the determination of the elution orders. Binaphthol (**13b**) [19] and biaryl carboxylic acid derivatives (**13c–i**) [20,21] were prepared by the literature procedure. Other samples used were of commercial origin.

Derivatization of these samples was according to the procedure described before [11,12].

3. Results and discussion

Chiral selector molecule (aR)-2 was prepared starting from bianthraquinone **3** according to the method reported by Bell and Warning [14] (Fig. 3). Oxidation of the methyl substituents of **3** via bis(dibromomethyl) derivative **4** to dicarboxylic acid **5** followed by quinone-carbonyl reduction by zinc dust gave racemic acid **2**. Optical resolution of this material with quinidine gave an (aR)-2-quinidine salt as the less soluble precipitate. After acidic workup to remove the base, two recrystallizations from acetic acid gave essentially enantiopure (aR)-2 as evidenced by HPLC analysis of the methyl ester on a Pirkle column. The atropisomeric (aR)-2 was bonded to a 3-aminopropylsilylated silica via an amide linkage in dimethyl formamide with the aid of EEDQ under ultrasonic irradiation at 20°C to give the bianthracene-modified silica gel. This was slurry packed into a 250 × 4.6 mm I.D. stainless-steel column using conventional packing techniques to give CSP 2 bearing the chiral selector of opposite axial chirality as compared to CSP 1 (Fig. 1).

Enantiomeric samples were amino acids as the N-3,5-dinitrobenzoyl butyl esters (**6**), amines as the 3,5-dinitrophenylureas (**7**), alcohols as the 3,5-dinitrophenylcarbamates (**8–10**), carboxylic acids as the 3,5-dinitroanilides (**11** and **12**), 1,1'-bi-2-naphthols (**13a, b**) and biarylcarboxylic acids as the N-butylamides (**13c–i**) as summarized in

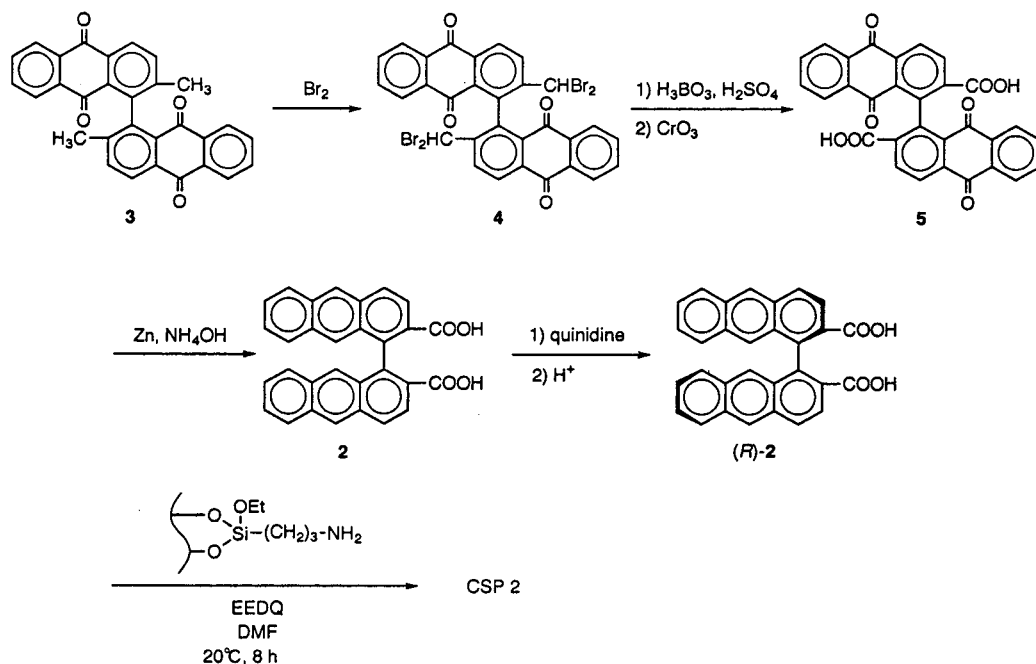


Fig. 3. Preparation of (aR)-2 and CSP 2. DMF = Dimethylformamide.

Fig. 4. They were eluted on CSP 2 with an alcohol–hexane mixture, the composition of which was varied to adjust the capacity factor, k' , in a comparable range. The results of the chromatographic resolution of these analytes are summarized in Table 1. A number of analytes could be resolved on CSP 2, and in favorable cases separation factors (α) greater than 3 were attained as seen for **8w**, **11k** and **q**. For comparison, also included in Table 1 are the results of the elution of the same samples on the binaphthalene-based CSP 1, some of which came from previous work [11,12]. Fig. 5 shows the resolutions of representative analytes on CSPs 1 and 2, illustrating the good performances of these CSPs.

Where chiral resolutions were attainable, the elution orders of each analyte were reversed from CSP 1 to CSP 2, which was consistent with the inverted axial configuration of the chiral selector molecules bonded to the silica support (Fig. 1). Thus, CSP 2 bearing (aR)-bianthracene axis retained more strongly the (S)-enantiomers of the derivatized amino acids, amines and

alcohols. This implies that similar chiral discrimination mechanisms are operative in these two phases, as supposed by the postulated mechanistic picture (Fig. 2). Generally speaking, CSP 2 showed considerably better separations than CSP 1 in terms of α values, although there were some cases where the latter showed almost equal or slightly superior separations to those obtained by the former. Considering the eluent compositions utilized, CSP 2 retained all the analytes examined more strongly than CSP 1. It seems that an increased π -donor–acceptor interaction plays a particularly important role for retention by incorporation of the bianthracene moiety in place of the binaphthalene residue (see below).

The importance of the presence of a π -accepting site in the analytes was discussed in detail in a previous paper for chiral recognition on CSP 1 [12]. It was shown that the 3,5-dinitrophenyl moiety is especially advantageous not only for electronic reasons but also because of steric arrangement of the nitro groups which seemingly enables hydrogen bonding to the 2'-carboxyl function of the binaphthalene selector (Fig. 2)

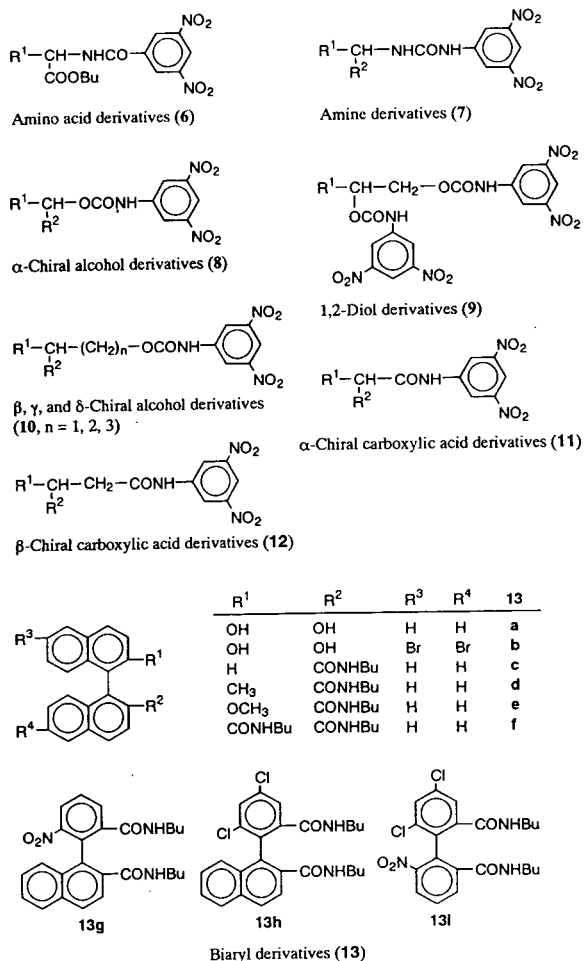


Fig. 4. Structures of enantiomers (see also Table 1).

[12]. Steric hindrance caused by *ortho* substituents on the aryl moieties was detrimental to chiral recognition on CSP 1. Similar situations also hold for CSP 2 as exemplified by Table 2 which compares the separations of ten carbamates prepared from 1-phenylethanol and ten amides from 2-phenylpropionic acid.

Close inspection of the data in Table 1 permits several comments on the chromatographic behaviours of the respective analytes on CSPs 1 and 2, although it should be noted that a wide spectrum of the analytes does not always allow a consistent clear-cut explanation by the proposed chiral discrimination model alone. Among the eleven analytes of derivatized amino acids **6** and

amines **7** examined, three samples (**6b**, **c** and **7a**) did not separate on CSP 1, but did separate with baseline resolution on CSP 2. Somewhat bothering is the behaviour of the derivatized phenylglycine **6d**. It was separated on CSP 1 but not on CSP 2. Only in this case, however, the elution order was reversed, i.e. the (*R*)-enantiomer eluted first on CSP 1 bearing (*aS*)-binaphthalene axis. As suggested previously [11], CSP 1 might recognize the phenyl substituent directly attached to the chiral centre being bulkier than the COOBu group. This situation may change by incorporation of the bianthracene moiety where enhanced π -donor–acceptor interactions of the CSP and the analyte may lead to too much spurious interactions which retain the analyte **6d** strongly as evidenced by the large k' value without distinguishing between the enantiomers.

As for aliphatic 2-alkanol carbamates (**8a–g**), derivatized 2-butanol separated on CSP 2, that is, the CSP discriminated the methyl from the ethyl unit. On both CSPs, the selectivity α increased but retention k' decreased with the increase of the alkyl chain length. This seems to show that the selectivity mainly depends on the difference of the bulk between the two alkyl substituents attached to the carbonyl carbon, while steric hindrance rather than the hydrophobic attractive force is operative between the CSPs and the alkyl chains of the analytes on the normal mode elution. In accordance with these assumptions, the selectivity of octanol derivatives (**8e**, **i** and **j**) decreased as the hydroxy group approached to the centre of the alkyl chain, while the retentions were kept within a rather comparable range. Both CSPs discriminated structural differences of the two alkyl substituents of the same carbon numbers as exemplified by **8l** and **8n**.

Although relative steric bulkiness of alkyl and alkenyl moiety is controversial ([22], see also [23]), CSP 1 seems to recognize vinyl to be bulkier than ethyl as judged by the separability of **8p** but not **8a** on CSP 1. This seems to imply that an unsaturated substituent in the vicinity of the chiral centre of the analyte causes electronic repulsion against the CSP, resulting in a bulkier exclusion volume than the Van der Waals radius.

Table 1
Separation of enantiomers on CSP 1 and CSP 2

No.	R ¹	R ²	CSP 1			CSP 2		
			Eluent	k' ₁	α	Eluent	k' ₁	α
<i>Amino acid derivatives (6)</i>								
6a	CH ₃ (Ala)		A	4.58 (S)	1.13 ^a	C	6.79 (R)	1.76
6b	Iso-C ₃ H ₇ (Val)		A	2.64	1.00 ^a	C	3.45 (R)	1.31
6c	Iso-C ₄ H ₉ (Leu)		A	2.71	1.00 ^a	C	3.46 (R)	1.63
6d	Ph (PhGly)		A	4.27 (R)	1.15 ^a	C	9.18	1.00
6e	CH ₂ Ph (Phe)		A	5.20 (S)	1.14 ^a	C	10.31 (R)	1.67
<i>Amine derivatives (7)</i>								
7a	CH ₃	Iso-C ₃ H ₇	D	5.59	1.00	E	6.69	1.17
7b	CH ₃	n-C ₆ H ₁₃	D	4.45	1.16 ^b	E	5.60	1.46
7c	CH ₃	Ph	E	4.48 (S)	1.30 ^b	G	6.61 (R)	1.73
7d	CH ₃	1-Naphthyl	E	5.47 (S)	1.24 ^b	G	8.56 (R)	1.53
7e	CH ₃	(CH ₂) ₂ Ph	E	3.86	1.10	G	5.20	1.18
7f	Ph	CH ₂ Ph	E	6.77	1.11	G	13.40	1.06
<i>α-Chiral alcohol derivatives (8)</i>								
8a	CH ₃	C ₂ H ₅	A	5.36	1.00	C	4.26	1.13
8b	CH ₃	n-C ₃ H ₇	A	4.78 (S)	1.08	C	3.86 (R)	1.20
8c	CH ₃	n-C ₄ H ₉	A	4.38	1.15	C	3.48	1.31
8d	CH ₃	n-C ₅ H ₁₁	A	4.11	1.19	C	3.36	1.46
8e	CH ₃	n-C ₆ H ₁₃	A	3.93 (S)	1.21 ^a	C	3.19 (R)	1.56
8f	CH ₃	n-C ₇ H ₁₅	A	3.76	1.22	C	3.10	1.66
8g	CH ₃	n-C ₈ H ₁₇	A	3.68	1.24	C	3.01	1.72
8h	C ₂ H ₅	n-C ₃ H ₇	A	4.27	1.09	C	3.94	1.05
8i	C ₂ H ₅	n-C ₅ H ₁₁	A	3.50	1.23	C	3.54	1.23
8j	n-C ₃ H ₇	n-C ₄ H ₉	A	3.64	1.08	C	3.47	1.15
8k	n-C ₃ H ₇	n-C ₅ H ₁₁	A	3.73	1.04	C	3.47	1.13
8l	n-C ₃ H ₇	Iso-C ₃ H ₇	A	3.81	1.10	C	3.65	1.05
8m	n-C ₄ H ₉	Iso-C ₃ H ₇	A	3.50	1.23	C	3.47	1.27
8n	n-C ₄ H ₉	Iso-C ₄ H ₉	A	3.60	1.22	C	3.37	1.27
8o	<i>trans</i> -2-Methylcyclohexanol		A	6.19	1.07	C	4.27	1.19
8p	CH ₃	CH = CH ₂	A	5.90	1.08	C	5.56	1.12
8q	2-Cyclohexene-1-ol		A	3.84	1.00	C	6.16	1.10
8r	CH ₃	Ph	B	3.86 (S)	1.54 ^a	E	3.93 (R)	2.31
8s	C ₂ H ₅	Ph	B	3.44	1.53 ^a	E	3.95	2.21
8t	n-C ₃ H ₇	Ph	B	3.33	1.43 ^a	E	3.82	2.04
8u	Iso-C ₃ H ₇	Ph	B	3.56	1.56	E	3.74	2.16
8v	Cyclo-C ₆ H ₁₂	Ph	B	4.08 (S)	1.38	E	4.17 (R)	1.99
8w	CH ₃	2-Naphthyl	B	5.62	1.55	E	5.25	3.10
8x	Ph	2-Naphthyl	B	12.12	1.04	E	16.95	1.28
8y	CH ₃	CH ₂ Ph	B	4.74 (S)	1.17	E	3.45 (R)	1.59
8z	C ₂ H ₅	CH ₂ Ph	B	4.18	1.18	E	3.44	1.49
8α	α-Tetralol		B	3.84	1.00	E	4.27	1.04
8β	β-Tetralol		B	5.28	1.08	E	4.18	1.05

Table 1 (continued)

No.	R ¹	R ²	CSP 1			CSP 2		
			Eluent	k' ₁	α	Eluent	k' ₁	α
<i>1,2-Diol derivatives (9)</i>								
9a	CH ₃		E	9.34	1.00	G	13.94	1.04
9b	C ₂ H ₅		E	7.87	1.06	G	12.04	1.27
9c	<i>n</i> -C ₄ H ₉		E	6.21	1.24	G	10.84	1.55
9d	<i>n</i> -C ₆ H ₁₃		E	5.38 (R)	1.31	G	10.20 (S)	1.80
9e	Ph		F	4.02 (R)	1.45	G	18.15 (S)	2.73
9f	<i>trans</i> -Cyclohexane-1,2-diol		E	6.43	1.00	G	8.63	1.20
<i>β, γ and δ-Chiral alcohol derivatives (10)</i>								
10a	CH ₃	Ph (<i>n</i> = 1)	B	5.05 (R)	1.09 ^b	E	3.99 (S)	1.13
10b	CH ₃	Ph (<i>n</i> = 2)	B	5.23	1.00 ^b	E	4.35 (R)	1.15
10c	CH ₃	Ph (<i>n</i> = 3)	B	4.99	1.00 ^b	E	4.57 (R)	1.03
<i>α-Chiral carboxylic acid derivatives (11)</i>								
11a	CH ₃	C ₂ H ₅	A	12.33	1.08 ^b	E	4.80	1.03
11b	CH ₃	<i>n</i> -C ₃ H ₇	A	9.73	1.09	E	4.04	1.04
11c	CH ₃	<i>n</i> -C ₄ H ₉	A	8.97 (R)	1.27 ^b	E	3.71 (S)	1.21
11d	CH ₃	<i>n</i> -C ₅ H ₁₁	A	8.49	1.31	E	3.49	1.32
11e	CH ₃	<i>n</i> -C ₆ H ₁₃	A	7.93	1.37 ^b	E	3.65	1.44
11f	CH ₃	<i>n</i> -C ₇ H ₁₅	A	7.60	1.37	E	3.14	1.54
11g	CH ₃	<i>n</i> -C ₈ H ₁₇	A	7.38	1.39	E	3.06	1.64
11h	C ₂ H ₅	<i>n</i> -C ₃ H ₇	A	9.36	1.00	E	3.27	1.03
11i	C ₂ H ₅	<i>n</i> -C ₄ H ₉	A	8.51	1.25	E	2.90	1.27
11j	C ₂ H ₅	<i>n</i> -C ₅ H ₁₁	A	8.04	1.29	E	2.75	1.40
11k	CH ₃	Ph	B	7.57 (R)	1.63 ^b	F	4.67 (S)	3.38
11l	C ₂ H ₅	Ph	B	7.26(R)	1.46 ^b	F	4.74 (S)	2.86
11m	<i>n</i> -C ₃ H ₇	Ph	B	7.02	1.47 ^b	F	4.34	2.76
11n	Iso-C ₃ H ₇	Ph	B	7.28	1.34	F	4.27	2.65
11o	<i>n</i> -C ₄ H ₉	Ph	B	8.03	1.19	F	4.76	2.30
11p	Cyclo-C ₆ H ₁₂	Ph	B	8.67	1.17	F	5.11	2.38
11q	CH ₃	5-OMe-(2-Naphthyl)	C	8.56	1.72	F	8.38	3.04
<i>β-Chiral carboxylic acid derivatives (12)</i>								
12a	CH ₃	Ph (<i>n</i> = 1)	B	7.82 (R)	1.50 ^b	F	5.09 (S)	2.61
<i>Biaryl derivatives (13)</i>								
13a			B	3.41 (S)	1.09 ^a	C	4.07 (R)	1.31
13b			B	5.86	1.24	C	6.38	1.81
13c			A	2.22	1.00 ^a	B	2.04	1.00
13d			A	1.46	1.00 ^a	B	1.39	1.00
13e			A	3.06 (S)	1.09 ^a	B	2.80 (R)	1.12
13f			B	5.41 (S)	1.38 ^a	B	5.09 (R)	1.47
13g			B	4.58 (R)	1.21 ^a	B	5.12 (S)	1.34
13h			B	3.25	1.26 ^a	B	3.18	1.29
13i			B	3.24 (S)	1.13 ^a	B	3.43 (R)	1.18

For structures, see Fig. 4. Mobile phases: hexane–2-propanol, (A) 90:10, (B) 85:15 and (C) 80:20; hexane–ethanol, (D) 90:10, (E) 80:20 and (F) 70:30; and (G) hexane–ethanol–methanol (70:20:10). Flow-rate: 1 ml/min. k'_1 = Capacity factor for the initially eluted enantiomer. The configuration of the initially eluted enantiomer is indicated in parentheses. The separation factor, α , is the ratio of the capacity factors of the enantiomers.

^a Data from Ref. 11.

^b Data from Ref. 12.

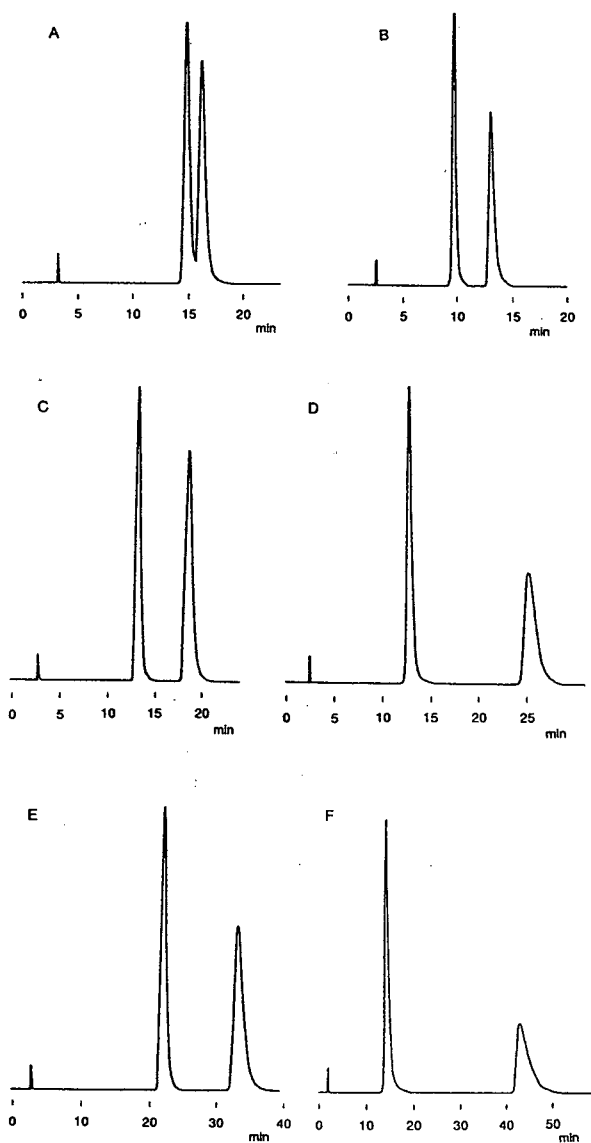


Fig. 5. Chromatographic separation of enantiomers. Separation of N-3,5-dinitrobenzoyl butyl ester of alanine (**6a**) on CSP 1 (A) and CSP 2 (B); separation of 3,5-dinitrophenylcarbamate of 1-phenylpropanol (**8s**) on CSP 1 (C) and CSP 2 (D); separation of 3,5-dinitroanilide of 2-phenylpropionic acid (**11k**) on CSP 1 (E) and CSP 2 (F). Conditions as in Table 1.

This electronic effect may be more operative in CSP 2 than in CSP 1; separations of alkyl aryl carbinol derivatives (**8r–w**) were greatly improved by changing CSP 1 to CSP 2. Conforma-

tional preferences of 6-membered cyclic systems may obscure the difference of the effective steric bulk of the relevant moieties attached to the carbinyl carbons to result in inferior separability of cyclohexenol derivatives (**8q**, α and β) [24].

Several 1,2-diols were converted into the bis(3,5-dinitrophenylcarbamate)s (**9**) and proved to separate well on CSP 2, although the separation of **9a** was not complete even on CSP 2. This means that the presence of an extra dinitrophenylcarbamate moiety at the terminus of an alkyl chain did not disturb the chiral recognition of alcohol derivatives. It should also be noted that CSP 1 discriminated at best the β -chiral centre of a homologous alcohol, while CSP 2 could recognize a chiral centre even at the γ -position (compare **10a** with **b**).

Carboxylic acids as the 3,5-dinitroanilides (**11**) also showed elution behaviours similar to those of the corresponding derivatized alcohols (**8**), except that the first-eluting enantiomers of the former belonged to the dissimilar stereochemistry of the latter enantiomers as fully discussed in a previous paper [12]. Good separations of α -aryl-substituted carboxylic acid derivatives are also noticeable, and derivatized naproxen (**11q**), an important non-steroidal anti-inflammatory agent, attained an α value as high as 3.04.

It is of particular interest to note that in case of the 3,5-dinitrophenyl derivatized analytes (**8–12**), CSP 2 required about twice the amount of the 2-propanol or ethanol content in the hexane-based eluent system to obtain retentions comparable to those obtained by CSP 1, suggesting a significantly enhanced π -donor–acceptor interaction between the anthracene donor and the 3,5-dinitrophenyl acceptor. On the other hand, in case of the biaryl analytes **13**, the retentions on CSP 2 did not so much increase as compared to those on CSP 1. Furthermore, the selectivity was not so much improved by changing from CSP 1 to 2. This is in good accordance with the chiral discrimination model (Fig. 6) which is based on that proposed for the separation of biaryl analytes **13** on CSP 1, where chiral discrimination and retention occur mainly via the hydrogen bonding interactions between the two sets of the 2,2'-substituents of the CSP and the

Table 2
Separation of carbamates of 1-phenylethanol and amides of 2-phenylpropionic acid on CSP 2

R	PhCH(CH ₃)–OCONH–R			PhCH(CH ₃)–CONH–R		
	Eluent	<i>k'</i> ₁	α	Eluent	<i>k'</i> ₁	α
3,5-(NO ₂) ₂ -C ₆ H ₃	C	10.36 (<i>R</i>)	2.80	E	7.64 (<i>S</i>)	3.30
2,4-(NO ₂) ₂ -C ₆ H ₃	C	4.26	1.00	E	3.14 (<i>S</i>)	1.09
<i>p</i> -NO ₂ -C ₆ H ₄	C	3.19 (<i>R</i>)	1.31	E	2.37 (<i>S</i>)	1.48
3,5-Cl ₂ -C ₆ H ₃	C	1.14 (<i>R</i>)	1.37	E	1.03 (<i>S</i>)	1.51
2,4-Cl ₂ -C ₆ H ₃	C	0.52	1.00	E	0.69	1.00
<i>p</i> -Cl-C ₆ H ₄	C	1.16 (<i>R</i>)	1.18	E	1.07 (<i>S</i>)	1.20
C ₆ H ₅	C	1.14	1.00	E	0.91 (<i>S</i>)	1.09
<i>p</i> -CH ₃ -C ₆ H ₄	C	1.06	1.00	E	1.04 (<i>S</i>)	1.09
<i>p</i> -OCH ₃ -C ₆ H ₄	C	1.91	1.00	E	1.61 (<i>S</i>)	1.09
Iso-C ₃ H ₇	C	0.42	1.00	E	0.85	1.00

Mobile phases: (C) hexane–2-propanol (80:20) and (E) hexane–ethanol (80:20). See Table 1 for HPLC conditions.

analyte, mostly irrespective of the backbone binaphthalene skeleton. Thus, biaryls bearing only one such polar substituent (**13c** and **d**) did not separate on both CSPs.

4. Conclusions

Highly efficient CSPs were prepared by bonding atropisomeric 1,1'-binaphthalene- and 1,1'-bianthracene-2,2'-dicarboxylic acid to 3-amino-propylsilanised silica (CSP 1 and 2, respectively),

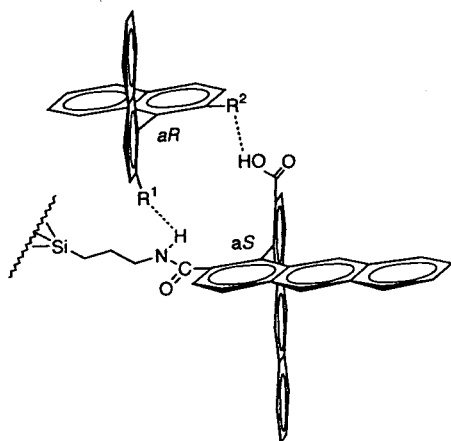


Fig. 6. Chiral discrimination model of biaryl analytes on CSP 2.

which can discriminate a wide range of amino acids, amines, alcohols and carboxylic acids as the 3,5-dinitrophenyl derivatives as well as biaryls bearing polar substituents on the 2,2'-positions. CSP 2 shows a similar elution order for an enantiomeric pair but greatly improved selectivity as compared to that of CSP 1, which is in good accordance with the proposed chiral recognition mechanism for CSP 1 (Fig. 2). These CSPs were quite stable under the experimental conditions used for the data accumulation during more than a year operation. Taking into account the ready availability of chiral selector molecule 1,1'-binaphthalene-2,2'-dicarboxylic acid **1** in both enantiomeric forms [25,26], the binaphthalene-based CSPs should be very useful for practical separation of a variety of 3,5-dinitrophenyl-derivatized enantiomers.

Acknowledgement

We are grateful to the Ministry of Education, Science and Culture, Japan (Grant-in-Aid No. 02555177) and to Tosoh Co. Ltd. for financial support. We thank Mitsui Toatsu Chemicals for a generous gift of a sample of 2,2'-dimethyl-1,1'-bianthraquinone.

References

- [1] S.G. Allenmark, *Chromatographic Enantioseparation, Methods and Application*, Ellis Horwood, Chichester, 1988.
- [2] W.H. Pirkle and T.C. Pochapsky, *Chem. Rev.*, 89 (1989) 347.
- [3] A.M. Krstulović (Editor), *Chiral Separation by HPLC*, Ellis Horwood, Chichester, 1989.
- [4] S. Miyano and H. Hashimoto, *Yuki Gosei Kagaku Kyokai-shi (J. Synth. Org. Chem. Jpn.)*, 44 (1986) 713; *Chem. Abstr.*, 106 (1987) 137988e.
- [5] C. Rosini, L. Franzini, A. Raffaelli and P. Salvadori, *Synthesis*, (1992) 503.
- [6] G.D.Y. Sogah and D.J. Cram, *J. Am. Chem. Soc.*, 97 (1975) 1259.
- [7] G.D.Y. Sogah and D.J. Cram, *J. Am. Chem. Soc.*, 101 (1979) 3035.
- [8] F. Mikeš and G. Boshart, *J. Chromatogr.*, 149 (1978) 455.
- [9] T. Shinbo, T. Yamaguchi, K. Nishimura and M. Sugiura, *J. Chromatogr.*, 405 (1987) 145.
- [10] J. Yamashita, H. Satoh, S. Oi, T. Suzuki, S. Miyano and N. Takai, *J. Chromatogr.*, 464 (1989) 411.
- [11] S. Oi, M. Shijo, H. Tanaka, S. Miyano and J. Yamashita, *J. Chromatogr.*, 645 (1993) 17.
- [12] S. Oi, H. Ono, H. Tanaka, Y. Matsuzaka and S. Miyano, *J. Chromatogr. A*, 659 (1994) 75.
- [13] S. Oi, M. Shijo and S. Miyano, *Chem. Lett.*, (1990) 59.
- [14] F. Bell and D.H. Waring, *J. Chem. Soc.*, (1949) 1579.
- [15] L.H. Ulich and W.R. Waldron, *US Pat.*, 2 666 768 (Jan. 19, 1954; *Chem. Abstr.*, 49 (1955) 1872e).
- [16] J.C.H. Hwa and H. Sims, *Org. Synth.*, V (1973) 608.
- [17] P.A. Levene and L.W. Bass, *J. Biol. Chem.*, 70 (1926) 211.
- [18] K. Petterson, *Ark. Kemi*, 10 (1956) 283.
- [19] A. Riecker, *Ann. Chem.*, 697 (1966) 1.
- [20] S. Miyano, S. Okada, T. Suzuki, S. Handa and H. Hashimoto, *Bull. Chem. Soc. Jpn.*, 59 (1986) 2044.
- [21] S. Miyano, H. Fukushima, S. Handa, H. Ito and H. Hashimoto, *Bull. Chem. Soc. Jpn.*, 61 (1988) 3249.
- [22] F. Yasuhara, S. Yamaguchi, M. Takeda, T. Abe and S. Miyano, *Bull. Chem. Soc. Jpn.*, 64 (1991) 3390.
- [23] R. Noyori, I. Tomino, M. Yamada and M. Nishizawa, *J. Am. Chem. Soc.*, 106 (1984) 6717.
- [24] S. Yamaguchi, F. Yasuhara and K. Kabuto, *Tetrahedron*, 32 (1976) 1363.
- [25] S. Oi, K. Matsunaga, T. Hattori and S. Miyano, *Synthesis*, (1993) 895.
- [26] T. Ohta, M. Ito, K. Inagaki and H. Takaya, *Tetrahedron Lett.*, 34 (1993) 1615.

Role of hydroxyl groups in chiral recognition of cannabinoids by carbamated amylose

Saleh Abu-Lafi, Marina Sterin, Shulamit Levin*

Pharmaceutical Chemistry Department, School of Pharmacy, P.O.B. 12065, Hebrew University of Jerusalem, Jerusalem 91120, Israel

First received 18 March 1994; revised manuscript received 1 June 1994

Abstract

The enantioselective retention of four pairs of enantiomeric cannabinoids that have hydroxyl groups was compared with that for the corresponding acetylated compounds, using amylose tris(3,5-dimethylphenylcarbamate) in the stationary phase. According to this study the hydroxyl groups were essential to the chiral discrimination by the amylose stationary phase, since blocking them by acetylation was detrimental to the enantioselective separation. Three of the four enantiomeric pairs had a relatively rigid tricyclic backbone, whereas the fourth, the cannabidiol, was a flexible compound. In contrast to the other three enantiomeric pairs, the resolution of the acetylated cannabidiol was not completely lost as a result of the acetylation, but it was decreased and the elution order was reversed. Conformational analysis of the acetylated and non-acetylated enantiomeric pairs was systematically performed, using molecular mechanics, in order to examine the effect of acetylation on the conformation of the molecules. The results indicated that acetylation did not change the conformations substantially and therefore the loss of resolution was attributed to the blockage of the hydroxyl groups. The molecular mechanics approach was validated by comparing the energy-minimized structure of cannabidiol with its X-ray crystallographic structure taken from the literature.

1. Introduction

With the increasing evidence of problems related to stereoselectivity in drug action, enantioselective analysis by liquid chromatography, using chiral stationary phases, has become a focus of intensive research [1]. One type of chiral stationary phase is an immobilized carbamated amylose, composed of D-glucose units that form a simple helical backbone [2]. This type of stationary phase has shown high capability of chiral discrimination [3–6]; however, it is not

known whether the chiral information is conveyed on the molecular level (the D-glucose units) and/or the supra-molecular level (helical backbone). The rationalization of the mechanism of chiral discrimination needs a structure–enantioselective retention relationship (SERR) approach, i.e., a comparative investigation of the chromatographic behaviour of solutes. The best strategy would be to use families of chiral compounds with diverse structural features.

The resolution of two such families of enantiomeric terpenoids and cannabinoids was reported previously [5,6]. A comparative study of the structural and chromatographic behaviour of the

* Corresponding author.

series of cannabinoids showed that enantiomeric pairs with very similar structures can be discriminated very differently, whereas very different enantiomeric pairs can be discriminated similarly [5]. The role of hydrogen bonding in the chiral discrimination of terpenoids was also investigated and it appeared as a major interaction [6]. The phenylcarbamated stationary phase resolved ketonic and alcoholic terpenoid enantiomers, although they had no aromatic moiety. Nevertheless, the presence of a hydroxyl group did not necessarily induce enantiomeric resolution, it had to be located in the right position on the molecular structure. The SERR studies were accompanied by a conformational analysis of the enantiomers, using molecular mechanics to verify that conformation was not different with derivatization of the solutes.

Some of the cannabinoids that were studied here had already been analysed by computer modeling as part of their structure–activity relationship (SAR) during the search for non-psychotropic therapeutic derivatives [7]. A major advancement in this field was achieved when this search brought about a therapeutic cannabinoid, devoid of tetrahydrocannabinol (THC)-like psychotropic effects [8]. This enantiomer was studied here, in addition to a natural enantiomer, (–)-cannabidiol (CBD), a non-psychotropic natural cannabinoid. The natural enantiomer has shown antiepileptic, anti-anxiety and antidystonia effects in man [9–11].

Comparisons between hydroxylated enantiomers and their alkyl analogues have been made in a few studies using chiral chromatography [12–14]. Enantiomers of *trans*-dihydrodiol derivatives of phenanthrene and benzopyrene, chrysene, and anthracene and their O-methyl ethers were separated by Yang et al. [12] using Pirkle chiral stationary phases. In contrast to the derivatized cannabinoids, the O-methyl ethers eluted with shorter retention times but were separated more efficiently than the enantiomers of underivatized dihydrodiols. Similarly, during the separation of bi- β -naphthols using a Pirkle-type stationary phase, the alkyl derivatives were less retained but were better resolved [13]. In

this example it seems that the position of the bulkier alkyl groups must have changed the overall conformation of the enantiomers, hence their resolution. Another example is the separation of alcoholic γ - and δ -lactones and their corresponding alkyl derivatives, using cellulose triacetate. Retention was increased and separation was improved when the OH group was blocked by an alkyl group [14].

2. Experimental

2.1. Instrumentation

HPLC analysis was performed using a HP1050 instrument (Hewlett-Packard, Palo Alto, CA, USA) equipped with a diode-array UV detector, an HPCHEM data station and a ThinkJet printer. A Rheodyne (Cotati, CA, USA) injection valve was used, equipped with a 20- μ l loop. The chiral column was a ChiralPak AD column (Daicel Chemical Industries, Tokyo, Japan) (250 mm \times 4.6 mm I.D., 10 μ m film thickness).

2.2. Materials and Methods

HPLC-grade solvents (*n*-hexane and 2-propanol) were purchased from LabScan (Dublin, Ireland) and ethanol from Merck (Darmstadt, Germany). The four pairs of cannabinoids were prepared as described previously [5]. Acetylation of all the (+)- and (–)-enantiomers was performed using acetic anhydride in an excess amount of freshly distilled pyridine as a catalyst. The mixture was stirred at room temperature overnight and the resulting mixture was then washed with ethanol. Evaporation under vacuum left a viscous oil that was checked by TLC. The synthesized cannabinoids obtained were submitted to further purification procedures using a silica HPLC column (Adsorbosphere, Alltech, Deerfield, IL, USA) before the chiral separations (whenever needed) for final chemical purification, using 2-propanol–*n*-hexane (5:95) in most instances.

2.3. Procedure for analysis

A flow-rate of 1 ml/min was used in all the experiments at room temperature. The mobile phase consisted of mixtures of *n*-hexane with ethanol or 2-propanol (5%, v/v). Each run was monitored at two wavelengths simultaneously, 260 and 240 nm. In each instance, approximately 0.1 mg of analyte was dissolved in 1 ml of the solvent and injected both individually and as a mixture.

2.4. Computational method

Construction and treatment of the cannabinoid structures were performed with the Insight II/Discover 2.0.0 software package from BIOSYM Technologies (San Diego, CA, USA). All calculations were made on a Silicon Graphics 4D/310VGX workstation. Molecular mechanics methods are based on a view of the molecular structures as set of balls and springs. The molecular force field is a sum of the potential energy functions in these sets. The following molecular mechanics (MM) potential energy function was used:

$$E_{\text{Tot.}} = E_s + E_q + E_f + E_{\text{VWD}} + E_{\text{elec}} \quad (1)$$

where E_s is the stretching energy, E_q is the bending energy, E_f is the dihedral (torsion) energy, E_{VWD} is the Van der Waals energy and E_{elec} is the electrostatic energy. The force field used in the calculations was CVFF (consistent valence force field). All parameters defining the geometry of the molecules were modified by small increments until the overall structural energy reached a local minimum. First, 1000 iterations were made in the steepest descent's algorithm, then it was swapped to the conjugate gradient minimizer, until a convergence criterion was reached. For CBD, a flexible compound that undergoes free rotation, the dihedral rotor was used to define a torsion angle in the segment of the free rotation and to determine the energy resulting from this rotation. The structure was minimized using 10° increments of the torsion angle over the entire range of 360°.

The fractional X-ray coordinates of CBD from the literature [15] were fed manually into personal CAChe software on a Macintosh IIC computer, and the resulting output file was transferred and rebuilt in the Silicon Graphics workstation to be used for the comparison.

The *RMS* value is a quantitative criterion for the difference between two structures or their portions when superimposed on each other. It is the least-squares fit between the two sets of xyz coordinates (Å units) of the two superimposed structures, and is calculated according to the following equation:

$$RMS = \sqrt{\sum_{i=1}^N \frac{(x - x_0)^2 + (y - y_0)^2 + (z - z_0)^2}{N}} \quad (2)$$

where N is the number of atoms compared.

3. Results and discussion

3.1. Structure–enantioselective retention relationship (SERR)

The structure–activity relationship (SAR) of cannabinoids has been extensively studied in the past, mainly to understand the structural features that are responsible for the therapeutic activity [16]. A similar approach can be adopted in order to investigate structural features of enantiomeric pairs that facilitate chiral discrimination. Chiral discrimination is measured chromatographically from the enantioselective retention or the selectivity and the resolution factors. This approach originates from the term “quantitative structure–enantioselective retention relation” (QSERR) that was pointed out by Kaliszan et al. [17].

A previous study using carbamated amylose as the stationary phase showed that the combination of hydrogen bonding by hydroxyl and ketonic groups in the appropriate positions played a key role in the chiral discrimination of enantiomeric terpenoids [6]. The role of the hydroxyl group in the enantioselective retention

of cannabinoids was therefore studied here. The hydroxyl groups were blocked by acetylation and the enantioselective retention was measured and compared with that of the non-acetylated compounds.

3.2. Chromatographic resolution of the enantiomeric cannabinoids

The structures of the four cannabinoids and their derivatives are presented in Fig. 1. The non-acetylated cannabinoids have already been resolved using amylose 3,5-dimethylphenyl carbamate. The enantioselectivity of the carbamated amylose towards all four non-acetylated cannabinoid enantiomers in this study was excellent, using any percentage of modifier [5]. A selectivity factor $\alpha > 1.2$ was obtained for all four using 2-propanol. The capacity factors k' , selectivity α and the resolution R_s of the non-acetylated cannabinoids were determined previously using the same type of stationary phase [5]. The values of k' and α in the present study were slightly higher than in the previous study, because the stationary phase originated from a different batch. In spite of the inconsistency in performance between two different batches, the reproducibility of k' and α was relatively good when the same column was used throughout the study.

All the chromatographic runs in this study were made using ethanol–or 2-propanol–*n*-hexane (5:95). Fig. 2 shows typical comparisons of the chromatographic resolution of three mixtures of cannabinoid enantiomeric pairs (1a–3a) and the corresponding acetylated compounds (pairs 1b–3b), using 2-propanol as the mobile phase modifier. Fig. 3 shows a mixture of the (+)- and (–)-enantiomers of CBD (pair 4a) vs. the corresponding mixture of the acetylated (+)- and (–)-enantiomers (pair 4), using (I) ethanol and (II) 2-propanol as modifier. As can be seen in Fig. 2, the separation of the acetylated enantiomeric pairs was lost owing to blocking of the hydroxyl groups. The loss of separation was especially dramatic for the two acetylated enantiomers HU-249 and HU-250 (pair 3b). The

enantioselectivity of the phenylcarbamated amylose towards this enantiomer pair was extraordinary [$\alpha = 4.8$ and $R_s = 19.9$ with 2-propanol–*n*-hexane (5:95)]; nevertheless, it disappeared completely when the hydroxyl groups of the two enantiomers were acetylated [Fig. 2(III)].

In contrast to pairs 1b–3b, the acetylated enantiomers of CBD (pair 4b) were still partially separated. Acetylation of the CBD resulted in a large decrease in the capacity factor (93% using ethanol and 80% using 2-propanol) and resolution (70% using ethanol and 50% using 2-propanol). Moreover, when the modifier was 2-propanol, inversion of the elution order was observed, i.e., the (–)-isomer eluted first. A similar inversion of elution order was observed in the separation of acetylated terpenoid enantiomers using the same stationary phase [6].

The loss of chromatographic resolution of the acetylated enantiomers (pairs 1b–3b) indicates that hydrogen bonding dominates the recognition process by the stationary phase. A similar loss of resolution was observed in the case of terpenoid chiral separations when acetylated [6]. The decrease in retention and the loss of separation could be explained also by a steric repulsion of the solutes from the chiral sites due to the bulkier acetoxy derivatives.

The chromatographic behaviour of the two acetylated CBD enantiomers was different from that of the other three enantiomeric pairs, probably owing to the difference in structure. Rings A and C in CBD are perpendicular to each other and can rotate freely. According to ^1H NMR measurements, acetylation of CBD did not restrict the free rotation of the two rings. The flexibility of these enantiomers facilitated a different fit to the stationary phase in spite of the loss of OH functionality. The acetoxy groups on the CBD could probably rearrange themselves so that weak hydrogen bonding between their two CO ester groups (hydrogen acceptors) and the NH of the carbamated residue (hydrogen donor) was still effective.

The loss of separation of pairs 1b–3b and the intriguing behaviour of pair 4b raised the question of whether the acetylation caused conformational changes in the enantiomeric pairs and

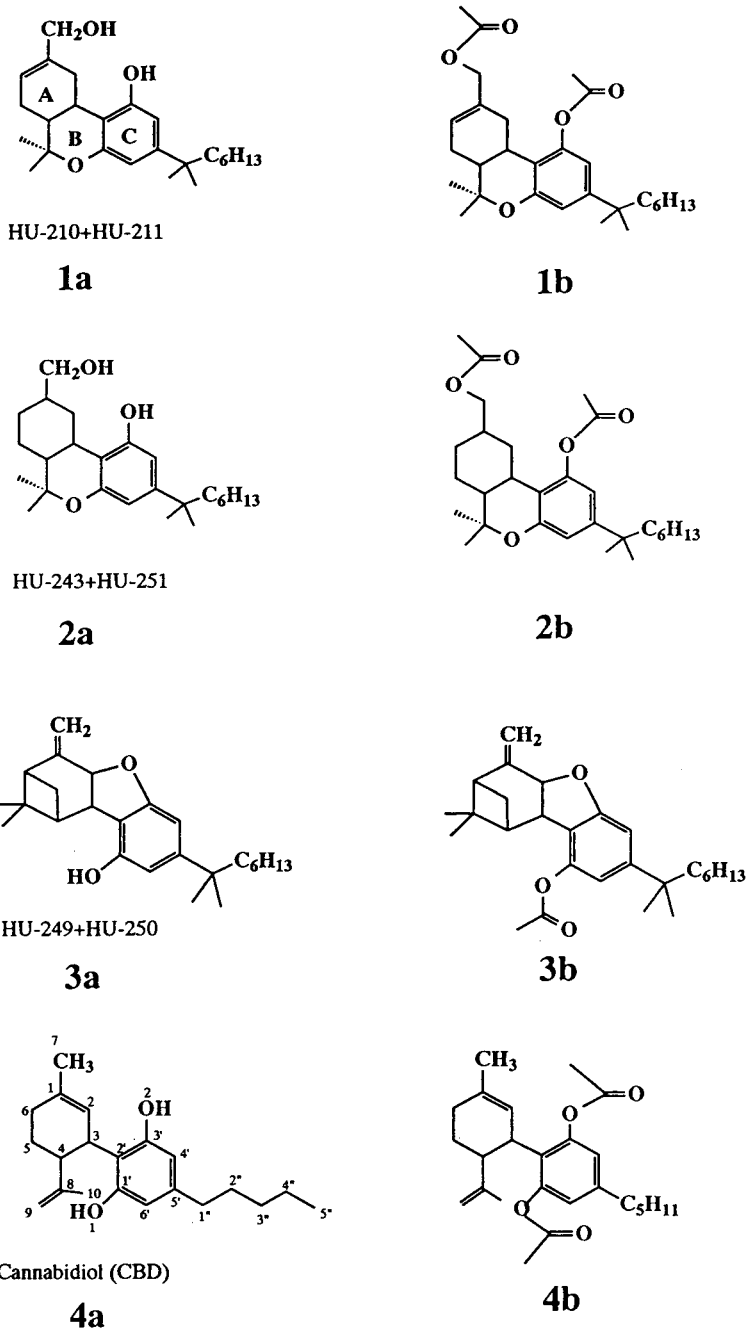


Fig. 1. Structures of the enantiomeric cannabinoids used in this study and their acetoxy derivatives.

these changes affected the discrimination. Conformational analysis of the four cannabinoids and their acetylated analogues was therefore per-

formed, and the energy-minimized structures of the original and the acetylated compounds were superimposed of each other.

I

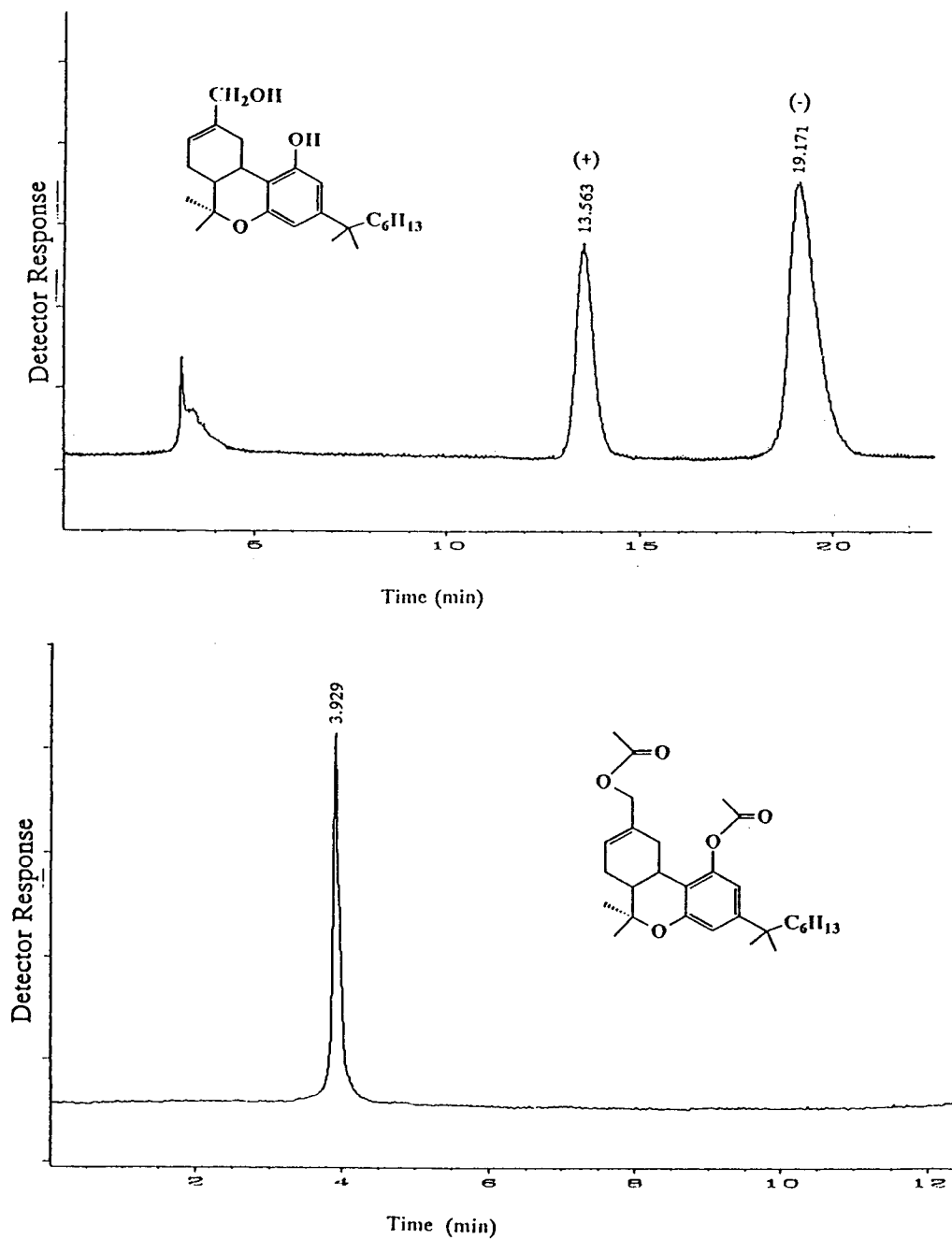


Fig. 2.

II

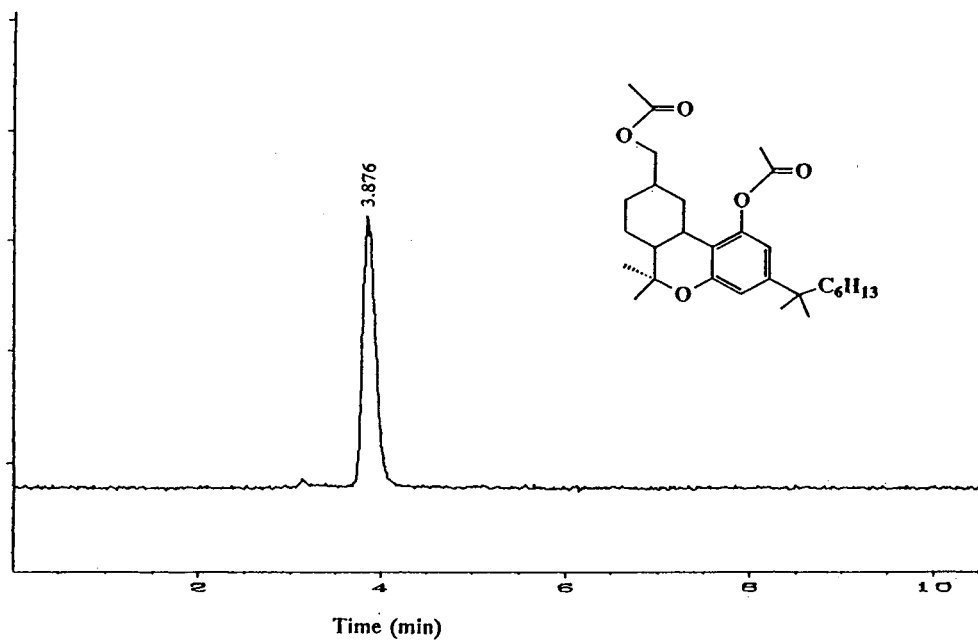
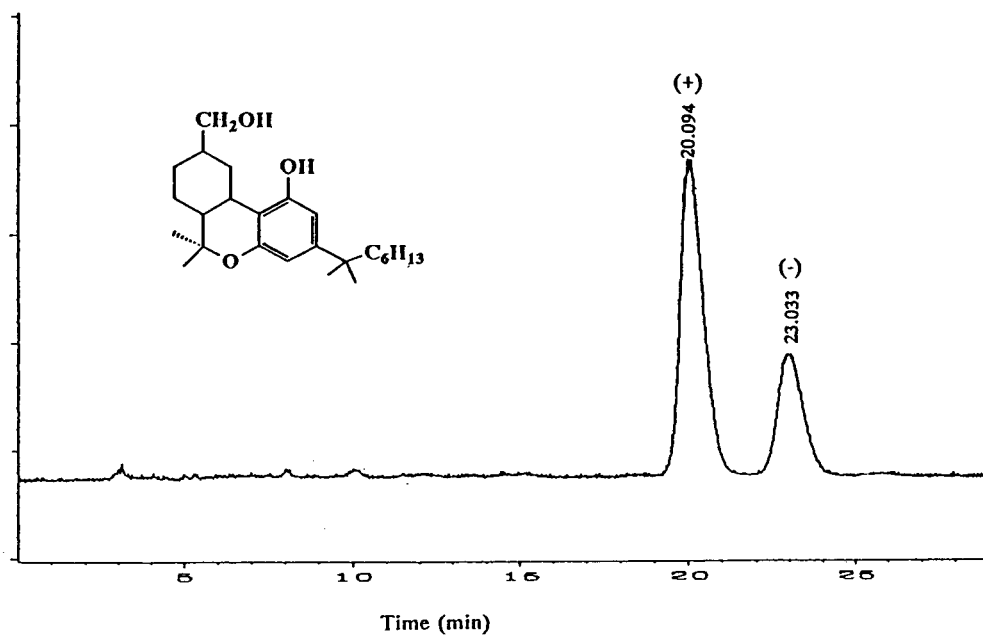


Fig. 2 (Continued on p. 54)

III

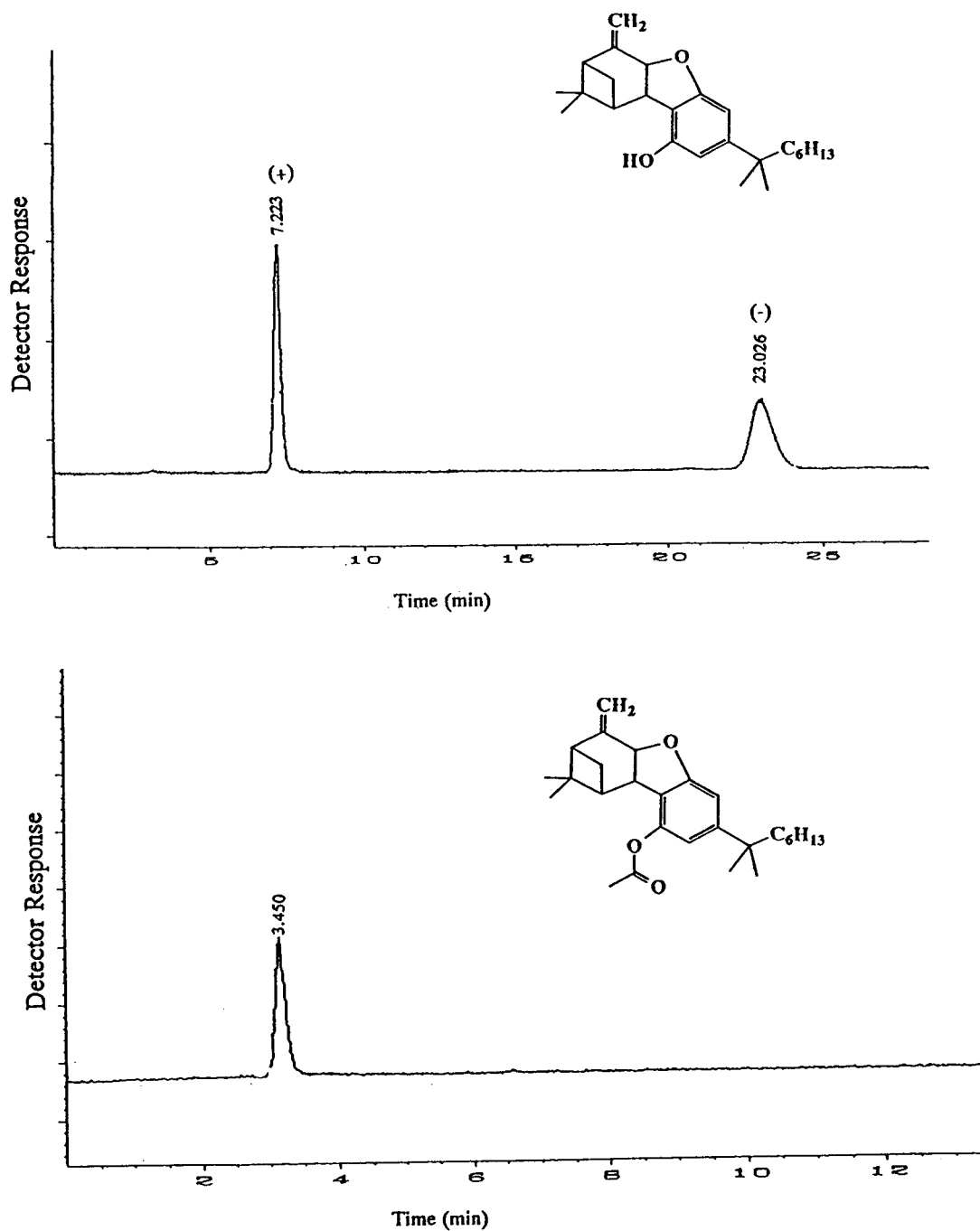


Fig. 2. Chromatograms showing the separation of mixtures of the enantiomeric pairs (I) 1a and 1b, (II) 2a and 2b and (III) 3a and 3b. Mobile phase, *n*-hexane-2-propanol (95:5, v/v); detection wavelength, 240 nm.

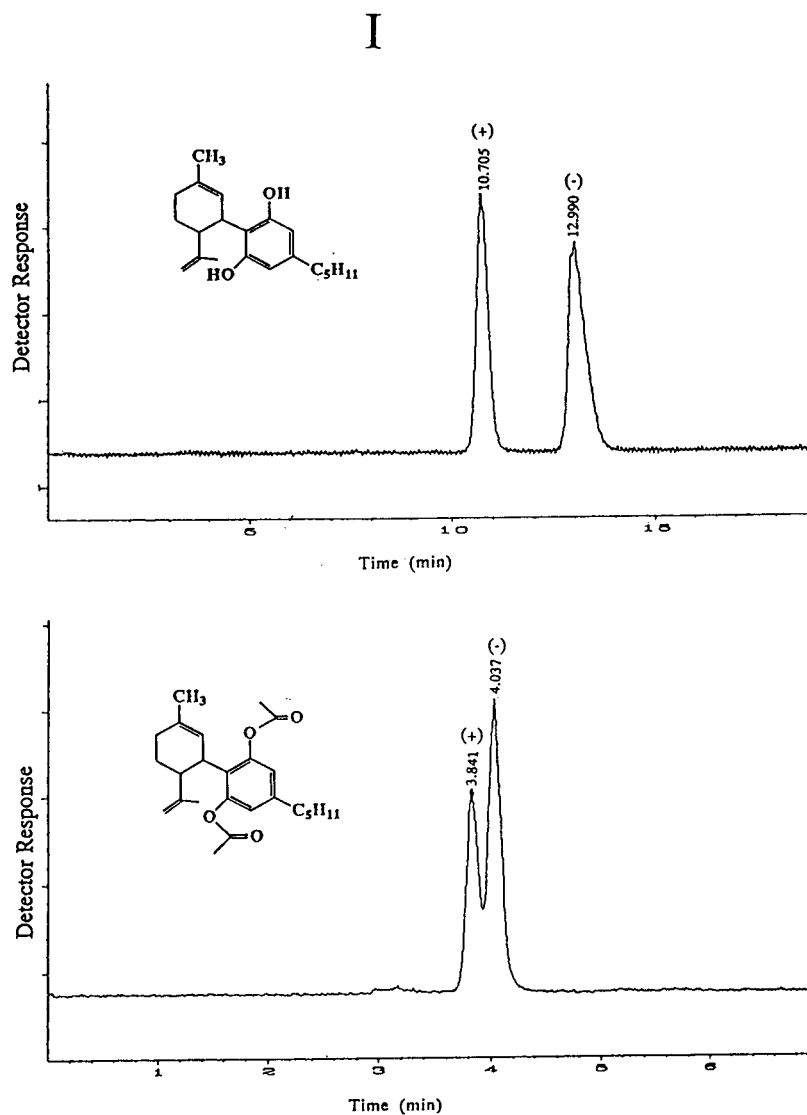


Fig. 3 (Continued on p. 56)

3.3. Conformational analysis

The tricyclic and tetracyclic fused rings of the three cannabinoids (see Fig. 1) provide considerable rigidity to these enantiomers, hence it was not surprising that according to molecular mechanics calculations, acetylation of the cannabinoids did not affect their conformational significantly. Superposition of each enantiomer

with its corresponding acetylated form gave rise to relatively small *RMS* values ($RMS \leq 0.126 \text{ \AA}$), as shown in Table 1. In the case of cannabidiol, in spite of its flexibility, the overall conformation of its acetylated derivative was approximately the same as that of the cannabidiol itself, as shown in Fig. 4, where the two structures are superimposed.

The similarity of the conformations of the

II

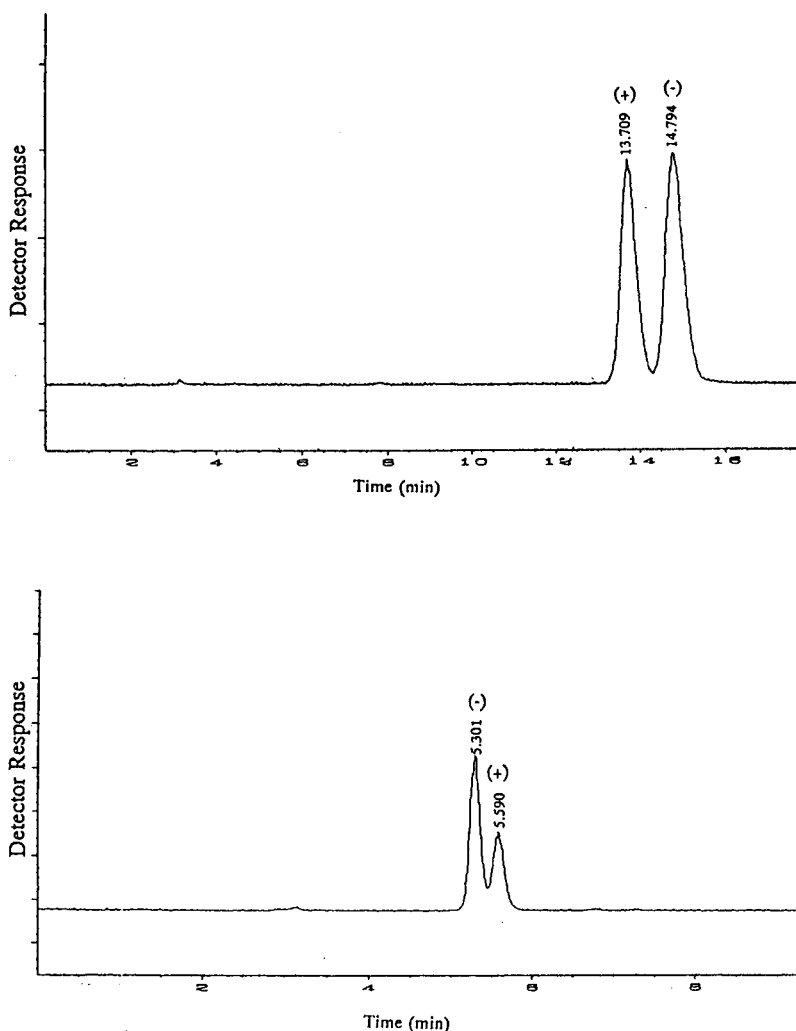


Fig. 3. Chromatograms showing the separation of a mixture of the enantiomeric pairs 4a and 4b. Mobile phase: (I) *n*-hexane–ethanol (95:5, v/v); (II) *n*-hexane–2-propanol (95:5, v/v). Detection wavelength, 240 nm.

acetylated and non-acetylated analogues supports earlier observations that the nature and position of the substituents is a determining factor in the chiral discrimination of cannabinoids rather than overall conformation [6].

3.4. Comparison with X-ray crystallography

The computational approach described above was validated by comparison with an X-ray crystallographic structure of cannabidiol from

the literature [15]. As shown in Fig. 1, cannabidiol has no ring B and rings A and C are almost perpendicular to each other, with two phenolic groups on ring C. The coordinates of the X-ray structure of cannabidiol were introduced into the DISCOVER software manually and the structure was reconstructed. Superposition of the reconstructed X-ray structure and the energy minimized structure revealed a small *RMS* value of 0.095 between them.

In CBD, the two torsion angles ψ (C5–C4–

Table 1

Values of root mean square (RMS) of the differences in xyz coordinates of the ten heavy atoms common to all the (+)-cannabinoid structures compared with the corresponding (+)-acetate isomers

Pair No.	Solute	RMS (Å)
1	HU-211	0.126
2	HU-251	0.056
3	HU-250	0.036
4	(+)-CBD	0.086

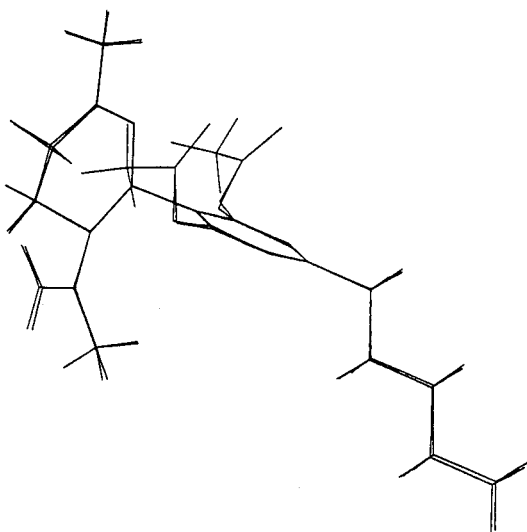


Fig. 4. Superposition of the common ten heavy atoms of the two structures of CBD and acetylated CBD.

C8–C10) and ϕ (C2–C3–C2'–C3') (Fig. 5) were calculated to be 120.7° and -59.9° , respectively, at the global minima. X-ray crystallography gave these torsion angles as 127° and -59.4° , respectively.

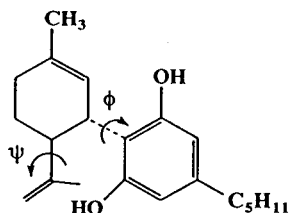


Fig. 5. Torsion angles ϕ and ψ of cannabidiol (CBD).

4. Conclusions

This systematic comparative study of four cannabinoids has highlighted the functionality of OH groups in chiral discrimination by phenylcarbamated amylose. When the OH groups of the cannabinoids were blocked, separation was completely lost for the three rigid enantiomeric pairs, and just partially lost for the flexible cannabidiol enantiomers. Molecular modelling, which was validated by comparison with an X-ray structure, indicated that the loss of separation was not caused by a change in conformation.

Acknowledgements

This work was financed by the Israel Ministry of Health. We thank Professor Raphael Mechoulam and Dr. Aviva Breuer of the Department of Natural Products, School of Pharmacy, for their guidance and assistance in preparing the acetylated cannabinoid enantiomers, and Galia Tawil for technical help.

References

- [1] S. Levin and S. Abu-Lafi, *Adv. Chromatogr.*, 33 (1993) 233.
- [2] Y. Hui and W. Zou, in H.J. Schneider and H. Durr (Editors), *Frontiers in Supramolecular Organic Chemistry and Photochemistry*, VCH, Weinheim, 1991, p. 203.
- [3] Y. Okamoto and Y. Kaida, *J. High Resolut. Chromatogr.*, 13 (1990) 708.
- [4] I.W. Wainer, R.M. Stiffin and T. Shibata, *J. Chromatogr.*, 411 (1987) 139.
- [5] S. Levin, S. Abu-Lafi, J. Zahalka and R. Mechoulam, *J. Chromatogr. A*, 654 (1993) 53.
- [6] S. Abu-Lafi, M. Sterin, S. Levin and R. Mechoulam, *J. Chromatogr. A*, 664 (1994) 159–167.
- [7] P.H. Reggio, G.B. McGaughey, D.F. Odear, H.H. Seltzman, D.R. Compton and B.R. Martin, *Pharmacol. Biochem. Behav.*, 40 (1991) 479.
- [8] J.J. Feigenbaum, F. Bergmann, S.A. Richmond, R. Mechoulam, N. Nadler, Y. Kloog and M. Sokolovsky, *Proc. Natl. Acad. Sci. U.S.A.*, 86 (1989) 9584.
- [9] J.M. Cunha, A.E. Carlini, A.E. Pereira, O.L. Ramos, C. Pimentel, R. Gagliardi, E.L. Sanvito, N. Lander and R. Mechoulam, *Pharmacologia*, 21 (1980) 175.

- [10] A.W. Zuardi, I. Shirakawa, E. Finkelfarb and I.G. Karniol, *Psychopharmacologia*, 76 (1982) 245.
- [11] S.R. Snider and P. Consroe, *Neurology*, 34, Suppl. (1984) 147.
- [12] S.K. Yang, M. Mushtaq, Z. Bao, H.B. Weems, M. Shou and X.L. Lu, *J. Chromatogr.*, 461 (1989) 377.
- [13] W.H. Pirkle and J.L. Schreiner, *J. Org. Chem.*, 46 (1981) 4988.
- [14] E. Francotte and D. Lohmann, *Helv. Chim. Acta*, 70 (1987) 1569.
- [15] P.G. Jones, L. Falvello, O. Kennard and G.M. Sheldrick, *Acta Crystallogr.*, Sect. B, 33 (1977) 3211.
- [16] R.K. Razdan, *Pharmacol. Rev.*, 38 (1986) 75.
- [17] R. Kaliszan, T.A.G. Noctor and I.W. Wainer, *Chromatographia*, 33 (1992) 546.



ELSEVIER

Journal of Chromatography A, 679 (1994) 59–66

JOURNAL OF
CHROMATOGRAPHY A

Preliminary computer simulation for fine tuning of the high-performance liquid chromatography of some phenolic acids

Tadeusz H. Dzido^{a,*}, Helena D. Smolarz^b

^a*Department of Inorganic and Analytical Chemistry, Medical Academy, Staszica 6, 20-081 Lublin, Poland*

^b*Department of Pharmaceutical Botany, Medical Academy, Staszica 4, 20-081 Lublin, Poland*

First received 16 March 1994; revised manuscript received 19 May 1994

Abstract

Computer simulation (Drylab G) was used to optimize the reversed-phase high performance liquid chromatography of eleven phenolic acids. On the basis of the data for two preliminarily optimized solvent systems (I = acetonitrile–water–1% acetic acid, II = acetonitrile–tetrahydrofuran–1% acetic acid) obtained by computer simulation the subsequent simple step-by-step procedure allowed conditions for the separation of all solutes to be found.

1. Introduction

Generally it is easy to separate simple mixtures consisting of several solutes and to ensure that the capacity factors are in the optimum range of 1–10. However, for more complex mixtures the optimization of the chromatographic system can be complicated and the trial-and-error procedures are time consuming and lead to a greater consumption of solvents and materials. Computer-assisted methods, which have been extensively developed in recent years, can be applied to solve the problems more readily [1]. However, before starting with any optimization procedure, it is worthwhile studying the literature on the subject. It is also well known from the chromatographic literature [2] that adsorbents differ from batch to batch, which can result

in selectivity changes, and it is often necessary to reoptimize the chromatographic system.

Examples of the chromatographic separations of phenolic acids are well documented [3–5]. The phenolic acids are relatively hydrophilic compounds and conventionally are separated by ion-pair or ion-suppression reversed-phase liquid chromatography. In this work, the latter mode was applied to obtain preliminary data for computer optimization. We used a typical procedure for optimization of the phenolic acid mixture by means of Drylab G software [6,7], which is based on the retention data of two preliminary runs and system variables. In our case the results for the two eluent systems investigated were only partially satisfactory. We could try other eluent systems or a longer, more efficient column, but the two experimental chromatograms obtained led us to the conclusion that the final chromatographic optimization could be easily performed by an additional simple step-by-step procedure.

* Corresponding author.

The method, which consists in the combination of two eluent systems, is presented below.

2. Experimental

An HP-1050 gradient liquid chromatograph (Hewlett-Packard, Palo Alto, CA, USA) equipped with a 20- μ l sample injector (Rheodyne, Cotati, CA, USA) and a variable-wavelength UV detector (HP-1050) operated at 254 nm was used. The chromatograms were recorded with a Hewlett-Packard Model 3396 A reporting integrator. Stainless-steel columns (250 \times 4.6 mm I.D. and 100 \times 4.6 mm I.D.) were packed with 7- μ m LiChrosorb RP-18 (Merck, Darmstadt, Germany) using laboratory-made apparatus with an Orlita pump. The first column had an efficiency of 6400 and the second 3600 theoretical plates, as determined using toluene as the test solute eluted with methanol–water

Table 1
System variables, compounds and retention times

System variables			
Dwell volume (ml)		0.90	
Column length (cm)		25.0	
Column diameter (cm)		0.46	
Flow-rate (ml/min)		1.00	
Starting B (ACN) concentration (%)		0.0	
Final B (ACN) concentration (%)		50.0	
Gradient time, 1st run (min)		30.0	
Gradient time, 2nd run (min)		90.0	
Retention times			
Band No.	Compound	t_R (min)	
		Run 1	Run 2
1	Gallic acid	6.66	8.18
2	Protocatechuic acid	9.52	13.52
3	Chlorogenic acid	11.94	22.07
4	Vanillic acid	13.42	23.25
5	<i>trans</i> -Caffeic acid	13.64	24.43
6	Syringic acid	13.76	25.17
7	<i>cis</i> -Caffeic acid	14.42	26.13
8	<i>trans-p</i> -Coumaric acid	16.56	31.48
9	<i>cis-p</i> -Coumaric acid	17.17	32.97
10	<i>trans</i> -Ferulic acid	17.42	34.39
11	<i>cis</i> -Ferulic acid	18.05	36.60

(60:40) at a flow-rate of 1 ml/min. The dwell volume of the equipment was determined by running a blank gradient without the column.

In two gradient runs, acetonitrile (ACN), tetrahydrofuran (THF) and water (doubly distilled) were used as components of the eluent; all solvents contained 1% (v/v) of acetic acid to suppress the ionization of phenolic acids. The sample was a mixture of eleven components (see Table 1) dissolved in methanol–water (1:1).

3. Results and discussion

In accordance with the Drylab G instruction manual, preliminary data are needed for the optimization of resolution in reversed-phase liquid chromatography. The data consist of system variables and retention times of solutes for two typical linear gradient runs from 5% to 100% of modifier in water. For acetonitrile as modifier, too low retention times for some of the solutes were obtained for the 25-cm column. Especially gallic and protocatechuic acids show retentions near the dead time. This means that these bands are eluted under isocratic conditions and it is difficult to obtain precise data on retention times. Taking into account the aspects discussed above, we decided to perform two preliminary linear gradient runs starting from 0% ACN plus a constant acetic acid concentration (1%) for gradient times of 30 and 90 min. From a practical point of view it was of interest to test whether Drylab G can be applied to the prediction of retention and resolution in the system investigated (basing on retention data for a 0–50% gradient range).

In Fig. 1 the resolution map is presented for the system using a 25-cm column with a real plate number $N = 6400$. It can be seen that good resolution can be obtained for a very long gradient time (90 min). The most efficient resolution was obtained by simulation of chromatogram using another gradient range. The final gradient range was found to be from 0 to 23.1% ACN during 46.2 min. The simulated chromatogram for this gradient is shown in Fig. 2 and the real chromatogram in Fig. 3. Good agreement of

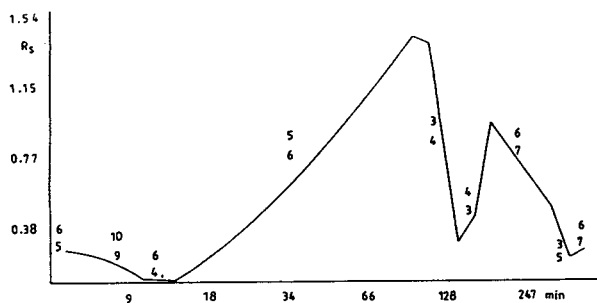


Fig. 1. Relative resolution map for phenolic acids. 0–50% acetonitrile–water gradient; compounds as in Table 1.

the simulated and real retention data is observed; compare also the data in Table 2.

Only the last band, *cis*-ferulic acid, shows a large deviation, 2.4%, from simulated value. Otherwise the resolution, especially of peaks 3–7, shows larger discrepancies which are probably due to the tailing of the peaks and/or the column being poorly packed. Instead of 6400 theoretical plates the efficiency of the column should be about 10 000.

In the subsequent experiments a new 10-cm column was packed with better efficiency per unit length, $N = 3600$, and the composition of the eluent was varied. THF as the second modifier with a low constant concentration, 2%, was introduced into the mobile phase. As reported earlier [8–10], a low concentration of another modifier with stronger hydrophobic properties than the first can lead to retention and selectivity changes, especially when the solutes interact specifically with the modifier. Modifiers such as

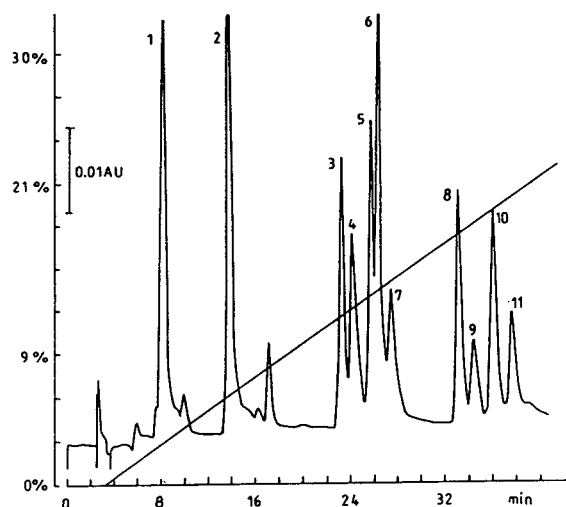


Fig. 3. Real chromatogram of phenolic acids. Conditions as in Fig. 2.

THF can be strongly extracted to the C_{18} stationary phase and then its interaction with proton-donor solutes (phenolic acids) in the stationary phase can introduce a marked influence on retention.

The optimization of the system with ACN–THF was performed as described above based on two linear gradient runs from 0% to 50% of ACN with constant THF (2%) and acetic acid (1%) concentrations. Table 3 reports the values of the system variables and retention times of the solutes for two runs of 20 and 60 min. The sequence of the solutes is different in comparison with the data in Table 1. Additionally, in Table 3 there is some sequence variation

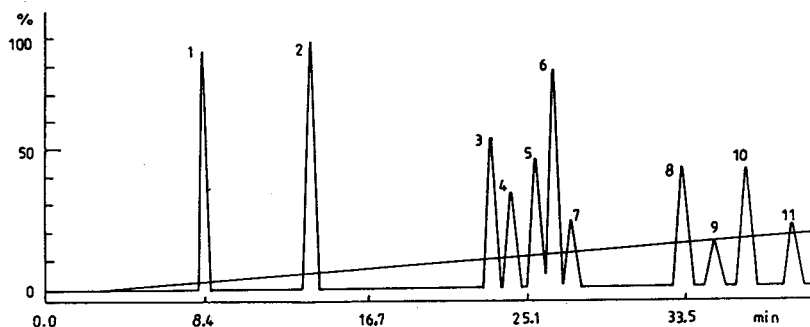


Fig. 2. Simulated chromatogram of phenolic acids by gradient elution with 0–23.1% acetonitrile–water during 46.2 min. Column length, 25 cm; compounds as in Table 1.

Table 2

Retention times for a linear gradient from 0.0 to 23.1% ACN in 46.2 min for simulated and experimental chromatograms using a 25-cm C₁₈ column

Band No.	Compound	t_R (min)	
		Simulated	Experimental
1	Gallic acid	8.30	8.23
2	Protocatechuic acid	13.90	13.95
3	Chlorogenic acid	23.39	23.65
4	Vanillic acid	24.41	24.53
5	<i>trans</i> -Caffeic acid	25.75	26.05
6	Syringic acid	26.60	26.68
7	<i>cis</i> -Caffeic acid	27.57	27.91
8	<i>trans-p</i> -Coumaric acid	33.39	33.56
9	<i>cis-p</i> -Coumaric acid	35.01	34.93
10	<i>trans</i> -Ferulic acid	36.64	36.57
11	<i>cis</i> -Ferulic acid	39.12	38.17

Table 3

System variables, compounds and retention times

System variables	
Dwell volume (ml)	0.90
Column length (cm)	10.0
Column diameter (cm)	0.46
Flow-rate (ml/min)	1.0
Starting B (ACN) concentration (%)	0.00 + 2% THF
Final B (ACN) concentration (%)	50.00 + 2% THF
Gradient time, 1st run (min)	20.0
Gradient time, 2nd run (min)	60.0

Retention times

Band No.	Compound	t_R (min)	
		Run 1	Run 2
1	Gallic acid	3.27	3.41
2	Protocatechuic acid	5.11	6.59
3	Chlorogenic acid	6.58	10.32
6	Syringic acid	7.15	10.41
4	Vanillic acid	7.41	10.24
5	<i>trans</i> -Caffeic acid	7.88	12.76
7	<i>cis</i> -Caffeic acid	8.14	13.12
8	<i>trans-p</i> -Coumaric acid	9.63	17.18
9	<i>cis-p</i> -Coumaric acid	9.87	17.18
10	<i>trans</i> -Ferulic acid	9.88	17.73
11	<i>cis</i> -Ferulic acid	10.23	18.58

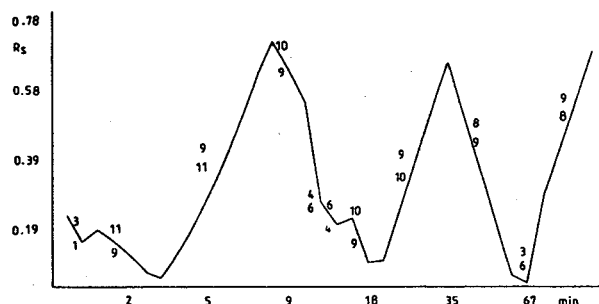


Fig. 4. Relative resolution map for phenolic acids. 0–50% acetonitrile–water gradient with constant concentration of THF (2%); compounds as in Table 1.

between the two runs, it is contrast to the data in Table 1 where the sequence of the solutes is the same in the two runs. Fig. 4 shows the relative resolution map for the system. The image is different to that in Fig. 1. No satisfactory resolution of the complete set of the solutes can be obtained in the gradient time range shown in Fig. 4.

It is interesting that generally in both Figs. 1 and 4 different pairs of bands show minimal resolution. This suggests that mixing of the two modifiers (ACN and THF) is another possibility for improving the separation. However, in our computer optimization procedure we obtained a new gradient range from 7 to 30% ACN (with constant THF and acetic acid concentrations) during 31 min.

Figs. 5 and 6 show the simulated and experimental chromatograms, respectively, of the mixture investigated. The retention times of the phenolic acids are about 0.7 min (mean value) lower in the real than in the simulated chromatogram (Table 4) but the resolutions are similar. In both Figs. 5 and 6 peaks 8–10 are only partially separated, in contrast to the chromatograms in Figs. 2 and 3, where the peaks are well separated. The opposite situation occurs for the peaks with lower retention. Bands 3–7 are poorly separated in Fig. 2 but show, in principle, acceptable resolution in Fig. 6. This means that bands 3–7 are well resolved with an eluent containing THF but bands 8–11 are better separated without THF in the mobile phase (compare also Fig. 7, where the chromatogram for the

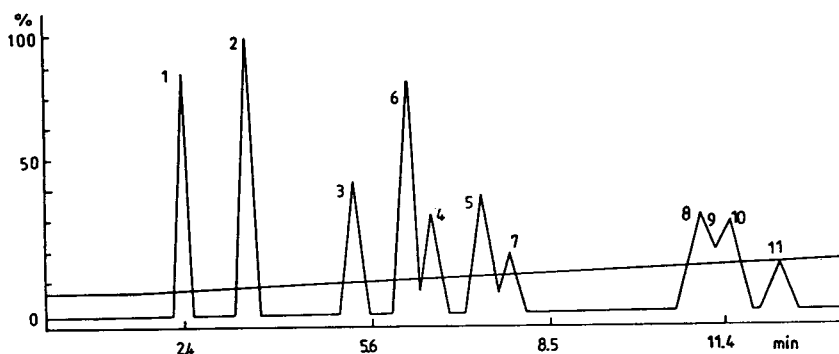


Fig. 5. Simulated chromatogram of phenolic acids by gradient elution with 7–30% ACN during 31 min with a constant concentration of THF (2%). Column length, 10 cm; compounds as in Table 1.

10-cm column, $N = 3600$, and an ACN gradient range of 7–30% is simulated based on the system variables in Table 1, without THF in the eluent).

The above observation can also be supplemented by the variation of the retention sequence within the band 3–7 set. Bands 3 (*cis*-chlorogenic acid) and 7 (*cis*-caffeic acid) are the first and the last band, respectively, in the set in both chromatograms. However, syringic acid shows a stronger retention than vanillic acid and *trans*-caffeic acid in the ACN system. In the

ACH–THF (2%) system the retention of syringic acid is weaker than that of vanillic acid and *trans*-caffeic acid. Also, *trans*-caffeic acid shows an increase in retention relative to *cis*-caffeic acid in the ACN–THF system in comparison with the ACN system. The retention variations suggest that the separation of bands 3–7 can possibly be achieved by fine tuning of the THF and ACN gradient simultaneously, e.g., by applying a procedure analogous to that described previously [11,12].

Instead of looking for another system with a different selectivity characteristic or changing the

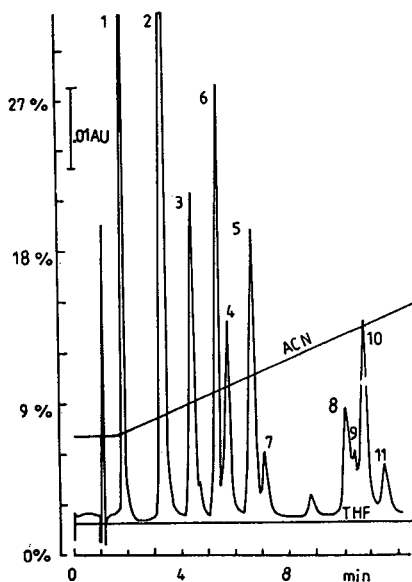


Fig. 6. Real chromatogram of phenolic acids. Conditions as in Fig. 5.

Table 4

Retention times for a linear gradient from 7.0 to 30.0% ACN and a constant THF concentration (2%) in 31 min for simulated and experimental chromatograms using a 10-cm C_{18} column

Band No.	Compound	t_R (min)	
		Simulated	Experimental
1	Gallic acid	2.43	1.81
2	Protocatechuic acid	3.37	3.32
3	Chlorogenic acid	5.09	4.42
6	Syringic acid	6.07	5.35
4	Vanillic acid	6.51	5.71
5	<i>trans</i> -Caffeic acid	7.32	6.61
7	<i>cis</i> -Caffeic acid	7.76	7.06
8	<i>trans-p</i> -Coumaric acid	10.95	10.07
9	<i>cis-p</i> -Coumaric acid	11.22	10.36
10	<i>trans</i> -Ferulic acid	11.48	10.76
11	<i>cis</i> -Ferulic acid	12.27	11.53

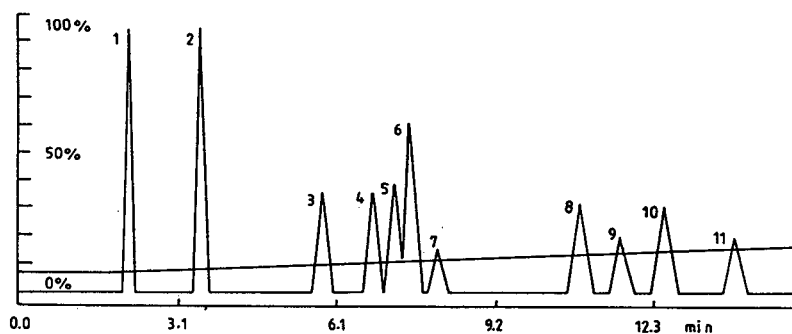


Fig. 7. Simulated chromatogram of phenolic acids by gradient elution with 7–30% ACN and a 10-cm column based on the data in Table 1.

operational parameters, e.g., column length, we decided to perform the next optimization procedure step by step based on the data for the chromatograms presented in Figs. 3, 6 and 7. We started using the same gradient of ACN as in Fig. 6 and the THF concentration was kept at the same level, 2%, during 0–6 min then decreased linearly to 0% from 6 to 12 min. The real chromatogram is shown in Fig. 8 and is very

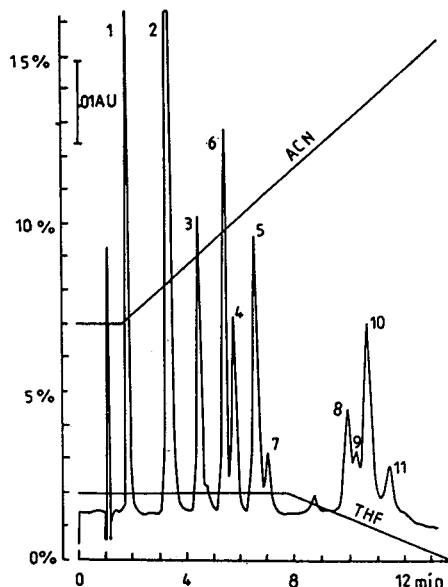


Fig. 8. Separation of phenolic acids by gradient elution with 7–30% ACN during 31 min, 2% THF during 0–6 min and 2–0% THF during 6–12 min. Compounds as in Table 1.

similar to that in Fig. 6. This means that the decrease in THF concentration in the last stage of the chromatographic process does not influence the retention of bands 8–11. The decrease should be greater to reflect the retention change of bands 8–11. The retention of these solutes is probably strongly influenced by extraction of THF into the stationary phase. Hence the expulsion of THF from the stationary phase in the later stages of the chromatographic process can be achieved by a higher ACN concentration.

We then decided to increase the gradient slope of ACN and to decrease the starting time of the THF gradient from the start of the chromatogram. The next chromatogram was obtained using a gradient of THF concentration from 2 to 0% during the initial 6 min. The gradient of ACN concentration was divided into two segments: (1) during the first 6 min the slope of the gradient was the same as in Figs. 6 and 8 (i.e., 7–11.6% ACN), and (2) during the next 6 min, i.e., from 6 to 12 min, the gradient was from 11.6 to 30% ACN (Fig. 9). The second segment with a higher slope of the ACN gradient was introduced mainly, as suggested above, to elute THF rapidly from the stationary phase.

The chromatogram shown in Fig. 9 demonstrates a good resolution of peaks 8–11, which now have decreased retention relative to the chromatogram in Fig. 8. However, peaks 6 and 4 overlap. The overlap of these peaks is probably caused by a too low concentration of THF in the

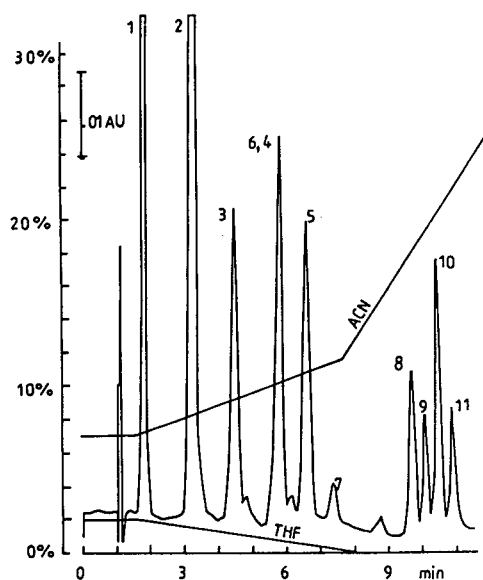


Fig. 9. Separation of phenolic acids by gradient elution with 7-11.6% ACN and 2-0% THF during 0-6 min and 11.6-30% ACN during 6-12 min. Compounds as in Table 1.

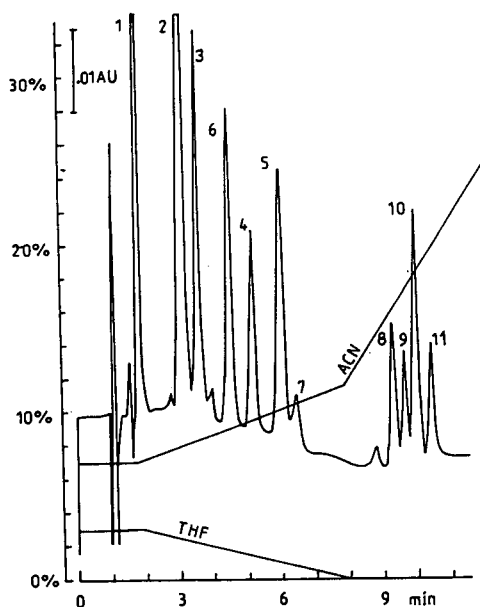


Fig. 10. Separation of phenolic acids by gradient elution with 7-11.6% ACN and 3-0% THF during 0-6 min and 11.6-30% ACN during 6-12 min. Compounds as in Table 1.

initial stage of elution relative to the conditions in Fig. 8. With a greater THF concentration, syringic acid shows a weaker retention than vanillic acid and the band of *trans*-caffeic acid is closer to that of *cis*-caffeic acid (Fig. 6). Therefore, for the next chromatogram a higher starting THF concentration (3%) was applied, which caused a poorer resolution of peaks 5 and 7 (Fig. 10). In the last stage of the fine tuning of the system, an intermediate starting concentration of THF was chosen, i.e., 2.5%. Fig. 11 shows the chromatogram with satisfactory resolution of all the bands under the final gradient conditions as follows: 0-6 min, gradient from 7% to 11.6% ACN and from 2.5 to 0% THF; 6-12 min, gradient from 11.6 to 30% ACN. In the whole gradient range the acetic acid concentration was constant at 1%.

The procedure described above for optimization of the chromatographic system is not typical in chromatographic practice but shows that it is a worthwhile effort to compare various chromatograms obtained after computer optimization. This can sometimes help to devise a more

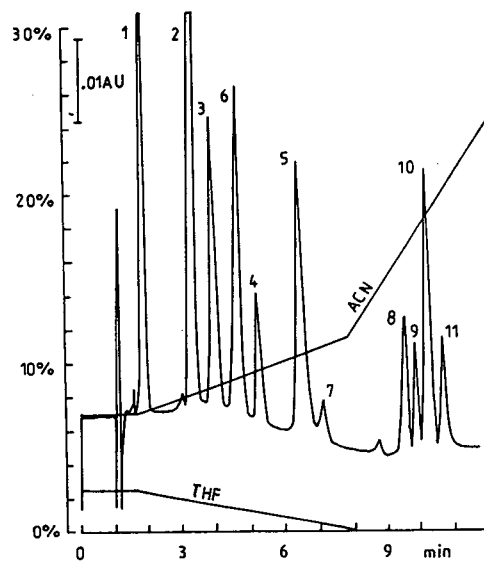


Fig. 11. Separation of phenolic acids by gradient elution with 7-11.6% ACN and 2.5-0% THF during 0-6 min and 11.6-30% ACN during 6-12 min. Compounds as in Table 1.

complicated chromatographic system permitting improved resolution of the solutes.

Acknowledgement

The donation of the Hewlett-Packard Model 1050 liquid chromatograph by the Alexander von Humboldt Foundation (Bonn, Germany) to T.H.D. is gratefully acknowledged.

References

- [1] A. Drouen, J.W. Dolan, L.R. Snyder, A. Poile and P.J. Schoenmakers, *LC·GC Int.*, 5 (1992) 28.
- [2] H. Engelhardt, B. Dreyer and H. Schmidt, *Chromatographia*, 16 (1982) 11.
- [3] L.W. Wulf and C.W. Nagel, *J. Chromatogr.*, 116 (1976) 271.
- [4] K. Van de Castele, H. Geiger and Ch.F. van Sumere, *J. Chromatogr.*, 258 (1983) 111.
- [5] A. Hasan, P. Waterman and N. Iftikhar, *J. Chromatogr.*, 446 (1989) 399.
- [6] J.W. Dolan, D.C. Lommen and L.R. Snyder, *J. Chromatogr.*, 485 (1989) 91.
- [7] L.R. Snyder and J.W. Dolan, *Drylab G Instruction Manual*, LC Resources, Lafayette, CA, 1987.
- [8] R.M. McCormick and B.L. Karger, *J. Chromatogr.*, 199 (1980) 259.
- [9] R.M. McCormick and B.L. Karger, *Anal. Chem.*, 52 (1980) 2249.
- [10] T.H. Dzido and H. Engelhardt, *Chromatographia*, in press.
- [11] P. Jandera, J. Churaček and H. Colin, *J. Chromatogr.*, 214 (1981) 35.
- [12] P. Jandera, *J. Chromatogr.*, 485 (1989) 113.

Purification of recombinant human granulocyte–macrophage colony-stimulating factor from the inclusion bodies produced by transformed *Escherichia coli* cells

M. Belew^{a,*}, Y. Zhou^b, S. Wang^c, L.-E. Nyström^a, J.-C. Janson^a

^aPharmacia Bioprocess Technology, S-751 82 Uppsala, Sweden

^bNational Laboratory of Molecular Biology and Genetic Engineering, Institute of Virology,
Chinese Academy of Preventive Medicine, 100 Yingxin Street, Beijing 100052, China

^cAntibiotic Institute, North China Pharmaceutical Corporation, 4 Heping Road, Shijiazhuang, Hebei, China

First received 8 March 1994; revised manuscript received 31 May 1994

Abstract

Recombinant human granulocyte–macrophage colony-stimulating factor (rhGM-CSF), produced as inclusion bodies in genetically transformed *Escherichia coli* cells was purified to homogeneity by a three-step chromatographic procedure involving hydrophobic interaction, ion exchange and gel filtration. Each purification step is reproducible and well suited for process-scale operations. The purification process also leads to a significant decrease in DNA and endotoxin levels in the final product. Of the three gel media used, Phenyl Sepharose 6 FF (high sub) was most effective in reducing the DNA content (by a factor of ca. 2000) while Superdex 75 prep grade was more effective for removing endotoxins (reduction factor ca. 15). The recovery of purified rhGM-CSF was 35% by enzyme-linked immunosorbent assay and 70% by a biological assay method. The overall purification factor obtained was about 4.6, which is in the range of those reported for recombinant proteins produced in *E. coli* as inclusion bodies. The purified rhGM-CSF is an acidic protein ($pI = 5.4$) and has a specific activity of ca. $3.3 \cdot 10^7$ units/mg, which is in excellent agreement with that reported for its natural counterpart. Its monomer molecular mass of 14 605, as determined by electrospray mass spectrometry, corresponds exactly to the mass calculated from its cDNA sequence. Its amino acid composition and partial NH_2 -terminal sequence (up to seventeen residues) are also identical with those reported for this protein. These and other results confirm the identity of the purified rhGM-CSF with its natural counterpart. However, the results also showed that it is apparently heterogeneous from its NH_2 -terminal side as it is composed of three polypeptides having Met, Ala and Pro as the NH_2 -terminal residues in which the intact Met analogue accounts for 60% for the mixture. This heterogeneity does not seem to have any biological significance since the specific activity of the purified rhGM-CSF is identical with that of its natural counterpart.

1. Introduction

The colony-stimulating factors (CSFs) are a

group of four glycoproteins which regulate the proliferation and differentiation of granulocytes, monocyte–macrophages and certain related haemopoietic cells [1]. Their classification is based on the stimulatory effects which they exert

* Corresponding author.

on various bone marrow progenitor cell lineages [2–6]. The granulocyte–macrophage CSF (GM-CSF) specifically stimulates the proliferation of cells of both the macrophage and granulocyte lineages [5,6]. The biological effects attributed to GM-CSF include (i) stimulation of the initial divisions of the erythroid and megakaryocyte progenitor cells [7], but mature cells in these lineages are produced only in the presence of either erythropoietin or a megakaryocyte stimulating factor [8]; (ii) prolonging the life span of mature granulocytes, macrophages and eosinophils [9–11]; (iii) inducing the accumulation of neutrophils at sites of infection or blood vessel damage [12]; (iv) inducing the secretion of interleukin-1 by GM-CSF-treated neutrophils, thereby involving other cells capable of fighting infections [13]; (v) stimulation of antibody-dependent T-cell-mediated cytotoxicity by neutrophils and macrophages [14,15]; and (vi) inducing macrophages to secrete a number of biological response modifiers including tumour necrosis factor [13].

Its important medical applications are (i) to restore haematopoietic dysfunction by raising cell counts from suppressed to normal levels; (ii) to stimulate the hyper-production of functionally primed effector cells [16]; and (iii) to augment host defence against infection and, possibly, malignant disease. It can thus help cancer patients to resist secondary infections developing either because of diminished resistance associated with some forms of cancer or in patients with suppressed bone marrow function after the use of myelotoxic chemotherapy or in those undergoing bone marrow transplantation following intense chemotherapy [1].

The natural human GM-CSF is composed of 127 amino acids including four cysteine residues that form two disulphide linkages [17,18]. It is a compact globular protein containing both α -helical and β -sheet structures [19]. It is also an acidic glycoprotein with a molecular mass of 18 000–30 000 and an isoelectric point ranging from 4.0 to 5.2, depending on the type of cells from which it is derived [20–22]. The molecular mass of the non-glycosylated protein is 14 700.

The cDNA of human GM-CSF has successful-

ly been cloned and expressed in both mammalian (monkey COS cells) [23,24] and bacterial (*Escherichia coli*) cells [25]. Characterization of the purified product showed that, despite the lack of glycosylation, the bacterially synthesized human GM-CSF is the same as its natural counterpart in both conformation and biological activity [25]. In order to improve its expression level in *E. coli*, polymerase chain reaction (PCR) technology and synthesized oligonucleotide primers have been used to modify its 5'-terminal cDNA to fit the *E. coli* system. Recently, the high yield expression plasmid (pBV₂₂₀/GM-CSF) has been obtained [26] which will allow the production of recombinant human (rh) GM-CSF in relatively large quantities. This in turn will make it possible to perform some detailed structure–function analysis on the purified protein and its use in diverse clinical trials.

Methods for the purification of rhGM-CSF are scanty and the few that are published are based either on immunoaffinity chromatography [27] or a combination of gel filtration, ion-exchange (IEC) and reversed-phase liquid chromatography (RPLC) [24,25,28]. This paper describes an optimized downstream purification procedure for rhGM-CSF expressed in *E. coli* as inclusion bodies. The adopted procedure is reproducible and well suited for process-scale operations. The purified rhGM-CSF is homogeneous when examined by several criteria of purity and its biological activity is apparently identical with that of its natural counterpart. It has also been characterized with respect to its amino acid composition, partial amino terminal sequence analysis and its molecular mass.

2. Experimental

Unless stated otherwise, all experiments were performed at room temperature (20°C). Chromatographic columns, gel media, recorders, detectors, fraction collectors, PhastSystem electrophoresis apparatus and the BioPilot chromatographic system were products of Pharmacia Bio-Process Technology (Uppsala, Sweden). During the developmental phase of the downstream

purification procedure and for establishing the reproducibility of the adopted purification process, XK16 and XK26 laboratory columns were used. For pilot-scale applications, XK50/30 and BioProcess glass columns (BPG 100/950) were used. Relevant details will be outlined in appropriate sections.

Guanidine hydrochloride ($\text{Gu} \cdot \text{HCl}$) (95%) was obtained from Aldrich Chemie, urea from Prolabo, Berol 185 from Berol Kemi (Stockholm, Sweden), EDTA (disodium salt, dihydrate) and 2-mercaptoethanol (2-ME) from Fluka, reduced glutathione (GSH) and oxidized glutathione (GSSG) from Sigma, RPMI 1640 medium and foetal calf serum from Gibco and a reference standard for rhGM-CSF (specific activity = $6 \cdot 10^7$ units/mg) from Boehringer (Mannheim, Germany).

The following buffers were used for extraction, solubilization and renaturation of the inclusion bodies and for the chromatographic experiments; they will be referred to in abbreviated form throughout:

- (A) 20 mM sodium phosphate (93 parts of 0.2 M Na_2HPO_4 solution + 7 parts of 0.2 M NaH_2PO_4 solution diluted 10-fold)–0.125 M NaCl–5 mM EDTA (pH 7.6).
- (B) 0.1% (v/v) Berol 185 in buffer A (pH 7.5).
- (C) 0.5 M urea in buffer A (pH 8.1).
- (D) 7 M guanidine hydrochloride–100 mM 2-mercaptoethanol–50 mM Tris–HCl–50 mM NaCl–1 mM EDTA (pH 7.5).
- (E) 20 mM Tris–HCl–1 mM reduced glutathione–0.1 mM oxidized glutathione–0.1% Berol 185 (pH 8.4).
- (F) 50 mM sodium phosphate (210 ml of 0.2 M Na_2HPO_4 + 40 ml of 0.2 M NaH_2PO_4 solutions diluted to 1 l)–10% (w/v) ammonium sulphate (pH 6.9).
- (G) 20 mM sodium phosphate (61 ml of 0.2 M Na_2HPO_4 + 39 ml of 0.2 M NaH_2PO_4 solutions diluted to 1 l) (pH 7.0).
- (H) 30% 2-propanol in buffer G.
- (I) 20 mM sodium phosphate buffer (31 ml of 0.2 M Na_2HPO_4 + 69 ml of 0.2 M NaH_2PO_4 solutions diluted to 1 l) (pH 6.5).
- (J) 20 mM sodium phosphate buffer (40 ml of 0.2 M Na_2HPO_4 + 60 ml of 0.2 M NaH_2PO_4 solutions diluted to 1 l)–0.15 M NaCl (pH 6.5).
- (K) 20 mM sodium phosphate buffer (58 ml of 0.2 M Na_2HPO_4 + 42 ml of 0.2 M NaH_2PO_4 solutions diluted to 1 l)–1.0 M NaCl (pH 6.4).

2.1. Production of rhGM-CSF

The procedure described here is essentially identical with that used in ref. [29]. *E. coli* strain DH5 α was transformed by plasmid pBV220/GM-CSF, which contains rhGM-CSF cDNA inserted downstream of P_{RPL} promoter and CIts857 regulator gene. Fermentation of the transformed cells was performed essentially as described by Song and Tong [30]. About 1000 ml of an overnight cell culture in LB medium was seeded into a 40-l fermenter containing 25 l of modified M 9 medium. The cells were allowed to grow at 30°C, maintaining the pH at 7.0 and the glucose concentration at 0.2–0.4% (w/v) until the absorbance of the cell suspension at 600 nm (A_{600}) was about 3. This was reached after about 9 h of continuous culturing. The temperature of the fermenter was then raised to 42°C to induce the expression of the rhGM-CSF [31,32]. The fermentation was allowed to continue for a further 4 h and the cells were then harvested by centrifugation at 10 000 rpm at 4°C in a Beckman J2-21 centrifuge fitted with a continuous rotor.

2.2. Extraction, solubilization and renaturation of the inclusion bodies

About 120 g of the *E. coli* cells were suspended in 1200 ml of buffer A followed by dispersion using an Ultra Turrax (IKA-Werk) run at moderate speed for about 5 min. The homogenized suspension was cooled to 15°C and passed through an APV Gaulin Press maintained at a pressure of 500 bar (50 MPa) throughout the milling operation. The temperature of the partially disrupted cell suspension rose to 30°C during this first passage. It was cooled to 20°C in an ice-bath and the milling operation was re-

peated twice more. At the third and last passage, the temperature of the disrupted cell suspension rose to 27°C. Microscopic examination of the milled suspension showed no intact *E. coli* cells, indicating that at least 98% of the cells were disrupted.

The suspension was centrifuged at 5000 g for 30 min and at 4°C. The supernatant was discarded and the pellet was resuspended in buffer B (600 ml) followed by homogenization for about 5 min using the Ultra Turrax and centrifugation as above. The resulting pellet was further washed by resuspension in buffer C (600 ml) followed by homogenization and centrifugation as above. The supernatant was discarded and the pellet was resuspended in 300 ml of buffer A followed by homogenization and centrifugation at 10 000 g for 30 min at 4°C. The supernatant was discarded and the pellet (ca. 14 g wet mass), containing highly purified inclusion bodies, was dissolved in 56 ml of buffer D by continuously stirring it for 3 h at 4°C. The resulting cloudy solution was centrifuged at 40 000 g for 30 min at 4°C to remove insoluble material and residual cell debris.

The clarified supernatant, containing denatured and solubilized proteins of the inclusion bodies, was renatured by stepwise dilution with buffer E (a total of seven steps were used). This procedure resulted in a significant decrease in the amount of precipitate formed during renaturation compared with a one-step dilution procedure we had previously used [29]. To 1 part of the supernatant was added sufficient amount of buffer E (1.17 parts) to decrease the concentration of Gu·HCl from 7 to 6 M. The solution was then stirred continuously for 10 min at 4°C and a further amount of buffer E was added to decrease the concentration of Gu·HCl to 5 M. The solution was stirred as above for 10 min and this process was repeated until the final concentration of Gu·HCl was decreased to 1 M. At this point, the solution turned cloudy. To this was added sufficient buffer E to decrease the concentration of Gu·HCl to 0.1 M (total dilution factor = 75) and the resulting cloudy suspension was stirred for 10 min and allowed to stand at 4°C overnight for optimum renaturation of the

proteins. The product obtained was distinctly cloudy, probably owing to the presence of partially renatured and/or aggregated proteins. It was clarified by centrifugation at 17 000 g for 30 min at 4°C and the clear supernatant, containing renatured rhGM-CSF, was used as the starting material for purifying the active protein according to the optimized procedure described below.

2.3. Hydrophobic interaction chromatography (HIC)

Phenyl Sepharose 6 Fast Flow (high sub) was packed in an XK50 column (bed height = 20 cm; bed volume = 400 ml) and washed with two bed volumes of deionized water followed by three bed volumes of equilibration buffer F. In the sample of renatured and clarified rhGM-CSF (4.3 l) was dissolved ammonium sulphate to a final concentration of 0.76 M (10%, w/v) before applying it to the equilibrated column at a flow-rate of 100 cm/h. After sample application, the column was washed with three bed volumes of the equilibration buffer F to elute the unbound fraction. The bound fraction, containing rhGM-CSF, was eluted by washing the column with 2.5 bed volumes of buffer G followed by about four bed volumes of buffer H. This last washing also serves to regenerate the column. For subsequent use, the column was washed with at least three bed volumes of deionized water to elute the 2-propanol prior to equilibrating it with buffer F. Fractions were pooled as they eluted from the column on the basis of their A_{280} recorder tracing.

After using the column for 3–5 consecutive runs, it was regenerated by washing with 2–3 bed volumes of 0.5–1 M NaOH. The column was allowed to stand in this solution overnight and then washed with deionized water (two bed volumes) followed by buffer F for re-equilibration (see above). This procedure serves to remove strongly bound proteins and lipids and thereby restore the function of the adsorbent.

2.4. Ion-exchange chromatography

The active fractions (B and C) obtained from

the HIC step were pooled (total volume 880 ml) and applied to an XK50 column (bed height = 22.5 cm; bed volume = 450 ml) packed with Q Sepharose Fast Flow which was equilibrated with buffer I. After sample application, the column was washed with the equilibration buffer I until all the unbound fraction was eluted, followed by 2.5–3 bed volumes of buffer J to elute the fraction containing active rhGM-CSF. The column was finally washed with three bed volumes of buffer K to elute the most strongly bound proteins and also to regenerate it.

2.5. Gel filtration

This was performed on a BioPilot glass column (BPG 100/950) packed with Superdex 75 prep grade (bed volume = 4.9 l). The column was equilibrated with buffer J and the flow-rate was maintained at 15 cm/h. The active fraction obtained from the IEC step (total volume = 620 ml) was applied to the column in portions, or after concentrating it over a PM 10 membrane fitted to an Amicon concentrating cell, such that the sample volume corresponded to approximately 5% of the total bed volume of the column. The eluted fractions were pooled directly on the basis of the continuous chart recording of the A_{280} of the effluent.

2.6. Analytical methods

The distribution of proteins in column effluents was determined by continuous on-line measurement of the absorbance at 280 nm and direct recording. Quantitative determinations were made according to a modified method of Lowry using a Sigma protein assay kit. The concentration of protein in solutions of purified rhGM-CSF was determined using a factor $A^{1\%}$ at 280 nm of 10.1 which we have established (see Results). Its amino acid composition was determined according to standard procedures on a purified sample which has been hydrolysed in 6 M HCl for 24 and 72 h at 110°C in evacuated and sealed glass tubes. Cysteine was determined as cysteic acid on an oxidized sample that was hydrolysed for 24 h. Tryptophan was determined

on a sample which was hydrolysed for 24 h in 3 M mercaptoethanesulphonic acid (MESA) to avoid its destruction by air oxidation. The hydrolysates were analysed on a Model 4151 Alpha Plus amino acid analyser (Pharmacia LKB Biotechnology).

The NH₂-terminal sequence of purified rhGM-CSF was determined using the Edman degradation method on an Applied Biosystems Model 477A sequencer. The resulting phenylhydantoin (PTH)-amino acid derivatives were identified using an Applied Biosystems Model 120A PTH analyser.

2.7. Determination of biological activity

This is based on determining the survival of TF-1 cells cultured in the presence of rhGM-CSF relative to those cultured in its absence. TF-1 (tri-factor dependent) is a unique cell line established from the bone marrow cells of a patient with erythroleukaemia that is dependent for its growth and proliferation on each of three haematopoietic factors, i.e. erythropoietin (EPO), granulocyte-macrophage colony-stimulating factor (GM-CSF) and interleukin 3 (IL-3) [33]. The procedure we employed routinely is an adaptation of the method described by Kitamura et al. [34]. The activity of rhGM-CSF was also determined by an indirect enzyme-linked immunosorbent assay (ELISA) using horseradish peroxidase conjugated with sheep anti-mouse (BALB/c) IgG.

2.8. Native or sodium dodecylsulphate-polyacrylamide gel electrophoresis (SDS-PAGE)

This was performed routinely according to the procedure outlined in Ref. [29] to follow the progress achieved at each stage of the downstream purification process and to examine the electrophoretic homogeneity of purified rhGM-CSF preparations. The dilute protein solutions were concentrated by lyophilization after desalting of each sample on a PD 10 (Sephadex G-25) column equilibrated with 50 mM ammonium acetate (pH 6.8). The dried samples were then dissolved in a suitable volume of distilled water

to obtain an A_{280} of ca. 10 (i.e. $10 \mu\text{g}/\mu\text{l}$). Low-molecular-mass marker proteins were also run simultaneously. Isoelectric focusing of the purified rhGM-CSF was performed on a PhastGel IEF 3–9 medium according to the standard procedure described in the PhastSystem manual.

Approximately $20 \mu\text{g}$ of each sample were applied to the gel for electrophoresis. The separated protein bands were stained using either the Coomassie Brilliant Blue (PhastGel Blue R) or silver staining techniques according to the detailed procedure outlined in the PhastSystem manual. The relative molecular mass of the purified rhGM-CSF was calculated by comparing its migration distance with that of standard calibration proteins run simultaneously.

2.9. Analytical gel filtration and ion-exchange chromatography

High-performance gel filtration was performed on a Superdex 75 HR 16 column ($48.5 \times 1.6 \text{ cm}$ I.D.; bed volume = 97 ml) equilibrated and eluted with buffer J. The sample of purified rhGM-CSF (2 ml) was applied to the column and eluted at a linear flow-rate of 15 cm/h. The effluent was monitored by continuous on-line detection at 280 nm. Analytical IEC was performed on a Mono Q HR 5/5 column fitted to a Pharmacia-LKB HPLC system. Various buffers (ranging in pH from 6.5 to 7.8) and salt gradient profiles were used to separate any minor component(s) that might be present in the purified sample of rhGM-CSF. The linear flow-rate was maintained at 150 cm/h in most routine analyses.

2.10. Mass spectrometry

The purified rhGM-CSF was analysed by electrospray (ES-MS; see [35] and [36]) or laser desorption (LS-MS) mass spectrometry to determine accurately its molecular mass. The results obtained, in conjunction with the published sequence of rhGM-CSF and its partial amino terminal sequence as determined by us, also formed the basis for further characterization of the purified molecule.

2.11. Quality control

These were performed in accordance with the detailed guidelines outlined in the WHO Expert Committee's Report on Biological Standardisation [37], whose aim is to ensure the safety of biological products which are to be used as therapeutic agents in human patients. Contaminating residual DNA in chromatographic fractions containing rhGM-CSF activity was determined using the Threshold total DNA detection system [38] after pretreating the samples with proteinase K. The content and concentration of endotoxins in the same samples were determined using a standard Limulus test [39].

In order to perform these analyses, all chromatographic experiments were carried out under aseptic conditions in an isolated room equipped with a continuously lit UV lamp. All buffers and vessels used for collecting fractions were sterilized by autoclaving for 1 h at 121°C . Sterile-filtered air was also circulated out of the room throughout the duration of the experiment. Each packed column was cleaned in place (CIP) with 2–3 bed volumes of 0.5 M NaOH which, after about a 15-h contact time, was washed out with 3–5 bed volumes of sterilized water. Each column was then equilibrated with the appropriate starting buffer and the chromatographic procedure described above was followed to purify the rhGM-CSF.

3. Results and discussion

During the initial stages of this investigation, the extraction, washing and renaturation of the inclusion bodies were performed following the procedure outlined in Ref. [29]. The results were unsatisfactory as relatively large amounts of protein impurities were co-extracted with the inclusion bodies and the activity of the renatured rhGM-CSF was low. The entire procedure was thus modified to circumvent this problem. A neutral detergent (0.1% Berol 185) was included in the washing buffer (buffer B) to remove impurities bound to inclusion bodies by hydrophobic forces [40,41]. Unlike other detergents

used for such purposes, e.g., sodium deoxycholate, Triton X-100 [40,41], any Berol 185 bound to the inclusion bodies (IBs) can be removed by washing with aqueous buffers. We believe that this washing procedure had resulted in highly purified inclusion bodies.

As concerns the renaturation of reduced proteins, a variety of recommendations have been published [41] whose basic aim was to obtain a high yield of correctly formed disulphide bonds and thereby of the active protein. Common to all the published procedures is the use of air oxidation or a variety of redox systems to obtain Cys–Cys linkages in the diluted protein solution. Of the various redox systems that are recommended [41], a 10:1 mixture of reduced to oxidized glutathione (introduced by Saxena and Wetlaufer [42]) was found to be an efficient system for generating disulphide bonds from reduced proteins. However, the ratio of reduced to oxidized glutathione is variable depending upon the number of disulphide bonds to be formed [41]. We have used this and other redox

systems to optimize the yield of the renatured rhGM-CSF. We also included 2-mercaptoethanol in the solubilizing buffer (buffer D) to stabilize the Cys residues in the denatured protein by forming mixed disulphides [41]. The results we obtained are summarized in Table 1 which indicate that the highest yield of active rhGM-CSF was obtained by using 7 M Gu·HCl (containing 100 mmol/l of 2-ME) for solubilizing the IBs followed by a 75-fold stepwise dilution of the solution in the presence of a 10:1 ratio of GSH–GSSG and a 0.1% (w/v) solution of Berol 185. Replacing Gu·HCl with urea markedly decreased the formation of active rhGM-CSF. The inclusion of PEG in the renaturation buffer, as suggested by Cleland et al. [43], had a marginal effect on the overall recovery of active protein.

Each of the chromatographic steps described below was optimized in order to obtain maximum selectivity and capacity of the media for the rhGM-CSF. The reproducibility of each step was checked with satisfactory results. The recovery, specific activity and homogeneity of the purified

Table 1
Effect of varying the conditions for solubilization and renaturation of the rhGM-CSF on the activity of the renatured product

Solubilization conditions			Renaturation conditions							
Denaturant	2-ME (mmol/l)	Berol (%, v/v)	GSH/GSSG (mmol/l)	PEG (μ mol/l)	Berol (%, v/v)	Sucrose (%, w/v)	Gu·HCl (mol/l)	Urea (mol/l)	Cys/Cys–Cys (mmol/l)	ELISA activity
Gu·HCl						5	0.2			2.4
Gu·HCl						5	0.2		3/0.3	2.3
Urea			2/0.2					4		5.9
Urea			2/0.2	70				4		7.5
Urea			2/0.2		0.1			4		8.6
Gu·HCl			2/0.2			5	0.1			4.5
Gu·HCl		7.5	2/0.2		0.1	5	0.1			8.4
Gu·HCl	100		1/0.1		0.1		1.0			8.6
Gu·HCl ^a	100		1/0.1		0.1		0.1			9.6
Urea	100		1/0.1		0.1			1		5.1
Urea	100		1/0.1		0.1			0.2		5.0

The concentration of urea for solubilizing the IBs was 8 M (pH 8.5) while that of Gu·HCl was 7.0 M (pH 7.5). About 1 g (wet mass) of inclusion bodies was used for each of the conditions listed. For details of the solubilization and renaturation procedure and the method for determining activity by indirect ELISA, see text. The unit for ELISA is mg of rhGM-CSF/g of inclusion bodies. GSH = reduced glutathione; GSSG = oxidized glutathione; PEG = polyethylene glycol (average molecular mass 3350); 2-ME = 2-mercaptoethanol.

^a Values in italics are optimal renaturation conditions that result in the highest yield of renatured protein.

rhGM-CSF was also found to be consistently high and reproducible in all the pilot experiments we performed.

3.1. Step 1: hydrophobic interaction chromatography

A typical elution profile obtained after chromatography of ca. 4.3 l of the renatured rhGM-CSF on a 400-ml column of Phenyl Sepharose 6 FF (high sub) is shown in Fig. 1. Fraction A was inactive and apparently contained very little protein as virtually no bands could be detected after PAGE of the concentrated sample followed by PhastGel Blue R staining (see Fig. 5). Pooled fractions B and C together account for approximately 40% of the A_{280} (60% of the proteins) and 92% of the rhGM-CSF activity applied to the column. This step is thus very effective in removing most of the impurities and also the buffer constituents (Gu·HCl, Berol 185, glutathione, etc.) found in the renatured sample. The overall degree of purification obtained is apparently low (twofold; see Table 2) and might be

due to the fact that the highly purified inclusion bodies contain very little extraneous protein contaminants.

In general, many proteins lose part or most of their activity on exposure to aqueous organic solvents. However, the rhGM-CSF was found to be stable when eluted with 30% 2-propanol from the Phenyl Sepharose 6 FF column. The possible denaturing effect of this solvent might be time dependent and it is advisable to avoid storage of the eluted fraction C for longer periods than necessary.

The capacity of Phenyl Sepharose 6 FF (high sub) for rhGM-CSF is low (about 1 mg/ml gel) and might be due to the presence of chaotropic ions (Gu·HCl), detergents and other competing solutes present in the renatured rhGM-CSF. However, this is compensated for by the fact that the partially purified rhGM-CSF so obtained is virtually free from buffer salts and DNA which can interfere with the subsequent IEC step. Another important advantage is that the active fractions 1B and 1C are eluted in a volume corresponding to approximately one fifth of the

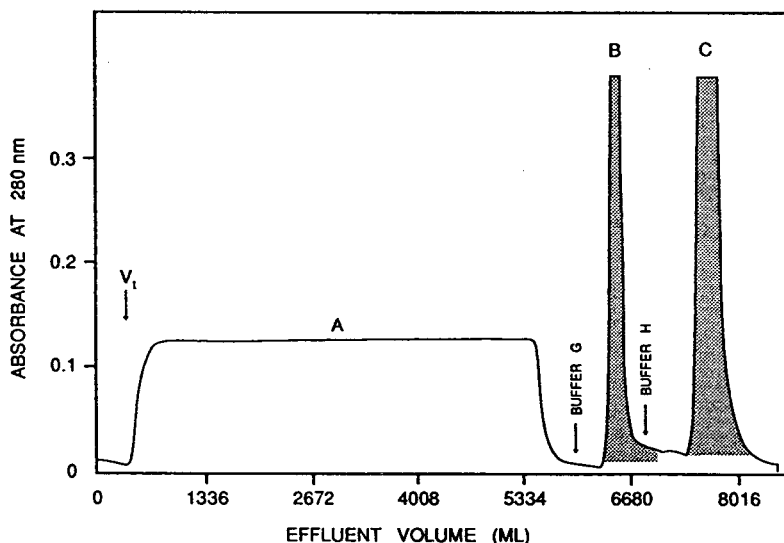


Fig. 1. Hydrophobic interaction chromatography (HIC) of 4340 ml of renatured crude extract ($A_{280} = 0.21$; total protein ≈ 580 mg) on an XK50/30 column packed with Phenyl Sepharose FF (bed height = 20 cm; bed volume = 400 ml). The renatured sample was centrifuged at 17 000 g to remove the suspension of finely divided precipitate prior to its application on the column that was equilibrated with buffer F. The flow-rate was 100 cm/h and fractions were pooled as they were eluted from the column. Fraction A was virtually inactive while pooled fractions B and C (shaded) contained approximately 96% of the activity (ELISA) and 40% of the A_{280} (ca. 60% of the protein) applied to the column.

Table 2
Recovery of rhGM-CSF activity after each chromatographic step used for its purification from the inclusion bodies of transformed *E. coli* cells

Step	Sample	Total protein (mg)	Total activity [biological] ($\times 10^7$ units)	Specific activity ($\times 10^7$ units/mg)	Recovery (%) (biological activity)	Total activity (ELISA) (mg)	Recovery (%) (ELISA)	Purification factor (-fold)
–	Renatured rhGM-CSF	578.6	416.6	0.72	100	181.6	100	1
I (HIC)	Pool 1 (B + C)	315	439.1	1.39	105 (68–125)	167.4	92.1 (85–97)	1.9
II (IEC)	Pool 2B	116	204.1	1.76	49 (33–72)	75.8	41.7 (35–47)	2.5
III (GF)	Pool 3B	88.4	289.8	3.28	70 (39–86)	64.1	35.3 (31–36)	4.6

The tabulated values are averages of three independent experiments covering the entire procedure adopted for its purification. The recovery in biological or ELISA activity is calculated relative to the corresponding total activity in the renatured sample. The purification factor is calculated on the basis of the specific activity obtained from the biological assay. Figures in parentheses indicate the range of values obtained. For identification of the samples referred to here, see Figs. 1–3. GF = Gel filtration.

volume of the renatured sample applied to the column. These considerations are especially important in reducing the processing time for large-scale applications. Finally, attempts have been made to elute the bound fraction (1B + 1C) by washing the column directly with buffer H but the recovery was found to be low. This might be due to the residual ammonium sulphate present in the column which must be washed out with buffer G prior to elution with buffer H.

3.2. Step 2: ion-exchange chromatography

The elution profile obtained after chromatography of 880 ml of pooled fractions 1B + 1C on a 450-ml column of Q Sepharose FF is shown in Fig. 2. The volume of media used is the minimum required to bind all of the rhGM-CSF activity in the pooled fractions. Neither the pH nor the salt concentration of the pooled sample was adjusted because the applied activity was bound satisfactorily to the column under the equilibration conditions used here.

Various salt gradient elution strategies have been tried but the activity was spread over several separated fractions and the total recovery in activity was not satisfactory. This also led to a

considerable dilution of the eluted fractions. Changing the pH of the equilibration buffer from 6.5 to 7.5 or 8.0 resulted in a progressive strong binding of the active protein but did not result in

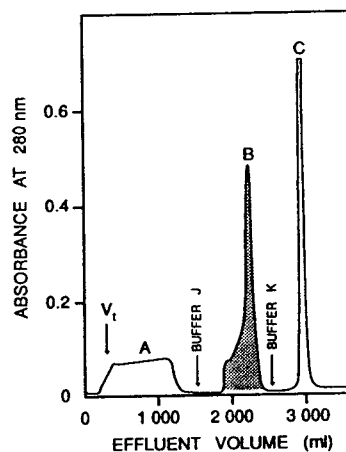


Fig. 2. Ion-exchange chromatography of 880 ml (ca. 300 mg of protein) of pooled fractions B + C (see Fig. 1) on an XK 50/30 column packed with Q Sepharose FF (bed height = 22.5 cm; bed volume = 450 ml). The column was equilibrated with buffer I and a flow-rate of 100 cm/h was used throughout. The bound fractions 2B and 2C were eluted by a stepwise change of the eluent buffers J and K and were pooled directly as they were eluted. Most of the applied activity (ca. 70%) was found in the shaded fraction 2B.

any improvement of the resolution obtained. It is therefore apparent that the procedure adopted here is simple, results in a high recovery of activity and leads to a concentration of the active protein in fraction 2B by a factor of about 1.4 relative to the volume applied to the column. All these considerations make this procedure well suited for large-scale operations.

Of the total ELISA activity applied to the column, less than 5% was found in the unbound fraction A, about 45–50% in fraction B and about 25–30% in fraction C. Electrophoretic analysis of these fractions (see Fig. 5) showed that the band corresponding to M_r 14 000 (i.e. the approximate molecular mass of rhGM-CSF) was predominantly found in fraction 2B. It is virtually absent in fraction 2A and is only a minor component of the many bands (most of which are of high molecular mass) detected in fraction 2C. The majority of the electrophoretic bands in fraction 2C might thus represent insufficiently renatured rhGM-CSF or its aggregation products.

3.3. Step 3: gel filtration

This step effectively removes the last traces of impurities (both high- and low-molecular mass proteins) present in the highly purified fraction 2B (see Fig. 3). The active fraction from the IEC step (pool 2B) can be applied as such or after concentration over an Amicon PM 10 membrane concentration cell such that the volume of sample applied to the Superdex 75 column corresponds to ca. 4–6% of the total bed volume. The active fraction 3B is diluted about 1.5-fold after elution from the column. Fractions 3A and 3C are inactive and together contain about 15% of the A_{280} applied to the column. The active fraction contains about 80% of the A_{280} and 90% of the rhGM-CSF activity applied to the column.

Based on the specific activity of the highly purified fraction 3B, the adopted downstream purification procedure leads to a 4.6-fold purification of the renatured rhGM-CSF (see Table 3). Such a low figure seems to be characteristic for recombinant proteins produced as inclusion

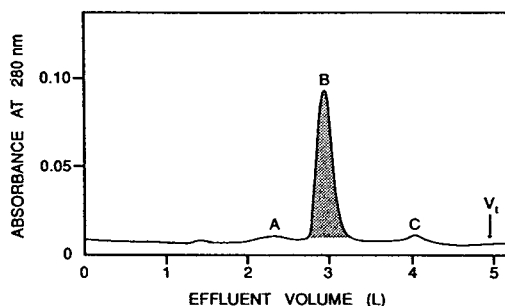


Fig. 3. Gel filtration of pooled fraction 2B (see Fig. 2) on Superdex 75 Prep Grade packed in a BioPilot glass column (BPG 100/950; bed volume = 4.9 l). The column was equilibrated and eluted with buffer J at a flow-rate of 15 cm h. The volume of sample applied was approximately 5% of the total bed volume of the column and fractions were pooled directly as they eluted from the column. Approximately 80% of the applied A_{280} and 90% of the rhGM-CSF activity was found in pooled fraction 3B.

bodies (cf., [29]) and might reflect the much lower level of extraneous protein contaminants present in highly purified inclusion bodies.

The entire purification scheme is presented in Fig. 4.

3.4. Criteria of purity

SDS-PAGE of the purified rhGM-CSF (fraction 3B) gave a single but diffuse band with an apparent molecular mass of 14 000 (see Fig. 5, lane 7 of each gel). Silver staining of an overloaded gel (not shown here) revealed the presence of a faint second band with a molecular mass of ca. 30 000. With all probability, this band represents a dimer of the single chain molecule.

The electrophoresis gels shown in Fig. 5 were overloaded with the purified sample (see lane 7 of each gel) in order to detect any minor impurities that might be present in the purified protein. This resulted in diffuse bands, especially with the SDS-treated samples, most likely due to the higher dye uptake of SDS-denatured proteins whose structure is in an extended, random coil state.

Isoelectric focusing of fraction 3B on PhastGel IEF 3–9 gave a single band with an isoelectric point near pH 5.2. Even when the gel was overloaded to the extent that the focused protein

Table 3
Stability of purified rhGM-CSF at pH 4.2 or 7.0 during storage for 45 days at 4 or at -20°C

Storage time (days)	pH	Temperature ($^{\circ}\text{C}$)	Activity (ELISA) ($\mu\text{g/ml}$)	Biological activity ($\times 10^7$ units/ml)
1	4.2	4	157	
	7.0	4	180	
15	4.2	4	152	
	4.2	-20	144	2.6
	7.0	4	170	
	7.0	-20	185	3.7
25	4.2	4	122	
	4.2	-20	137	2.4
	7.0	4	158	
	7.0	-20	183	1.0
35	4.2	4	81	
	4.2	-20	135	
	7.0	4	156	
	7.0	-20	167	
45	4.2	4	84	
	4.2	-20	121	1.3
	7.0	4	155	
	7.0	-20	178	1.4

About 12 ml of a purified sample of rhGM-CSF in 20 mM sodium phosphate buffer (pH 7.0) (protein concentration = 0.34 mg/ml) was used in this study. From this sample, 0.5-ml aliquots were transferred to ten plastic tubes of which five were stored at 4°C and the other five were stored at -20°C . To the remaining solution (7 ml) was added 0.7 ml of 1 M acetic acid dropwise until the pH decreased to 4.2. From this solution, 0.5-ml aliquots were transferred to ten plastic tubes of which five were stored at 4°C and the remaining five were stored at -20°C . One tube from each of the four categories was then taken at intervals of several days (see tabulated values) and the activity in each was determined by ELISA or by using cultured cells as described in detail in the text. The tabulated values are averages of triplicate analyses performed on the same sample.

could be seen as a distinct opalescent band without staining, no further bands were seen after staining the gel. The results indicate that the purified protein is homogeneous with respect to surface charge and any variants or deamidation products could not be detected by this method. This leads us to conclude that deamidation of the four asparagine or eight glutamine residues in this protein [18,24,26] has not occurred during the extraction and purification process.

High-performance gel filtration of fraction 3B on an analytical column of Superdex 75 HR 16 showed a single symmetrical peak eluting at a position corresponding to an apparent molecular mass of ca. 28 000. This result seems to suggest that the rhGM-CSF exists as a dimer in its native state in a neutral pH milieu. However, this is

contrary to the report by Wingfield et al. [19], who found that the rhGM-CSF is a monomeric protein with a molecular mass of 14.7 000, as determined by sedimentation equilibrium analysis. The reason for this anomaly is difficult to explain. It is worth mentioning, however, that we obtained a similar result for rhIFN- γ [29] when run under the same experimental conditions as used here.

High-performance IEC of fraction 3B on a Mono Q HR 5/5 column run at different pH values (6.5–7.8) and salt gradient elution profiles gave a single symmetrical peak. Some of our earlier preparations showed a minor peak (ca. 2–5%) eluting slightly earlier than the major peak, but this was not seen on later preparations carried out according to the standardised protocol described in this paper.

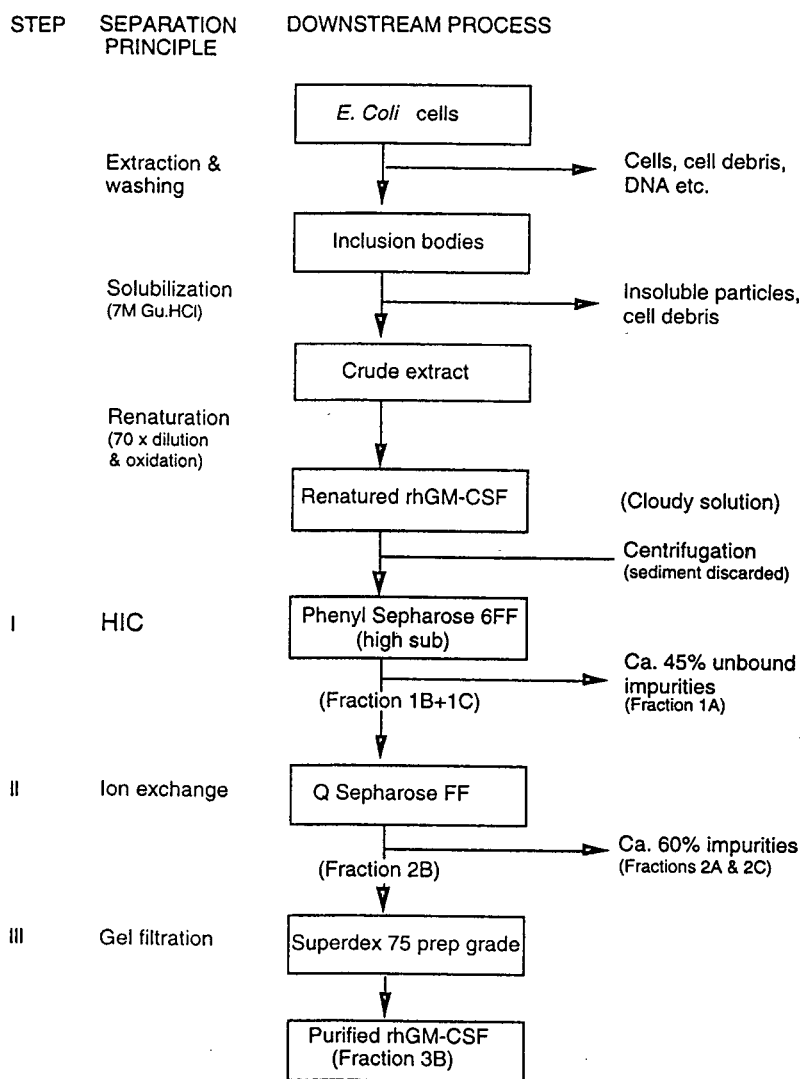


Fig. 4. Pilot-scale purification scheme for rhGM-CSF.

High-performance RPLC of fraction 3B on a column of Pep-S, C_2-C_{18} ($5\text{-}\mu\text{m}$ silica particles) showed one major peak (representing ca. 96% of the eluted material) and two very minor peaks eluting just in front of it. This indicates that the otherwise homogeneous preparation of rhGM-CSF can be further purified by RPLC, if required, to remove the last traces of impurities it might contain.

3.5. Biological potency and stability

The specific biological activity of the purified rhGM-CSF is about $3.3 \cdot 10^7$ units/mg (Table 2), which is comparable to the values reported for this protein derived from mammalian cell cultures [24] or *E. coli* cells [25]. The results in Table 2 also show that the specific biological activity of fraction 3B (Fig. 3) is almost double

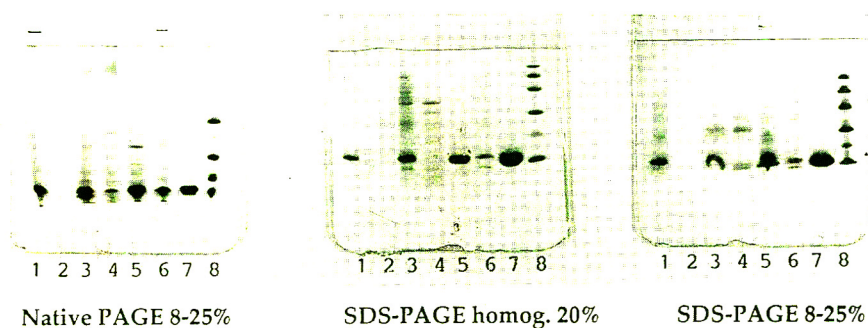


Fig. 5. PhastGel PAGE patterns of the various chromatographic fractions obtained during the three-step purification process for rhGM-CSF. About 20 μg of each sample (native or reduced) were applied to the gels and analysed by three PAGE techniques as indicated under each photograph. The gels were stained with PhastGel Blue R according to a standardized procedure. Lanes: 1 = renatured rhGM-CSF; 2, 3 = unbound (inactive) and buffers G- and H-desorbed and combined fractions, respectively, from a Phenyl Sepharose 6 FF (high sub) column; 4–6 = unbound (inactive); buffer J- and K-desorbed fractions, respectively, from Q Sepharose FF column; 7 = the main fraction 3B (see Fig. 3) that was eluted from a Superdex 75 prep grade column (purified rhGM-CSF); 8 = molecular mass marker proteins (top to bottom: 94 000, 67 000, 43 000, 30 000, 20 000, 14 000). The variations in the densities of the stained bands of the native and SDS-treated samples might be due to the higher dye uptake of the latter.

that of fraction 2B (Fig. 2), indicating that the gel filtration step is very effective in removing some crucial contaminants present in fraction 2B.

Purified rhGM-CSF showed no significant loss in its ELISA activity when stored for 4 weeks at -20°C and pH 7.0, but lost about 60% of its biological activity (Table 3). Storing it for 4 weeks at -20°C and pH 4.2 decreased its ELISA activity by ca. 15% and its biological activity by ca. 50%. The results thus indicate that, irrespective of the pH at which it is stored, the biological activity of purified rhGM-CSF progressively decreases with time of storage. Moreover, although there is an initial drop of its biological activity by 30% on lowering the pH from 7.0 to 4.2, the long-term effects on its biological activity are negligible if stored at -20°C . However, there is a significant loss in ELISA activity (45%) when it was stored for 4 weeks at 4°C and pH 4.2 compared with a loss of only 10% at pH 7.0 during the same period.

3.6. Molecular size and structure

The amino acid composition of the purified rhGM-CSF is shown in Table 4. The total

number of residues found in the purified protein is 127, which is less by one residue of glutamic acid compared with the composition calculated from the cDNA sequence coding for this protein [26]. This discrepancy might be due to the limits of accuracy of this analytical method when a single amino acid residue (glutamic acid + glutamine) represents 16% of the total amino acids in this protein. With this exception, the number of residues for the other amino acids is identical with those calculated from its cDNA sequence data [26]. The data also show that, of the charged amino acids, 60% are acidic (Asp + Glu) and 40% are basic (Arg + Lys), which accounts for the low isoelectric point which we have determined for the purified protein (approximately pH 5.2). Based on the quantitative amino acid composition data and the absorption spectrum of purified rhGM-CSF, we have established that its $A^{1\%}$ at 280 nm (10 mm light path) is 10.1, which is in good agreement with the reported value of 9.58 [19].

The NH_2 -terminal sequence of the first seventeen residues of the purified protein is shown in Table 5. The results are based on two independent analyses of two different preparations of purified rhGM-CSF and were found to be identi-

Table 4
Amino acid composition of purified rhGM-CSF

Amino acid	Notation	Relative No. of residues	Residues per mole
Lysine	K	6.1	6
Histidine	H	2.9	3
Arginine	R	6.2	6
Half-cystine	C	4.1	4
Aspartic acid	D	8.2	8
Threonine	T	11.0	11
Serine	S	9.4	9
Glutamic acid	E	20.0	20 (21)
Proline	P	10.9	11
Glycine	G	3.3	3
Alanine	A	7.8	8
Valine	V	5.1	5
Methionine	M	4.9	5
Isoleucine	I	4.9	5
Leucine	L	14.0	14
Tyrosine	Y	2.1	2
Phenylalanine	F	5.2	5
Tryptophan	W	2.0	2
Total		128.1	127

The numbers of amino acid residues per molecule are averages of the values calculated from the analyses performed on 24- and 72-h hydrolysed samples. They represent the nearest integers obtained from the normalized values for each amino acid so obtained. Tryptophan was determined on a sample hydrolysed for 24 h in the presence of 3 M mercaptoethanesulphonic acid. The value obtained for Glu (20) is less by one residue compared with that expected from its sequence, probably owing to limits of accuracy of this type of analysis. Glu and Gln account for 16% of the total number of residues in this protein.

cal. In both instances, three NH₂-terminal residues (i.e., Met, Ala and Pro) were found, indicating that the purified protein is apparently heterogeneous from its amino-terminal end. This heterogeneity is not due to extraneous protein impurities or other artefacts in the purified rhGM-CSF since the sequence for all three

variants is identical from the third amino acid up to fifteen stages of the Edman degradation cycle. The sequence we obtained corresponds exactly to that reported for this protein [18,24,26], suggesting that the purified rhGM-CSF is identical with its natural counterpart. Based on the area of the peaks for each amino acid after stage

Table 5
Amino-terminal sequence of residues 1–17 of purified rhGM-CSF

I	1	5	10	15	H ₂ N · Met–Ala–Pro–Ala–Arg–Ser–Pro–Ser–Pro–Ser–Thr–Gln–Pro–Trp–Glu ······ COOH (128)
II	1	5	10	15	H ₂ N · Ala–Pro–Ala–Arg–Ser–Pro–Ser–Pro–Ser–Thr–Gln–Pro–Trp–Glu–His ······ COOH (127)
III	1	5	10	15	H ₂ N · Pro–Ala–Arg–Ser–Pro–Ser–Pro–Ser–Thr–Gln–Pro–Trp–Glu–His–Val ··· COOH (126)

The sequence was generated from data obtained after analysis of a purified sample of rhGM-CSF on an Applied Biosystems Model 477A automatic micro-sequencing apparatus according to standardized procedures. The relative occurrence of the three variants of rhGM-CSF is 58% for variant I (i.e., the full length sequence of rhGM-CSF), 29% for II and 12% for III.

1 of the Edman degradation cycle, the relative occurrence of each amino acid was calculated and the values obtained were Met = 58%, Ala = 29% and Pro = 12%. This indicates that the majority (58%) of the molecules are in their intact form with Met as the NH₂-terminal residue.

The occurrence of the above three variants of rhGM-CSF is further supported by data obtained from LS-MS and ES-MS analyses which showed that the purified protein is composed of three distinct components with molecular masses of 14 605, 14 474 and 14 402. The difference in their molecular masses can be accounted for by the lack of Met (residue $M_r = 131$) and Met + Ala (combined residue $M_r = 202$) from the main component whose molecular mass is 14 605. This value is in excellent agreement with that determined by SDS-PAGE (14 000, see Fig. 5) or that determined from the gene sequence (14 650, see ref. [24]) or from ultracentrifugal analysis (14 700, see ref. [19]). The spectrum also shows that each of these variants contains at least 1 mol of Na per mole of protein and that the main component accounts for 55% of the total area of the three peaks seen in the spectrum.

We can only speculate at this stage about the occurrence of the two modified variants of the

parent Met (1) analogue of rhGM-CSF. Despite this apparent molecular heterogeneity, the mixture of the three variants showed a specific biological activity (Table 2) that is comparable to that reported for the recombinant protein produced in mammalian or bacterial cells [24,25]. This might indicate that the occurrence of this protein as three variants may not have any biological significance.

3.7. Quality control

Recombinant proteins intended for use as biopharmaceuticals must not only fulfil the rigorous requirements of purity, identity and biological efficacy vis-à-vis their natural counterparts, but must also fulfil the safety requirements related to their content of DNA, endotoxins and chromatographic artefacts [37]. The first set of these requirements have been satisfactorily fulfilled by the results we have presented above. The results in Table 6 relate to the reduction in DNA and endotoxin levels obtained at each stage of the downstream purification process. According to a WHO Study Group on Biologicals, the probability of risk associated with heterologous contaminating DNA is negligible when the amount of such DNA is 100 pg or less

Table 6

Levels of DNA and endotoxins in renatured rhGM-CSF and the active fractions obtained after each chromatographic purification step

Step	Sample	Total volume (ml)	Total protein (mg)	Endotoxin (EU/ml) ^a	Total endotoxin (EU) ^a	DNA (ng/ml)	Total DNA (ng)
–	Renatured rhGM-CSF	4340	490	421	1 827 140	180	781 200
I (HIC)	Pool 1 (B + C)	880	220	243	213 840	0.46	405
II (IEC)	Pool 2B	620	88	251	155 620	0.14	87
III (GF)	Pool 3B	1045	62	9	9405	0.08	84

The results serve as guidelines in assessing the efficiency of removal of these impurities by the gel media used for chromatography. For identification of the samples referred to here, see Figs. 1–3.

^a EU = Endotoxin units.

in a single dose administered parenterally [37]. The DNA content in the purified rhGM-CSF is 80 pg/ml, which corresponds to 1.4 pg of DNA per μg of protein. For comparison, the level of DNA in the sterilized buffer used for the final gel filtration step is approximately 10 pg/ml. The results thus indicate that a single dose of ca. 70 μg of the purified protein contains a level of DNA that is within the acceptable upper limit recommended by the WHO study group.

The results also show that Phenyl Sepharose 6 FF (high sub) decreases the DNA content effectively (by a factor of ca. 2000), probably because most of the DNA does not bind to it. The anion-exchange step further reduces the level about fivefold. The reduction obtained here is less than expected but might be due to the fact that some of the DNA bound by Q Sepharose FF co-elutes with the rhGM-CSF at pH 6.5. Taken as a whole, the combination of gel media used here for removing protein impurities from the rhGM-CSF is also effective in removing minor amounts of DNA present in the crude extract.

The total decrease in the level of endotoxins in the purified product is about 190-fold relative to the renatured rhGM-CSF. After chromatography on Phenyl Sepharose 6FF, an eightfold decrease was obtained, indicating that most of the endotoxins are not bound under the experimental conditions employed. An even higher reduction (seventeenfold) was obtained after chromatography on Superdex 75, probably owing to large differences in the molecular size of the rhGM-CSF and the contaminating endotoxins. On the other hand, the reduction obtained after the anion-exchange step on Q Sepharose FF (ca. twofold) is much less than expected considering that endotoxins are negatively charged at pH 6.5 and should have been bound strongly. This result seems to suggest that some of the endotoxins and the rhGM-CSF have similar surface charge characteristics and therefore co-elute from the column at pH 6.5. If such is the case, it may be possible to bind the endotoxins more strongly than the rhGM-CSF at a higher pH (e.g., pH 8.0), thereby facilitating their efficient removal.

Acknowledgements

The support and continuing interest of Mr. Yong-hui Liu, Director, China National Centre for Biotechnology Development (CNCBD), Beijing, and Professor Yunde Hou, Director, National Laboratory of Molecular Biology and Genetic Engineering, Institute of Virology, Chinese Academy of Preventive Medicine, Beijing, is gratefully acknowledged. We also thank Dr. Bengt Norén (Kabi Pharmacia) for the ES-MS analysis and Mr. Åke Hammarström of Pharmacia Bioprocess Technology for his expert help in the extraction of the inclusion bodies.

References

- [1] D. Metcalf, *Cancer*, 65 (1990) 2185.
- [2] J.N. Ihle, J. Keller, L. Henderson, F. Klein and E. Palaszynski, *J. Immunol.*, 129 (1982) 2431.
- [3] E.R. Stanley, *Proc. Natl. Acad. Sci. U.S.A.*, 76 (1979) 2969.
- [4] N.A. Nicola, D. Metcalf, M. Matsumoto and G.R. Johnson, *J. Biol. Chem.*, 258 (1983) 9017.
- [5] A.W. Burgess and D. Metcalf, *Blood*, 56 (1980) 947.
- [6] A.W. Burgess, J. Camakaris and D. Metcalf, *J. Biol. Chem.*, 252 (1977) 1998.
- [7] G. Kannourakis and G.R. Johnson, *Blood*, 71 (1988) 758.
- [8] A.R. Migliaccio, M. Bruno and G. Migliaccio, *Blood*, 70 (1987) 1867.
- [9] J.F. Di Persio, P. Billing, R. Williams and J.C. Gasson, *J. Immunol.*, 140 (1988) 4315.
- [10] B.D.-M. Chen, M. Mueller and T.-H. Chou, *J. Immunol.*, 141 (1988) 139.
- [11] C.G. Begley, A.F. Lopez, N.A. Nicola, D.J. Warren, M.A. Vadas, C.J. Sanderson and D. Metcalf, *Blood*, 68 (1986) 162.
- [12] R.H. Weisbart, D.W. Golde, S.C. Clark, G.G. Wong and J.C. Gasson, *Nature*, 314 (1985) 361.
- [13] A. Lindermann, D. Riedel, W. Oster, S.C. Meuer, D. Blohn, R.H. Mertelsmann and F. Hermann, *J. Immunol.*, 140 (1988) 837.
- [14] A.F. Lopez, N.A. Nicola, A.W. Burgess, D. Metcalf, F.L. Battye, W.A. Sewell and M. Vadas, *J. Immunol.*, 131 (1983) 2983.
- [15] K.H. Grabstein, D.L. Urdal, R.J. Tushinski, D.Y. Mochizuki, V.L. Price, M.A. Cantrell, S. Gillis and P.J. Conlon, *Science*, 232 (1986) 506.
- [16] S.C. Clark and R. Kamen, *Science*, 236 (1987) 1229.
- [17] K. Kaushanky, P.J. O'Hara, K. Berkner, G.M. Segal, F.S. Hagen and J.W. Adamson, *Proc. Natl. Acad. Sci. U.S.A.*, 83 (1986) 3101.

- [18] M.A. Cantrell, D. Anderson, D.P. Cerretti, V. Price, K. McKereghan, R.T. Tushinski, D.Y. Mochizuki, A. Larsen, K. Grabstein, S. Gillis and D. Cosman, *Proc. Natl. Acad. Sci. U.S.A.*, 82 (1985) 6250.
- [19] P. Wingfield, P. Graber, P. Moonen, S. Craig and R.P. Pain, *Eur. J. Biochem.*, 173 (1988) 65.
- [20] N.A. Nicola, D. Metcalf, G.R. Johnson and A.W. Burgess, *Leukemia Res.*, 2 (1978) 313.
- [21] G.B. Price, J.S. Senn, E.A. McCulloch and J.E. Till, *Biochem. J.*, 148 (1975) 209.
- [22] S.S. Fojo, M.-C. Wu, M.A. Gross, Y. Purcell and A.A. Yunis, *Biochemistry*, 17 (1978) 3109.
- [23] F. Lee, T. Yokota, T. Otsuka, L. Gemmell, N. Larson, J. Luh, K.-I. Arai and D. Rennick, *Proc. Natl. Acad. Sci. U.S.A.*, 82 (1985) 4360.
- [24] G.G. Wong, J.S. Witek, P.A. Temple, K.M. Wilkens, A.C. Leary, D.P. Luxenberg, S.S. Jones, E.L. Brown, R.M. Kay, E.C. Orr, C. Shoemaker, D.W. Golde, R.J. Kaufman, R.M. Hewick, E.A. Wang and S.C. Clark, *Science*, 228 (1985) 810.
- [25] A.W. Burgess, C.G. Begley, G.R. Johnson, A.F. Lopez, D.J. Williamson, J.-J. Mermod, R.J. Simpson, A. Schmitz and J.F. DeLamarter, *Blood*, 69 (1987) 43.
- [26] J.Q. Zhang, Y. Zhang, X.H. Lu, S.C. Wang, K. Shao, Y. Zhou, L.J. Ma, Y.Y. Li, L.H. Yao, B.K. He, Y.D. Hou, *Chin. J. Virol.*, 9 (1993) 136.
- [27] P. Moonen, J.-J. Mermod, J.F. Ernst, M. Hirschi and J.F. DeLamarter, *Proc. Natl. Acad. Sci. U.S.A.*, 84 (1987) 4428.
- [28] J. Schrimsher, K. Rose, M. Simona and P. Wingfield, *Biochem. J.*, 247 (1987) 195.
- [29] Z. Zhang, K.-T. Tong, M. Belew, T. Pettersson and J.-C. Janson, *J. Chromatogr.*, 604 (1992) 143.
- [30] Y.M. Song, and K.T. Tong, *Selected Papers of the Shanghai Institute of Biological Products*, Chinese Academy of Sciences, Beijing, 1990.
- [31] Z. Zhang, Y.-D. Hou, Y.Y. Li, X.X. Zhao, Y. Zhou, S.M. Duan and L.H. Yao, *Chin. J. Virol.*, 4 (1988) 97.
- [32] Z. Zhang, L.H. Yao and Y.-D. Hou, *Chin. J. Virol.*, 6 (1990) 111.
- [33] T. Kitamura, T. Tange, S. Chiba, T. Kuwaki, Y.-F. Piao, K. Miyazono, A. Urabe, F. Takaku, *J. Cell. Physiol.*, 140 (1989) 323.
- [34] T. Kitamura, A. Tojo, T. Kuwaki, S. Chiba, K. Miyazono, A. Urabe and F. Takaku, *Blood*, 73 (1989) 375.
- [35] J.B. Fenn, M. Mann, C.K. Meng, S.F. Wong and C.M. Whitehouse, *Science*, 246 (1989) 64.
- [36] B. Monegier, F.F. Clerck, A.V. Dorselaer, M. Vuilhorgne, B. Green and T. Cartwright, *Pharm. Technol. Int.*, Nov. (1990) 19.
- [37] WHO Expert Committee on Biological Standardization, *Thirty-Ninth Report. Technical Report Series 786*, World Health Organization, Geneva, 1989.
- [38] S. McKnab, R. Rupp and J.L. Tedesco, *Biotechnology*, 7 (1989) 343.
- [39] P. Friberger, in J.W. Cate, H. Büller, A. Sturk and J. Levin (Editors), *Bacterial Endotoxins: Structure, Biomedical Significance and Detection With the Limulus Amoebocyte Lysate Test*, Alan R. Liss, New York, 1985, p. 139.
- [40] G.A. Bowden, A.M. Paredes and G. Georgiou, *Bio/Technology*, 9 (1991) 725.
- [41] B. Fischer, I. Sumner and P. Goodenough, *Biotechnol. Bioeng.*, 41 (1993) 3.
- [42] V.P. Saxena and D.B. Wetlaufer, *Biochemistry*, 9 (1970) 5015.
- [43] J.L. Cleland, S.E. Builder, J.R. Swartz, M. Winkler, J.Y. Chang and D.I.C. Wang, *Bio/Technology*, 10 (1992) 1013.

Limited enzymatic digestion for the determination of the quantities of minor diastereomeric impurities in preparations of RMP-7, a peptide containing a reduced peptide bond

Julie Ann Straub*, Alan Akiyama, Parul Parmar, Gary F. Musso
Alkermes, Inc., 64 Cambridge Street, Cambridge, MA 02139, USA

First received 18 May 1994; revised manuscript received 31 May 1994

Abstract

RMP-7 is a bradykinin analogue containing all "L" amino acids and a reduced dipeptide bond between amino acids eight and nine. This reduced dipeptide bond [4-Me-Tyr- Ψ (CH₂NH)-Arg] is created under synthetic conditions which could result in inversions of the chiral centers of either 4-Me-Tyr or Arg. Stereoisomers of RMP-7 would be expected to have altered biological specificity. Current chromatographic methods are not sufficiently sensitive to distinguish the anticipated stereoisomeric variants of the intact molecule. Therefore we have devised an analytical method based on limited enzymatic digestion of the compound followed by reversed-phase HPLC analysis of the peptide fragments. Using this method we have been able to carry out precise and reliable quantitative analysis of the stereoisomeric content of different batches of peptide prepared for biological testing.

1. Introduction

RMP-7 [H-Arg-Pro-Hyp-Gly-Thi-Ser-Pro-4-Me-Tyr- Ψ (CH₂NH)-Arg-OH; Thi = thienylalanine] is an analogue of the vasodilatory hormone bradykinin. Biological activity of bradykinin is known to be triggered by interaction with a specific cell surface receptor molecule. The kinetics of elimination of bradykinin are influenced by enzymatic digestion of the molecule in circulation. The RMP-7 molecule is a synthetic agonist of the naturally occurring compound designed to interact with the normal bradykinin B₂ receptor and to be more resistant to enzymatic degradation [1]. We are currently evaluating RMP-7 as a receptor mediated per-

meabilizer of the blood-brain barrier. Our strategy is to administer RMP-7 in combination with therapeutic molecules to which the blood-brain barrier would otherwise be impermeable. Working as an adjuvant, RMP-7 is intended to assist in delivery of these molecules to the brain or brain tumors in order to treat specific disease states [2].

A key structural feature of RMP-7 is the reduced peptide bond, 4-Me-Tyr- Ψ (CH₂NH)-Arg which was incorporated into the sequence in order to increase metabolic stability and receptor specificity. This strategy has been used for other biologically active peptides such as somatostatin [3] and tetragastrin [4]. Key to the overall strategy is the targeting of such molecules to specific biological receptors. Implicit in any such model is the assumption that only one stereo-

* Corresponding author.

isomer will have the specificity to result in biological potency. The presence of varying amounts of other stereoisomers in individual batches of material prepared for biological testing could result in quantitative variations in response or therapeutic effect.

We have devised a synthesis of the overall molecule in which reductive amination of a Boc-protected amino aldehyde with cyanoborohydride forms the reduced peptide bond isostere [5,6]. Reaction conditions at this step of the synthesis are sufficiently vigorous that epimerization of the key chiral centers might be expected for several reasons, including (1) reported lability of amino aldehydes [7], (2) sensitivity of the imine formed in situ during the reductive amination [8] and (3) inversion of the C-terminal arginine upon esterification to the resin or following HF cleavage

Since we expect the pharmacologically active stereoisomer of RMP-7 to be that with all L-amino acid constituents, epimerization of any single chiral center might lead to undesirable isomers. Centers 8 and 9 are those of most concern and we have conducted several studies of reaction strategies designed to minimize inversions at these carbons. In order to measure the effectiveness of our synthetic strategies we needed a sensitive quantitative analytical method to detect the relative amounts of the three major stereoisomers: 8_L,9_L; 8_D,9_L; and 8_L,9_D. To assist in our analysis we synthesized the two major putative impurities which we labeled RMP-10 and RMP-12:

RMP-7: all L chiral centers;

RMP-10: 8_D,9_L;

RMP-12: 8_L,9_D.

We anticipated that few, if any molecules would be formed by inversion of both chiral centers and we have never found evidence for the 8_D,9_D stereoisomer.

Analysis of batches of RMP-7 prepared during scale-up for clinical trial testing required validation of the quantitative method for detecting the levels of the two contaminating stereoisomers in the presence of the major component. We did not find an analytical HPLC method capable of resolving mixtures of all three stereoisomers.

Acid or enzymatic digestion of the peptides followed by chromatography on chiral supports could be used to assay the purity of the individual amino acids [9–11]. Such a method might have been used to generate the reduced dipeptide and measure the ratios of the three anticipated species. However, acid hydrolysis can cause racemization itself and reliable measurements based on this method must be assessed by GC-MS technology which was not readily available. We were also concerned that the reduced dipeptide fragment formed by such digestion might not be suitable for derivatization for GC analysis. Therefore, we devised a method for enzymatic digestion coupled to HPLC analysis.

We considered two enzyme/HPLC-based strategies: (1) complete enzymatic digestion of RMP-7 to amino acids followed by chiral chromatography and (2) partial digestion to peptide fragments followed by non-chiral chromatography. We examined enzymes known to degrade the parent molecule (bradykinin; H-Arg-Pro-Pro-Gly-Phe-Ser-Pro-Phe-Arg-OH), and enzymes which act as general peptidases. These included angiotensin-converting enzyme (ACE; cleaves bonds 7–8 and 5–6 of bradykinin), prolidase (cleaves bond 1–2 of bradykinin) and α -chymotrypsin (cleaves bonds 8–9 and 5–6 of bradykinin) [12], as well as aminopeptidase M [13], papain [14], pepsin [15], subtilisin [16] and pronase [9]. In this report, we detail our findings with respect to the applicability of these enzymes for use in limited proteolysis of RMP-7. In addition, we report our analysis of various batches of RMP-7 when analyzed by limited proteolysis with pronase followed by HPLC analysis.

2. Experimental

2.1. Materials

RMP-7 triacetate salt was prepared for Alkermes by Peninsula Labs. (Belmont CA, USA) using solid-phase peptide synthesis on a Merrifield resin using the N^α-Boc protecting group strategy. The reduced peptide bond between

residues 8 and 9 was initially synthesized according to the method described by Coy and Sasaki (synthetic route 1) [5]. In later lots of RMP-7, the reduced peptide bond was synthesized according to the method of Ho et al. (synthetic route 2) [6]. Authentic samples of 8D,9L-RMP-7 (RMP-10 trifluoroacetate salt, lyophilized powder) and 8L,9D-RMP-7 (RMP-12 trifluoroacetate salt, lyophilized powder) were prepared for Alkermes by Peninsula Labs. using solid-phase peptide synthesis. ACE (rabbit lung), α -chymotrypsin (bovine pancreas), prolidase (porcine kidney), papain (*Papaya latex*), pepsin (porcine stomach mucosa), and subtilisin Carlsberg (*Bacillus licheniformis*) were purchased from Sigma (St. Louis, MO, USA). Aminopeptidase M (hog kidney) was purchased from Pierce (Rockford IL, USA). Pronase (Protease, non-specific from *Streptomyces griseus*) was purchased from Boehringer Mannheim Biochemicals. Phosphate-buffered saline (PBS) consisted of 1.15 g Na_2HPO_4 (8.1 mM), 0.26 g $\text{NaH}_2\text{PO}_4 \cdot \text{H}_2\text{O}$ (1.9 mM), 0.20 g KCl (2.7 mM) and 7.0 g NaCl (120 mM) in 1 l water (Milli-Q).

2.2. Enzymatic methods

Angiotensin-converting enzyme

RMP-7 (4 $\mu\text{g}/\mu\text{l}$, 25 μl), PBS (375 μl) and ACE (0.1 U in 100 μl PBS) were mixed and incubated at 37°C for 21.5 h. The reaction mixture was assayed using HPLC system B.

α -Chymotrypsin

RMP-7 (1 $\mu\text{g}/\mu\text{l}$ solution in saline, 25 μl), buffer (0.2 M triethylammonium acetate, pH 8.0, 100 μl) and α -chymotrypsin (1.1 U enzyme activity in 25 μl buffer) were mixed and incubated at 37°C for a total of 25 h. The reaction mixture was assayed using HPLC system A.

Prolidase

A solution of manganese chloride (1.0 M, 400 μl), glutathione (reduced form, 0.03 M, 100 μl) and buffer [0.1 M 4-(2-hydroxyethyl)-1-piperazineethanesulfonic acid (HEPES), pH 8.0, 2.4 ml] was made. RMP-7 (2.0 $\mu\text{g}/\mu\text{l}$ solution in saline, 10 μl), buffer (0.1 M HEPES, pH 8.0,

165 μl) and prolidase (25 μl , 53.4 U enzyme activity) were mixed. A 100- μl aliquot of the RMP-7/prolidase solution was mixed with 100 μl of manganese chloride/glutathione solution. The resulting mixture allowed to stand at room temperature for 30 min, and was then assayed using HPLC system C.

Papain

RMP-7 (4 $\mu\text{g}/\mu\text{l}$ solution in water, 25 μl), buffer (0.1 M ammonium acetate, pH 5.7, 454 μl), mercaptoethanol (diluted 1:32 with water, 5 μl) and papain (21 μl ; 10 U enzyme activity) were mixed and incubated at 37°C at 22.5 h. The reaction mixture was assayed using HPLC system B.

Pepsin

RMP-7 (4 $\mu\text{g}/\mu\text{l}$ solution in water, 25 μl), buffer (24 mM citrate, pH 4.6, 471 μl) and pepsin (11.8 U enzyme activity in 4 μl buffer) were mixed and incubated at 37°C for 24 h. The reaction mixture was assayed using HPLC system B.

Subtilisin

RMP-7 (4 $\mu\text{g}/\mu\text{l}$, 25 ml), PBS (345 μl) and subtilisin Carlsberg (1.0 U enzyme activity in 130 μl buffer) were mixed and incubated at 37°C for 23.5 h. The reaction mixture was assayed using HPLC system B.

Aminopeptidase M

RMP-7 (1.0 $\mu\text{g}/\mu\text{l}$ solution in saline, 25 μl), buffer (0.1 M HEPES, pH 8.5, 25 μl), glutathione (reduced form, 9.2 mg/ml solution in saline, 25 μl) and aminopeptidase M solution (50 μl , 1 U enzyme activity) were mixed and incubated at 37°C for a total of 17 days. The reaction mixture was assayed periodically using HPLC system A.

Pronase

RMP-7 drug substance (1 $\mu\text{g}/\mu\text{l}$ in water, 100 μl), Tris-calcium chloride dihydrate buffer (53.3 μl ; 0.2 M Tris, 5 mM calcium chloride, pH adjusted to 7.5 with 1 M HCl) and pronase (9.3 μl of a solution of 5.2 mg solid dissolved in 10 ml

Tris–calcium chloride dihydrate buffer; 0.56 U enzyme activity) were mixed and incubated at 37°C for 24 h. HPLC system A was used for initial studies of cleavage patterns. HPLC systems D and E were used for analysis of diastereomeric ratio. RMP-12 was analyzed using the same conditions as were used for RMP-7. Due to limited sample availability, when RMP-10 was analyzed, a concentration of 0.25 $\mu\text{g}/\mu\text{l}$ in water was used in place of the 1 $\mu\text{g}/\mu\text{l}$ solution used for RMP-7.

2.3. HPLC Analysis

System A: A Hewlett-Packard 1090 HPLC system with a diode-array detector set at 210, 214, 230 and 280 nm; a Vydac C₁₈ protein and peptide column (5 μm particle size, 300 Å average pore diameter, 250 mm \times 4.6 mm); a linear gradient system of 10% eluent B to 40% eluent B over 30 min (eluent A: 0.1 M aqueous sodium perchlorate/0.1% phosphoric acid (85%), pH 2.5; eluent B: acetonitrile); flow-rate: 1 ml/min.

System B: HP 1090 system with a diode-array detector set at 210, 214, 230 and 280 nm; a Phenomenex Bondclone C₁₈ column (300 mm \times 3.9 mm); a linear gradient system of 0% eluent B to 39% eluent B over 39 min (eluent A: 0.1 M aqueous sodium perchlorate/0.1% phosphoric acid (85%), pH 2.5; eluent B: acetonitrile); flow-rate: 1 ml/min.

System C: a Beckman system with a Model 166 UV detector set at 210 nm; a Waters μ Bondapak C₁₈ column (300 mm \times 3.9 mm, 10 μm particle size); a linear gradient system of 10% eluent B to 40% eluent B over 30 min [eluent A: 0.1% trifluoroacetic acid in water; eluent B: acetonitrile]; flow-rate: 1 ml/min.

System D: HP 1090 system with a diode-array detector set at 210 nm; a Vydac C₁₈ protein and peptide column (5 μm particle size, 300 Å average pore diameter, 250 mm \times 4.6 mm); an isocratic elution system [96% eluent A and 4% eluent B; eluent A: 0.2% aqueous triethylamine, pH adjusted to 5.2 with phosphoric acid (85%); eluent B: MeOH]; flow-rate: 1 ml/min; 45 min run time.

System E: HP 1090 Series II system with a diode-array detector set at 210 nm; a Zorbax 300SB-C₈ (5 μm particle size, 300 Å average pore diameter, 250 mm \times 4.6 mm); an isocratic elution system (0.2% aqueous triethylamine, pH adjusted to 3.1 with phosphoric acid); flow-rate: 1 ml/min; 45 min run time.

3. Results and discussion

Initially we evaluated the fragmentation pattern resulting from incubation of RMP-7 with various enzymes. Digestion conditions were based on procedures recommended by the supplier of each enzyme. The reaction progress was monitored over time by HPLC. For practical purposes, 1–3 days incubation times were used. Aminopeptidase M was monitored over 17 days, because the digestion appeared to be incomplete at earlier times.

These studies used HPLC analysis on C₁₈ reversed-phase columns with UV detection to determine the extent of digestion of RMP-7 by various enzymes. The structures of the fragments of RMP-7 produced by enzymatic digestion were assigned based on UV spectral data, and a comparison of HPLC retention times of these fragments to the retention times of known structures derived from RMP-7. Monitoring the enzymatic digestions using a diode-array detector at multiple wavelengths that included 280 nm allowed us to identify HPLC peaks associated with fragments containing 4-Me-Tyr- $\Psi(\text{CH}_2\text{NH})$ -Arg (in RMP-7, 4-Me-Tyr $\lambda_{\text{max}} = 274$ nm). The retention times of des-Arg¹-RMP-7 and the C-terminal tetrapeptide [H-Ser-Pro-4-Me-Tyr- $\Psi(\text{CH}_2\text{NH})$ -Arg-OH] were known, as these compounds had been isolated by HPLC and identified by fast atom bombardment MS analysis, as a part of a study of the metabolism of RMP-7 [1]. Authentic C-terminal dipeptide [H-4-Me-Tyr- $\Psi(\text{CH}_2\text{NH})$ -Arg-OH] had been synthesized previously. Thienylalanine was the only free amino acid that could be easily detected in the HPLC systems used, as it has a characteristic 230 nm absorbance, and is sufficiently hydrophobic to be retained on the col-

umn. Any fragment of RMP-7 with a significant absorbance at 230 nm, but not at 280 nm, was assumed to contain thienylalanine but not 4-Me-Tyr.

Observed enzymatic cleavage sites of RMP-7 are summarized in Fig. 1. Only aminopeptidase M appeared able to hydrolyze RMP-7 to constituent amino acids and the C-terminal reduced dipeptide [H-4-Me-Tyr⁸-Ψ(CH₂NH)-Arg-OH; $t_R = 5.5$ min in system A). However, this digestion was incomplete after 17 days, and the observed remaining C-terminal tetrapeptide resulted from one (or both) of the minor stereoisomeric impurities (RMP-10 and/or RMP-12) in the preparation of RMP-7 (the C-terminal tetrapeptide resulting from RMP-7 had been completely digested). Prolidase cleaved the Arg¹-Pro² bond resulting in the formation of des-Arg¹-RMP-7 ($t_R = 21.0$ min in system C). Enzymatic digestions employing ACE, α -chymotrypsin, papain or pronase resulted in the formation of diastereomeric C-terminal tetrapeptides, H-Ser-Pro-4-Me-Tyr-Ψ(CH₂NH)-Arg-OH [$t_R = 11.6$ min (8L,9L isomer) and 12.5 min (8D,9L and 8L,9D isomers) in system A; $t_R = 23.0$ min (8L,9L isomer) and 24.0 min (8D,9L and 8L,9D isomers) in system B]. With ACE, papain or pronase, the remainder of RMP-7 appeared to be digested to single amino acids, since free thienylalanine was detected in the analyte. Based on substrate specificity, free thienylalanine was not expected to be formed in the digestions using

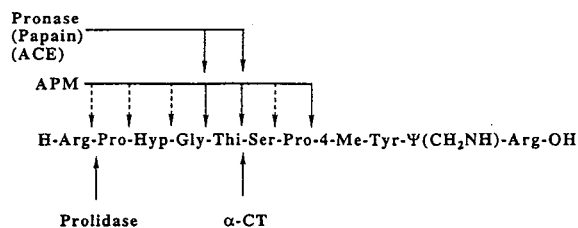


Fig. 1. Sites of enzymatic cleavage of RMP-7. APM = Aminopeptidase M; α -CT = α -chymotrypsin; ACE = angiotensin-converting enzyme. Solid lines indicate sites of cleavage detected directly via product analysis. Dashed lines indicate expected sites of cleavage that were not directly observed via product analysis. ACE and papain are in parentheses as the observed sites of cleavage were not predicted based on the site specificity of these enzymes.

ACE or papain. It is possible that the observed hydrolysis of RMP-7 with ACE or papain was the result of impurities in the enzyme preparations. Only α -chymotrypsin appeared to have a single cleavage site at the Thi⁵-Ser⁶ bond, which resulted in the formation of the diastereomeric C-terminal tetrapeptides along with the N-terminal pentapeptide ($t_R = 8.5$ min in system A). Pepsin and subtilisin did not cleave RMP-7.

Since the C-terminal tetrapeptides were small fragments in which the single-center epimers of interest are diastereomers rather than enantiomers, we concentrated on their separation. Based on the initial studies, the pronase reaction appeared to be a simple and clean method of generating the tetrapeptides; therefore, all later separation studies were performed with pronase digests. In addition to RMP-7, these studies used samples of authentic RMP-10 and RMP-12 as standards. These molecules appeared to be completely digested to the C-terminal tetrapeptides by pronase under the conditions used.

Studies of non-chiral HPLC conditions for separation of the tetrapeptides were performed. The first system found to separate all three isomeric C-terminal tetrapeptides derived from RMP-7 used a Vydac C₁₈ column (system D; 8L,9L derived peak $t_R = 26$ min; 8L,9D derived peak $t_R = 31$ min; 8D,9L derived peak $t_R = 34$ min). Unfortunately, quantification of small percentages of the 8L,9D isomer was problematic, since the peaks were broad and the peak from the 8L,9L isomer frequently tailed into the 8L,9D derived peak. The tetrapeptides were composed of one primary amine, one secondary amine, one guanidinium group, and one carboxylic acid moiety, resulting in an overall charge of +2. Such basic molecules tend to tail on reversed-phase chromatographic systems due to ionic interactions with incompletely capped silica. Therefore, other columns reported by their suppliers to be good for separation of basic molecules (such as the Zorbax 300SB-C₈ used in HPLC system E) were examined. HPLC system E resulted in improved separation of all three diastereomeric C-terminal tetrapeptides, as illustrated in Fig. 2.

This method has been subsequently used to

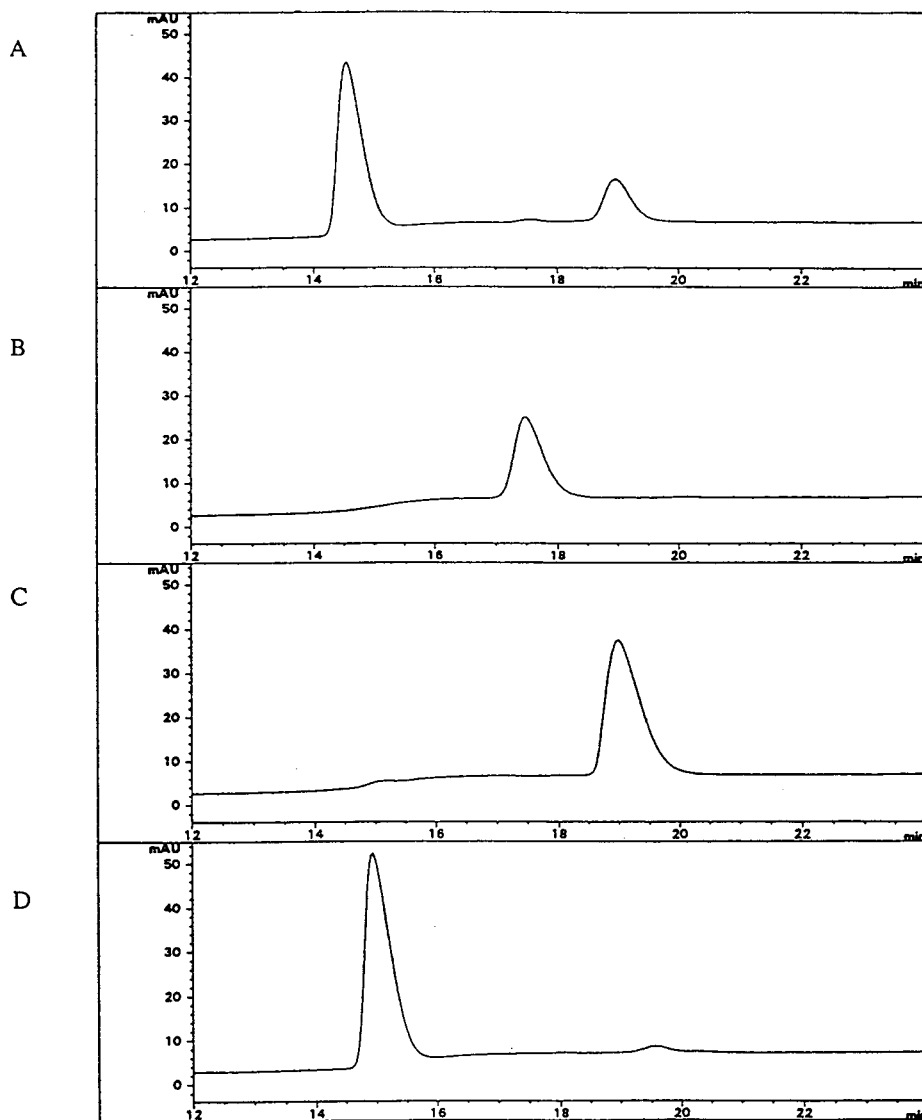


Fig. 2. HPLC analysis using system E. (A) RMP-7 (via synthetic route 1) treated with pronase. (B) RMP-10 treated with pronase. (C) RMP-12 treated with pronase. (D) RMP-7 (via synthetic route 2) treated with pronase. *y*-Axes: absorbance at 210 nm.

assess the ratios of diastereomers present in various batches of RMP-7. The 8_D,9_L-diastereomer was the major undesired isomer in the early lots (produced using synthetic route 1) as shown in Fig. 2A. This demonstrated that the reductive amination used to prepare the reduced peptide bond between residue 8 and 9 resulted in significant epimerization at the 8 position. This knowledge led to modifications of the synthetic process

to minimize the presence of the undesired diastereomers [6]. Later lots (produced using synthetic route 2) had significantly reduced amounts of the 8_D,9_L isomer, and only trace amounts of the 8_L,9_D isomer (Fig. 2D).

This paper demonstrates the use of limited enzymatic degradation of a peptide (RMP-7) to determine the ratios of diastereomers present in the peptide. Such an analysis is important for

those peptides whose manufacturing process might result in the presence of diastereomers. While the strategy of limited enzymatic digestion is not a general method of analysis, the limited digestions can be particularly useful in cases of peptides containing unusual components such as the reduced dipeptide bond in RMP-7. The limited digestions also have the advantage in that they employ non-chiral column supports and equipment that is present in most analytical laboratories.

Acknowledgments

The authors thank Timothy Curran for helpful discussions and William Kelley for his comments on the manuscript.

References

- [1] J.A. Straub, A. Akiyama and P. Parmar, *Pharmaceutical Res.*, in press.
- [2] T. Inamura, T. Nomura, R.T. Bartus and K.L. Black, *J. Neurosurgery*, in press.
- [3] Y. Sasaki, W.A. Murphy, M.L. Heiman, V.A. Lance and D.H. Coy, *J. Med. Chem.*, 30 (1987) 1162–1166.
- [4] J. Martinex, J.P. Bali, M. Rodriguez, B. Castro, R. Magous, J. Laur and M.F. Lignon, *J. Med. Chem.*, 28 (1985) 1874–1879.
- [5] D.H. Coy and Y. Sasaki, *Peptides*, 8 (1987) 119–121.
- [6] P.T. Ho, D. Chang, J.W.X. Zhong and G.F. Musso, *Peptide Res.*, 6 (1993) 10–12.
- [7] K.E. Rittle, C.F. Homnick, G.S. Ponticello and B.E. Evans, *J. Org. Chem.*, 47 (1982) 3016–3018.
- [8] M. Cushman, Y. Oh, T.D. Copeland, S. Oroszlan and S.W. Snyder, *J. Org. Chem.*, 56 (1991) 4161–4167.
- [9] A. Daniello, G. Donofrio and M. Pischetola, *Biochim. Biophys. Acta*, 1037 (1990) 200–208.
- [10] C. Celma and E. Giralt, *J. Chromatogr.*, 562 (1991) 447.
- [11] M. De Bondt, J. Couder, L. Van der Auwera, M. Van Marsenille, M. Elseviers and N. Delaet, *J. Chromatogr.*, 442 (1988) 165–173.
- [12] D. Regoli and J. Barabe, *Pharmacol. Rev.*, 32 (1980) 1–46.
- [13] G.P. Royer and J.P. Andrews, *J. Biol. Chem.*, 248 (1973) 1807–1812.
- [14] L.A.E. Sluyterman, *Biochim. Biophys. Acta*, 85 (1964) 305–315.
- [15] F.A. Bovey and S.S. Yanari, *Enzymes*, 4 (1960) 63–92.
- [16] A.N. Glazer, *J. Biol. Chem.*, 243 (1968) 1344–1348.



ELSEVIER

Journal of Chromatography A, 679 (1994) 93–98

JOURNAL OF
CHROMATOGRAPHY A

Complete purification of tRNA, charged or modified with hydrophobic groups, by reversed-phase high-performance liquid chromatography on a C₄/C₁₈ column system

Jeroen R. Mesters, Erik L.H. Vorstenbosch, Aldo J. de Boer, Barend Kraal*

Department of Biochemistry, Leiden University, P.O. Box 9502, 2300 RA Leiden, Netherlands

First received 7 February 1994; revised manuscript received 26 May 1994

Abstract

Phe-tRNA^{Phe}, N-acetyl-Phe-tRNA^{Phe} and Leu-tRNA^{Leu-4} (from brewer's yeast and *Escherichia coli*) were each separated with baseline resolution from the uncharged tRNA species by using a wide-pore C₄ column and inverse salt gradient elution. The alterations at the 3' end of the tRNAs result in a considerable shift of retention time on this column. The method is useful not only for obtaining tRNA preparations as required for poly(U) translational studies, but also for producing 20–50-mg amounts of tRNA for NMR and X-ray analysis. These aminoacylated species (charged by crude synthetase mixtures) can be purified from the crude tRNA mixtures in a one-step procedure.

1. Introduction

In protein synthesis, the aminoacyl-tRNA (aa-tRNA) molecules are the key to the decoding of the RNA messenger. A proper and productive interaction of aa-tRNA with the A site on the ribosome-mRNA complex is mediated by elongation factor (EF) Tu · GTP. The formation of the ternary complex EF-Tu · GTP · aa-tRNA and the tRNA-mRNA-ribosome interactions are of critical importance for an accurate peptide-chain elongation. Most studies on polypeptide-chain elongation are performed in poly(U) translating systems and require pure preparations of N-acetyl-Phe-tRNA^{Phe}, Phe-tRNA^{Phe},

deacylated tRNA^{Phe} and Leu-tRNA^{Leu-4} (for error frequency analysis). Large quantities are needed for NMR or crystallographic analysis of complexes such as EF-Tu · GTP · aa-tRNA. Purification of wild-type and mutant EF · Tu species for such purposes is fairly easy (for recent approaches see [1–4]). In contrast, it is more complicated to completely purify large quantities of specifically charged aminoacyl-tRNA as single species and in the literature we could not find an efficient and suitable procedure. We here describe a reversed-phase high-performance liquid chromatographic method with a wide-pore C₄ column for the efficient and large-scale purification of these charged and modified tRNA species from a crude mixture. This is the first comprehensive report on a methodology that can provide all the tRNA species necessary for

* Corresponding author.

poly(U) translation and error frequency analysis studies.

2. Materials and methods

2.1. HPLC instrumentation and methods

As HPLC-columns we used 250 × 4.6 mm I.D. Hypersil with 300 Å pore-size and 5 μm particles C₄ and C₁₈ columns from Phenomenex (Torrance, CA, USA). As guard columns we used 30 × 4.6 mm I.D. C₄ and C₁₈ Nucleosil columns from Macherey–Nagel (Düren, Germany) with the same particle and pore sizes.

The columns were operated at room temperature (about 20°C) on a Beckman System Gold HPLC system (Beckman Instruments, Fullerton, CA, USA). Gradient elution was performed with buffer A and buffer B, both containing 0.1 M potassium phosphate (final pH of 5.7), 1 mM sodium azide, and either 1.5 M ammonium sulphate or 4% 2-propanol, respectively. They were filtered through a Millipore HVLP filter (Millipore Intertech, Bedford, MA, USA), pore size 0.45 μm, prior to use. To increase reproducibility, each day buffer B was freshly prepared and 2-propanol was added *after* filtering. For HPLC analysis the samples were dissolved in 0.1 M potassium phosphate (pH 5.7), 1 mM sodium azide and 2 M ammonium sulphate prior to injection. The samples were eluted at a flow-rate of 0.75 ml/min using gradients as depicted in Figs. 1–3.

2.2. Isolation of crude tRNA synthetase mixtures

Crude tRNA synthetase mixtures were isolated from fresh baker's yeast (a kind gift of P.H.J. Mesters, Royal Gist Brocades, Delft, Netherlands) and *Escherichia coli* MRE600 (purchased from Porton Products, Maidenhead, UK). Cells were disrupted by grinding them in a mortar at 4°C with a double mass portion of alumina type A-5 (Sigma, St. Louis, MO, USA) and a trace of bovine pancreas deoxyribonuclease I (P-L Biochemicals, Milwaukee, WI,

USA). Thereafter, the paste was diluted with standard buffer (64 mM TrisHCl pH 7.6, 5 mM MgCl₂, 60 mM NH₄Cl, 10 mM 2-mercaptoethanol, 1 mM sodium azide) and the alumina was removed by centrifugation at 3000 g for 30 min. The supernatant was subjected to ammonium sulphate fractionation at 4°C: the fraction of interest, between 45 and 68% saturation, was collected by centrifugation at 14 000 g for 30 min. The precipitate was redissolved in, and dialysed against standard buffer. This fraction was applied to a DEAE-Sephadex column in standard buffer. After thorough washing with standard buffer, the column was eluted with 300 mM NaCl in standard buffer. Fractions with absorbance at 280 nm were pooled and the tRNA-free crude synthetases were precipitated (70% saturated ammonium sulphate), redissolved and dialysed against standard buffer with 5% glycerol and stored at –80°C. For both preparations the protein concentration was about 15 μg/μl as determined with the "Coomassie Protein Assay Reagent" kit from Pierce (Rockford, IL, USA).

2.3. Aminoacylation of tRNA

Crude tRNA mixtures from *E. coli* MRE600 and brewer's yeast were bought from Boehringer Mannheim (Mannheim, Germany) whereas pure *E. coli* tRNA^{Leu-4} (NAA), with 1.5 nmol of amino acid esterified per absorbance (260 nm) unit of tRNA, was bought from Subriden RNA (Rollingbay, Washington, DC, USA). Partially purified tRNA^{Phe} from brewer's yeast was obtained as described in the Results section.

The crude tRNA mixtures were aminoacylated at 37°C for 20 min, using 0.75 mg of the homologous crude synthetase mixtures per 300 absorbance (260 nm) units of crude tRNA mixture in 1 ml standard buffer containing 1 mM ATP, 0.1 mM CTP, 10 μg/ml pyruvate kinase, 5 mM phosphoenolpyruvate and 0.1 mM of each of the 17 amino acid as present in the "Amino Acid Standard H" mixture from Pierce.

The (partially) pure tRNA^{Phe} and tRNA^{Leu} preparations were aminoacylated at 37°C for 20

min, using 0.75 mg of the homologous crude synthetase mixture per 10 absorbance (260 nm) units of tRNA in 0.5 ml of the same reaction mixture as above but with 0.15 mM Phe or Leu instead of the amino acid mixture. The aminoacylated tRNAs were subjected to one phenol extraction, followed by three times ethanol precipitation at -80°C for 30 min. The precipitates were lyophilised, in order to avoid interference by traces of ethanol with the proper elution of the tRNAs from the C_4 column.

Acetylation of the α -amino group of Phe-tRNA was carried out as described in Ref. [5].

3. Results

3.1. The effect of aminoacylation and acetylation on the retardation of tRNA on a C_4 column

Aminoacylation or modification of tRNA with hydrophobic groups might significantly influence its retention on a C_4 column. Accordingly Fig. 1 shows optimized separation of charged and acetylated partially purified brewer's yeast tRNA^{Phe}. In a control experiment, the acetylation procedure itself has no effect on the retention time of uncharged tRNA^{Phe}. In the same way, aminoacylation of tRNA^{Leu} retards its migration significantly (Fig. 2). The elution order is tRNA^{Phe}, tRNA^{Leu}, Phe-tRNA^{Phe}, Leu-tRNA^{Leu} and N-acetyl-Phe-tRNA^{Phe}, according to increasing hydrophobicity. To further investigate the effect of aminoacylation on the retardation of tRNA, we also compared crude uncharged *E. coli* tRNA with the same tRNA mixture charged in the presence of only phenylalanine, only leucine or the "Amino Acid Standard H" mixture (17 different amino acids). All the elution patterns are shown in Fig. 3. The Phe-tRNA^{Phe} is clearly visible as a new peak beyond the bulk of uncharged tRNAs. The same is true for the aminoacylation of two out of the six iso-acceptors of tRNA^{Leu}. Similar results were obtained with a crude brewer's yeast tRNA mixture and phenylalanine (not shown).

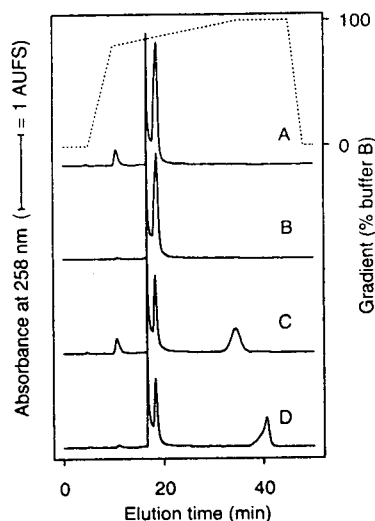


Fig. 1. The effect of aminoacylation and acetylation on the retention time of tRNA^{Phe} from brewer's yeast. Elution patterns of non-aminoacylated (A, B) and aminoacylated (C, D) tRNA of about 2 absorbance (258 nm) units are shown, before (A, C) or after (B, D) acetylation with acetic anhydride. The retention times of residual traces of ATP and phenol are about 7 and 11 min, respectively. The dotted line indicates the elution gradient of buffers A and B. For further details see Materials and methods.

3.2. Collecting the C_4 column effluent directly on an in-line C_{18} column

The tRNA peaks cannot simply be recovered by ethanol precipitation because of coprecipitation of considerable amounts of sulphate and phosphate salts that are present in the column effluent. We therefore developed a new strategy

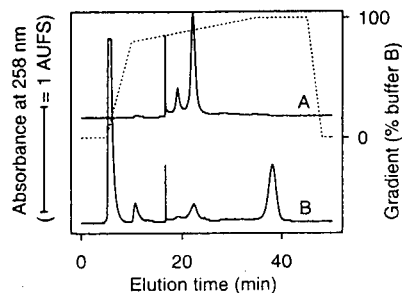


Fig. 2. The influence of aminoacylation on the retention time of tRNA^{Leu-4} from *E. coli*. Elution patterns of non-aminoacylated (A) and aminoacylated (B) tRNA samples of about 1 absorbance (258 nm) unit are shown (see caption to Fig. 1).

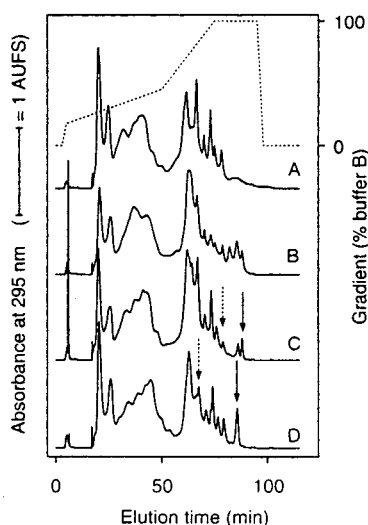


Fig. 3. The resolution of aminoacylated tRNAs from *E. coli*. Elution patterns are shown of samples [about 300 absorbance (258 nm) units each] of non-aminoacylated crude tRNAs (A) or tRNA aminoacylated in the presence of either the "Amino Acid Standard H" mixture (B), leucine (C) or phenylalanine (D). For tRNA^{Leu-4} (C) and tRNA^{Phe} (D), the positions of uncharged (dotted arrow) and charged (solid arrow) species are indicated (see caption to Fig. 1).

by connecting one or several wide-pore C₁₈ columns via a switching valve to the outlet of the detector (Fig. 4). In this way, the peak (or peaks) of interest can be loaded in-line onto the C₁₈ column(s). The macromolecules in the C₄ column effluent will again bind to the C₁₈ column because its matrix is much more hydrophobic. One or more other peaks can be collected onto a subsequent C₁₈ column and used for other purposes. After the C₄ run is finished, each C₁₈ column is in turn directly connected to the HPLC pump, thoroughly washed with distilled water, and the absorbed tRNA is eluted with 35% (v/v) ethanol. Finally, the collected tRNA can be concentrated by simple ethanol precipitation with 70% (v/v) ethanol or by

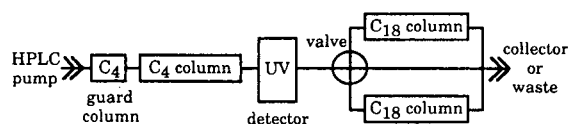


Fig. 4. Schematic illustration of the C₄/C₁₈ chromatographic system for the preparative isolation of tRNAs.

lyophilisation, whichever is more convenient. Both aminoacyl- and acetylaminoacyl-tRNA can be recovered without significant deacylation as judged by an analytical run on a C₄ column. Very satisfying results are also obtained with a preparative C₄ column (250 × 22.5 mm I.D.) for large-scale isolations of tRNA^{Phe}. For example, the uncharged but partially purified brewer's yeast tRNA^{Phe} [of about 0.9 nmol of phenylalanine esterified per absorbance (260 nm) unit] that we used in this paper, was isolated from crude brewer's yeast tRNA [about 55 pmol of phenylalanine esterified per absorbance (260 nm) unit] with a yield of 80% according to the methodology described above (see Fig. 1).

4. Discussion and conclusions

Although the isolation of some species of non-aminoacylated tRNA is relatively easy and well documented (see for example [6–8] and references cited therein), this is less so for aminoacylated tRNA, whereas for certain applications the availability of pure and fully aminoacylated tRNA preparations is essential. In some methods of aa-tRNA purification, affinity chromatography on a column with immobilized EF-Tu is used [9,10] and in other cases use is made of mixed-mode columns [7,11] or C₁₈ columns [12]. However, there are several important drawbacks to these procedures. Except for the C₁₈ support, the columns are not commercially available and laborious to prepare. In the mixed-mode methodologies the tRNA cannot simply be recovered by ethanol precipitation (as discussed further on). Additional drawbacks of the affinity chromatography methodology are (a) the large amounts of expensive EF-Tu that are needed for the coupling to the matrix, (b) the relatively short durability of the affinity column (several months), (c) the inability to separate iso-accepting tRNA species after aminoacylation, and (d) the inability to separate uncharged from N-acetylated aminoacyl-tRNA. The normal-pore (100 Å) C₁₈ HPLC columns lack sufficient tRNA-binding capacity [for a 300 × 3.9 mm I.D. column this is only 50 absorbance (260 nm)

units], although they can separate complex mixtures of uncharged tRNA species as shown recently [13].

In our view the wide-pore C_4 column is the optimal choice for the purification of tRNA charged or modified with hydrophobic groups (see also [14]). In addition to the high level of resolution (see Figs. 1–3), the wide-pore C_4 column is durable and has a relatively large binding capacity: the 250×4.6 mm I.D. Hypersil 300-5 C_4 column can be loaded with 600 absorbance (260 nm) units of tRNA. This is much more than the 10–20 absorbance (260 nm) units of tRNA a 100 \AA C_4 column of the same dimensions can handle [15]. This can be explained by the diameter of the tRNA molecule which is about 75 \AA (see also the 100 \AA pore C_{18} column mentioned above).

The main bottleneck of previous mixed-mode and C_4 HPLC methods is the somewhat inefficient and time-consuming diafiltration or precipitation procedure [7,14,15] of the pooled tRNA fractions. Especially for aa-tRNA with its labile ester bond, a fast isolation procedure is commendatory. The in-line C_{18} column (see Fig. 4) provides an adequate solution. Now, Phe-tRNA^{Phe}, N-acetyl-Phe-tRNA^{Phe} and Leu-tRNA^{Leu-4} can individually be separated from the bulk of tRNAs (Figs. 2 and 3) and immediately loaded onto the C_{18} column. This dramatically simplifies the purification of amounts up to 1 mg of these charged species. For NMR and X-ray applications large amounts (20–50 mg) of aa-tRNA are needed and the desired species of non-aminoacylated tRNA can be collected on an in-line C_{18} column with repetitive sample applications of the crude tRNA mixture on the C_4 column. The collected enriched tRNA fraction is afterwards aminoacylated and separated from non-aminoacylated tRNA as described. The method may be of more general use, because the relatively large effects of aminoacylation and N-acetylation on the retention time point to an exposed position of both the amino acid side chain and the N-acetyl group. For example, tyrosine has a similar effect as phenylalanine (results not shown) and also Trp-tRNA was recently found at a retarded position on a 100 \AA

C_4 column [15]. The change in retention time may also reflect changes in the overall three-dimensional structure of the tRNA molecule upon charging and modification.

It is important to check the technical specifications of the detector cell for the increased back pressures. A proper choice of the dimensions and specifications (pore and particle size) of the C_{18} column can thus be made. In our case the C_{18} column has a back pressure of about 4.5 MPa at a flow-rate of 0.75 ml/min whereas the Beckman 166 detector module can withstand pressures up to 7 MPa.

In conclusion, the in-line combination of both a wide-pore C_4 and C_{18} column provides an efficient system for the purification of tRNA charged or modified with hydrophobic groups. The above described methodology can provide all the tRNA species necessary for poly(U) translation studies. The same approach may be successful for the purification of other tRNA species as well. It can easily be scaled up to meet the quantitative and qualitative requirements of NMR or X-ray experiments.

Acknowledgement

E.L.H.V. was supported by a grant from the Netherlands Foundation for Chemical research (SON).

References

- [1] K. Boon, E. Vijgenboom, L.V. Madsen, A. Talens, B. Kraal and L. Bosch, *Eur. J. Biochem.*, 210 (1992) 177.
- [2] C.R. Knudsen, B.F.C. Clark, B. Degn and O. Wiborg, *Biochem. Int.*, 28 (1992) 353.
- [3] J.R. Mesters, J.M. de Graaf and B. Kraal, *FEBS Lett.*, 321 (1993) 149.
- [4] L.A.H. Zeef and L. Bosch, *Mol. Gen. Genet.*, 238 (1993) 252.
- [5] A.-L. Haenni and F. Chapeville, *Biochim. Biophys. Acta*, 114 (1966) 135.
- [6] I. Gillam, S. Millward, D. Blew, M. von Tigerstrom, E. Wimmer and G.M. Tener, *Biochemistry*, 6 (1967) 3043.
- [7] R. Bischoff and L.W. McLaughlin, in C.W. Gehrke and K.C.T. Kuo (Editors), *Chromatography and Modification of Nucleosides, Part A*, Elsevier, Amsterdam, 1990, p. 73.

- [8] G. Keith, in C.W. Gehrke and K.C.T. Kuo (Editors), *Chromatography and Modification of Nucleosides, Part A*, Elsevier, Amsterdam, 1990, p. 103.
- [9] A. Louie, E. Masuda, M. Yoder and F. Jurnak, *Anal. Biochem.*, 141 (1984) 402.
- [10] M. Sprinzl and K.H. Derwenskus, in C.W. Gehrke and K.C.T. Kuo (Editors), *Chromatography and modification of nucleosides, Part A*, Elsevier, Amsterdam, 1990, p. 143.
- [11] R.D. Ricker and A. Kaji, *Anal. Biochem.*, 175 (1988) 327.
- [12] O.W. Odom, H.-Y. Deng and B. Hardesty, *Methods Enzymol.*, 164 (1988) 174.
- [13] D. Kanduc, *Nucl. Acids Res.*, 21 (1993) 2778.
- [14] B.S. Dudock, in M. Inouye and B.S. Dudock (Editors), *Molecular Biology of RNA: New Perspectives*, Academic Press, San Diego, CA, 1987, p. 321.
- [15] H. Xue, W.Y. Shen and J.T.F. Wong, *J. Chromatogr.*, 613 (1993) 247.



ELSEVIER

Journal of Chromatography A, 679 (1994) 99–104

JOURNAL OF
CHROMATOGRAPHY A

Determination of copper(II) chlorophyllin by reversed-phase high-performance liquid chromatography

H. Inoue^{a,*}, H. Yamashita^a, K. Furuya^a, Y. Nonomura^a, N. Yoshioka^a, S. Li^b

^aDepartment of Applied Chemistry, Keio University, 3-14-1 Hiyoshi, Kohoku-ku, Yokohama 223, Japan

^bDepartment of Technological Physics, Peking University, Beijing 100871, China

First received 6 April 1994; revised manuscript received 14 June 1994

Abstract

Copper(II) chlorophyllin, consisting of copper(II) pheophorbide *a*, copper(II) chlorin *e*₆, copper(II) rhodin *g*₇ and copper(II) chlorin *e*₄, was prepared and separated by semi-preparative high-performance liquid chromatography (HPLC). The components of copper(II) chlorophyllin were determined on a reversed-phase Inertsil ODS-2 column using a mobile phase of methanol–water (97:3, v/v) containing 1% (v/v) of acetic acid. Linear calibration plots were obtained for copper(II) chlorophyllin in the concentration range of 0–30 $\mu\text{g cm}^{-3}$ with photometric detection at 407 or 423 nm. The detection limits of copper(II) pheophorbide *a*, copper(II) chlorin *e*₆, copper(II) rhodin *g*₇ and copper(II) chlorin *e*₄ were 3.5, 1.5, 3.3 and 1.4 ng cm^{-3} with relative standard deviations ($n = 10$) of 1.8, 1.6, 5.2 and 3.6%, respectively. The reversed-phase HPLC method proposed here was demonstrated to be useful for the determination of the components of sodium copper(II) chlorophyllin.

1. Introduction

In recent years metallochlorophyllins have received a great deal of attention because of their importance in food additives, pharmaceuticals and electrode materials of photoelectron conversion. Sodium copper(II) chlorophyllin is utilized as food additive due to its high light-stability and applied to medicine owing to its antioxidative effect [1,2]. Some kinds of copper(II) chlorophyllins, including copper(II) pheophorbides, are useful in the functionalized electrode for artificial photosynthetic systems [3]. Commercially available sodium copper(II) chlorophyllins consist of a few kinds of copper(II)

chlorophyll derivatives, e.g. copper(II) pheophorbide *a*, copper(II) chlorin *e*₆, copper(II) chlorin *e*₄, copper(II) rhodin *g*₇ and their degradation products (cf. Fig. 1). Spectrophotometry, widely used for the determination of metallochlorophyllins, is insufficient for the accurate determination of each component of sodium copper(II) chlorophyllin, because all components have similar absorption spectra. Recently high-performance liquid chromatography (HPLC) without any time-consuming pretreatment techniques prior to the quantitation step has been exploited for zinc(II) chlorophyllin [4]. The potential usefulness of HPLC has been demonstrated for the separation and determination of metallochlorophylls such as iron(III) [5], nickel(II) [6], copper(II) [7] and zinc(II)

* Corresponding author.

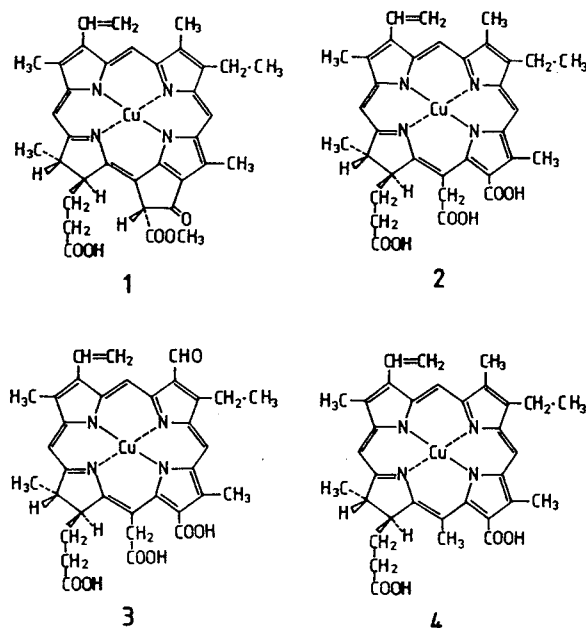


Fig. 1. Structures of copper(II) chlorophyllin components. 1 = Copper(II) pheophorbide *a*; 2 = copper(II) chlorin *e*₆; 3 = copper(II) rhodin *g*₇; 4 = copper(II) chlorin *e*₄.

chlorophylls [8]. The present study has focused on both the preparation of pure copper(II) chlorophyllin by semi-preparative HPLC and rapid and accurate determination of each component of copper(II) chlorophyllin by analytical HPLC. A development of the preparation and purification method of copper(II) chlorophyllin would provide a basis for a comparison of its spectroscopic and structural properties and reveal its previously unrecognized functions.

2. Experimental

2.1. Reagents and instruments

All chemicals were of analytical-reagent grade and used as supplied without further purification. Pheophorbides *a* and *b*, chlorin *e*₆ and rhodin *g*₇ were prepared according to the method of Hyninen [9]. Chlorin *e*₄ was prepared from chlorin *e*₆ by a modification of the literature method [10]. Organic solvents were purchased from Kanto Chemical and of LC quality. The JASCO

BIP-1 liquid chromatograph, equipped with a Uvidec-1000 variable-wavelength UV-Vis detector or a JASCO MULTI-340 multichannel detector, a Shimadzu C-R3A chromatopac integrator, an Inertsil ODS-2 column (5- μ m spherical ODS, 250 mm \times 4.6 mm I.D., Gasukuro Kogyo), and a Rheodyne Model 7125 injector with a 20-mm³ injection loop, was used for analytical HPLC. A semi-preparative Develosil ODS column (10- μ m spherical octadecyl silica, 25 cm \times 3 cm I.D., Nomura Chemical, Aichi, Japan) equipped with a Kusano-Kagaku KV-3W loop injector (0.59 cm³) was used for semi-preparative HPLC. Each HPLC solvent or solvent mixture was filtered through a fresh 0.45- μ m hydrophilic Millipore filter and degassed every time before use by ultrasonically vibrating the solvent container. The flow-rate of the analytical HPLC was 1.4 cm³ min⁻¹, the inlet pressure was 5.0–10 MPa depending on the mobile phase and the analytes were usually detected at 407 nm. The column temperature was set at 35°C by dipping the analytical column in a thermostat bath. The electronic absorption spectra were recorded with a Hitachi U-2000 spectrophotometer using 1-cm quartz cells. The mass spectra of copper(II) chlorophyllin were measured with a JEOL JMS-AX505H fast atom bombardment (FAB) mass spectrometer.

2.2. Preparation of copper(II) chlorophyllin

Copper(II) pheophorbide *a* was prepared by adding a 5-fold molar excess of Cu(CH₃COO)₂ · H₂O (8.4 mg) to pheophorbide *a* (5 mg) in 10 cm³ of glacial acetic acid. The reaction mixture was stirred at 20°C for 15 min and the extent of insertion reaction was monitored spectrophotometrically via the Soret band of copper(II) pheophorbide *a* (λ_{max} , 423 nm). The reaction mixture was allowed to cool, followed by addition of 20 cm³ of chloroform. The mixed solution was washed five times with distilled water to remove the residual copper(II) acetate and acetic acid. The dark green chloroform solution was concentrated by rotary evaporation to obtain copper(II) pheophorbide *a*. The copper(II) pheophorbide *a* obtained was purified with a

semi-preparative Develosil ODS column at a flow-rate of $7.4 \text{ cm}^3 \text{ min}^{-1}$. All operations were carried out in the dark under an argon atmosphere at an ambient temperature of 20°C . Copper(II) chlorin e_6 , copper(II) rhodin g_7 and copper(II) chlorin e_4 were prepared in a manner similar to that for copper(II) pheophorbide a .

2.3. Analytical procedures

A $50 \mu\text{g cm}^{-3}$ stock solution of each copper(II) chlorophyllin component was prepared in glass-stoppered volumetric flasks, which were then sealed and stored at 5°C in the dark. Standard solutions for calibration graphs were prepared with a solvent composition as near to the sample solution as possible, by diluting the appropriate volume of the stock solution with a mixture of methanol–water (97:3, v/v) containing 1% (v/v) of acetic acid. All the samples of commercially available sodium copper(II) chlorophyllin were treated as follows. A certain amount of sodium copper(II) chlorophyllin (30 mg) was dissolved in 40 cm^3 of distilled water. After the pH value of the aqueous solution was adjusted to 2.3 with 0.1 M hydrochloric acid (30 cm^3), 40 cm^3 of diethyl ether was added to the copper(II) chlorophyllin solution. Copper(II) chlorophyllin was extracted by vigorously shaking and the ether layer was washed five times with distilled water. Then the extract was brought to dryness by rotary evaporation and subjected to the HPLC determination of each

copper(II) chlorophyllin component. All sample solutions were filtered prior to injection into the chromatograph with a Toyo Roshi DISMIC-25JP filter ($0.45 \mu\text{m}$).

3. Results and discussion

3.1. Preparation and identification of copper(II) chlorophyllin

Copper(II) chlorophyllin is usually available as sodium salt and a mixture of copper(II) chlorin e_6 , copper(II) rhodin g_7 and their degradation products. A preliminary study revealed that most of commercially available copper(II) chlorophyllin preparations consists of copper(II) pheophorbide a , copper(II) chlorin e_6 and copper(II) rhodin g_7 [11]. In fact a few chromatographic peaks were observed on a typical three-dimensional chromatogram measured for commercially available copper(II) chlorophyllin (cf. Fig. 2). In order to identify and determine each peak component on the high-performance liquid chromatogram, copper(II) pheophorbide a , copper(II) chlorin e_6 , copper(II) rhodin g_7 and copper(II) chlorin e_4 were prepared according to the methods described under Experimental. Each component of copper(II) chlorophyllin thus prepared was purified by semi-preparative HPLC and then the absorption spectrum was measured in a solution of methanol–water (97:3, v/v) containing 1% (v/v) of acetic acid. The absorption spectra of the components of cop-

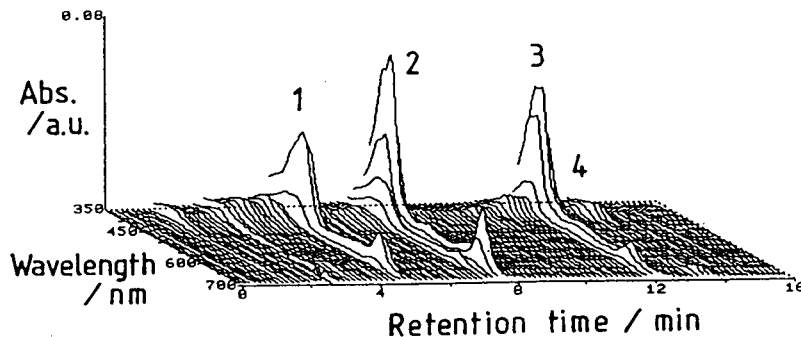


Fig. 2. Three-dimensional chromatogram of copper(II) chlorophyllin. Peaks: 1 = copper(II) rhodin g_7 ; 2 = copper(II) chlorin e_6 ; 3 = copper(II) chlorin e_4 ; 4 = copper(II) pheophorbide a .

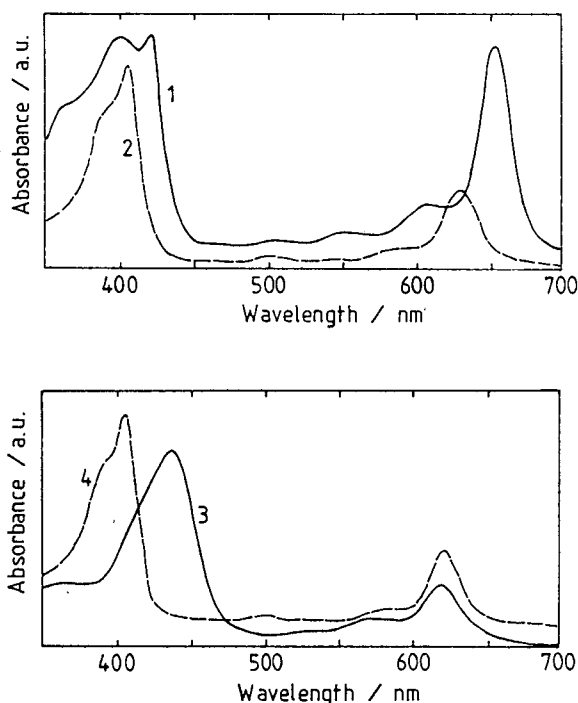


Fig. 3. Absorption spectra of copper(II) chlorophyllin components. 1 = Copper(II) pheophorbide *a*; 2 = copper(II) chlorin *e*₆; 3 = copper(II) rhodin *g*₇; 4 = copper(II) chlorin *e*₄.

per(II) chlorophyllin are shown in Fig. 3, and the spectral data are summarized in Table 1. All spectra are very similar to each other, but slightly different in the spectral shape and ab-

sorption maxima. Each peak component on the chromatogram of copper(II) chlorophyllin was fractionated and carefully concentrated by a rotary evaporator. The sample obtained by evaporating the residual acetic acid was subjected to FAB mass spectrometry to identify each peak component. The mass spectrum of each fraction showed the presence of the chlorophyllin component with a molecular ion M^+ : copper(II) chlorin *e*₆, 657 (M^+ , 45%); copper(II) chlorin *e*₄, 613 (M^+ , 65%). Each peak component on the chromatogram was also identified by a comparison of the retention times with those of the corresponding pure compounds and the absorption spectra.

3.2. Chromatographic separation of copper(II) chlorophyllin

Commercially available sodium copper(II) chlorophyllin is soluble in water, but hardly distributed to octadecyl silica(ODS). Therefore, it is necessary to convert sodium metallochlorophyllins to their corresponding carboxylic acids by the release of sodium ions using hydrochloric acid. Octadecyl silica was selected as a stationary phase in combination with a mobile phase of methanol–water (97:3, v/v). The best separation and retention of copper(II) chlorophyllin were achieved using a mobile phase of methanol–water (97:3, v/v) containing 1% (v/v) of acetic acid. The small amount of acetic acid

Table 1
Absorption maxima and molar extinction coefficients (ϵ) of copper(II) chlorophyllin components

Compound	λ_{\max} (nm)		$\epsilon \times 10^4$ (cm ⁻¹ mol ⁻¹ dm ³)	
	Soret band	Q band	Soret band	Q band
Copper(II) pheophorbide <i>a</i>	401, 423	653	5.14, 4.86	4.71
Copper(II) chlorin <i>e</i> ₆	407	633	8.08	3.20
Copper(II) rhodin <i>g</i> ₇	436	622	4.35	1.38
Copper(II) chlorin <i>e</i> ₄	404	626	2.70	0.95

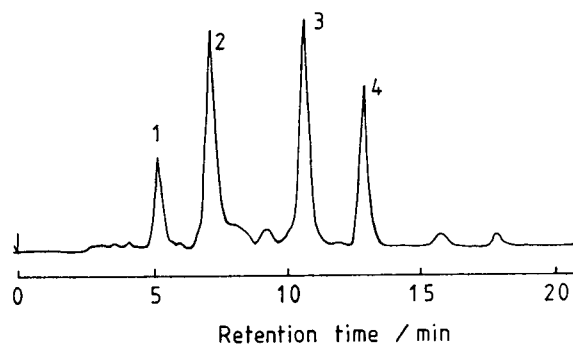


Fig. 4. Typical chromatogram of copper(II) chlorophyllin. Peaks: 1 = copper(II) rhodin g_7 ; 2 = copper(II) chlorin e_6 ; 3 = copper(II) chlorin e_4 ; 4 = copper(II) pheophorbide a .

was added to the mobile phase to prevent the liberation of protons at the carboxyl group. A typical high-performance liquid chromatogram of copper(II) chlorophyllin is shown in Fig. 4. Four well-resolved peaks were obtained using UV detection at 423 nm and copper(II) rhodin g_7 , copper(II) chlorin e_6 , copper(II) chlorin e_4 and copper(II) pheophorbide a eluted in the order given. The retention time of copper(II) chlorophyllin decreases with the increasing number of carboxyl groups, indicating that the carboxyl group attached to the chlorin ring allows greater interactions with the mobile phase. As expected, rhodin g_7 is eluted fast compared with chlorin e_6 due to less interaction of the former with the non-polar ODS stationary phase. This elution order agrees with the general tendency that the

aldehyde group attached to the chlorin ring is more polar than the methyl group.

3.3. Determination of copper(II) chlorophyllin

The preparation of working standard solutions by diluting the stock solution in methanol–water (97:3, v/v) yielded a standard solution of copper(II) chlorophyllin which was stable over 24 h. The calibration graphs for four components of copper(II) chlorophyllin were constructed in the concentration range of 0–30 $\mu\text{g cm}^{-3}$. The minimum detectable concentrations of copper(II) pheophorbide a , copper(II) chlorin e_6 , copper(II) rhodin g_7 and copper(II) chlorin e_4 were 3.5, 1.5, 3.3 and 1.4 ng cm^{-3} with relative standard deviations ($n = 10$) of 1.8, 1.6, 5.2 and 3.6% at a concentration level of 1 $\mu\text{g cm}^{-3}$, respectively. They were calculated from that amount of copper(II) chlorophyllin which yielded a signal-to-noise (S/N) ratio of 2. The HPLC method proposed here was applied to the assay of commercially available sodium copper(II) chlorophyllin. The analytical results obtained for samples A–D are summarized in Table 2. The sum total of the analytical values of individual components is less than 100% (w/w), because the samples assayed are contaminated by degradation products other than copper(II) chlorophyllin which was identified in the present study. It is noteworthy that one of the most abundant components in commercial sodium copper(II) chlorophyllin is chlorin e_4 . The chlorophyll a in

Table 2
Analytical results on commercially available sodium copper(II) chlorophyllin

Sample	Content (% w/w)			
	Copper(II) pheophorbide a	Copper(II) chlorin e_6	Copper(II) rhodin g_7	Copper(II) chlorin e_4
A	8.7 (0.1)	8.0 (0.2)	10.1 (0.2)	57.1 (1.1)
B	17.1 (0.2)	3.7 (0.2)	10.7 (0.2)	60.2 (2.4)
C	5.4 (0.1)	8.4 (0.3)	9.0 (0.2)	34.7 (1.0)
D	3.8 (0.1)	13.2 (0.1)	6.7 (0.1)	56.6 (0.6)

The number in parentheses is the standard deviation of the analytical values ($n = 5$).

the starting material of copper(II) chlorophyllin must be converted to copper(II) chlorin e_4 in the course of the production processes. This is supported by the fact that the starting material of copper(II) chlorophyllin contains much chlorophyll a compared with chlorophyll b and chlorin e_4 is easily derived from pheophorbide a or chlorin e_6 . The HPLC method described above has been applicable to commercially available sodium copper(II) chlorophyllin. Consequently, it will be very useful for the evaluation of food additives and effective to the study of the antioxidative and antimutagenic components in metallochlorophyllins.

Acknowledgements

This work was partially supported by a Grant-in-Aid for scientific research, No. 06453071, from the Ministry of Education, Science and Culture, Japan.

References

- [1] M. Ishidate and A. Tanimura, *Shokuhintenkabutsu-Kouteisho-Kaisetsusho*, Hirokawa Shoten, Tokyo, 1979, pp. B-655, B-678.
- [2] M. Sato, I. Fujimoto, T. Sakai, R. Kimura and T. Murata, *Yakugaku Zasshi*, 99 (1979) 1055.
- [3] T. Watanabe, K. Machida, H. Suzuki, M. Kobayashi and K. Honda, *Coord. Chem. Rev.*, 64 (1985) 207.
- [4] H. Yamashita and H. Inoue, *Anal. Sci.*, 7 Suppl. (1991) 1371.
- [5] K. Furuya, H. Inoue and T. Shirai, *Anal. Sci.*, 3 (1987) 353.
- [6] K. Furuya, N. Ohki, H. Inoue and T. Shirai, *Chromatographia*, 25 (1988) 319.
- [7] H. Inoue, K. Furuya, K. Watanabe, K. Tanaka, T. Shirai and E. Miyoshi, *Anal. Sci.*, 4 (1988) 599.
- [8] H. Inoue, M. Imai, T. Naemura, K. Furuya and Y. Shizuri, *J. Chromatogr.*, 645 (1993) 259.
- [9] P.H. Hynninen, *Acta Chem. Scand.*, 27 (1973) 1771.
- [10] H. Fischer, J. Heckmaier and E. Plots, *Justus Liebigs Ann. Chem.*, 500 (1933) 215.
- [11] K. Furuya, H. Inoue and T. Shirai (edited by Shokuhin-kagaku-Kenkyukai), *Shokuhin-Bunseki Data Book*, Vol. 1, Tokyo, 1988, p. 78.

Comparison of isocratic and gradient elution reversed-phase behaviour of high-molecular-mass polystyrenes in dichloromethane and acetonitrile

Ross Andrew Shalliker^a, Peter Edwin Kavanagh^{a,*}, Ian Maxwell Russell^b

^a*School of Biological and Chemical Sciences, Deakin University, Waurn Ponds, Victoria 3217, Australia*

^b*CSIRO Division of Wool Technology, Belmont, Victoria 3216, Australia*

First received 10 May 1994; revised manuscript received 27 May 1994

Abstract

Isocratic and gradient elution of high-molecular-mass polystyrenes were compared in a dichloromethane–acetonitrile mobile phase and C₁₈ bonded phase on a variety of different pore size silicas. Plots of the capacity factor versus the solvent composition were drawn from which solvent strength parameters, *S*, were determined for different molecular masses. Linear gradient elution data were also used to estimate *S* values using a graphical procedure. It was found that *S* depended on gradient rate and that only gradient rates of less than 2%/min gave constant values of *S*. Only molecular masses less than 50 000 gave good agreement with isocratic values. Plots of log *S* against log molecular mass were different for isocratic and gradient determined values of *S*.

1. Introduction

Several studies are reported [1] to have shown that the log of the isocratic capacity factor, *k'* varies linearly with φ , the volume fraction of good solvent, for low-molecular-mass compounds in water–methanol and water–acetonitrile reversed-phase solvent systems. The empirical relationship initially discussed by Snyder and co-workers [2,3] is

$$\log k' = \log k_0 - S\varphi \quad (1)$$

where *k*₀ is capacity factor in the poor solvent and *S* is a constant. Aguilar and Hearn [4] have proposed that the constant *S* is related to the

contact area of the molecule with the stationary phase surface and that log *k*₀ values reflect the affinity of the solute for the poorer solvent. Schoenmakers et al. [5,6] have argued on theoretical grounds that a quadratic relationship is more precise but that for normal operating conditions in an analytical separation, any differences would be negligible for low-molecular-mass compounds. With high-molecular-mass compounds the situation is less clear. Hearn [7] has clearly shown that plots of log *k'* against φ are curved due to two different modes of adsorption for peptides and proteins over large ranges of φ . Nevertheless, they have continued to use Eq. 1 over narrow ranges of φ . Polystyrenes are non-polar and would not be expected to show silanophilic interactions as do

* Corresponding author.

peptides and proteins. However, as the proportion of good solvent in the mobile phase increases, the capacity factors are expected to go to zero as size-exclusion chromatography becomes dominant.

Using gradient elution data to determine S and k_0 is of special importance in the reversed-phase separation of high-molecular-mass synthetic polymers because, as the molecular mass increases, isocratic elution becomes more and more difficult to observe [8–11] and the direct application of Eq. 1 is difficult. Nevertheless, Lochmuller and McGranaghan [9] have been able to compare isocratically obtained values of S with gradient estimated values S for polystyrenes up to M_r 300 000 in a dichloromethane–acetonitrile solvent system. They found linear relationships between $\log k'$ and solvent composition for both tetrahydrofuran–water and dichloromethane–acetonitrile solvent systems using a 10 nm pore size, C_{18} column. A 30 nm pore size C_8 bonded phase column also gave a linear plot. Using this column, agreement between isocratic and gradient S values was good, for both the dichloromethane–acetonitrile and the tetrahydrofuran–water systems. Gradient rates were between 1.6 and 5.0%/min. Alhedai et al. [10] investigated polystyrenes up to M_r 390 000 in dichloromethane–methanol with 10 nm and 30 nm pore size C_{18} columns. They found a non-linear relationship between \log capacity factor and mobile phase composition. They also found poor agreement between isocratic and gradient estimated values of S . The gradient estimated values of S were considerably higher than the isocratic values but agreement improved as molecular mass increased. The gradient rates used were 2 to 4% dichloromethane per minute. Larman et al. [8] investigated the gradient elution of polystyrenes on four different pore size C_{18} columns, in a tetrahydrofuran–methanol mobile phase but only up to a molecular mass of 50 000. They found reasonable agreement between isocratic and gradient derived S values. Gradient rates up to 15%/min were used. Later work by Quarry et al. [12] reexamined this work and concluded that better results were obtained when two well separated

gradient rates were used to estimate S and k_0 . However, the highest gradient rate used in this later study was lowered to 2%/min.

Hearn [7] has found little correlation of S with molecular mass for peptides and proteins. However, this is to be expected in adsorption type chromatography of polymers with different chemical structures. All workers have found that S generally increases with molecular mass for synthetic polymers with the same chemical structure. Boehm et al. [13,14] found this increase to be monotonic for polystyrenes in both the dichloromethane–methanol and tetrahydrofuran–acetonitrile solvent systems. However, Lochmuller and McGranaghan [9] found a monotonic increase in S with molecular mass for a 30 nm pore size C_8 column but not with a 10 nm pore size C_{18} column. They attributed this to available surface area effects. The BMAB theory [13–15] predicts that the slope of a $\log S$ versus $\log M$ plot should be one. However, all results reported so far, are lower than one.

When linear solvent strength (LSS) gradients [3] are used, Eq. 1 can be used to predict isocratic retention data from two or more gradient elution experiments [12]. The gradient steepness parameter, b , is proportional to S and given by

$$b = \Delta\phi St_0/t_G \quad (2)$$

where $\Delta\phi$ is the change in the gradient in time t_G and t_0 is the column void volume. To determine S and k_0 for a solute, this relationship can be combined with Eq. 1 to give

$$t_g = (t_0/b) \log [2.3bk_0(t_s/t_0) + 1] + t_s + t_d \quad (3)$$

where t_g is the solute gradient elution time, t_s is the retention time of the solute under non-retained conditions and t_d the delay time of the gradient to column inlet [8]. Larman et al. [8] used an iterative method to estimate average values for S and k_0 . Lochmuller and McGranaghan [9] used two gradient runs to solve for the two unknowns. Alhedai et al. [10] used a graphical method which allowed them to estimate S and the critical solvent composition from the gradient data. The critical solvent

composition was defined as the composition when $k' = 1$.

The aim of this paper is to report a simple graphical procedure for estimating S and k_0 from gradient elution data and to compare S values for polystyrenes determined by both isocratic and gradient elution. The results were obtained using C_{18} bonded phases in a dichloromethane–acetonitrile solvent system, and were conducted over a wider range of molecular masses and column pore sizes than previous work. A column packed with pellicular material is included.

2. Experimental

All chromatographic experiments were performed using two M6000A pumps, a 660 solvent programmer and a U6K injector (Waters, Milford, MA, USA). The detector was a variable wavelength UVIS 200 set at 262 nm (Linear Instruments, NV, USA). Column temperature was maintained at 25°C in a thermostatted water jacket. In this work, flow-rates were 1.0 ml/min unless otherwise stated. All gradients were linear and started at 0.4 volume fraction of dichloromethane. Injection mass was 10 μ g. Injection volume was 10 μ l. Data acquisition was done with a laboratory-built system. Table 1 lists the columns that were used throughout this study. All columns were packed at 400×10^6 Pa into 150 mm \times 4.6 mm diameter column blanks. These columns are described in more detail elsewhere [16].

Acetonitrile and dichloromethane (HPLC

grade) were obtained from Mallinckrodt Australia. The monodisperse polystyrene standards used were molecular masses $2.35 \cdot 10^3$, $1.1 \cdot 10^5$, $2.0 \cdot 10^5$ (Waters) and $9.00 \cdot 10^3$, $1.75 \cdot 10^4$, $5.0 \cdot 10^4$, $4.10 \cdot 10^5$ and $9.29 \cdot 10^5$ (Polysciences, Warrington, PA, USA).

In the present study, the parameters S and k_0 were determined by the following graphical method. Rearranging Eq. 2 gives

$$t'_G = \left(\frac{t_G}{\Delta\varphi} \right) = S \left(\frac{t_0}{b} \right) \quad (4)$$

where t'_G is the gradient time from 0 to 100%.

If $t'_g = t'_g - t_s - t_d$, the gradient elution time corrected for size exclusion and gradient delay, then by substitution of Eq. 4 and t'_g into Eq. 3 we obtain,

$$t'_g = \left(\frac{t'_G}{S} \right) \log \left[\left(\frac{2.3Sk_0t_s}{t'_G} \right) + 1 \right] \quad (5)$$

If k_0 is very large as would be the case for high-molecular-mass polymers in most circumstances, (typically 10^4 – 10^5 [9–11]) then the 1 could be neglected in Eq. 5, assuming realistic values of b , $\Delta\varphi$ and t_G are used. Rearrangement of Eq. 5 gives

$$\left(\frac{t'_g}{t'_G} \right) = \frac{1}{S} \log(2.3Sk_0t_s) - \frac{1}{S} \log t'_G \quad (6)$$

By plotting t'_g/t'_G against $\log t'_G$, a straight line with a slope of $-1/S$ should be obtained with an intercept of $1/S \log(2.3Sk_0t_s)$. This allows S and k_0 to be determined.

Table 1
Column data

Column	Silica	Surface area (m ² /g)	Carbon (%)	Reduced plate height ^a	
Pore size (nm)	Particle size (μ m)				
7	6	Zorbax	350	14.5	2.08
50	10	LiChrospher	60	4.6	3.39
100	10	LiChrospher	30	1.8	10.0
Pellicular	30–40	Perisorb	14	0.9	20.4

^a Measured from phentole using conditions of Bristow and Knox [20].

3. Results and discussion

The isocratic elution of high-molecular-mass polystyrenes was observed in agreement with previous workers [8–11]. The isocratic elution of the higher-molecular-mass polymers became increasingly more difficult to observe as the molecular mass increased and this was also found by these previous workers. Typically, the solvent range would vary by as little as 1% between complete retention and elution at the solvent front for the M_r $4.10 \cdot 10^5$ and $9.29 \cdot 10^5$ polystyrenes. Without making solvent mixtures, which introduces composition stability problems with such volatile solvents as dichloromethane, we observed the isocratic elution of these polystyrenes but only by chance. Increasing the column pore size allowed observance of isocratic elution of higher molecular masses, as Fig. 1 illustrates for the M_r 929 000 polystyrene on the 100 nm pore size column.

To determine the capacity factor, the unretained elution volume of the solute is required. For small molecules this is closely approximated by the solvent void volume. This approximation worsens on porous columns as the size of the solute increases relative to the solvent. Previous workers [8–12] have used the size-exclusion volume of the solute in pure good solvent as a measure of the unretained retention volume.

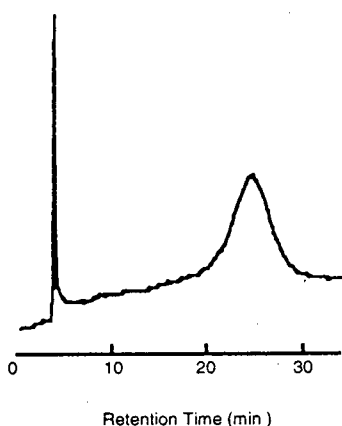


Fig. 1. Isocratic elution of M_r 929 000 polystyrene. Mobile phase dichloromethane–acetonitrile (58:42), flow-rate 1.0 ml/min, sample $10 \mu\text{g}$ in $10 \mu\text{l}$ dichloromethane, 100 nm pore size, $10 \mu\text{m}$ particle size C_{18} column.

However it is known [17] that the hydrodynamic volume of a polymer molecule varies with the solvent composition. Viscosity measurements [18] indicate that the radius of gyration of an M_r 113 000 polystyrene molecule in 0.6 volume fraction dichloromethane–acetonitrile solvent is about 15% smaller than in pure dichloromethane. For M_r 470 000 polystyrene the percentage decrease is 25. Hence the size-exclusion elution volume will only be an approximation to the unretained retention volume.

Size-exclusion experiments in dichloromethane–acetonitrile solvent mixtures with decreasing dichloromethane composition show that the elution volume increases exponentially with acetonitrile volume fraction. Fig. 2 shows these results for M_r 110 000 polystyrene on the 50 nm pore size column. Benzene showed an elution volume of 2.0 ml on this column which does not change with mobile phase composition. The mobile phase composition at which the M_r 110 000 polystyrene just dissolves (solubility composition) is 0.465 volume fraction dichloromethane [19]. Yet at a volume fraction of 0.6 dichloromethane, considerably higher than the solubility composition where size exclusion might

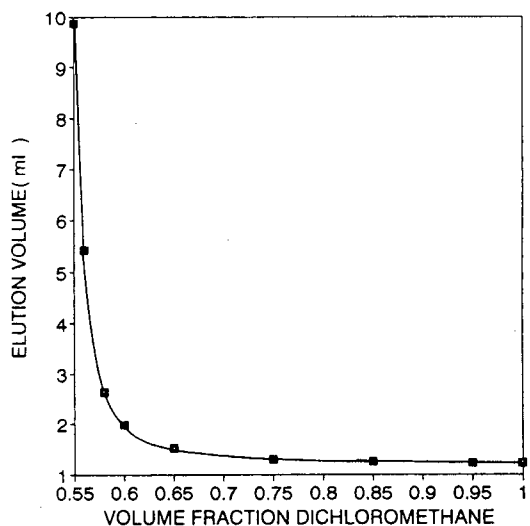


Fig. 2. Retention volume as a function of dichloromethane composition; $10 \mu\text{g}$ M_r 110 000 polystyrene in $10 \mu\text{l}$ dichloromethane, flow-rate 1.0 ml/min, 50 nm pore size, $10 \mu\text{m}$ particle size C_{18} column.

be expected to be dominant, the elution volume was 2.0 ml. Obviously M_r 110 000 polystyrene cannot have the same size as benzene and there must be retention to explain the same elution volume. There was no sharp change from size-exclusion to reversed-phase chromatography. Adsorption effects must be present at much higher concentrations of dichloromethane than the solubility composition. In these circumstances an accurate estimate of the unretained elution volume is not possible from chromatography and so we also used the elution volume in 100% dichloromethane as a measure of the unretained volume of a solute for capacity factor calculations. These elution volumes, for each column and each molecular mass, are shown in Table 2.

Fig. 3 illustrates the relationship between $\log k'$ and the solvent composition for various molecular mass polystyrenes up to M_r 200 000 eluted isocratically on the 50 nm pore size column. This graph used isocratic retention times reported in Table 3 and the size-exclusion volumes reported in Table 2. Similar graphs were drawn for the other columns using data reported in Tables 3 and 4. Isocratic S values for each column were determined from these graphs. There is evidence of very slight curvature in

Table 2
Size-exclusion volumes on the various columns for the polystyrenes

Molecular mass	Size-exclusion elution volume (ml) on column of pore size			
	7 nm	50 nm	100 nm	Pellicular
78	1.600	2.000	2.150	1.030
800	1.310	1.935	2.150	0.980
$2.35 \cdot 10^3$	1.225	1.885	2.080	0.980
$9.00 \cdot 10^3$	1.115	1.783	2.050	0.970
$1.75 \cdot 10^4$	1.090	1.666	2.030	0.950
$5.00 \cdot 10^4$	1.075	1.475	1.970	0.950
$1.10 \cdot 10^5$	1.060	1.240	1.850	0.950
$2.00 \cdot 10^5$	1.048	1.075	1.580	0.950
$4.10 \cdot 10^5$	1.035	1.036	1.570	0.950
$9.29 \cdot 10^5$	1.032	0.975	1.570	0.950

Flow-rate = 0.5 ml/min, 1.0 dichloromethane.

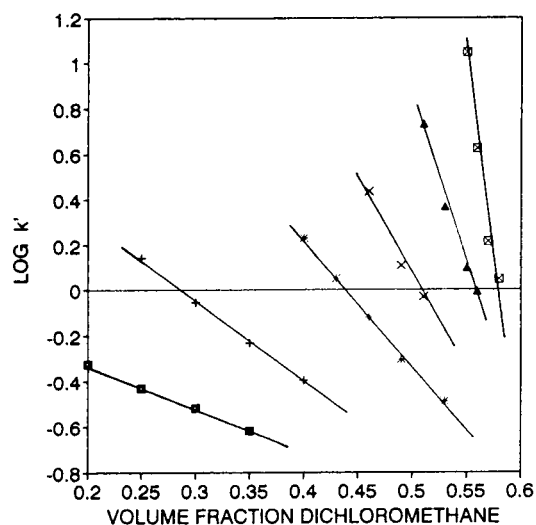


Fig. 3. Isocratic $\log k'$ against volume fraction dichloromethane. Sample $10 \mu\text{g}$ polystyrene in $10 \mu\text{l}$ dichloromethane, flow-rate 1.0 ml/min, 50 nm pore size, $10 \mu\text{m}$ particle size C_{18} column. Polystyrene M_r : \square = 800; + = 2350; * = 9000; \times = 12 500; \blacktriangle = 50 000; \square = 110 000.

some of these graphs at the highest molecular masses. Curvature in these graphs has also been reported by Alhedai et al. [10]. The S values reported are obtained from the slopes of straight lines of best fit in all cases.

Gradient elution of the polystyrenes became more difficult to observe as the molecular mass decreased and as the gradient rate decreased. As the molecular mass and gradient rate decreased, peaks became broader and eventually merged into the baseline. Table 5 lists the retention data for the polystyrenes on the various C_{18} columns for various gradient rates. Fig. 4 illustrates a graph of t'_g/t'_G versus $\log t'_G$ for molecular masses 17 500 to 929 000 on the 50 nm pore size column, using data from Table 5 and values of the size-exclusion elution volume, given in Table 2. Graphs for the other columns were similar. When steep gradients were used, the graphs were initially curved and became linear as the gradient steepness decreased. At gradient rates greater than 2%/min, curvature was evident even for the lowest molecular mass studied (17 600) but the curvature increased as the molecular mass increased. This implies that the

Table 3
Isocratic retention times for 7 nm and 50 nm pore size columns

Dichloromethane (volume fraction)	Retention time (min) for molecular mass						
	800	2350	9000	17 500	50 000	110 000	200 000
<i>7 nm pore size column</i>							
0.32	3.50						
0.38	2.92						
0.42	2.63	4.87					
0.46	2.48	3.58					
0.50		2.78					
0.52			4.52				
0.54		2.23	3.30	7.10			
0.56			2.50	3.78	15.00		
0.57				2.89	6.45		
0.58		1.58	2.03	2.42	3.52	13.05	
0.59				2.07	2.34	3.25	
0.60					2.05	2.45	
<i>50 nm pore size column</i>							
0.20	2.35						
0.25	2.65	4.50					
0.30	2.52	3.55					
0.35	2.40	2.99					
0.40		2.65	4.80				
0.43			3.78				
0.46			3.13	6.20			
0.49				3.81			
0.50			2.03	3.22			
0.51					9.40		
0.53					4.90		
0.55					3.73	15.00	
0.56					2.93	6.44	
0.57						3.26	7.26
0.58						2.62	3.44

rate of diffusion of mobile phase into and from these large solvated molecules may be a limiting factor in this chromatography. Similar suggestions have been made by Lochmuller and McGranaghan [9] and Shalliker [18] to explain anomalous elution behaviour of polystyrenes. S values were estimated from the slopes of these curves using only gradient rates of less than 2% dichloromethane per minute. S values were also estimated from these same data using the method described by Larman et al. [8]. No significant differences were observed.

The large variations in S values observed by other workers for high-molecular-mass polymers

may have resulted because of this curvature when steep gradients were used. The result of this curvature is that values of S , estimated at high gradient rates, are lower than values estimated at gradient rates less than 2%/min as the slope equals $-1/S$. In the study by Larman et al. [8], S values were estimated from gradient rates between 0.75 and 16%/min. Data from Larman et al.'s study for two different columns were plotted to produce graphs of t'_g/t'_G versus $\log t'_G$ that were non-linear (Fig. 5). Later work by this group [12] used gradients of lower steepness and ascribed the differences in S obtained at different gradient rates to errors introduced by large

Table 4
Isocratic retention times for 100 nm pore size and pellicular columns

Dichloromethane (volume fraction)	Retention time (min) for molecular mass						
	800	2350	9000	17 500	50 000	110 000	200 000
<i>100 nm pore size column</i>							
0.20	2.55						
0.25	2.41	3.21					
0.30	2.30	2.76					
0.35	2.20	2.45					
0.40		2.29	3.16				
0.43			2.67	4.46			
0.46			2.40				
0.49				2.91			
0.50			2.39	2.71	5.23		
0.51			2.26	2.48	3.42		
0.53				2.34	2.79	5.40	
0.55						3.90	
0.56					2.24	2.88	6.41
0.57						2.60	3.46
0.58							2.30
<i>Pellicular column</i>							
0.25		1.62					
0.30		1.42					
0.35		1.29					
0.42			1.90	6.00			
0.46			1.37	3.00			
0.50				1.54	18.80		
0.52				1.29	4.12		
0.54					1.75		
0.55					1.43		

values of k_0 . It seems likely that at least part of this difference can be assigned to obtaining low values of S for high gradient rates, especially as a similar trend has now been obtained by different workers, in two different solvent systems and on columns of different pore sizes.

S values estimated from isocratic and gradient data are shown in Table 6. Where possible a range, estimated from all possible slopes, is included. The range of molecular masses for which a comparison of the S values can be made is not large. The range is smaller when gradient rates of less than 2% dichloromethane per minute are used and larger when larger pore size columns are used. Reasonable agreement was obtained for molecular masses up to 50 000.

Above this molecular mass, isocratic S values tend to be higher than gradient S values. The differences are of the order of 100% for molecular masses 110 000 and 200 000. This is too large to be experimental error. The error of neglecting the size decrease in poorer solvents and hence underestimating the unretained retention volume can be estimated for the M_r 110 000 polystyrene. By using size estimates from viscosity data of M_r 110 000 polystyrene, it was estimated that S values would increase by only about 5% for both isocratic and gradient determined values. Thus the reasons for the difference remain unclear. Lochmuller and McGranaghan [9] obtained good agreement between isocratic and gradient S values, with a 30 nm pore size C_8 column up to a

Table 5
Retention times at various gradient rates for the polystyrenes

Molecular mass	Retention time (min) at gradient rate					
	10%/min	5%/min	2%/min	1%/min	0.5%/min	0.25%/min
<i>7 nm C₁₈ column</i>						
1.75 · 10 ⁴	9.55	11.25	15.80	22.67	34.58	
5.00 · 10 ⁴	9.50	11.37	16.51	24.83	39.92	
1.10 · 10 ⁵	9.50	11.35	16.71	26.05	43.33	
2.00 · 10 ⁵			16.80	26.47	44.20	
4.10 · 10 ⁵	9.50	11.37	16.85	26.50	44.40	
9.29 · 10 ⁵			16.85	26.54	44.71	
<i>50 nm C₁₈ column</i>						
1.75 · 10 ⁴	9.38	10.30	12.38	14.77	18.15	21.28
5.00 · 10 ⁴	9.77	11.25	14.86	20.58	29.70	45.82
1.10 · 10 ⁵	9.88	11.70	16.30	23.97	37.75	63.08
2.00 · 10 ⁵			16.83	25.43	41.43	71.22
4.10 · 10 ⁵	9.87	11.88	16.88	25.78	42.48	72.19
9.29 · 10 ⁵			16.90	26.22	43.28	76.36
<i>100 nm C₁₈ column</i>						
1.75 · 10 ⁴			12.07	11.55	12.35	
5.00 · 10 ⁴			14.15	18.78	27.40	
1.10 · 10 ⁵			16.06	23.43	37.73	
2.00 · 10 ⁵			16.58	24.77	39.93	
4.10 · 10 ⁵			17.00	25.65	41.00	
9.29 · 10 ⁵			17.23	26.03	42.81	
<i>Pellicular column</i>						
1.75 · 10 ⁴			10.90	13.57	17.95	
5.00 · 10 ⁴			13.40	19.35	29.98	
1.10 · 10 ⁵			15.10	22.91	37.36	
4.10 · 10 ⁵			15.55	24.20	40.58	
9.29 · 10 ⁵			15.68	24.62	41.55	
7.00 · 10 ⁶			15.85	24.98	42.48	
1.50 · 10 ⁷			15.85	25.00	42.65	

Delay time, $t_d = 5.4$ min. Flow-rate = 1.0 ml/min. Initial $\varphi = 0.40$ dichloromethane, final $\varphi = 1.0$ dichloromethane.

molecular mass of 300 000 in a dichloromethane–acetonitrile mobile phase. Gradient rates were 1.7 and 2.5% dichloromethane per minute. Alhedai et al. [10] found differences of greater than 100% between gradient and isocratic S values on 10 nm and 30 nm pore size C_{18} columns using dichloromethane–methanol solvent system. Gradient rates were 2–4% dichloromethane per minute. These workers found gradient S values to be significantly higher than

isocratic values with agreement improving as the molecular mass increased to 100 000. This is directly opposite to the trend reported here. The three sets of results are not directly comparable because they were conducted with different columns and mobile phases. However it is clear that more effort is required to reconcile these disparate trends.

Fig. 6 shows plots of $\log S$ versus \log molecular mass for the isocratically determined values

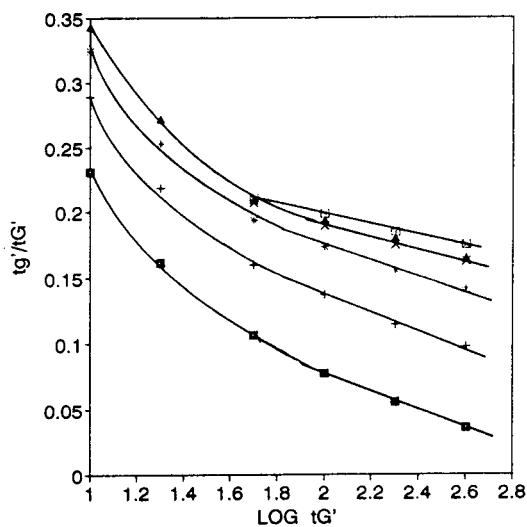


Fig. 4. Gradient S determination. Initial composition 0.4 dichloromethane, final composition 1.0 dichloromethane, flow-rate 1.0 ml/min, delay time 5.4 min, 50 nm pore size, 10 μ m particle size column. Polystyrene M_r : \blacksquare = 17 500; + = 50 000; * = 110 000; \times = 200 500; \blacktriangle = 410 000; \square = 929 000.

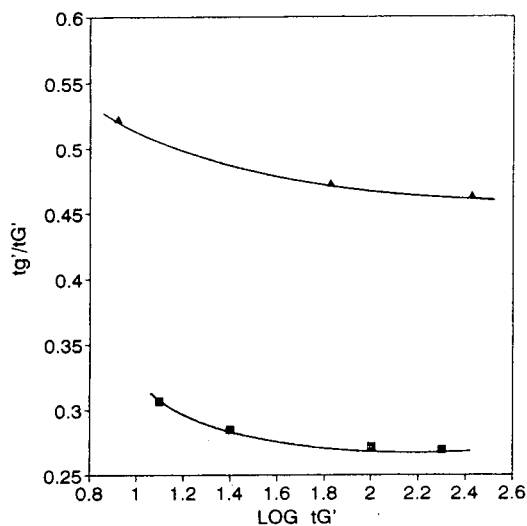


Fig. 5. Gradient t'_g/t'_G against $\log t'_G$ using data of Larman et al. [8]. Mobile phase tetrahydrofuran–water, flow-rate 2.0 ml/min, delay time 2.2 min, sample M_r 50 000 polystyrene. \blacksquare = 15 nm pore size C_{18} column, gradient 0.6 to 1.0 tetrahydrofuran; \blacktriangle = 30 nm pore size C_{18} column, gradient 0.4 to 1.0 tetrahydrofuran.

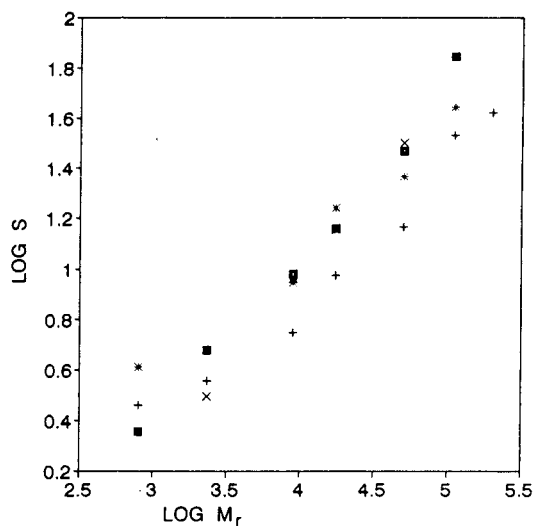


Fig. 6. Isocratic $\log S$ against \log molecular mass. \blacksquare = 7 nm pore size C_{18} column; + = 50 nm pore size C_{18} column; * = 100 nm pore size C_{18} column; \times = pellicular C_{18} column.

on the four different columns. There is not much difference. The slopes of all plots are similar and equal to 0.6. There is no evidence of a lower slope for the higher molecular masses and the virtually non-porous and low surface area pellicular column falls into the same set as the porous supports. Fig. 7 shows the same plots with S values obtained from gradient elution data and the plots differ appreciably. Closest agreement with isocratic data is shown by the 7 nm pore size column and the pellicular column. Both these columns do not allow significant pore access to the polystyrenes for which gradient elution data could be obtained. However, both plots tail off at higher molecular masses and only have slopes of 0.4 on the linear portion at low molecular masses. The graphs for the two columns with larger pores have much smaller slopes than the equivalent isocratic ones. Possible reasons for the poor agreement between isocratic and gradient results are that either LSS theory does not hold for large molecules, or that different mechanisms, or different available surface areas operate in the retention of large molecules for gradient elution versus isocratic elution.

Table 6
S values for isocratic and gradient elution

Molecular mass	S							
	Isocratic				Gradient			
	Column pore size		100 nm	Pellicular	Column pore size		100 nm	Pellicular
7 nm	50 nm	7 nm			50 nm			
800	2.3 ± 0.1	3.1 ± 1.3	4.1 ± 0.6					
2350	4.7 ± 0.2	3.6 ± 0.2	4.9 ± 0.3	3.2 ± 0.2				
9000	9.6 ± 0.3	5.6 ± 0.3	5.6 ± 1.3	9.2				
17 500	15.9 ± 1.5	9.4 ± 2.5	8.8 ± 1.5	14.4 ± 1.4	13.2 ± 0.9	10.1 ± 3.1	18.0	18.2 ± 3.0
50 000	29.4 ± 3.0	14.7 ± 2.3	17.5 ± 5.2	31.5 ± 3.8	18.0 ± 0.5	15.9 ± 3.7	17.0 ± 2.9	26.3 ± 1.1
110 000	69.9	34.1 ± 6.6	22.3 ± 7.6		29.4 ± 4.0	18.6 ± 2.5	25.3 ± 6.7	30.2 ± 1.1
200 000		41.7	44.1 ± 2.8		33.0 ± 7.0	21.1 ± 2.3	22.1 ± 1.5	46.9 ± 7.9
410 000					33.3 ± 7.3	22.4 ± 1.8	20.0 ± 1.0	56.8 ± 20
929 000					36.4 ± 7.3	26.0 ± 3.8	23.2 ± 3.3	64.4 ± 17

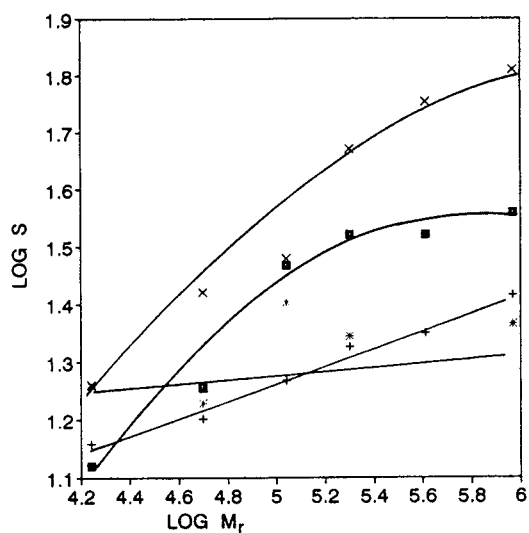


Fig. 7. Gradient log *S* against log molecular mass. ■ = 7 nm pore size C₁₈ column; + = 50 nm pore size C₁₈ column; * = 100 nm pore size C₁₈ column; × = pellicular C₁₈ column.

References

- [1] L.R. Snyder, J.W. Dolan and J.R. Gant, *J. Chromatogr.*, 165 (1979) 3.
- [2] J.W. Dolan, J.R. Gant and L.R. Snyder, *J. Chromatogr.*, 165 (1979) 31.
- [3] L.R. Snyder, in Cs. Horváth (Editor), *High Performance Liquid Chromatography—Advances and Perspectives*, Vol. 1, Academic Press, New York, 1980, p. 207.
- [4] M.I. Aguilar and M.T.W. Hearn, *Chem. Aust.*, (1993) 284.
- [5] P.J. Schoenmakers, H.A.H. Billiet and L. de Galan, *J. Chromatogr.*, 185 (1979) 179.
- [6] P.J. Schoenmakers, H.A.H. Billiet and L. de Galan, *J. Chromatogr.*, 218 (1981) 261.
- [7] M.T.W. Hearn, *HPLC of Proteins, Peptides and Polynucleotides*, VCH, New York, 1991, Ch. 8.
- [8] J.P. Larman, J.J. Stefano, A.P. Goldberg, R.W. Stout, L.R. Snyder and M.A. Stadalius, *J. Chromatogr.*, 255 (1983) 165.
- [9] C.H. Lochmuller and M.B. McGranaghan, *Anal. Chem.*, 61 (1989) 2449.
- [10] A. Alhedai, R.E. Boehm and D.E. Martire, *Chromatographia*, 29 (1990) 313.
- [11] D.M. Northrup, D.E. Martire and R.P.W. Scott, *Anal. Chem.*, 64 (1992) 16.
- [12] M.A. Quarry, R.L. Grob and L.R. Snyder, *Anal. Chem.*, 58 (1986) 907.
- [13] R.E. Boehm, D.E. Martire, D.W. Armstrong and K.H. Bui, *Macromolecules*, 16 (1983) 466.
- [14] R.E. Boehm, D.E. Martire, D.W. Armstrong and K.H. Bui, *Macromolecules*, 17 (1984) 400.
- [15] R.E. Boehm and D.E. Martire, *Anal. Chem.*, 61 (1989) 471.
- [16] R.A. Shalliker, P.E. Kavanagh and I.M. Russell, *J. Chromatogr. A*, 664 (1994) 221.
- [17] J.M.G. Cowie, *Polymers: Chemistry and Physics of Modern Materials*, International Textbook, Aylesbury, UK, 1973.
- [18] R.A. Shalliker, *Ph.D. Thesis*, Deakin University, Waurin Ponds, 1992.
- [19] R.A. Shalliker, P.E. Kavanagh and I.M. Russell, *J. Chromatogr.*, 558 (1991) 440.
- [20] P.A. Bristow and J.H. Knox, *Chromatographia*, 10 (1977) 279.



ELSEVIER

Journal of Chromatography A, 679 (1994) 115–121

JOURNAL OF
CHROMATOGRAPHY A

Determination of reactive hydrocarbons by capillary gas chromatography with the reduction gas detector

Xu-Liang Cao, C. Nicholas Hewitt*, K.S. Waterhouse

Institute of Environmental and Biological Sciences, Lancaster University, Lancaster LA1 4YQ, UK

First received 7 December 1993; revised manuscript received 3 May 1994

Abstract

The reduction gas detector has been used successfully for the capillary GC determination of C₂–C₆ alkenes and isoprene. The detection limits have been improved by using a capillary GC column. The peak shapes for hydrocarbons above C₆ (benzene, toluene, *p*-xylene, *o*-xylene, α -pinene and β -pinene) are very broad and tailing due to their slow and incomplete reactions with HgO at the maximum temperature (300°C) achievable with the present reduction gas detector. If the HgO bed temperature of the detector could be increased, the system might be applicable to the detection of higher-molecular-mass compounds.

1. Introduction

Few hydrocarbons are toxic in their own right at the concentrations found in the ambient atmosphere. Their main contribution to air pollution stems from their atmospheric degradation to ozone, peroxyacetyl nitrate (PAN), hydrogen peroxide and other secondary air pollutants. Because of their extremely low concentrations [volume mixing ratios of 10⁻⁹ (ppb, v/v), or 10⁻¹² (ppt, v/v)], hydrocarbons are difficult to monitor at ambient concentration levels. Development of more sensitive detection systems for hydrocarbons, compatible with gas chromatographic (GC) separation methods, is therefore an urgent priority. Since the more reactive hydrocarbons (e.g., alkenes) have much higher

potentials for ozone formation than the non-reactive hydrocarbons (e.g., alkanes), the priority in atmospheric monitoring programmes which focus on photochemical ozone production is therefore the quantitation of the reactive volatile organic compounds (VOCs), rather than of the non-reactive species. Under some circumstances it would therefore be advantageous to utilize a detection system that has enhanced sensitivity towards alkenes but is relatively insensitive to alkanes and other less reactive VOC species. This would result in a less complex chromatogram than is obtained with other universal detectors, for example the flame ionization detector, and so simplify peak identification.

The reduction gas detector was originally developed for detecting the reducing gases CO and H₂ [1]. It has also been used for the detection of acetaldehyde and acetone [2] and of isoprene. Recently, the reduction gas detection

* Corresponding author.

(RGD) response to the reactive hydrocarbons has been investigated using GC with a packed column [3]. It was shown that RGD is considerably more sensitive to alkenes than is flame ionization detection (FID), and it has much greater sensitivity to alkenes than alkanes.

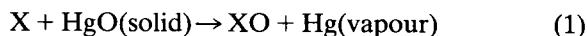
Because the RGD system was designed for the simple reducing gases, the detector is engineered for use with packed GC columns. However, in order to use RGD for environmental analysis, it is very desirable that it should be compatible with high-resolution capillary GC columns. This would allow advantage to be taken of the high resolving power of capillary columns and may also improve the detection limits of the detector. One of the disadvantages of using packed GC columns is that the analysis has to be carried out isothermally, since RGD is very sensitive to changes in the carrier gas flow-rate. This is adequate for the analysis of simple reducing gases (e.g., H₂, CO), but prevents the separation of compounds with a wide range of boiling points (e.g., C₂–C₁₀ hydrocarbons). Moreover, because the carrier gas flow-rate through the capillary column is only a small part of that of the make-up gas (<0.5%), the total carrier gas flow-rate will not change significantly when the GC oven temperature changes. Thus, temperature programming may be employed for the analysis of hydrocarbons when using a capillary GC column.

In this work, a make-up gas line was made in order to render RGD compatible with capillary GC columns. The response of RGD to alkenes and other hydrocarbons was investigated using GC with four different capillary columns.

2. Experimental

2.1. Principle of the reduction gas detector

The principle of operation of the reduction gas detector has been described elsewhere [3,4]. Briefly, it depends upon the reduction of solid mercuric oxide by a reducing gas X on a heated bed:



The resultant mercury vapour concentration is directly proportional to the inlet gas concentration and is quantitatively detected by means of an ultraviolet photometer located immediately downstream of the reaction bed.

2.2. Analytical system

GC measurements were made using a Hewlett-Packard 5890 Series II gas chromatograph fitted with the reduction gas detector. The carrier gas used was helium. The reduction gas detector employed in this work was an RGD-2 (Trace Analytical, Menlo Park, CA, USA). Four different capillary columns were used in this work to investigate the RGD responses to different hydrocarbons: (i) porous-layer open tubular (PLOT; Al₂O₃/KCl), 50 m × 0.32 mm (Chrompack); (ii) Ultra 2 (cross-linked 5% phenyl methylsilicone), 25 m × 0.2 mm, film thickness (*d_f*) 0.33 μm (Hewlett-Packard); (iii) HP-1 (cross-linked methylsilicone gum), 10 m × 0.53 mm, *d_f* 2.65 μm (Hewlett-Packard); (iv) HP-1 (cross-linked methylsilicone gum), 25 m × 0.32 mm, 1.05 μm film thickness (Hewlett-Packard).

A make-up gas line (stainless-steel tube, 1/8 in. I.D.; 1 in. = 2.54 cm) was made in order to use the RGD system with the capillary GC. A catalytic combustion filter was used in conjunction with an organic–water vapour trap (molecular sieve) for carrier gas purification. An uncoated fused-silica capillary (15 cm × 0.53 mm) was used as the transfer line and was connected to the capillary GC column by a glass press-fit connector (Hewlett-Packard).

Sample vapours were injected into the carrier gas stream by means of a gas-tight syringe via a Chrompack TCT injector. The injected vapours were then carried by helium gas through a heated (220°C) empty Perkin-Elmer stainless-steel tube to a coated (CP-Sil 8CB, *d_f* = 5 μm) fused-silica capillary trap [5] which was cooled by liquid nitrogen. After sample concentration, the trap was flash-heated to 220°C at 15°C/s for 1

min, and the trapped vapours injected onto the GC capillary column in the splitless mode. A schematic diagram of the whole TCT-GC-RGD system is shown in Fig. 1.

2.3. Analytes

The RGD responses of C_2 – C_6 alkenes, isoprene, benzene, toluene, *p*-xylene, *o*-xylene, α -pinene and β -pinene were investigated. A 15 ppm (v/v) Scotty standard calibration mixture (Chrompack) was used as the standard for C_2 – C_6 alkenes. Dilutions of these standards were made by injecting known volumes of vapours into a 1-l glass flask. Mixtures of isoprene, benzene, toluene, *p*-xylene, *o*-xylene, α -pinene and β -pinene vapours were prepared using the static dilution bottle method [6,7].

3. Results and discussion

3.1. The RGD responses to alkenes and other hydrocarbons

RGD has been shown to be considerably more sensitive and selective for the detection of C_2 – C_6 alkenes than the commonly used FID [3]. In order to investigate if RGD can be used for the detection of other hydrocarbons, the RGD responses to C_5 – C_{10} hydrocarbons were studied using different capillary GC columns.

Fig. 2a shows GC-RGD responses to these C_5 – C_{10} hydrocarbons from the Ultra 2 capillary column. It can be seen that the peak of isoprene is relative sharp with slight tailing, while peak tailing is a severe problem for all the other hydrocarbons, especially for the heavier ones. This may be due to the extremely low carrier gas

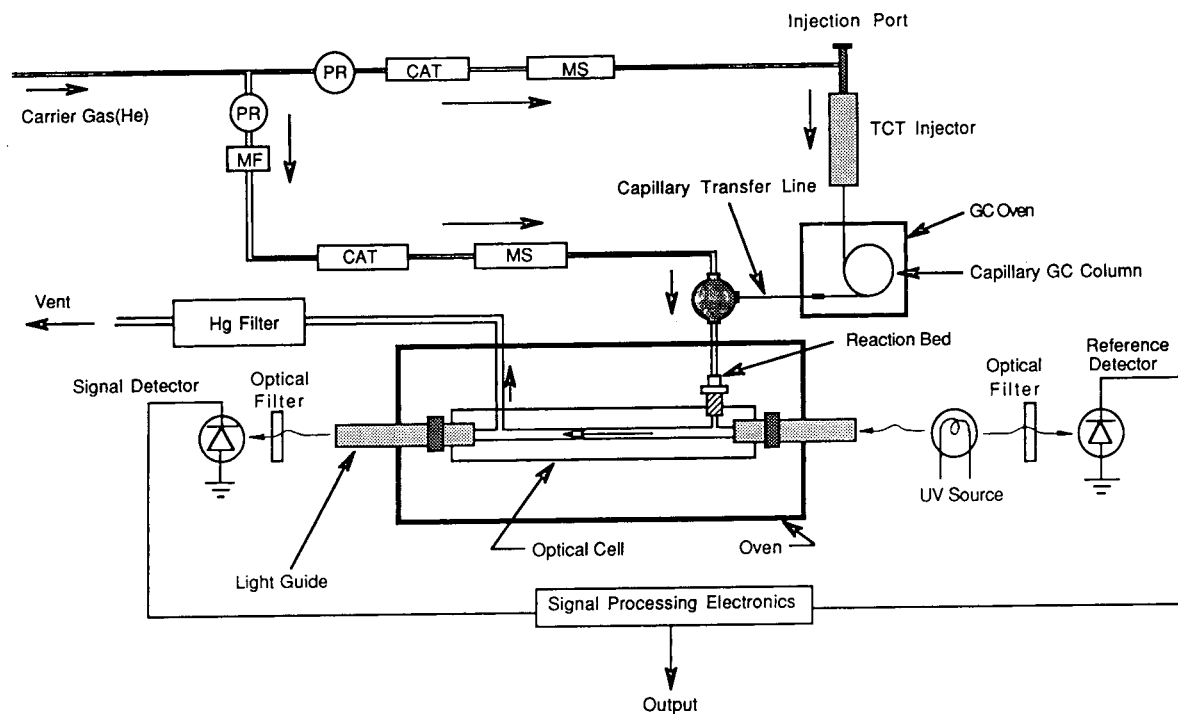


Fig. 1. Schematic diagram for the TCT-GC-RGD system. MS = Molecular sieve; CAT = catalytic combustion filter; MF = mass flow regulator; PR = pressure regulator.

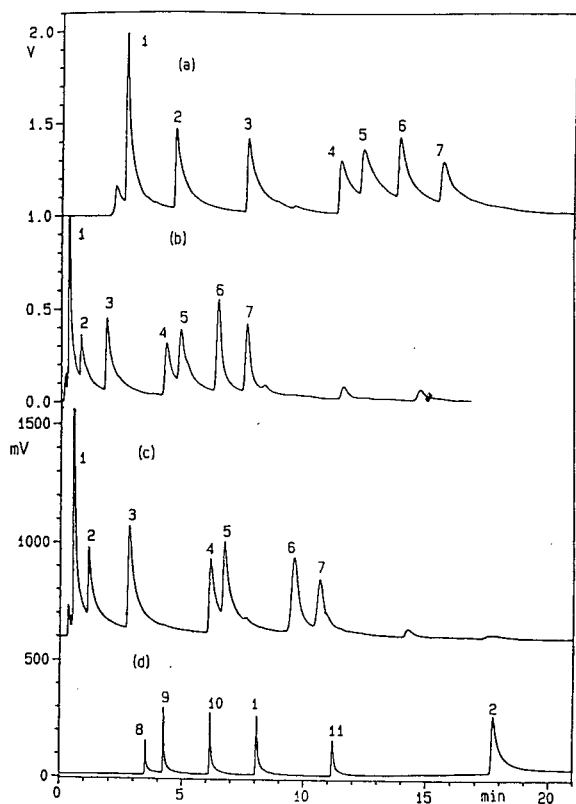


Fig. 2. GC-RGD chromatograms of hydrocarbons. TCT conditions: desorption temperature 220°C (2 min), injection temperature 210°C (1 min), cold trap temperature -190°C. (a) Ultra 2 column (25 m \times 0.2 mm), temperature programme 35°C (3 min) to 200°C at 5°C/min, flow-rate through HgO 23 ml/min. (b) HP-1 column (10 m \times 0.53 mm), temperature programme as in (a), flow-rate through HgO 35 ml/min. (c) HP-1 column (25 m \times 0.32 mm), temperature programme as in (a), flow-rate through HgO 40 ml/min. (d) PLOT column (50 m \times 0.32 mm), temperature programme 160°C (8 min) to 180°C at 3°C/min, flow-rate through HgO 28 ml/min. Peaks: 1 = isoprene; 2 = benzene; 3 = toluene; 4 = *p*-xylene; 5 = *o*-xylene; 6 = α -pinene; 7 = β -pinene; 8 = propene; 9 = 1-butene; 10 = 1-pentene; 11 = 1-hexene.

(He) flow-rate through the capillary column (< 1 ml/min) because the Ultra 2 is a very-narrow-bore (I.D. 0.2 mm) capillary. In order to investigate if a higher flow-rate of carrier gas through the column can improve the peak shape or not, two capillary columns with wide bores were used.

The flow-rate of carrier gas through the 25

m \times 0.32 mm I.D. HP-1 capillary is about 3 ml/min. While the 10 m \times 0.53 mm I.D. HP-1 is a wide-bore capillary, its performance is similar to a packed GC column. The flow-rate through this column can be higher than 30 ml/min depending on the head pressure. The RGD responses to the C₅-C₁₀ hydrocarbons from these two capillary columns are shown in Fig. 2b and c. It can be seen that the peak shapes for these hydrocarbons were indeed improved, but not significantly. Moreover, these peaks are still very broad despite the high resolving power of the capillary used. The effect of make-up gas flow-rates (from 20 to 50 ml/min) on the peak shape was also investigated, and it was found that different make-up gas flow-rates can only change the retention times and the sensitivity, but the peak shapes cannot be improved even at higher make-up gas flow-rates.

Because RGD was designed for the detection of simple reducing gases, the HgO bed temperatures can only be adjusted between 200 and 300°C. Thus, the peak shapes (broad, tailing) of these hydrocarbons with RGD may be due to their slow and incomplete reaction (1) even at the highest HgO bed temperature achievable. In order to check this possibility, the RGD responses to C₂-C₆ alkenes, isoprene and benzene were investigated using a PLOT capillary column. A typical chromatogram is shown in Fig. 2d.

It can be seen that the peak shapes for C₃-C₆ alkenes (ethene cannot be trapped) and isoprene are relative sharp with slight tailing. This may be due to the sudden change of temperature from 160°C in the GC oven to the room temperature to which part of the transfer line (ca. 10 cm) was exposed. It is expected that the peak shapes will be improved further if the transfer line is heated. However, the peak shape of benzene is still broad and tailing as observed above with the other capillary columns. This may confirm that the broad and tailing peaks for those C_≥6 hydrocarbons from RGD are due to the slow and incomplete reaction (1). It is suggested that the temperature range of the HgO bed should be broadened in order to detect heavier compounds with this detector.

It can also be seen from all the chromatograms in Fig. 2 that the baseline drift with increasing GC oven temperatures was eased significantly with the capillary columns. This is in marked contrast to the very significant baseline drift that was observed with a temperature-ramped packed column.

3.2. The response linearity of the capillary GC–RGD system

In order to investigate the response linearity of the capillary GC–RGD system to different hydrocarbons, different amounts of C₂–C₆ alkenes, isoprene and benzene vapours were injected onto the GC–RGD system with the PLOT capillary column. Their responses in both area and height counts were plotted against the mass of hydrocarbons injected, and the results shown in Figs. 3–8.

It can be seen that the linearity ranges of the RGD responses generally increase with the carbon number of the hydrocarbon, from ca. 0.3 ng for propene to ca. 2.0 ng for benzene. This is because the linearity range of the RGD responses depends very much on the peak height, rather than peak area. It can be seen from Figs. 3–8 that generally the RGD responses will begin to deviate when the peak height is greater than

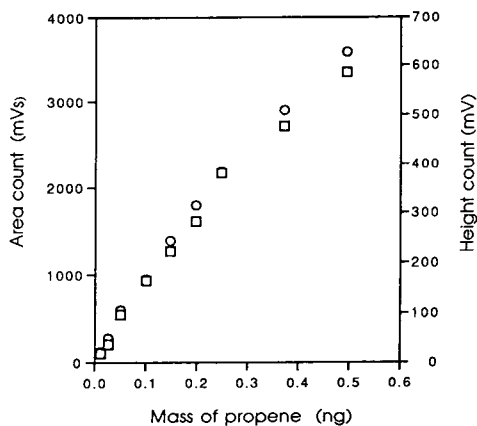


Fig. 3. Linearity of the RGD responses to propene. □ = Height; ○ = area.

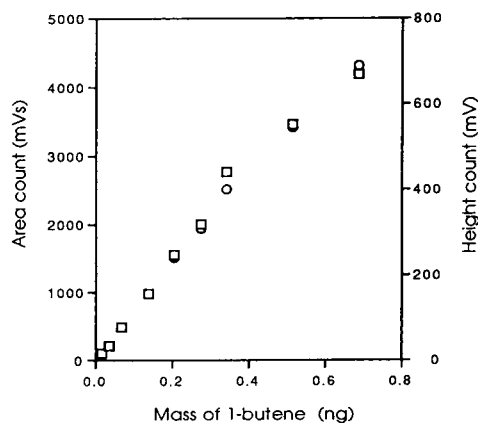


Fig. 4. Linearity of the RGD responses to 1-butene. □ = Height; ○ = area.

500–600 mV. Although a capillary GC column was used, peak tailing and broadening still occurred due to the problems of the detector itself. Thus, for the lighter hydrocarbons which appear at the beginning of the chromatogram, their peaks will be very sharp, and their linearity range will be very narrow; while the peaks of the relatively heavier hydrocarbons will be broader, and their linear range will be wider. Therefore, although the capillary columns can be used for environmental analysis, the linearity range of RGD will be narrow.

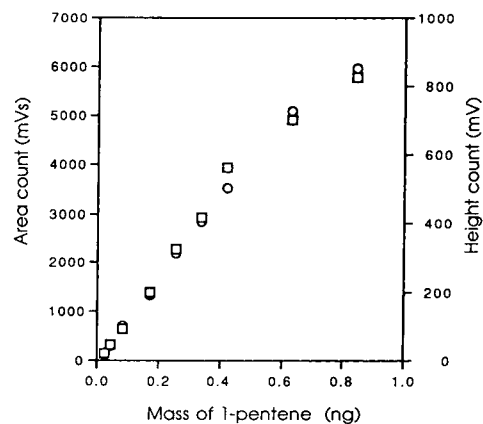


Fig. 5. Linearity of the RGD responses to 1-pentene. □ = Height; ○ = area.

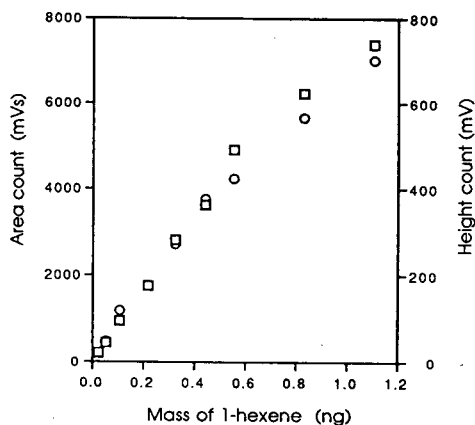


Fig. 6. Linearity of the RGD responses to 1-hexene. □ = Height; ○ = area.

3.3. Detection limits of the capillary GC-RGD system for hydrocarbons

The minimum detectable amounts of alkenes, isoprene and benzene using the capillary GC-RGD system were determined, based on a signal-to-noise ratio of 2, and the results shown in Table 1.

It can be seen from Table 1 that the detection limits have been improved indeed by using the capillary GC column, but not substantially because peak tailing is still a problem even when a capillary column is used, and the signals are much more noisy when using thermal desorption

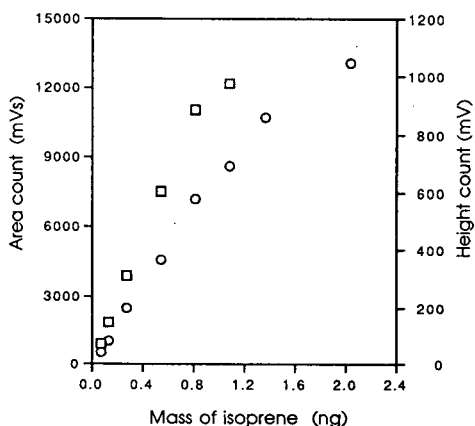


Fig. 7. Linearity of the RGD responses to isoprene. □ = Height; ○ = area.

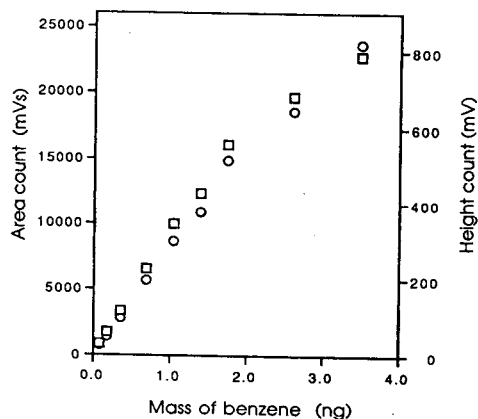


Fig. 8. Linearity of the RGD responses to benzene. □ = Height; ○ = area.

injection than when using direct injection with syringe.

4. Conclusions

RGD, which has been applied to the quantitation of hydrocarbons separated with a packed column, has been further developed for detecting reactive hydrocarbons using capillary GC. This capillary GC-RGD system can be successfully used for the analysis of C₃-C₆ alkenes and isoprene using a 50-m PLOT capillary column. The detection limits have been improved by using the capillary GC column, but not substantially. It is expected that they can be improved further by heating the transfer line and designing a micro-RGD system. The peak shapes for hydrocarbons \geq C₆ are broad and tail severely,

Table 1
Detection limits of the capillary GC-RGD systems for hydrocarbons.

Compounds	Detection limits (ng)
Propene	0.006
1-Butene	0.008
1-Pentene	0.010
1-Hexene	0.014
Isoprene	0.010
Benzene	0.030

due to their slow and incomplete reactions with HgO even at the maximum HgO bed temperature (300°C) achievable with the present RGD system. It is suggested that the HgO bed temperature range of the detector should be broadened in order to use RGD for the analysis of heavier molecules. RGD therefore may, with further development, offer advantages over FID for selective development of ozone-precursor hydrocarbons in ambient air.

Acknowledgements

We would like to thank the Government of China, the British Council, and the Natural Environment Research Council for funding. We appreciate the helpful suggestions and critical comments of an anonymous referee.

References

- [1] W.M. Doizaki and M.D. Levitt, *J. Chromatogr.*, 285 (1984) 210–213.
- [2] D. Ohara and H.B. Singh, *Atmos. Environ.*, 22 (1988) 2613–2615.
- [3] X.-L. Cao, C.N. Hewitt and K.S. Waterhouse, *Anal. Chim. Acta*, (1994) submitted for publication.
- [4] *Reduction Gas Detector (RGD-2) Operating Manual*, Trace Analytical, Menlo Park, CA, 1989.
- [5] X.-L. Cao and C.N. Hewitt, *J. Chromatogr.*, 627 (1992) 219–226.
- [6] C.M. Morris, R. Berkley and J. Bumgarner, *Anal. Lett.*, 16 (1983) 1585.
- [7] C.M. Morris, J.V. Dangtridge and J. Bumgarner, *AREAL/RTP-SOP-MRDD-036*, US Environmental Protection Agency, Research Triangle Park, NC, 1990.



ELSEVIER

Journal of Chromatography A, 679 (1994) 123-132

JOURNAL OF
CHROMATOGRAPHY A

Retention of halocarbons on a hexafluoropropylene epoxide-modified graphitized carbon black

II. Ethane-based compounds[☆]

Thomas J. Bruno*, Michael Caciari¹

Thermophysics Division, National Institute of Standards and Technology, Boulder, CO 80303, USA

First received 14 March 1994; revised manuscript received 16 May 1994

Abstract

The retention characteristics of 18 ethane-based chlorofluorocarbon, bromochlorofluorocarbon and fluorocarbon fluids have been studied as a function of temperature on a stationary phase consisting of a 5% (mass/mass) coating of a low-molecular-mass polymer of hexafluoropropylene epoxide on a graphitized carbon black adsorbent. Measurements were made at -20, 0, 20 and 40°C for hexafluoroethane (R-116), pentafluoroethane (R-125), 1,1,2,2-tetrafluoroethane (R-134), 1,1,1,2-tetrafluoroethane (R-134a), 1,1,2-trifluoroethane (R-143), 1,1,2-trifluoroethane (R-143a), 1,1-difluoroethane (R-152a), and fluoroethane (R-161). Measurements were made at 40, 60, 80 and 100°C for 1,2-dichlorotetrafluoroethane (R-114), 1,1-dichlorotetrafluoroethane (R-114a), chloropentafluoroethane (R-115), 2,2-dichloro-1,1,1-trifluoroethane (R-123), 2-chloro-1,1,1-trifluoroethane (R-133a), 1,1-dichloro-1-fluoroethane (R-141b), 1-chloro-1,1-difluoroethane (R-142b), and 1-chloroethane (R-160). Measurements were performed at 60, 80, 100 and 120°C for 1-bromo-2-chlorotetrafluoroethane (R-114B1). Net retention volumes, corrected to a column temperature of 0°C, were calculated from retention time measurements, the logarithms of which were fitted against reciprocal thermodynamic temperature. The relative retentions, also as a function of temperature, were calculated with respect to the retention of tetrafluoroethane and hexafluoroethane. Qualitative features of the data are examined, and trends are identified. In addition, the data were fitted to linear models for the purpose of predicting retention behavior of these compounds to facilitate chromatographic analysis.

1. Introduction

Many laboratories are engaged in a comprehensive research program geared toward the development of new fluids for use as refriger-

ants, blowing and foaming agents, and propellants. These new materials are needed to replace the fully halogenated materials that are thought to contribute to atmospheric ozone depletion, and which will be phased out of production by law. The research that comprises this effort includes thermophysical properties measurements and correlation, materials compatibility testing, chemical stability measurement, and cycle suitability studies [1,2]. An important part of all of these research programs

* Corresponding author.

[☆] Contribution of the USA Government. For Part I, see Ref. [10].

¹ Permanent address: Fort Lupton High School, Fort Lupton, CO, USA.

is the chemical analysis of new fluids that are tested [3–6].

Gas chromatography is one of the major chemical analysis methods that is applied to the study of alternative refrigerants for several important reasons, not the least of which are simplicity and economics of operation [7,8]. It is used both as a qualitative identification tool and for quantitative analysis of impurities that are known to be present in a sample [7,9]. A knowledge of the retention characteristics of important fluids on the more useful stationary phases is an important component in the design of effective qualitative and quantitative chromatographic analyses. This information would facilitate the identification of unknown or unfamiliar peaks that appear on a chromatogram obtained from, for example, the analysis of a field sample of a new refrigerant fluid. Moreover, these data would facilitate optimization of chromatographic separations by allowing us to predict the response of elution times and separation factors to controllable instrumental parameters. Corrected retention parameters, such as the net retention volume, V_N^0 (corrected to a column temperature of 0°C), and relative retentions, $r_{a/b}$, provide the simplest avenue to achieve these goals.

In an earlier paper, we discussed in detail the pitfalls and necessary caution that one must use in the application of such retention data [10]. In that paper, we also presented measurements for several methane-based fluids. In this paper, we present temperature-dependent measurements of the net retention volume, corrected to a column temperature of 0°C, of 18 ethane-based fluids that are commonly encountered in alternative refrigerant research and testing. The fluids we have studied are all gaseous at room temperature and pressure. To facilitate the data analysis and comparison, one measurement (at 40°C) is also provided for ethane (R-150). A listing of all the fluids studied is provided in the left-hand column of Table 1, along with the accepted code numbers. An explanation of the numbering system for these compounds has been provided elsewhere [10,11]. The measurements were made on the packed-column stationary phase that has

proven to be very useful for refrigerant analysis; a 5% coating of a low-molecular-mass polymer of hexafluoropropylene epoxide on a graphitized carbon black. The relative retentions were then calculated with respect to tetrafluoromethane and hexafluoroethane. In addition to the discussion of qualitative trends in the data, fits to linear models are presented of the logarithms of the net retention volumes and the relative retentions against thermodynamic temperature, thus providing a predictive capability.

2. Theory

A discussion of the basic definitions, theory and application of corrected retention parameters was presented earlier [10], and only a brief review will be presented here. If the volumetric carrier gas flow-rate (at the column exit) is measured and multiplied by the retention time, the retention volume, V_R , is obtained. The adjusted retention volume, V'_R , is the retention volume corrected for the void volume (or mobile phase holdup) of the column. It is obtained by simply subtracting the retention volume of an unretained solute (V_M) such as air:

$$V'_R = V_R - V_M \quad (1)$$

The net retention volume, V_N^0 , is obtained by applying the Martin–James compressibility factor, j , to account for the pressure drop across the column [7]:

$$V_N^0 = jV'_R \quad (2)$$

The specific retention volume, V_g^0 , in units of volume per unit mass of stationary phase, corrects the net retention volume for the amount of stationary phase, and the column temperature is adjusted to 0°C:

$$V_g^0 = 273.15 \cdot \frac{V_N^0}{W_s T_{col}} \quad (3)$$

where T_{col} is the column temperature and W_s is the mass of stationary phase in the column. This value is a characteristic for a particular solute on a particular stationary phase in a particular

Table 1
Net retention volumes, V_N^0 , and their logarithms, of the fluids measured in this study

Name	V_N^0 (ml)	$\log V_N^0$	-20°C (253.15 K)	0°C (273.15 K)	20°C (293.15 K)	40°C (313.15 K)	60°C (333.15 K)	80°C (353.15 K)	100°C (373.15 K)	120°C (393.15 K)	0°C (273.15 K)	20°C (293.15 K)	40°C (313.15 K)	60°C (333.15 K)	80°C (353.15 K)	100°C (373.15 K)	120°C (393.15 K)
Hexafluoroethane (R-116)	178.9 ± 1.37 0.76%	82.4 ± 0.82 0.99%	43.2 ± 0.49 1.13%	24.6 ± 0.36 1.48%							2.25	1.92	1.64	1.39			
Pentafluoroethane (R-125)	407.3 ± 3.03 0.96%	172.8 ± 1.74 1.00%	83.5 ± 0.73 0.88%	43.4 ± 0.85 1.90%							2.61	2.24	1.92	1.64			
1,1,2,2-Tetrafluoroethane (R-134)	517.8 ± 4.37 0.84%	216.2 ± 2.69 1.2%	104.3 ± 0.91 0.87%	53.8 ± 0.45 0.84%							2.71	2.34	2.02	1.73			
1,1,1,2-Tetrafluoroethane (R-134a)	481.4 ± 5.43 1.13%	202.5 ± 1.39 0.69	98.0 ± 0.85 0.87%	48.7 ± 0.88 1.80%							2.68	2.31	1.99	1.69			
1,1,2,2-Trifluoroethane (R-143)	633.1 ± 3.48 0.55%	257.8 ± 3.77 1.46%	121.8 ± 1.09 0.89%	61.1 ± 0.51 0.84%							2.80	2.41	2.09	1.79			
1,1,1,1-Trifluoroethane (R-143a)	315.7 ± 3.43 1.09%	141.8 ± 1.96 1.38%	70.9 ± 0.60 0.85%	37.5 ± 0.56 1.48%							2.50	2.15	1.85	1.57			
1,1-Difluoroethane (R-152a)	412.8 ± 4.52 1.09%	176.8 ± 2.42 1.36%	88.2 ± 0.76 0.86%	46.4 ± 0.53 1.14%							2.62	2.25	1.95	1.67			
Fluoroethane (R-161)	338.0 ± 3.17 0.94%	148.2 ± 2.01 1.35%	75.2 ± 0.65 0.86%	40.0 ± 0.34 0.86%							2.53	2.17	1.88	1.60			
1,2-Dichlorotetrafluoroethane (R-114)	652.3 ± 10.70 1.60%	302.8 ± 2.78 0.92%	161.3 ± 1.04 0.65%	89.0 ± 1.42 1.60%							2.81	2.48	2.21	1.95			
1,1-Dichlorotetrafluoroethane (R-114a)	682.5 ± 7.10 1.04%	319.0 ± 2.65 0.83%	169.4 ± 1.19 0.70%	93.2 ± 1.59 1.70%							2.83	2.50	2.23	1.97			
Chloropentafluoroethane (R-114b)	145.2 ± 0.96 0.66%	73.5 ± 0.82 1.12%	41.9 ± 0.66 1.58%	25.9 ± 0.15 0.58%							2.16	1.87	1.62	1.41			
2,2-Dichloro-1,1,1-trifluoroethane (R-123)	1413.6 ± 44.3 3.15%	613.7 ± 4.95 0.81%	308.1 ± 1.94 0.66%	162.8 ± 2.62 1.61%							3.15	2.79	2.49	2.21			
2-Chloro-1,1,1,2-tetrafluoroethane (R-124)	274.7 ± 1.55 0.56%	128.5 ± 0.94 0.74%	71.8 ± 0.47 0.65%	42.2 ± 0.24 0.58%							2.44	2.11	1.86	1.63			
2-Chloro-1,1,1-trifluoroethane (R-133a)	304.5 ± 4.90 1.60%	144.9 ± 1.08 0.75%	80.0 ± 0.47 0.58%	47.1 ± 0.26 0.55%							2.48	2.16	1.90	1.67			
1,1-Dichloro-1-fluoroethane (R-141b)	918.3 ± 9.71 1.06%	462.5 ± 3.47 0.81%	224.1 ± 1.39 0.62%	124.3 ± 1.99 1.60%							2.96	2.63	2.35	2.09			
1-Chloro-1,1-difluoroethane (R-142b)	210.1 ± 2.71 1.29%	103.2 ± 0.76 0.73%	59.6 ± 0.38 0.64%	35.8 ± 0.20 0.56%							2.32	2.01	1.78	1.55			
1-Chloroethane (R-160)	238.9 ± 2.01 0.84%	126.1 ± 1.40 1.11%	71.3 ± 1.10 1.54%	42.2 ± 0.27 0.65%							2.38	2.10	1.85	1.63			
1-Bromo-2-chlorotetrafluoroethane (R-114B1)	631.3 ± 7.75 1.22%	314.5 ± 1.92 0.61%	167.0 ± 2.69 1.61%	97.4 ± 0.94 0.97%							2.80	2.50	2.22	1.99			

The uncertainties cited are propagated from replicate measurements of the experimental parameters.

carrier gas, and is instrument independent. This is a quantity that may be compared from instrument to instrument, and laboratory to laboratory with a high level of confidence provided the stationary phase used is a single, pure compound. If the mass of stationary phase is not known, or is not meaningful, it is still of value to correct the net retention volume to a column temperature to 0°C (represented by V_N^0) by simply not including the term for W_s (setting it equal to unity). In the present study, the stationary phase is a solid sorbent modified with a liquid coating. Since the retention in this case is not caused exclusively by either adsorption or absorption processes, we will use the net retention volume, V_N^0 , corrected to 0°C (that is, V_g^0 , with $W_s = 1$).

It is also extremely valuable to calculate a relative retention, $r_{a/b}$:

$$r_{a/b} = \frac{V_g^b}{V_g^a} = \frac{V_N^b}{V_N^a} \quad (4)$$

where the alphabetic superscripts refer to the retention volumes of solutes a and b, solute a serving as the reference. The relative retention is dependent only on the column temperature and the type of stationary phase. For reasons of operational simplicity, this parameter is usually one of the best to use for qualitative analysis [7,9]. When measurements are performed carefully, the relative retention varies only with column temperature and stationary phase, and thus forms a reasonable basis for qualitative identification.

To extend the applicability of relative retention data, it is possible to account for temperature by plotting $\ln r_{a/b}$ against $1/T$, where T is the thermodynamic temperature. Such plots are nearly linear (especially in gas-liquid chromatography), and allow comparisons at many column temperatures. The plots can become very non-linear when measured with unmodified solid sorbents as the stationary phase, depending upon the detailed characteristics of the adsorption isotherms. The use of a surface modifier (as was done in the present study) on a solid phase will often increase the linearity of the plots, and shorten retention times.

Although it is not generally considered good practice to extrapolate the plot beyond the temperature range for which experimental data are available, we have found with this class of compounds that extrapolation to temperatures 50°C higher than that used in the correlation can provide acceptable predictions. Naturally, interpolation within the region covered by the experimental data provides very good predictions of both the relative retentions and the net retention volumes. These data can even provide the basis for scaling isothermal analyses to temperature-programmed analyses.

3. Experimental

The measurements presented in this paper were performed on a commercial gas chromatograph that had been modified to provide high-precision retention data. All of the experimental details were described earlier [10], so only a very general description will be provided here. The chromatograph was modified to provide a highly stable column temperature which was measured with a quartz-crystal oscillator thermoprobe (calibrated against a NIST-standard platinum resistance thermometer) that was accurate to within $\pm 0.01^\circ\text{C}$. Injection was done with a valve containing a sample loop of 0.1 ml volume. The valve was pneumatically actuated with pilot valves using helium as the actuation gas to inject very rapidly and thereby minimize the injection pressure pulse. The injection valve and loop were maintained at 50°C for all measurements. The carrier gas line to the injection valve was modified to allow the column head pressure to be measured with a calibrated Bourdon tube gauge. This gauge was calibrated against a dead weight pressure balance traceable to a NIST standard. The column outlet pressure was measured with an electronic barometer that had a resolution of 1.3 Pa (approximately 0.01 Torr). This barometer was also calibrated against a dead-mass pressure balance. The column carrier gas flow-rate (corrected for water vapor pressure) was measured with an electronic soap-bubble flow meter. Retention times were measured

by a commercial integrator. A Ranque–Hilsch vortex tube was used to provide cooling in the column oven for the subambient temperature measurements (see [12]). Thermal conductivity detection (TCD) was used with a carrier gas of research-grade helium. The TCD system was maintained at 50°C for all measurements.

The stationary phase was a commercially prepared packing material consisting of a 5% (mass/mass) coating of a low-molecular-mass polymer of hexafluoropropylene epoxide modifier on a 60–80 mesh (177–250 μm) graphitized carbon black [13]. Some representative properties of this modifier and the column preparation procedure were presented earlier [10].

For each retention time measurement, five fluid injections were performed at each column temperature. Each series of injections was preceded and followed by five measurements of the carrier gas flow-rate, and the injection of five aliquots of air. The air was injected separately, before and after the injection of fluid, to measure the void volume of the column without introducing air as an impurity into the fluid containers. The corrected retention time was simply obtained by subtracting the average air retention time. At the start of each of these fifteen injections (5 air, 5 fluid, 5 air), the requisite temperatures (column, flowmeter, and barometer) and pressures (column head and column exit) were recorded. These replicate measurements furnished the uncertainties used for the error propagation that provided the overall experimental uncertainties that are reported. The column head pressure was maintained uniformly at 137.9 ± 0.3 kPa (approximately 20 p.s.i.g.) for the measurements, although measurements were initially performed at several other pressures to verify consistency in the operation of the chromatograph. The carrier gas flow-rate at the column exit was maintained at 45 ± 0.3 ml/min.

Measurements were performed on four isotherms for each fluid, approximately equally divided between two temperature ranges, -20 to 40°C and 40 to 100°C . One fluid, 1-bromo-1-chlorotetrafluoroethane (R-114B1), was measured between 60 and 120°C . The samples were

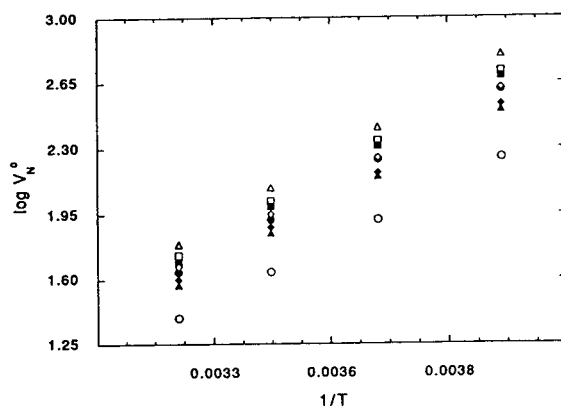


Fig. 1. Plot of the logarithm of the net retention volume, $\log V_N^0$, against $1/T$, for each fluid measured between -20 and 40°C . \circ = R-116; \bullet = R-125; \square = R-134; \blacksquare = R-134a; \triangle = R-143; \blacktriangle = R-143a; \diamond = R-152a; \blacklozenge = R-161.

all obtained from commercial sources in the highest available purity, and were used without further purification.

4. Results and discussion

The corrected net retention volumes, V_N^0 , for each fluid are presented in Table 1. The reported uncertainties are the result of an error propagation performed with the standard deviations

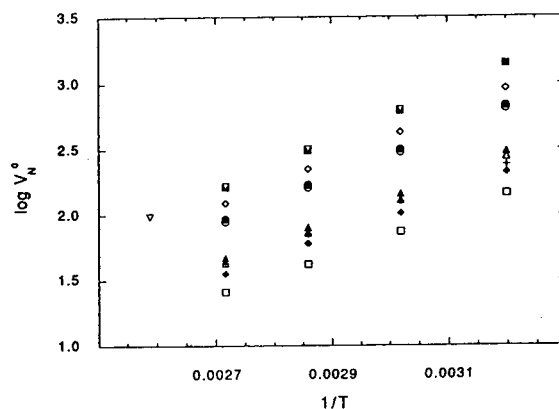


Fig. 2. Plot of the logarithm of the net retention volume, $\log V_N^0$, against $1/T$, for each fluid measured between 40 and 120°C . \circ = R-114; \bullet = R-114a; \square = R-115; \blacksquare = R-123; \triangle = R-124; \blacktriangle = R-133a; \diamond = R-141b; \blacklozenge = R-142b; $+$ = R-160; ∇ = R-114B1.

Table 2

Coefficients of the fits of $\log V_N^0$ against $1/T$, with the respective correlation coefficients

Compound	Model	m	b	r	Temperature range (°C)
R-116	L	1138.5	-2.25	0.99999	-20 to 40
R-125	L	1280.89	-2.45	0.99999	-20 to 40
R-134	L	1297.06	-2.41	0.99997	-20 to 40
R-134a	L	1306.11	-2.47	0.99986	-20 to 40
R-143	L	1332.40	-2.46	0.99997	-20 to 40
R-143a	L	1224.56	-2.33	0.99988	-20 to 40
R-152a	L	1244.01	-2.30	0.99989	-20 to 40
R-161	L	1220.87	-2.29	0.99986	-20 to 40
R-114	L	1675.55	-2.54	0.99989	40 to 100
R-114a	L	1676.43	-2.52	0.99993	40 to 100
R-115	P	2.43	6.932	0.99989	40 to 100
R-123	L	1821.42	-2.67	0.99990	40 to 100
R-124	P	2.28	6.088	0.99982	40 to 100
R-133a	P	2.26	6.033	0.99993	40 to 100
R-141b	L	1688.50	-2.43	0.99994	40 to 100
R-142b	P	2.29	6.084	0.99973	40 to 100
R-160	L	1466.95	-2.30	0.99998	40 to 100
R-114B1	L	1773.22	-2.52	0.99994	60 to 120

Note that for R-115, R-124, R-133a and R-142b the coefficients are for the power (P) model rather than the simple linear (L) model.

obtained from replicate measurements of each experimental parameter. The errors were found to be uncorrelated (as determined by examination of Spearman's ρ and Kendall's τ ; see [14]), and the deviations were found to fit a normal distribution and were therefore treated as being entirely random. In addition to the uncertainty,

the relative standard deviation is provided. The precision of the measurements is generally between 0.5 and 1.5%, with the average precision of all the measurements being 1.04%. This figure compares very well with the precision of typical retention parameters (generally between 1 and 2%) obtained in other physicochemical gas chro-

Table 3

Relative retentions, $r_{a/b}$, and their logarithms, of the more volatile fluids measured in this study, with respect to tetrafluoromethane, R-14

Compound	$r_{a/b}$				$\log r_{a/b}$			
	-20°C (253.15 K)	0°C (273.15 K)	20°C (293.15 K)	40°C (313.15 K)	-20°C (253.15 K)	0°C (273.15 K)	20°C (293.15 K)	40°C (313.15 K)
R-116	9.72	8.32	6.65	6.15	0.99	0.92	0.82	0.79
R-125	22.14	17.45	12.85	10.85	1.35	1.24	1.11	1.04
R-134	28.14	21.84	16.05	13.45	1.45	1.34	1.21	1.13
R-134a	26.16	20.45	15.08	12.18	1.42	1.31	1.18	1.09
R-143	34.41	26.04	18.74	15.28	1.54	1.42	1.27	1.18
R-143a	17.16	14.32	10.91	9.38	1.23	1.16	1.04	0.97
R-152a	22.43	17.86	13.57	11.60	1.35	1.25	1.13	1.06
R-161	18.37	14.97	11.57	10.00	1.26	1.18	1.06	1.00

matographic measurements [15]. A plot of $\log V_N^0$ against $1/T$ is provided in Fig. 1 for each fluid that was measured from between -20 and 40°C . A similar plot is provided in Fig. 2 for the fluids measured between 40 and 120°C . These temperature-dependent data were then fit with the best linear model (simple linear, logarithmic, power or exponential) [10]. The results of these fits are provided in Table 2. Included with each fluid are the coefficients, the Pearson correlation coefficient of the fit, and the temperature range over which the fit was taken. Most of the measurements are represented very well (within experimental error) with the simple linear model:

$$\log V_N^0 = m/T + b \quad (5)$$

where m is the slope and b is the intercept. For four fluids, the power model was slightly better able to account for all of the structure in the data, and therefore provides a somewhat more accurate representation of the measurements. The form of this model is:

$$\log^2 V_N^0 = m[\log(1/T)] + b \quad (6)$$

To recover the V_N^0 value from this model, one must take the antilogarithm (that is, 10^x) twice.

The relative retentions, $r_{a/b}$, were calculated with tetrafluoromethane (R-14) and hexafluoroethane (R-116) as reference compounds. Tetrafluoromethane was chosen because it is the least retained of all the fluids examined [10], and was used only for the more volatile fluids studied here. These values are provided in Table 3. Relative retentions with respect to hexafluoroethane were calculated for all of the fluids, however, and are provided in Table 4. Plots of $\log r_{a/b}$ against $1/T$ for each reference are provided in Figs. 3 and 4. The expected trend with temperature is observed, and the plot and fits can therefore be used for prediction of the retention behavior on other columns containing the same stationary phase.

In addition to the quantitative relationships and correlations presented above, the retention parameters we have measured appear to fit an important qualitative scheme that is useful in

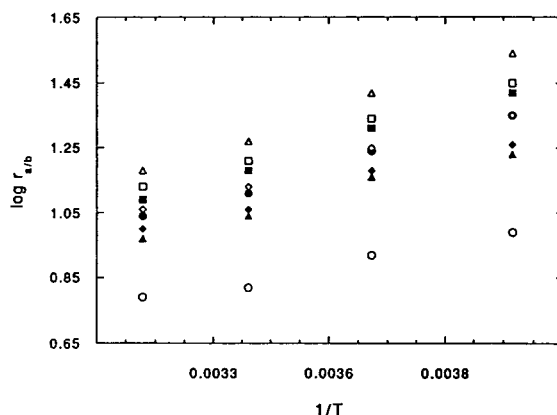


Fig. 3. Plot of the logarithm of the relative retention, $\log r_{a/b}$, with respect to tetrafluoromethane (R-14), against $1/T$, for the fluids measured between -20 and 40°C . \circ = R-116; \bullet = R-125; \square = R-134; \blacksquare = R-134a; \triangle = R-143; \blacktriangle = R-143a; \diamond = R-152a; \blacklozenge = R-161.

understanding the behavior of chlorofluorocarbons and fluorocarbons. One can construct a kind of "periodic chart" or property diagram for these types of compounds [2]. The chart has a triangular format that groups the fluids according to their molecular structures and properties. We present in Fig. 5 such a chart for two-carbon fluids. The top of the chart represents compounds rich in hydrogen (with ethane being the extreme member); the right-hand side represents compounds rich in fluorine (with hexafluoroethane being the extreme member); and the left-hand side represents compounds rich in chlorine (with hexachloroethane being the extreme member). Such charts have been successful in systematizing, in a semiquantitative manner, properties such as normal boiling point, atmospheric lifetime, flammability and toxicity [2]. The retention parameters measured in this study fit this scheme qualitatively, with expected minima in the fluorine-rich section, and expected maxima predicted to occur in the chlorine-rich section. This chart can provide guidance in the design of analyses of (1) compounds not measured in this study, and (2) analyses done with somewhat different modifier concentration on the stationary phase.

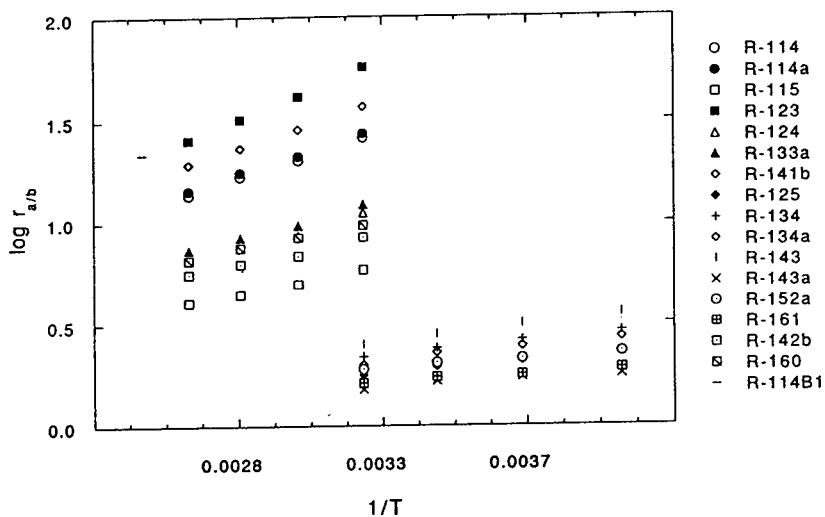


Fig. 4. Plot of the logarithm of the relative retention, $\log r_{a/b}$, with respect to hexafluoromethane (R-116), against $1/T$, for all fluids measured in this study.

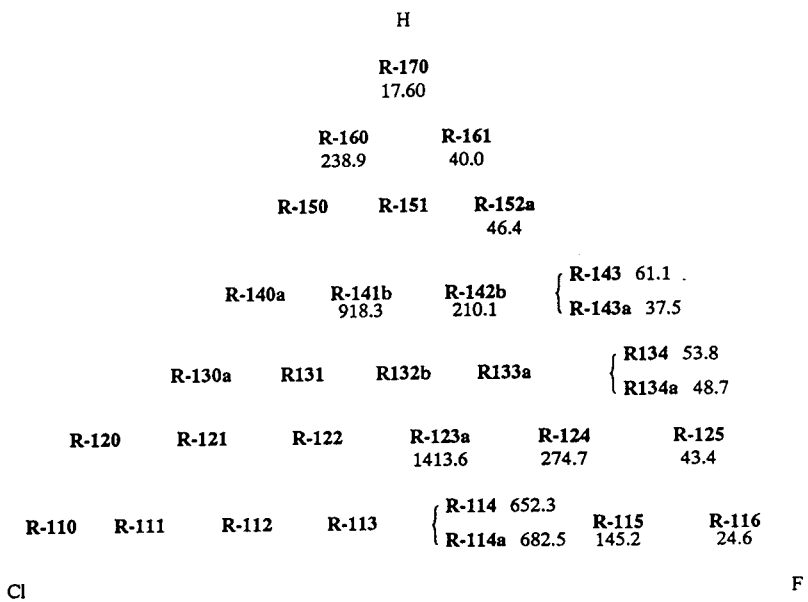


Fig. 5. Triangular diagram that provides a semiquantitative representation of refrigerant properties correlated with molecular structure. In this diagram, we have listed the net retention volumes, V_N^0 , for each of the indicated fluids measured at 40°C (313.15 K).

5. Conclusions

Measurements of the corrected net retention volume and relative retentions of 18 two-carbon halocarbon fluids that are relevant to research on alternative refrigerants have been presented. The logarithms of these data were fitted against reciprocal thermodynamic temperature to several linear models. In most cases, a simple linear relationship accounts for all structure in the data; in a few cases, a power model is slightly better. These derived equations can be used for the prediction of the retention behavior of these fluids on this important stationary phase, and therefore can be used for solute identification and analytical separation design. In addition, we note that the retention parameters also qualitatively fit the triangular diagram scheme that successfully describes the normal boiling point, flammability, atmospheric lifetime and toxicity of these compounds.

Acknowledgement

The financial support of the Colorado Alliance for Science is gratefully acknowledged.

References

- [1] E.J. Lizardos, *Maint. Tech.*, 6, No. 8 (1993) 17–19.
- [2] M.O. McLinden and D.A. Didion, *ASHRAE J.*, 29, No. 12 (1987) 32–42.
- [3] T.J. Bruno, *Spectroscopic Library for Alternative Refrigerant Analysis, Special Publication 794*, National Institute of Standards and Technology (USA) (NIST), Boulder, CO, 1990.
- [4] T.J. Bruno, *Strategy of Chemical Analysis of Alternative Refrigerants, Technical Note 1340*, National Institute of Standards and Technology (USA), Boulder, CO, 1990.
- [5] T.J. Bruno, *ASHRAE Trans.*, 98, No. 2 (1992) 204–208.
- [6] T.J. Bruno, *ASHRAE Trans.*, 98, No. 2 (1992) 210–215.
- [7] R.L. Grob (Editor), *Modern Practice of Gas Chromatography*, Wiley, New York, 2nd ed., 1985.
- [8] T.J. Bruno, *Chromatographic and Electrophoretic Methods*, Prentice-Hall, Englewood Cliffs, NJ, 1991.
- [9] J.E. Willett, *Gas Chromatography (Analytical Chemistry by Open Learning)*, Wiley, Chichester, 1987.
- [10] T.J. Bruno and M. Caciari, *J. Chromatogr. A*, 672 (1994) 149–158.
- [11] T.J. Bruno (Editor), *CRC Handbook for the Analysis and Identification of Alternative Refrigerants*, CRC Press, Boca Raton, FL, 1994.
- [12] T.J. Bruno, *Anal. Chem.*, 58 (1986) 1596.
- [13] J.L. Glajch and W.G. Schindel, *LC·GC*, 4 (1986) 574.
- [14] J.D. Gibbons and S. Chakraborti, *Nonparametric Statistical Inference*, Marcel Dekker, New York, 1992.
- [15] T.J. Bruno and D.E. Martire, *J. Phys. Chem.*, 87 (1986) 2430.

Combined solvent extraction–mass spectrometry determination of free phenol traces in poly(vinyl chloride) products

Joaquín Vilaplana^{a,*}, Juan López^a, Alfonso Jiménez^b

^a*Instituto Tecnológico del Juguete (AIJU)., Av. Industria s/n, Ibi (Alicante) 03440, Spain*

^b*Analytical Chemistry Department, University of Alicante, Ap. 99, 03080, Alicante, Spain*

First received 7 March 1994; revised manuscript received 7 June 1994

Abstract

A gas chromatography–mass spectrometry technique was used for the analysis of trace phenol in poly(vinyl chloride) products. A pre-concentration of samples was made by using a solid-phase extraction cartridge, previously developed for wastewater. The cartridge extraction of several samples yielded recoveries better than 90%. The relative standard deviation of overall recoveries for ten different samples was less than 7%. The detection limit achieved was less than 10 ppb (w/w) for free phenol measured in plastic materials.

1. Introduction

Increasing interest in the determination of free phenol in environmental samples has prompted the development of numerous methods for their quantitation. In terms of instrumentation, the proposed procedures are diverse. Colorimetry, gas–liquid and liquid–solid chromatography, and mass spectrometry have been most popular. The colorimetric standard procedure [1] is based on the reaction with 4-aminoantipyrine and oxidation under alkaline conditions to give a colored product. The main problem in using this method is the unspecificity among various phenols. For improved specificity, chromatographic methods have replaced colorimetry. Gas chromatography (GC) with flame ionization, electron-capture or mass spectrometric (MS) detection is commonly

used [2–9]. In other cases, phenols have been separated by liquid chromatography [10,11].

In polymer processing, a great number of additives can be used. Some of them, mainly antioxidants and ultraviolet absorbers, are typically phenol derivatives with sterically protected phenolic hydroxyl groups. Low-molecular-mass substituted phenols are too volatile for use in poly(vinyl chloride) (PVC). 2,2-Bis(*p*-hydroxyphenyl)propane, commonly known as bisphenol A, and 2,6-di-*tert*-butyl-*p*-cresol, commonly known as BHT, are the most widely used materials. Products such as alcohols and phenols can be the result of stabilizer hydrolysis or oxidation.

Several chromatographic techniques can be applied to the analysis of polymer additives, including high-performance liquid chromatography [12–15], supercritical fluid chromatography [16–19] and capillary GC [20,21], which can be easily combined with MS. This technique offers better resolution and higher sensitivity.

* Corresponding author.

This is the reason why this technique has been chosen to identify and quantify free phenol in polymers.

Solid-phase extraction has been a very adequate method to isolate and purify many chemical compounds in a complex matrix, being a fast and reproducible method. It has been applied as a sample purification technique, trace enrichment and quick separation method. A great number of analytical techniques have used this extraction procedure as a complementary method, mainly GC [22].

Recently developed bonded-phase silica adsorbents have been used for the specific adsorption of organic compounds from water [23–25]. The wide variety of bonded phases available allowed the selection of the most effective sorbent for a particular application [26]. Several bonded phase materials have been evaluated for the sampling/concentration of phenols [27]. However, there are few examples of application to actual polymers.

The aim of this study is the extension of the GC–MS and solid-phase extraction technologies, used in other samples as wastewaters, to polymers and in particular to PVC products.

2. Experimental

2.1. Materials

All chemicals were analytical grade and were supplied by Panreac (Barcelona, Spain). Reagent-grade water was obtained from a Barnstead E-pure system (Barnstead, Dubuque, IA, USA). Bond Elut cartridges (Analytichem International, Harbor City, CA, USA) containing cyclohexyl (CH) as a bonded phase adsorbent were used for phenolic pollutants in wastewaters [22]; these were considered the best choice for a solid-phase adsorbent (containing 1000 mg per cartridge) in polymer studies.

As a first material Vestolit B 7021 (Huls) PVC resin has been used. This is a homopolymer, non-prestabilized, and capable of forming low-viscosity pastes easily. This suspension PVC resin, normally used for rotational moulding, has

been characterized by calculating the K value, using DIN 53726 standard, giving a final result of $K = 72.0$. By measuring mean molecular mass a value of 130 000 has been obtained. As phenol sources some industrial antioxidants as Irganox 1076 have been used.

2.2. Equipment

Analyses were carried out using a Shimadzu QP 1100 EX gas chromatograph–mass spectrometer (Shimadzu, Kyoto, Japan) equipped with a split/splitless injection system and an electron multiplier with ion converter as a detector. The limit of detection is 100 pg methyl stearate in the electronic ionization mode. Eluate samples were analyzed on a 30 m × 0.25 mm fused-silica SPB-5 capillary column (Supelco, Bellefonte, PA, USA) with a film thickness of 0.20 μm . The column temperature program was as follows: 55°C no hold, 10°C/min to 185°C with a 5-min hold, 10°C/min to 250°C with a final hold of 5 min. The linear rate of the helium carrier gas was 20 cm/s. A 2- μl volume of sample was introduced in the splitless mode with the injector at 250°C and the solvent vent was closed for 90 s after injection. The column was heat-traced (250°C) directly from the GC oven into the heated (250°C) mass spectrometer ion source. The MS was scanned from 10 to 1000 u twice every second, under standard electron impact conditions (70 eV). Data were collected and analyzed with an MS-PAC 1000 data system (Shimadzu) including the automatic quantitation software.

2.3. Operating procedure

Phenol pre-treatment in PVC derivatives is made by a Soxhlet extraction using sodium hydroxide aqueous solution (pH 10) over 1.000 ± 0.001 g of PVC product. This sample amount has been chosen because it has been previously considered as appropriate to obtain a representative quantity of phenol in final samples. The extracted phase is diluted to 70 ml with deionized water and stored in the dark until it would be pre-concentrated.

The phenol pre-concentration is made by using Bond Elut cartridges. First the cartridge was conditioned by addition of 1 ml of methanol, which was allowed to set for 5 min before being drawn off and 1 ml of 0.01 M HCl afterwards. The pH of samples was adjusted to 1–2 by addition of concentrated HCl to obtain the conversion of phenolate ion into phenol and 17.5 g of NaCl were added to the sample to decrease phenol solubility. It has been demonstrated that phenol recoveries in wastewaters are improved at NaCl concentrations between 20 and 25% [22].

Then the cartridge was adapted to a vacuum pump, Visiprep Vacuum Mainfold (Supelco) and the extract was aspirated through sorbent at 20 ml/min. Finally, the cartridge was washed with 0.01 M HCl and the vacuum left on for 10 min to dry the sorbent. The cartridge was eluted with 2 ml of methanol which was allowed to remain on the cartridge for a few minutes before being drawn off. After measuring the volume, the eluate was stored in glass-sealed vials in the dark until analysis.

GC-MS analysis was performed by injecting 2 μ l of eluate in the splitless mode as described above. The use of methanol solutions for splitless injections is made because split injections resulted in poorly shaped chromatographic peaks. Quantitation of free phenol was done by comparing chromatographic peak areas for sample eluates with those of standards in the same concentration range.

3. Results and discussion

Because of its relatively high solubility in water and ionic characteristics, phenol has a short retention time. That is the reason why the GC-MS run must be started at low temperatures. A typical GC-MS run of a free phenol standard using selected ion monitoring (SIM) mode and centering on ion 94.0 is given in Fig. 1. It will be noted that a sharp peak is obtained at a relatively short retention time. The use of SIM mode in mass spectrometry results in a

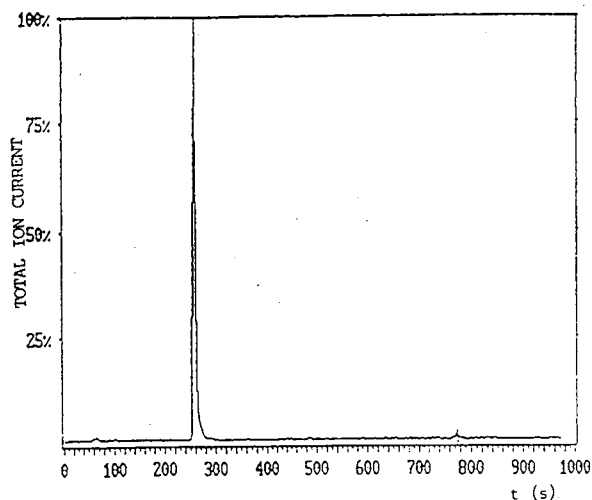


Fig. 1. Free phenol standard (5.0 ppm) chromatogram obtained by using the SIM mode.

better separation and peak quantitation and sensitivity improvement.

By operating with the method described above and preparing some adequate standards, a calibration line can be obtained as shown in Fig. 2. Samples can be quantitated by interpolation from a standard curve with linearity extending from 1.6 to 16.0 ng injected (slope = $1.22 \cdot 10^3$, y intercept = $-1.17 \cdot 10^3$, correlation coefficient = 0.9991).

Hydrophobic sample cleanup cartridges, as Bond Elut, offer a rapid alternative to other preconcentration techniques, which are necessary when the sample concentration is less than about 500 ppb. The common practice with these materials is to pass as much sample volume through as possible, without permitting breakthrough and a concomitant loss of recovery [28,29]. Unfortunately, for phenols, breakthrough occurs early so that the concentration advantage is reduced.

Moreover, in polymer samples it is important to assess the influence from other species in the matrix on free phenol recovery. A number of experiences have been made in order to quantify the breakthrough point of Bond Elut cartridges and to give a security interval of work. As shown by Fig. 3, a 70-ml sample can be considered as

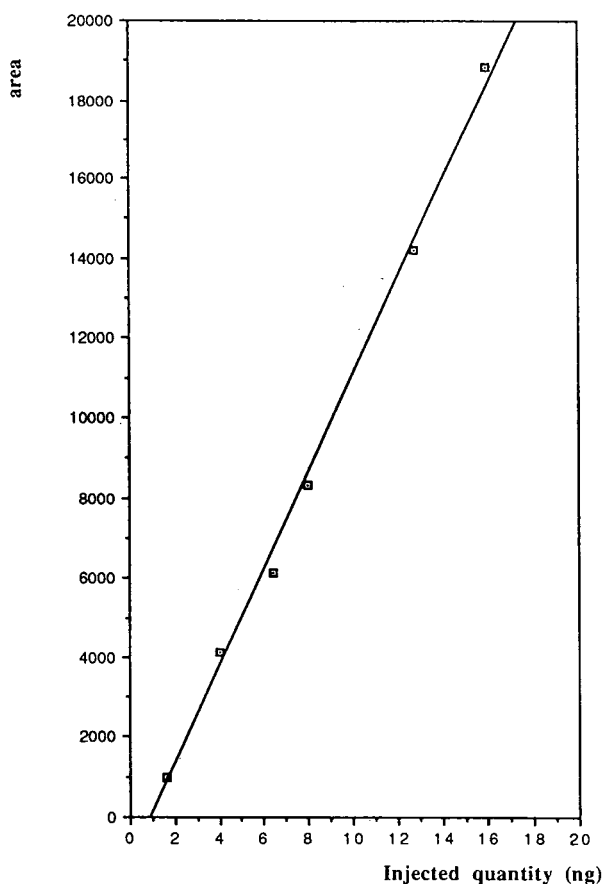


Fig. 2. Calibration curve for free phenol (SIM mode).

the maximum quantity allowed to avoid break-through problems in a 5-ng free phenol extract.

By equilibrating the entire cartridge with solute, careful control of flow-rate is unnecessary. However, the absolute amount of solute trapped depends on the amount of adsorbent material in the cartridge. The standard deviation by mass of packaging material is approximately 2%, comparable to the precision in common solvent extractions.

A number of experiments have been carried out to obtain recoveries of phenol from some samples which were considered representative for the amount of free phenol in real samples. The results of analyses using the conditions described above are summarized in Table 1. As can be seen from Table 1, better recoveries are

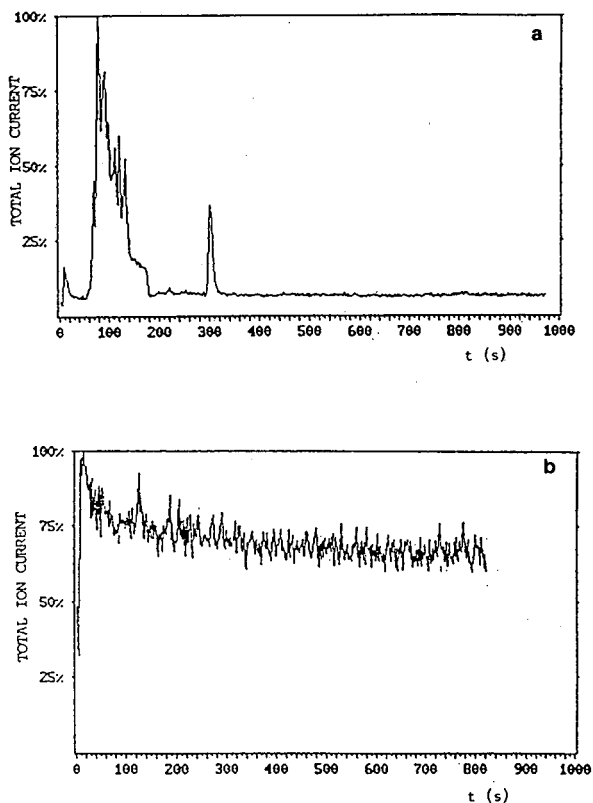


Fig. 3. Chromatograms of two 5-ng free phenol extracts: (a) 70 ml extract, (b) 90 ml extract.

obtained in the interval 120–150 ppb. These results can be explained by some differences in apparatus sensitivity.

Some samples have been prepared in order to determine detection limits for free phenol in polymers. The restricted amount of sample that

Table 1
Free phenol recoveries from polymer samples

Phenol (ppb)	Recovery (%)	S.D. (%)
100	89	5
110	95	2
120	99	3
130	99	4
140	99	3
150	99	3

A 2- μ l volume was injected; 55 to 185°C at 10°C/min. Three injections of every sample have been made.

Table 2
Sunlight and time of exposure effect in free phenol polymer sample

Time of exposure (min)	Apparent concentration (ppm)
0	4.9
30	4.6
60	3.7
90	3.2
120	2.9
150	2.5
180	2.0
210	1.8
240	1.6

can be passed through the cartridges is a real problem to obtain better detection limits. However, it was found that detection limits below 10 ppb for free phenol could still be achieved by GC–MS. This value could be improved by using larger injection volumes, but it has been proved that some problems could arise with capillary columns utilized during the present study using volumes larger than 2 μ l. Thus, this method applied to polymers permits us to obtain detection limits very similar to wastewaters [4,5,22].

Finally, a study has been made to determine if sample degradation occurs if the sample is stored in any particular way. We have studied photochemical degradation for a 5-ppm phenol sample and some phenol loss due to sunlight has been observed. Results are summarized in Table 2.

As can be seen from Table 2 there is an important effect of sunlight in phenol apparent concentration. Hence, it would be better to store samples in the dark to avoid photochemical degradation.

4. Conclusions

From a practical standpoint, a new GC–MS method to determine free phenol in polymers has been proved to be as consistent as used in waters. Moreover, the cartridge adsorbent extraction method has several advantages: (a) very little solvent (2 ml) is needed for extraction so

that the evaporative concentration step is eliminated; (b) the labor and equipment required for sample preparation are greatly reduced; (c) selective elution procedures yield a final eluate with fewer background interferences than obtained by common extraction procedures in complex samples as polymers. This factor could improve the accuracy and precision of the analysis.

References

- [1] F.D. Snell and L.S. Ettore (Editors), *Encyclopedia of Industrial Chemical Analysis*, Vol. 19, Interscience, New York, 1974, p. 386.
- [2] T.R. Edgerton, R.F. Moseman, E.M. Lores and L.H. Wright, *Anal. Chem.*, 52 (1980) 1774.
- [3] A.B. McKague, *J. Chromatogr.*, 208 (1981) 287.
- [4] Y.I. Korenman, V.A. Minasyants and V.N. Fokin, *Zh. Anal. Khim.*, 43 (1988) 1303.
- [5] M.M. Kopečni, M.V. Tarana, S.D. Cupic and J.J. Comor, *J. Chromatogr.*, 462 (1989) 392.
- [6] Y.I. Korenman and V.N. Fokin, *Zh. Anal. Khim.*, 44 (1989) 1607.
- [7] Y.I. Korenman, A.I. Kryukov and V.N. Fokin, *Zh. Anal. Khim.*, 45 (1990) 1027.
- [8] D.I. Welch and C.D. Watts, *Int. J. Environ. Anal. Chem.*, 38 (1990) 185.
- [9] C. Brage and K. Sjoostrom, *J. Chromatogr.*, 538 (1991) 303.
- [10] R.E. Shoup and G.S. Mayer, *Anal. Chem.*, 54 (1982) 1164.
- [11] K. Kuwata and S. Tanaka, *J. Chromatogr.*, 442 (1988) 407.
- [12] F. Sevini and B. Marcato, *J. Chromatogr.*, 260 (1983) 507.
- [13] J.D. Vargo and K.L. Olson, *Anal. Chem.*, 57 (1985) 672.
- [14] J.D. Vargo and K.L. Olson, *J. Chromatogr.*, 353 (1986) 215.
- [15] D. Munteanu, A. Isfan, C. Isfan and I. Tincul, *Chromatographia*, 23 (1987) 7.
- [16] J. Doehl, A. Farbrot, J. Greibrokk and B. Iversen, *J. Chromatogr.*, 392 (1987) 175.
- [17] M.W. Raynor, K.D. Bartle and I.L. Davies, *Anal. Chem.*, 60 (1988) 427.
- [18] P.J. Arpino, D. Dilettato, K. Nguyen and A. Bruchet, *J. High Resolut. Chromatogr.*, 12 (1989) 688.
- [19] M. Ashraf-Khorassani and J.M. Levy, *J. High Resolut. Chromatogr.*, 13 (1990) 742.
- [20] G. di Pasquale, L. Giambelli, A. Soffientini and R. Paiella, *J. High Resolut. Chromatogr. Chromatogr. Commun.*, 8 (1985) 618.

- [21] W. Blum and L. Damasceno, *J. High Resolut. Chromatogr. Chromatogr. Commun.*, 10 (1987) 472.
- [22] E. Chladek and R.S. Marano, *J. Chromatogr. Sci.*, 22 (1984) 313.
- [23] E. Grushka, *Bonded Stationary Phases in Chromatography*, Ann Arbor Sci. Publ., Ann Arbor, MI, 1978.
- [24] F. Eisenbeiss, H. Heln, R. Joesler and G. Naundorf, *Chem. Tech.*, 6 (1977) 8.
- [25] R.A. Dylar, D.L. Bodenner and K.J. Welch, *Anal. Chem.*, 50 (1978) 837.
- [26] T.J. Good, *Am. Lab.*, 13 (1981) 36.
- [27] P. Dimson, *LC Mag.*, 1 (1983) 236.
- [28] P. Schauwecker, R.W. Frei and F. Erni, *J. Chromatogr.*, 136 (1977) 63.
- [29] R.J. Bushway, *J. Chromatogr.*, 211 (1981) 135.



ELSEVIER

Journal of Chromatography A, 679 (1994) 139–146

JOURNAL OF
CHROMATOGRAPHY A

Direct and indirect approaches to enantiomeric separation of benzodiazepines using micro column techniques

Susanne R. Almquist^a, Patrik Petersson^a, Willi Walther^b, Karin E. Markides^{a,*}

^aDepartment of Analytical Chemistry, Uppsala University, P.O. Box 531, S-75121 Uppsala, Sweden

^bPharmaceutical Research Department, F. Hoffmann-La Roche, Ltd., CH-4002 Basle, Switzerland

First received 1 March 1994; revised manuscript received 8 June 1994

Abstract

The ability of gas chromatography, supercritical fluid chromatography (SFC) and subcritical fluid chromatography to separate ten benzodiazepine racemates, using both direct and indirect methods, has been investigated. Racemic lorazepam, oxazepam, ethyl loflazepate and dihydrodiazepam were baseline separated in open tubular column SFC using a permethylated β -cyclodextrin stationary phase. Racemic oxazepam, lorazepam, temazepam and ethyl loflazepate, derivatized with (*S*)-trolox methyl ether, were separated on a non-chiral packed capillary column with diol functionality, employing a subcritical fluid as mobile phase. The temazepam derivatives were also baseline separated using an open tubular biphenyl column in SFC.

1. Introduction

A racemic mixture should be considered as a mixture of two different substances since optical isomers may differ in biological activity, toxicity and metabolism [1]. Enantiomeric separation can be achieved using either direct or indirect methods. The direct methods include the use of a chiral stationary (or mobile) phase, while the indirect methods are based on chiral derivatizations, i.e. conversion of the enantiomers into diastereomers, and separations using non-chiral stationary phases. Chiral derivatization is unfortunately not a straightforward procedure as the optical purity of the reagent must be known and high, the yield of the reaction must be carefully controlled and racemisation of the

sample during reaction must be prevented. On the other hand, with the indirect method the elution order of the diastereomers can be altered by using either the (*R*)- or the (*S*)-form of the chiral reagent. A broad range of non-chiral columns is also commercially available, for both gas chromatography (GC) and supercritical fluid chromatography (SFC).

The most widely used chiral stationary phases in both GC and SFC are based on permethylated β -cyclodextrin (β -CD-M) [2–6]. It is believed that the cavity of the cyclodextrin-bucket empowers chiral recognition through the formation of inclusion complexes [6,7]. Due to the solvating power of supercritical carbon dioxide, the stationary phases used in open tubular column SFC must be carefully immobilised [8]. Several reports have been published on the synthesis of stable chiral open tubular columns for SFC [2–

* Corresponding author.

4,9,10]; but yet there are no such columns commercially available. In packed-column SFC, as in liquid chromatography (LC), this becomes a minor problem since the chiral selector is covalently bound to the packing material. Most chiral LC columns can also be used in enantiomeric separations carried out by SFC.

Benzodiazepines are tranquillising and anti-convulsive drugs and can be classified as compounds of medium to high polarity. According to the literature most separations of benzodiazepines have been carried out using LC and in a recent article the advantages of using normal-phase LC (NPLC) instead of reversed-phase LC (RPLC) were pointed out [11]. Also the direct enantiomeric separation of these types of analytes is favoured by NPLC [12]. Wännman et al. [13] reported of the difficulties using RPLC in enantiomeric separation of oxazepam, which undergoes racemisation in aqueous media leading to the formation of a diffuse zone between the two enantiomeric peaks. In a comparative study between NPLC and subcritical fluid chromatography (SubFC) using chiral stationary phases, Macaudière et al. [6] showed that SubFC can be used with advantage for the resolution of various classes of racemates. Racemic oxazepam was, for example, separated both in SubFC and NPLC with a resolution of 3.5. The separation took less than 5 min employing SubFC but more than 20 min in LC [6]. Separations of racemic benzodiazepines using a supercritical fluid as mobile phase and a cyclodextrin-based open tubular column have been reported [3].

The use of GC for separation of benzodiazepine-like compounds is often hindered by thermolability [7], high molecular mass and high polarity. Some of the benzodiazepines have, nevertheless, been routinely analysed by GC [14–16], but to our knowledge no enantiomeric separation has been reported. The efficiency is generally higher in GC than in SFC and SubFC. On the other hand, the lower temperatures used in SFC and SubFC are advantageous as the chiral selectivity generally increases with decreasing temperature [17–19]. Additional advantages with a supercritical fluid mobile phase is the minimal consumption of organic solvents and

the possibility to use lower UV wavelengths for detection.

In this work both direct and indirect micro-column techniques (SFC, SubFC and GC) for enantiomeric separations of several benzodiazepines are compared and discussed.

2. Experimental

2.1. Instrumentation

The studies with open tubular columns and unmodified carbon dioxide as mobile phase were carried out using a series 600 SFC system equipped with a flame ionisation detection (FID) system (Dionex, Salt Lake City, UT, USA). Time-split injections were performed with a Valco C14W high-pressure four-port valve (Valco Instruments, Houston, TX, USA) equipped with a 0.2- μ l sample loop. Both the 7.5 m \times 50 μ m I.D. (originally 10 m) SB-Biphenyl-30 (30% biphenyl methylpolysiloxane, film thickness d_f = 0.25 μ m) column, and the fused-silica frit restrictor were obtained from Dionex. Chromatograms were recorded with a W + W 1100 recorder (Kontron Instruments, Zurich, Switzerland).

Separations on the packed capillary column, using methanol-modified carbon dioxide as mobile phase were carried out using a Carlo Erba SFC 3000 series (Fison Instruments, Milan, Italy) connected to a Phoenix 20 CU pump equipped with a Phoenix 20 slave pump (Fison Instruments). The SFC system was programmed using an IBM PC XT Model 286 computer and software from Fison Instruments. Time-split injections were, also in this set-up, carried out using a Valco C14W high-pressure four-port valve equipped with a 0.2- μ l sample loop. UV detection was performed at 254 nm using a capillary detector 433 with a 0.2- μ l fused-silica Z-cell (Kontron Instruments). The 30 cm \times 320 μ m I.D. packed capillary column, with LiChrosorb Diol as stationary phase (5 μ m), was purchased from LC Packings (Zurich, Switzerland). A fused-silica frit restrictor 50 μ m I.D. (Dionex) was mounted after the UV detector.

Chromatograms were recorded with a W + W 1100 recorder (Kontron Instruments)

GC separations were carried out using a Carlo Erba GC 6000 Vega Series 2, equipped with an FID system (Fison Instruments). The injections were performed with split flow (ca. 1:40) and the injection temperature was 250°C. Chromatograms were recorded with a Chrom Jet integrator (Spectra-Physics, Houston, TX, USA)

The chiral stationary phases that were used in open tubular column SFC and in GC were based on permethylated β -cyclodextrin. In the GC experiments, 25 m \times 320 μ m I.D. and 17 m \times 320 μ m I.D. deactivated fused-silica capillaries coated with β -CD-M dissolved in OV-61 (33% diphenyl dimethylpolysiloxane) were used. The separations carried out with SFC were obtained using a 5 m \times 50 μ m I.D. deactivated fused-silica capillary coated with approximately 0.25 μ m side-arm substituted methyloctylsiloxane, having β -CD-M as chiral selector [20].

2.2. Chemicals

SFC-grade carbon dioxide was obtained from Scott Speciality Gases (Plumsteadville, PA, USA). Oxazepam, temazepam, lorazepam, ethyl loflazepate, dihydrodiazepam, camazepam, flutazolam, cloxazolam, tofisopam and otazolam were all kindly supplied by Hoffmann-La Roche (Basle, Switzerland). The derivatization reagents, acetic anhydride (AA), trifluoroacetic anhydride (TFAA), dicyclohexylcarbodiimide (DCC) and 4-dimethylaminopyridine (DMAP) were obtained from Fluka (Buchs, Switzerland). (*S*)-Trolox methyl ether was prepared at Hoffmann-La Roche but can also be obtained from Fluka. All solvents were of analytical grade.

2.3. Derivatization procedures

Derivatization using acetic anhydride and DMAP

The analyte was dissolved in water-free pyridine and derivatized with AA using DMAP as a catalyst. The reaction time was 2 h at 70°C. The reaction mixture was first dried under a

stream of nitrogen and was then dissolved in methylene chloride.

*Chiral derivatization using (*S*)-trolox methyl ether*

The analyte was first dissolved in methylene chloride (*S*)-trolox methyl ether, DCC and DMAP were then added. The reaction time was 1 h at room temperature. Because of the formation of dicyclohexyl urea, the mixture was filtered through a 0.45- μ m filter prior to injection. Ethyl loflazepate, otazolam and cloxazolam were derivatized, although not quantitatively, using higher amounts of DCC and DMAP and a reaction time of 10 h at room temperature.

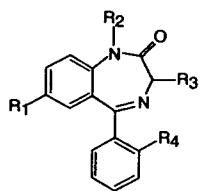
3. Results and discussion

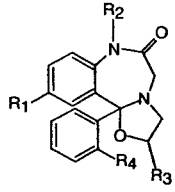
3.1. Direct separation of benzodiazepine enantiomers

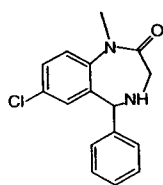
The underivatized benzodiazepine standards, shown in Table 1, were chromatographed by chiral open tubular column SFC, using a slow density program (starting at 0.20 g ml⁻¹, with 0.007 g ml⁻¹ min⁻¹ up to 0.750 g ml⁻¹) under isothermal conditions (60°C). The enantiomers having the longest retention times and thus the highest elution densities, i.e. dihydrodiazepam, oxazepam, lorazepam and ethyl loflazepate were separated. To obtain high resolution (i.e. $R_s = 1.5$) in a minimum amount of time, the separation of dihydrodiazepam, oxazepam, lorazepam and ethyl loflazepate was optimised according to the procedure described in Refs. 21 and 22. The optimised separations (Table 2) were performed using a short focusing step, i.e. a low density (e.g. 0.20 g ml⁻¹) was maintained for a short initial period (e.g. 2 to 3 min) as part of the injection procedure, after which the density was rapidly increased (e.g. 0.20–0.50 g ml⁻¹ min⁻¹) to the calculated optimal density. This density was then maintained until the analyte had eluted.

In a recent work [23] little or no enantio-

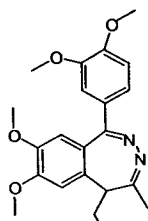
Table 1
Structures and names of the ten racemic benzodiazepines used in this study

Name				
	R ₁	R ₂	R ₃	R ₄
Temazepam	Cl	CH ₃	OH	H
Oxazepam	Cl	H	OH	H
Lorazepam	Cl	H	OH	Cl
Ethyl loflazepate	Cl	H	COOCH ₂ CH ₃	F
Camazepam	Cl	CH ₃	OCN(CH ₃) ₂	H

				
	R ₁	R ₂	R ₃	R ₄
Flutazolam	Cl	CH ₂ CH ₂ OH	H	F
Otazolam	Cl	H	CH ₃	H
Cloazolam	Cl	H	H	Cl



Dihydrodiazepam



Tofisopam

selectivity was observed for oxazepam and lorazepam using a cyclodextrin-based open tubular column in SFC. As shown in Table 2 and Fig. 1a, separation of these analytes is indeed possible, although the optimised separations of oxazepam and ethyl loflazepate gave R_s values below 1.5, due to a slight tailing of the peaks. As can be seen in Fig. 1b, baseline-separated peaks

in less than 4 min were obtained for dihydrodiazepam.

A general advantage with open tubular columns in SFC is the ability to obtain well-deactivated columns and thereby the possibility to use a non-modified mobile phase for elution. This enables the use of the "universal" FID as detection method. However, all test compounds in this study, except dihydrodiazepam gave poor FID responses. The smaller signal-to-noise ratio for e.g. lorazepam compared to dihydrodiazepam can be seen in Fig. 1. Poor FID sensitivity for these analytes has earlier been reported by Chiarotti et al. [24].

None of the underivatized benzodiazepines could be eluted using a chiral open tubular column (β -CD-M/OV-61) in GC, using a temperature program from 100 to 220°C.

3.2. "Direct" separation of benzodiazepine enantiomers after a non-chiral derivatization

Oxazepam, lorazepam and ethyl loflazepate were derivatized with AA and TFAA according to the method described in the Experimental section. While the derivatization of lorazepam and oxazepam, that contains a hydroxyl group, gave a quantitative yield, ethyl loflazepate was not quantitatively derivatized.

In chiral open tubular column SFC, this approach resulted in decreased retention times, improved peak shapes and an almost unchanged resolution for the acetylated analytes compared to that for the underivatized analytes. This is illustrated by underivatized and AA-derivatized oxazepam in Fig. 2. Under the same SFC conditions for the acetylated compounds as for the underivatized, the FID response was still not sufficient although a small increase in the signal was observed for the compounds derivatized with AA (Fig. 2). UV detection or electron-capture detection could be an alternative for this type of analytes, the latter especially after a derivatization with TFAA.

None of the AA or TFAA derivatives could be eluted in GC using the β -CD-M/OV-61 column, and a temperature program from 170 to 215°C.

Table 2

Resolution of racemic benzodiazepine standards using a β -CD-M open tubular column in SFC

Compound	Density (g ml ⁻¹)	Temperature (°C)	<i>t_R</i> (min)	<i>R_s</i>
Dihydrodiazepam	0.520	85	3.6	1.6
Oxazepam	0.445	55	44.9	1.2
Lorazepam	0.635	60	17.1	1.7
Ethyl loflazepate	0.400	50	23.1	1.3

Open tubular column SFC. Column 5 m × 50 μm I.D. fused-silica capillary, coated with side-arm substituted methyloctylsiloxane having β -CD-M as chiral selector, $d_t = 0.25$ μm. Supercritical carbon dioxide as mobile phase. *t_R* = Retention time for the last-eluting peak. The densities shown in Table 2 are the calculated optimal densities.

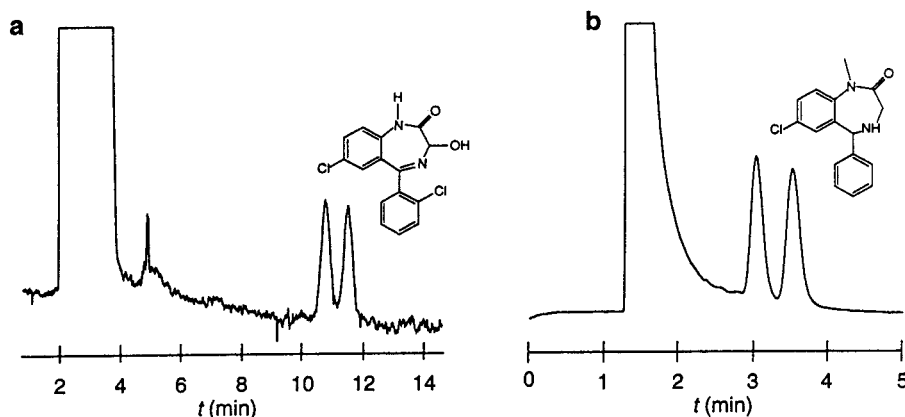


Fig. 1. Enantiomeric separation of (a) lorazepam (5 mg ml⁻¹), CO₂ at 0.79 g ml⁻¹, 60°C and (b) dihydrodiazepam (5 mg ml⁻¹), CO₂ at 0.52 g ml⁻¹, 85°C. Using an open tubular column (5 m × 50 μm), coated with side-arm substituted methyloctylsiloxane, having β -CD-M as a chiral selector, $d_t \approx 0.25$ μm.

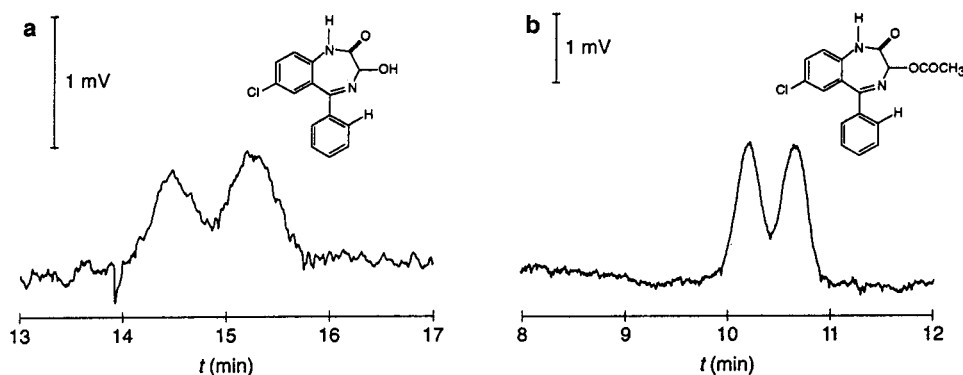


Fig. 2. Enantiomeric separation of (a) oxazepam (5 mg ml⁻¹) and (b) oxazepam derivatized with acetic anhydride (5 mg ml⁻¹). Using an open tubular column (5 m × 50 μm), coated with side-arm substituted methyloctylsiloxane having β -CD-M as a chiral selector, $d_t \approx 0.25$ μm. CO₂ at 0.79 g ml⁻¹, 60°C.

3.3. Indirect separation of benzodiazepine as diastereomers

Chiral derivatization of enantiomers into diastereomers is an alternative to the separation on chiral stationary phases. Today there are more than 20 chiral reagents commercially available and most of them have been tested for a broad range of racemic compounds. Esterification using (*S*)-trolox methyl ether (Fig. 3) as chiral reagent has proved to be a versatile method for preparing diastereomers from enantiomers [25,26]. As the indirect separation approach requires that the analyte contains a functional group, derivatization is not possible for tofisopam and camazepam.

The racemic benzodiazepine standards, with exception for dihydrodiazepam, were derivatized with (*S*)-trolox methyl ether. While the derivatization of flutazolam, oxazepam, lorazepam and ethyl loflazepate gave a quantitatively yield, ethyl loflazepate, otazolam and cloxazolam could not be quantitatively derivatized. Using an open tubular column coated with biphenyl methylpolysiloxane (7.5 m × 50 μm I.D.) and supercritical carbon dioxide as mobile phase all derivatives eluted. While the temazepam derivatives were baseline separated (Fig. 4), the separations of the derivatives of oxazepam, lorazepam, otazolam, cloxazolam and ethyl loflazepate were poor due to peak tailing. No separation was obtained for the flutazolam derivatives, presumably because the derivatization takes place too far away from the chiral centre.

When tested in GC the (*S*)-trolox methyl ether derivatives did not elute, even from a short (5 m) open tubular column coated with SE-30 (methylpolysiloxane, $d_f = 0.4 \mu\text{m}$) at temperatures up to 350°C.

The (*S*)-trolox methyl ether derivatives were

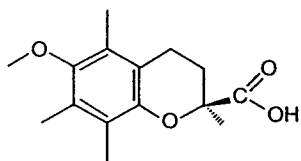


Fig. 3. Structure of (*S*)-trolox methyl ether.

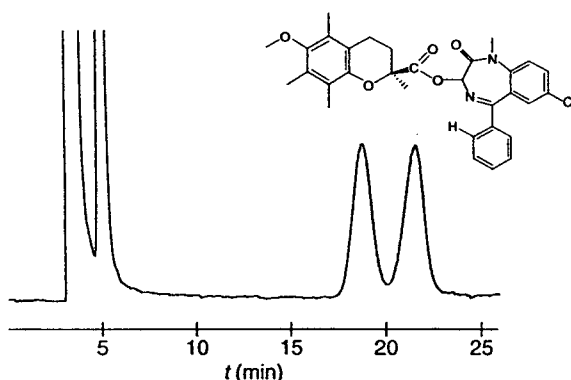


Fig. 4. Separation of (*S*)-trolox methyl ether derivatives of racemic temazepam using an open tubular column (5 m × 50 μm) coated with biphenyl methylpolysiloxane, $d_f \approx 0.25 \mu\text{m}$. CO_2 at 0.75 g ml⁻¹, 60°C.

also chromatographed using a packed fused-silica capillary column with diol functionality, and subcritical methanol-modified carbon dioxide as mobile phase. The large surface area of packed columns contains residual silanol groups that can cause adsorption of polar solutes, an effect that is not seen in deactivated open tubular columns. Addition of a polar modifier decreases adsorption in packed columns via competition for these active sites. The change of the mobile phase density (at constant temperature and pressure) and polarity when adding a modifier, will also facilitate the solubility of more polar solutes [27]. Elution of the (*S*)-trolox methyl ether derivatized analytes in approximately 1 h was observed at a methanol concentration of 8% (as defined in the Carlo Erba software) or higher. All separations were carried out in the subcritical region, at isothermal conditions (80°C), with methanol concentrations between 8.5 and 10%, and at isopycnic conditions. Fig. 5 shows the separation of racemic oxazepam derivatized with (*S*)-trolox methyl ether, using the above-mentioned conditions. The small rise in background signal before the peaks, is believed to be due to a minor change in flow-rate, leading to a change in the amount of added modifier. As shown in Table 3, the (*S*)-trolox methyl ether derivatives of temazepam, lorazepam, oxazepam and ethyl loflazepate were separated with a resolution

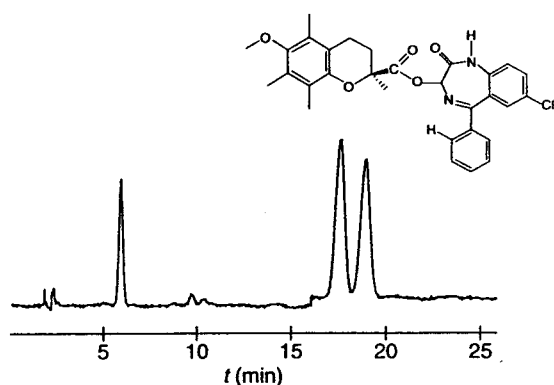


Fig. 5. Separation of (*S*)-trolox methyl ether derivatives of racemic oxazepam using a packed capillary column (30 cm \times 320 μ m), LiChrosorb Diol (5 μ m). CO₂-MeOH (90:10) at 0.65 g ml⁻¹, 80°C.

higher than 1.0 when using the packed capillary column.

In conclusion, racemic lorazepam, oxazepam, ethyl loflazepate and dihydrodiazepam were separated using a chiral β -cyclodextrin column in open tubular SFC. The peak shapes and FID responses were enhanced by a derivatization with AA. The racemates of temazepam, oxazepam, lorazepam and ethyl loflazepate were, after a chiral derivatization with (*S*)-trolox methyl ether, separated using a packed capillary column in SubFC. The temazepam derivatives were also separated using a non-chiral open tubular column in SFC. Flutazolam that was quantitatively derivatized both using an

anhydride and (*S*)-trolox methyl ether, could not be separated using either of the discussed approaches, possibly as the derivatization takes place too far away from the chiral centre. Otazolam, cloxazolam, tofisopam and camazepam, could not be separated using the direct method and the two latter could not be derivatized due to the lack of a functional group. Although derivatization was possible for cloxazolam and otazolam, no separation was obtained for the (*S*)-trolox methyl ether derivatives.

The direct separation method is recommended since additional steps in the analysis are excluded. A disadvantage with the direct approach employing SFC is, at present, the lack of commercially available chiral open tubular columns.

GC and SFC are complementary methods in this area, but when analysing thermolabile and highly polar compounds like the benzodiazepines it must be concluded that SFC or SubFC is usually preferable over GC. Compared to LC, packed-column SFC and SubFC are techniques well worth considering since the analysis times often can be shortened.

Acknowledgements

Financial support from the Swedish National Research Council, project K-KU 1439-307, is gratefully acknowledged. The authors also wish

Table 3

Resolution of (*S*)-trolox methyl ether derivatives of racemic benzodiazepines using a packed capillary column, LiChrosorb Diol, in SubFC

Compound	Density (g ml ⁻¹)	Mobile phase: carbon dioxide-methanol	<i>t_R</i> (min)	<i>R_s</i>
Temazepam	0.510	91.5:8.5	64.2	1.1
Oxazepam	0.650	90:10	19.1	1.4
Lorazepam	0.620	91.5:8.5	50.2	1.2
Ethyl loflazepate	0.700	90:10	11.8	1.2

Packed capillary column SubFC. Column 30 cm \times 320 μ m I.D. fused-silica packed capillary column, LiChrosorb Diol, 5 μ m. Subcritical methanol-modified carbon dioxide as mobile phase. The compounds are derivatized with (*S*)-trolox methyl ether. All separations were carried out at 80°C. *t_R* = Retention time for the last-eluting peak.

to thank Drs. U.B. Ranalder and W. Vetter for helpful ideas and advice.

References

- [1] E.J. Ariëns, *Eur. J. Clin. Pharmacol.*, 26 (1984) 663.
- [2] D.W. Armstrong, Y. Tang, T. Ward and M. Nichols, *Anal. Chem.*, 65 (1993) 1114.
- [3] V. Schurig, Z. Juvancz, G.J. Nicholson and D. Schmalzing, *J. High Resolut. Chromatogr.*, 14 (1991) 58.
- [4] P. Petersson, S.L. Reese, G. Yi, H. Yun, A. Malik, J.S. Bradshaw, B.E. Rossiter, M.L. Lee and K.E. Markides, *J. Chromatogr. A*, submitted.
- [5] V. Schurig and H.-P. Nowotny, *J. Chromatogr.*, 441 (1988) 155.
- [6] P. Macaudière, M. Caude, R. Rosset and A. Tambuté, *J. Chromatogr. Sci.*, 27 (1989) 583.
- [7] P. Macaudière, M. Caude, R. Rosset and A. Tambuté, *J. Chromatogr.*, 405 (1987) 135.
- [8] L.G. Blomberg, *J. Microcol. Sep.*, 2 (1990) 62.
- [9] D.F. Johansson, J.S. Bradshaw, M. Eguchi, B.E. Rossiter, M.L. Lee, P. Petersson and K.E. Markides, *J. Chromatogr.*, 594 (1992) 283.
- [10] T.L. Chester, J.D. Pinkston, D.E. Raynie, *Anal. Chem.*, 64 (1992) 153R; and references cited therein.
- [11] I. Choma, A.L. Dawidowicz and R. Lodkowski, *J. Chromatogr.*, 600 (1992) 109.
- [12] X.-L. Lu and S.K. Yang, *J. Chromatogr.*, 535 (1990) 229.
- [13] H. Wännman, A. Walhagen and P. Erlandsson, *J. Chromatogr.*, 603 (1992) 121.
- [14] M. Japp, K. Garthwaite, A.V. Geeson and M.D. Osseltton, *J. Chromatogr.*, 439 (1988) 317.
- [15] C. Drouet-Coassolo, C. Aubert, P. Coassolo and J.-P. Cano, *J. Chromatogr.*, 487 (1989) 295.
- [16] H. Maurer and K. Pflieger, *J. Chromatogr.*, 422 (1987) 85.
- [17] X. Lou, Y. Sheng and L. Zhou, *J. Chromatogr.*, 514 (1990) 253.
- [18] P. Mourier, P. Sassiati, M. Caude and R. Rosset, *J. Chromatogr.*, 353 (1986) 61.
- [19] B. Koppenhoefer and E. Bayer, *Chromatographia*, 19 (1985) 123.
- [20] P. Peterson, J. Malmquist, K. Markides and S. Sjöberg, *J. Chromatogr. A*, 670 (1994) 239.
- [21] P. Petersson, N. Lundell and K.E. Markides, *Chromatographia*, 35 (1993) 479.
- [22] P. Petersson, N. Lundell, K.E. Markides, in P. Sandra, K. Markides and G. Devos (Editors), *Proceedings of the 2nd European Symposium on Analytical Supercritical Fluid Chromatography and Extraction, Riva del Garda, May 1993*, Hüthig, Heidelberg, 1993, p. 8.
- [23] M. Jung and V. Schurig, *J. High Resolut. Chromatogr.*, 16 (1993) 215.
- [24] M. Chiarotti, N. Giovanni and A. Fiori, *J. Chromatogr.*, 358 (1986) 169.
- [25] W. Walther, W. Vetter, M. Vecchi, H. Schneider, R.K. Müller and T. Netscher, *Chimia*, 45 (1991) 121.
- [26] W. Walther, W. Vetter and T. Netscher, *J. Microcol. Sep.*, 4 (1992) 45.
- [27] P.J. Schoenmakers, L.G.M. Uunk and H.-G. Janssen, *J. Chromatogr.*, 506 (1990) 563.



ELSEVIER

Journal of Chromatography A, 679 (1994) 147–152

JOURNAL OF
CHROMATOGRAPHY A

Supercritical fluid extraction using a new restrictor design

F. Mellor^a, U. Just^{b*}, Th. Strumpf^c

^a*E. Merck, Frankfurter Strasse 250, D-64271 Darmstadt, Germany*

^b*Bundesanstalt für Materialforschung und -prüfung (BAM), Unter den Eichen 87, D-12205 Berlin, Germany*

^c*Biologische Bundesanstalt für Land- und Forstwirtschaft (BBA), Königin-Luise-Strasse 19, D-14195 Berlin, Germany*

First received 4 March 1994; revised manuscript received 7 June 1994

Abstract

A simple SFE apparatus is presented. Particular emphasis is placed on the design of the restrictor, whereby the advantages of a special restrictor nozzle are discussed in relation to problems in conjunction with the use of capillary restrictors. The rubber additives, fullerenes and soil constituents used as example application underline the possibilities offered by the new restrictor presented here.

1. Introduction

Supercritical fluid extraction (SFE) is today frequently used as an alternative to Soxhlet extraction, because substance solubility and diffusion coefficients in supercritical fluids can be varied over a wide range [1] and, for example, biogenic and anthropogenic compounds can be extracted mildly from very different matrices. Currently a shift in interest from supercritical fluid chromatography (SFC) to SFE can be observed [2]. On the one hand, this is due to the fact that, in spite of all the advances made in the field of chromatography and spectroscopy, there are still crucial unsolved problems involved in specimen preparation procedures; on the other hand, particularly SFE can provide very promising initiation points for specimen preparation procedures in the future [3–7]. Particular emphasis is placed on on-line and off-line coupling

of SFE with chromatographic and spectroscopic techniques.

Compared with conventional extraction methods (e.g. Soxhlet), SFE can provide a drastic reduction in the time required for the extraction and relocation of substances from a wide range of analytes. Furthermore, the solvent quantities required for extraction are considerably reduced.

A basic problem in SFE, which will continue to be a point of study in the future, is the strong matrix dependency of the extraction yield. In order to facilitate an easier detachment of the analytes from the matrix, modifiers such as alcohols, methylene chloride or carbon disulphide may be added to the supercritical carbon dioxide, as applicable from case to case. This eases the extraction of more polar compounds [8–12]. In our applications only pure, unmodified carbon dioxide was used.

The solvent characteristics of supercritical carbon dioxide (0.8–0.9 g/ml) have been compared with those of benzene [13] and toluene [14].

Besides the difficult methods involved in

* Corresponding author.

procedural development, on-line SFE methods have the disadvantage that only small amounts of specimen can be used. They are well suited for trace analysis in matrices that are not co-extracted [15]. The advantage of off-line extractions is that traces of substances are enriched and subsequently extracts can be analysed using the established analytical procedures HPLC and GC or GC-MS, respectively. Off-line extraction is thus particularly suited for instances where larger specimen amounts are available [15], and it was therefore used in our applications.

Although positioned at the end of the apparatus—as seen in the solvent flow direction—the restrictor unit is the crucial component of every SFE apparatus, and it will accordingly be dealt with in more detail here. However, in discussing the restrictor design, the problems involved in off-line extraction will also become evident [7,15–18]. As a result of the Joule-Thompson effect, the tip of fused-silica capillary restrictors commonly used in commercial extractors cools down when the carbon dioxide transits from the supercritical state to the gas phase. As a result, the extracted components fall out more easily and block the restrictor.

Burford et al. [18] present three different types of restrictors, with particular consideration being given to their heatability and the transfer of the extracted substances to different recipient vessels. The most effective arrangement was found to be with the capillary directly submerged in the recipient liquid and the upper part heated in a heater block.

For these reasons we led the restrictor nozzles directly into simple recipient vessels.

2. Experimental

HPLC columns were used as extraction cells. Stainless steel capillaries 1/16-inch (1.6 mm) O.D. having an internal diameter of 0.25 mm were used as connecting capillaries; the screw connections were based on the Knauer Dynaseal system. A column thermostat was used to provide the correct temperature for the extraction cells.

A Knauer HHPN nozzle was used as a restrictor. This nozzle is normally part of the hydraulic high-pressure nebulizer system used for injecting specimens in atomic absorption spectrometry, and is suitable for pressures up to 40 MPa. It was not absolutely necessary to make changes in the nebulizer system, but it is planned to lengthen the nozzle mount in order to optimize the restrictor outlet. The o-ring is not used in SFE; instead of a polyether ether ketone (PEEK) capillary we used a stainless steel capillary.

To feed the liquid carbon dioxide, we used on the one hand the injection pumps used in commercial SFC units by Fisons and Dionex (density programming possible) and, on the other hand, the isocratic HPLC double-piston pump L-6000 by Merck. To provide a means of cooling the pump head of the Merck L-6000, this pump head was bored and threads were tapped from both sides to accommodate coolant tubes; the pump head was then integrated into a coolant circuit.

The Merck pump can be flow controlled as well as pressure controlled. The Teflon tube on the suction side was replaced by steel capillaries (0.5 mm diameter) and the valve mount on the suction side was replaced by a valve mount on the pressure side.

3. Results and discussion

The following solutions are apparent for preventing restrictor blockages, currently the main problem in off-line SFE [15,18]:

1. Minimising the pressure drop between the extraction cell and the restrictor outlet
2. Heating the restrictor
3. Using a “suitable” solvent in which the substances are dissolved when the supercritical fluid expands
4. Extracting smaller amounts of specimen
5. Using restrictors which afford a greater amount of flow

Fig. 1 shows the cross section of the entire nozzle. The nozzle plates are offered with laser boreholes of various sizes (one each). Nozzle plates (thickness 0.3 mm) having bore diameters of 5, 10 and 20 μm were tested for their

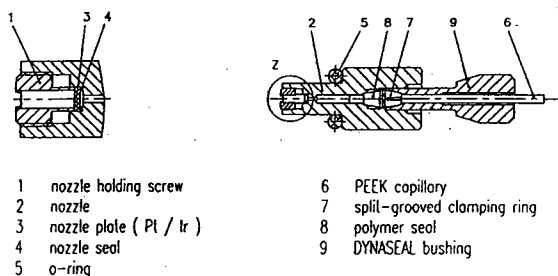


Fig. 1. Cross section of nebulizer nozzle (restrictor) and nozzle mount Z. (expanded plot). Reproduced with permission of Dr. Ing. H. Knauer GmbH.

suitability. Compared with fused-silica capillary restrictors, this nozzle is easier to handle in off-line operation because the nozzle plates can readily be replaced and blockages in the nozzle openings can easily be eliminated by turning the nozzle plate around.

Thus, once the nozzle plates have been acquired, when the task for which the equipment is being used is changed, it presents no problem to clean the nozzle plates and reuse them. On the other hand, capillary restrictors block up relatively quickly when in use, particularly in conjunction with soil extractions, and have then to be discarded and replaced with new ones [16].

A further advantage of the tested restrictor is that the supercritical medium only expands when it reaches the borehole in the plate; the expansion does not take place over a length of feed. This provides an exceptional solution for meeting the requirement stated under item 1.

Temperature control of the restrictor ($\sim 50^{\circ}\text{C}$) may serve not only to prevent blockages but also to facilitate “fine-tuning” of the volume flow [18]. Since the nozzle mount is made of titanium, temperature control can be provided by wrapping heater wire around the upper part of the nozzle mount and the capillary connection, and then heating (item 2). The temperature can be measured at the upper part of the nozzle mount beside the Dynaseal bushing. That part of the nozzle mount that extends into the recipient liquid (20 ml of toluene at room temperature) is to be inserted in a PEEK or PTFE tube to avoid heat transition from the nozzle mount to the recipient liquid.

Toluene was used as the recipient liquid since it proved to be a universally applicable solvent for compounds having aromatic structure components (item 3).

Blockages only occurred with soil extractions, not with fullerenes or rubber additives, using $5\text{-}\mu\text{m}$ nozzles without heating. In our applications with soil extractions, heating of the nozzle was not necessary when nozzle plates with a larger bore diameter, e.g. $20\ \mu\text{m}$ were used (item 5); this resulted in a higher consumption of liquid carbon dioxide and an occurrence of bigger gas bubbles in the recipient vessel.

Table 1 shows the experimental conditions of three applications using SFE with this restrictor.

Extractions of rubber additives are chosen because they are less frequently described in the literature.

The main components of the extracted addi-

Table 1
SFE conditions

	Rubber additives	Fullerenes	Soil extract
Extraction cell	Empty column 30×4 mm I.D.	30×4 mm I.D.	60×4 mm I.D.
Weighed specimen	Finely ground rubber, 0.05 g	Soot, 0.04 g	Air-dried soil, 1 g
Oven temperature	70°C	40°C	40°C
Pressure of CO_2	41.5 MPa	25 MPa	30.5 MPa
Density of CO_2	0.87 g/ml	0.88 g/ml	0.92 g/ml
Volume flow	2 ml/min liquid CO_2	2.4 ml/min	1 ml/min
Nozzle aperture	$20\ \mu\text{m}$	$20\ \mu\text{m}$	$10\ \mu\text{m}$
Extraction time	30 min	30 min	30 min
Recipient liquid	Toluene	Toluene	Toluene

tive of the rubber specimen in our example are N-(1,3-dimethyl-butyl)-N'-phenyl-*p*-phenylene-diamine, alkylated phenols and alkylphenylic sulfonates.

Fig. 2 shows the SFC chromatograms created on the Dionex SFC unit of the extract on SB-Biphenyl-30 and, for comparison, the following components: N-(1,3-dimethyl-butyl)-N'-phenyl-*p*-phenylene-diamine, octylated diphenylamine, alkylphenylic sulfonates and stearic acid.

A total of 9.4% extractable components [approximately 90% of the amount of extractable components that can be attained with Soxhlet extraction (1 h) using acetone] was found.

A further example of the possibilities offered by SFE using pure carbon dioxide is shown with the extraction of fullerenes.

Fig. 3, lower trace, shows the HPLC sepa-

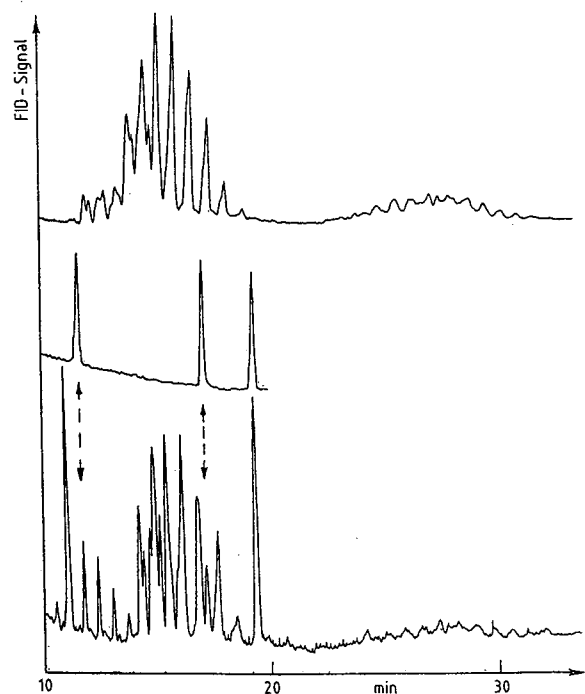


Fig. 2. SFC chromatograms of the rubber extract (lower trace), of stearic acid, octylated diphenylamine and N-(1,3-dimethyl-butyl)-N'-phenyl-*p*-phenylene-diamine (in this order, middle trace) and of alkylphenylic sulfonates (upper trace). SFC conditions: Column, SB-Biphenyl-30 (ID 50 μ m; 10 m); temperature, 120°C. Density program: initial density 0.2 g/ml, increase to 0.6 g/ml at 0.025 g/ml/min, then increase to 0.65 g/ml at 0.002 g/ml/min.

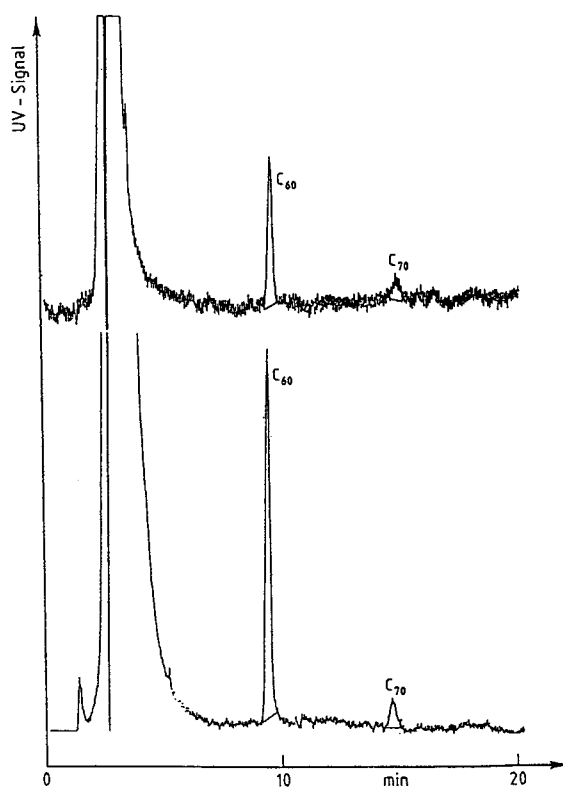


Fig. 3. HPLC chromatogram of fullerenes C₆₀ and C₇₀ following their SFE with pure carbon dioxide (lower trace) and with carbon dioxide/10% acetone (upper trace). HPLC conditions: Column, Inertsil ODS 2, 150 A, 5 μ m; flow: 1.0 ml/min; dimensions, 250 \times 4.6 mm I.D.; injection, 20 μ l; eluent, CH₂CL₂-MeOH (60:40, v/v); detector, UV, 260 nm.

ration of C₆₀ and C₇₀ out of the SFE recipient in accordance with the described example in Table 1. The extraction using supercritical carbon dioxide yielded 6% extractable components. The fraction of C₆₀ and C₇₀ is unknown [19].

Fig. 3, upper trace, shows the result of the SFE for C₆₀ and C₇₀ using supercritical carbon dioxide and 10% acetone as a modifier in accordance with Ref. 20. A lower yield was obtained under similar SFE conditions using carbon dioxide-10% acetone.

As investigations by Jinno et al. [21] show, the yield can be increased through the addition of toluene as a modifier.

Our third application example involves a soil extraction. Before a soil-humus complex is char-

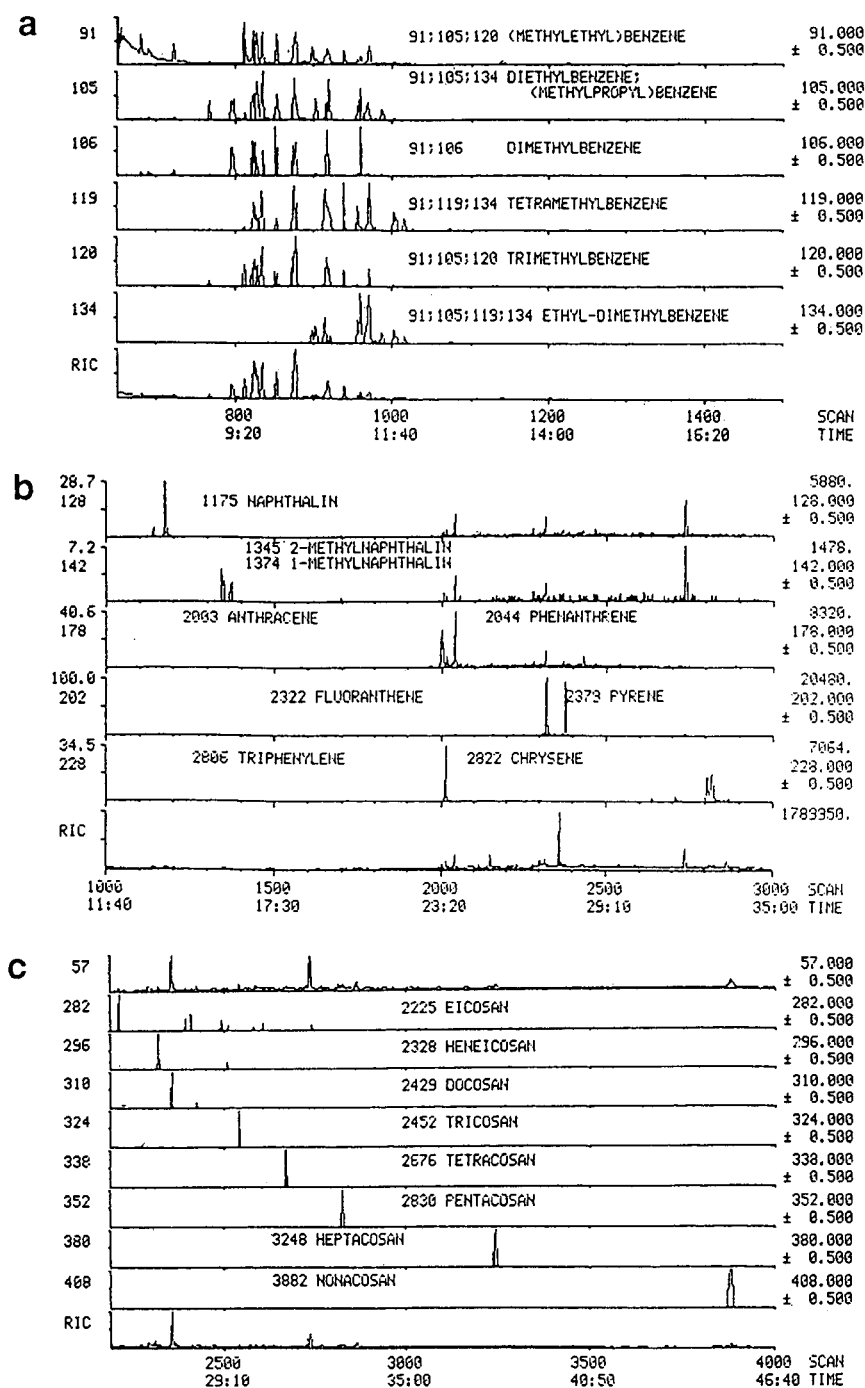


Fig. 4. GC-MS chromatogram of an SFE extracted soil in the Dahlem test field, Plot 21, soil horizon 1...30 cm. (a) alkylated benzenes; (b) polyaromatic hydrocarbons; (c) hydrocarbons (eluting in this order out of the column). GC conditions: column, DB1 (30 m × 0.25 mm I.D., 0.25 μm film thickness); injection 2 μl; injector, 270°C. Temperature program: initial temperature 50°C, hold 3 min, then increase to 100°C at 15°C/min, then increase to 280°C at 9°C/min, hold 20 min.

acterized, it is necessary to separate from it any unincorporated organic components, and to do so in such a way that its primary structure is not considerably denaturalised, so that subsequent fractionation of the humin substances into fulvic acids, humic acids and humin can provide a realistic interpretation of the structural composition of the individual fractions. This can be achieved through the mild SFE process, whereby, if necessary, modifiers may be added.

In our example, a soil from an exposed position on the Dahlem test field of the Federal Biological Research Centre for Agriculture and Forestry (BBA) was selected for presenting the results. The components were extracted from 1 g of soil each ranging from 1...30 cm soil horizon, and were determined using GC-MS (Finnigan MAT).

Fig. 4a, b and c are parts of the same GC-MS chromatogram. Fig. 4a shows alkylated benzenes eluting first out of the column (8 to 12 min elution time), then polyaromatic hydrocarbons (Fig. 4b) and hydrocarbons up to 46 min elution time (Fig. 4c). Evidence of approximately 20 compounds of the classes alkylated benzenes (Fig. 4a) and hydrocarbons (4c), and approximately 10 compounds of the class polyaromatic hydrocarbons (Fig. 4b) was found in the soil extract.

4. Summary

The point of emphasis in the above paper is the presentation of a new restrictor design as part of a simple SFE apparatus. The advantages of the restrictor nozzle are discussed in comparison with capillary restrictors.

Handling of the presented restrictor nozzle proved to be good, as shown by a number of selected examples in SFE practice.

The apparatus is suitable for extraction with supercritical carbon dioxide as well as with

mixtures of carbon dioxide and modifiers. In order to set solvent gradients for SFE, it is necessary to use 2 pumps and a mixing chamber.

References

- [1] St. Küppers, *Chromatographia*, 33 (1992) 434.
- [2] J.M. Levy, M. Ashraf-Khorassani, A.C. Rosselli, D. Boyer, L.A. Dolota, R.M. Ravey and E. Storożnyski, *SFE Applications*, Suprex Corporation, Pittsburgh, PA, 1989.
- [3] R.E. Majors, *LC·GC*, 4 No. 2 (1991) 10.
- [4] R.E. Majors, *LC·GC*, 4 No. 3 (1991) 10.
- [5] W. Pipkin, *LC·GC*, 5 No. 1 (1992) 8.
- [6] F. Höfler, *Labor-Praxis*, 16 (1992) 350.
- [7] J.W. King and M.L. Hopper, *J. Assoc. Off. Anal. Chem.*, 75 (1992) 375.
- [8] E. Stahl and K.W. Quirin, *Naturwissenschaften*, 71 (1984) 181.
- [9] W.M.A. Niessen, P.J.M. Bergers, U.R. Tjaden and J. van der Greef, *J. Chromatogr.*, 454 (1988) 243.
- [10] J. Doehl, A. Farbrot, T. Greibrokk and B. Iversen, *J. Chromatogr.*, 392 (1987) 175.
- [11] M. Ashraf-Khorassani and L.T. Taylor, *Anal. Chem.*, 61 (1989) 145.
- [12] S.B. Hawthorne, D.J. Miller and J.J. Langenfeld, in P. Sandra (Editor), *Proceedings of the 13th International Symposium on Capillary Chromatography*, Riva del Garda, May 1991, Hüthig, Heidelberg 1991.
- [13] V. Janda, G. Steenbeke and P. Sandra, *J. Chromatogr.*, 479 (1989) 200.
- [14] J.A. Hyatt, *J. Org. Chem.*, 49 (1984) 5097.
- [15] S.B. Hawthorne, D.J. Miller and J.J. Langenfeld, in K. Jinno (Editor), *Hyphenated Techniques in Supercritical Fluid Chromatography and Extraction (Journal of Chromatography Library, Vol. 53)*, 1992, p. 225.
- [16] Y.Y. Wigfield and M. Lauouette, *J. Agric. Food Chem.*, 41 (1993) 84.
- [17] H. Engelhardt, J. Zapp and P. Kolla, *Chromatographia*, 32 (1991) 527.
- [18] M.D. Burford, S.B. Hawthorne, D.J. Miller and T. Braggins, *J. Chromatogr.*, 609 (1992) 321.
- [19] H.J. Möckel, Hahn-Meitner-Institut GmbH, Abt. S3, Berlin, personal communication.
- [20] F. Höfler, *SFE-Applikation*, Dionex GmbH, Idstein, 1992.
- [21] K. Jinno, H. Nagashima, K. Itoh, M. Saito and M. Buonoshita, *Fresenius' J. Anal. Chem.*, 344 (1992) 435.



ELSEVIER

Journal of Chromatography A, 679 (1994) 153–165

JOURNAL OF
CHROMATOGRAPHY A

UV detection in capillary zone electrophoresis Peaks or dips – that is the question

J.L. Beckers

Laboratory of Instrumental Analysis, Eindhoven University of Technology, P.O. Box 513, 5600 MB Eindhoven, Netherlands

First received 30 March 1994; revised manuscript received 27 May 1994

Abstract

Applying capillary zone electrophoresis with UV detection, both UV-absorbing and UV-transparent components can be present in electropherograms as negative peaks (dips) or as positive peaks. Starting from Kohlrausch's regulation function, derived for fully ionized monovalent ionic constituents and under the assumption that the molar absorptivities of the UV-absorbing components are identical, eight different cases can be distinguished and in several cases components can occur both as peaks or as dips depending on their mobilities and those of the co-ions of the system. Applying background electrolytes containing two co-ions, system peaks are present, with a mobility that is between the mobilities of the two co-ions and determined by the concentration ratio of these two co-ions. In the background electrolytes studied, containing the co-ions potassium and histidine, UV-transparent sample components with a mobility higher than that of the system peak migrate as a positive peak, whereas UV-transparent components with lower mobilities migrate as negative peaks. System peaks themselves can also be peaks or dips depending on the sample composition. Sample peaks in the vicinity of system peaks interact with the system peaks through which both sample and system peaks are enlarged and quantitative properties are lost. Similar phenomena can be measured for anions in background electrolytes containing the co-ions phenylacetate and acetate, indicating that these phenomena are probably not associated with adsorption phenomena of cations on the fused-silica surface.

1. Introduction

Most commercially available capillary zone electrophoresis (CZE) apparatus is equipped with selective detectors, such as UV and laser-induced fluorescence (LIF) detectors, and not with a universal detector, such as a conductivity detector. Applying selective detectors, e.g., a UV detector, UV-absorbing components can be measured in the "direct UV mode". UV-transparent components, however, often have to be detected in the indirect mode. With indirect detection, the analyte displaces a chromophore

present in the background electrolyte (BGE), whereby the concentration of the limit of detection, c_{LOD} , can be determined by

$$c_{\text{LOD}} = c_{\text{M}}/RD_r \quad (1)$$

with c_{M} is the concentration of the BGE constituent that is being monitored, R is the response factor or transfer ratio and D_r is the dynamic reserve, equal to the signal-to-noise ratio (S/N) [1]. From Eq. 1, it could be concluded that a low c_{LOD} can be obtained by applying low c_{M} values and a high D_r [1–3], although in practice also D_r decreases at lower

c_M values [4]. Nielen [5] calculated the response factor, dependent on the mobilities. Foret et al. [6] discussed that the highest sensitivity can be achieved for sample ions having an effective mobility close to the mobility of the absorbing co-ion. So far, less attention has been paid to the presence of more than one UV-absorbing component in CZE systems. In that case both UV-absorbing and UV-transparent components can be met as negative or as positive peaks, depending on their molar absorptivity and transfer ratio. In this paper we discuss the question “peaks or dips?”, due to the presence of both UV-absorbing counter- and co-ions, and the effect of the presence of two co-ions in a BGE on system peaks in UV detection and the influence on calibration graphs.

2. Theoretical

Assuming only the presence of fully ionized monovalent ionic constituents, the electrophoretic separation mechanism can be approximately described by Kohlrausch's regulation function [7]:

$$\sum_i \frac{c_i}{m_i} = \omega \quad (2)$$

where c_i and m_i represent the ionic concentrations and absolute values of the effective mobilities of all ionic constituents and the numerical value of the Kohlrausch function ω is locally invariant in time [8]. If the separation compartment in CZE is filled with a background electrolyte AC, consisting of a co-ion A and a counter ion C, for the relationship between the concentration of the co-ions in the BGE, c_A^{BGE} , and in a sample zone S, c_A^{S} , containing also the sample ions i , can be derived [9,10]:

$$c_A^{\text{BGE}} = c_A^{\text{S}} + c_i^{\text{S}} k_i \quad (3)$$

with

$$k_i = \frac{m_i + m_c}{m_A + m_c} \cdot \frac{m_A}{m_i} \quad (4)$$

The superscripts BGE and S refer to the compo-

sition of the pure background electrolyte AC and the sample zone, respectively. The concentration of the counter ion C is determined by the electroneutrality condition.

The transfer ratio or response factor, often denoted as R , is defined as the number of molecules of the BGE displaced by each analyte molecule and is in fact equal to the constant k_i in Eq. 4:

$$R = \frac{c_A^{\text{BGE}} - c_A^{\text{S}}}{c_i^{\text{S}}} = \frac{|\Delta c_A|}{c_i^{\text{S}}} = k_i \quad (5)$$

Applying a UV detector, the measured absorbance A will be

$$A = \epsilon c l \quad (6)$$

where ϵ is the molar absorptivity ($l/\text{mol} \cdot \text{cm}$) and l is the effective path length in the detector (cm). For the carrier electrolyte this means

$$A^{\text{BGE}} = (\epsilon_A + \epsilon_C) c_A^{\text{BGE}} l \quad (7)$$

For a sample zone the absorbance will be

$$A^{\text{S}} = (\epsilon_A + \epsilon_C) c_A^{\text{S}} l + (\epsilon_i + \epsilon_C) c_i^{\text{S}} l \quad (8)$$

For the UV signal of a sample zone, applying Eq. 3, we can derive

$$\begin{aligned} dA &= A^{\text{S}} - A^{\text{BGE}} = c_i^{\text{S}} l [(\epsilon_i + \epsilon_C) - (\epsilon_A + \epsilon_C) k_i] \\ &= c_i^{\text{S}} l [\epsilon_i - k_i \epsilon_A - (k_i - 1) \epsilon_C] = c_i^{\text{S}} l K_i \end{aligned} \quad (9)$$

If the bracketed term in Eq. 9 is indicated by K_i , the spatial peak area will be proportional to $K_i Q_{\text{inj}}$ and the measured peak area on a temporal basis to $K_i Q_{\text{inj}} t_i$, where Q_{inj} is the injected amount and t_i is the migration time of a sample ion i [10].

If sample components have an equal concentration c_i in their zones, the peak heights are proportional to K_i . Generally, the concentrations c_i will not only be determined by the sample concentration but by several other factors such as the concentrating effect, electrodispersive effects and diffusion.

From Eq. 9, all possible situations in UV detection in CZE can be deduced. If for ease of survey components are considered to be UV transparent or UV absorbing with equal molar

Table 1

All possible combinations of (+) UV-absorbing or (–) UV-transparent sample components i , co-ions A and counter-ions C, the expressions of K_i values according to Eq. 9 and values for K_i for the UV modes and indirect UV modes assuming equal molar absorptivities ϵ for the UV-absorbing ionic species

No.	Component			K_i : $\epsilon_i - k_i\epsilon_A - (k_i - 1)\epsilon_C$	K_i	
	i	A	C		UV mode	Indirect UV mode
1	+	+	+	$\epsilon_i - k_i\epsilon_A - (k_i - 1)\epsilon_C$	$(2 - 2k_i)\epsilon$	
2	+	+	–	$\epsilon_i - k_i\epsilon_A$	$(1 - k_i)\epsilon$	
3	+	–	+	$\epsilon_i - (k_i - 1)\epsilon_C$	$(2 - k_i)\epsilon$	
4	+	–	–	ϵ_i	ϵ	
5	–	+	+	$-k_i\epsilon_A - (k_i - 1)\epsilon_C$		$(1 - 2k_i)\epsilon$
6	–	+	–	$-k_i\epsilon_A$		$-k_i\epsilon$
7	–	–	+	$-(k_i - 1)\epsilon_C$		$(1 - k_i)\epsilon$
8	–	–	–	No UV absorption		

absorptivities ϵ , eight different cases can be distinguished as indicated in Table 1. In Table 1 the values of K_i are given for all combinations of the ionic components i , A and C if they are UV absorbing (+) or are UV transparent (–). The concepts usable in UV detection of “direct UV mode” and “indirect UV mode”, whereby generally a BGE is chosen without any UV-absorbing properties or a BGE the co-ion of which has UV-absorbing properties respectively, correspond to cases 4 and 6 in Table 1, respectively. However, we shall use the term “direct UV mode” for cases 1–4 where the sample component has UV-absorbing properties and the term “indirect UV mode” for cases 5–7 where the sample component is UV transparent and these modes are given in the columns “UV mode” and “indirect UV mode”. Case 8 is not useful, because no UV signal will be observed.

2.1. Optimization in UV detection

From Table 1, it is clear that there are several ways to optimize the UV signal. In all cases in Table 1 an optimum UV response (optimum K_i) value can be obtained for minimum k_i values or very large k_i values, except for case 4 (K_i is always ϵ) and case 6 where a maximum (negative) K_i value is obtained for a maximum k_i value. This means that the crucial point in the optimization of the absorbance A is the value of

K_i and by this maximizing or minimizing the value of k_i . To give an indication of the values of k_i , in Fig. 1 calculated lines of constant k_i values are given, corresponding to sets of m_A and m_C values and a constant value for a sample ionic mobility m_i of $40 \cdot 10^{-9} \text{ m}^2/\text{V} \cdot \text{s}$. The arrows indicate increasing k_i values. From Fig. 1 (and Eq. 4), it can be seen that for $m_i = m_A$, the k_i values and therefore the transfer ratios are always unity. Minimum k_i values are obtained for a minimum mobility of the A ions, and maximum k_i values for a maximum mobility of the A ions, both at a maximum mobility of the C ions. It should be noted that minimum k_i values, obtained for $m_i > m_A$, mean that one ion of the BGE is displaced by more than one sample ion, through which the total ionic strength increases.

2.2. Peaks or dips?

The question of whether components can be detected as peaks or dips is answered by the values of K_i given in Table 1. For positive values of K_i positive peaks and for negative values of K_i negative peaks (dips) are obtained. For an impression of the size of the UV signals in the different modes of UV detection, in Fig. 2 the calculated parameter K_i/ϵ is given for all (A, C) direct UV modes and (B, D) indirect UV modes for varying mobilities of the (A, B) co-ions A and of (C, D) the sample ions i . All other

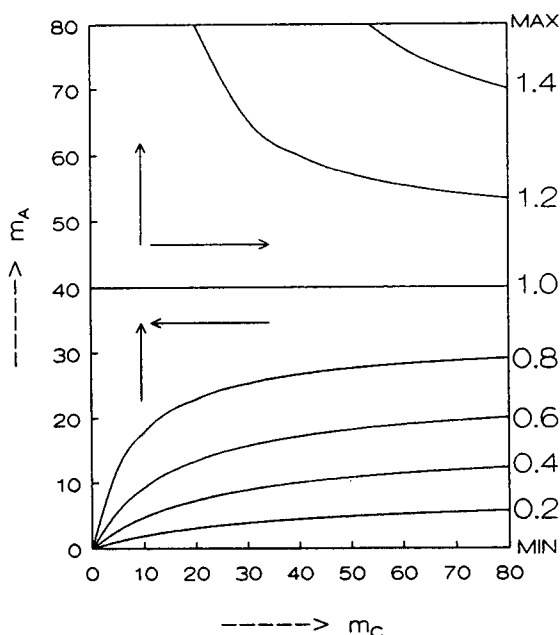


Fig. 1. Calculated lines of constant k_i values for various mobilities of the co-ions m_A and of the counter ions m_C for a constant mobility of the sample ionic species of 40. All mobilities are given in $10^{-9} \text{ m}^2/\text{V}\cdot\text{s}$. The lines are indicated with numbers referring to the constant k_i values of the corresponding lines. Maximum and minimum values of k_i are obtained for a maximum and minimum value of m_A , respectively, in combination with a maximum mobility of the counter ions C. The arrows indicate increasing k_i values.

mobilities are always taken as $40 \cdot 10^{-9} \text{ m}^2/\text{V}\cdot\text{s}$. From Table 1 and Fig. 2, some interesting conclusions can be drawn. For the conventional direct UV mode, case 4, the K_i/ϵ value is always 1 (see Fig. 2A and C). For cases 1 and 2, positive peaks are obtained if $m_i > m_A$. Negative peaks (dips) are obtained, however, if $m_i < m_A$. This means that the UV signal, although the sample and co-ion are assumed to have the same molar absorptivity, can be positive or negative depending on the mobility of the sample component. The explanation is simple. If the sample ionic mobility is lower than that of the co-ions, the response factor is larger than one through which the total ionic strength decreases, and although both ionic species are UV absorbing, the net UV signal decreases. If $m_i = m_A$ the transfer ratio is just one and the UV signal is constant. For case

3, negative peaks are obtained for very low mobilities of the sample ionic species.

If $m_i > m_A$ the application of UV-absorbing counter-ions ($K_i/\epsilon = 2 - k_i$) gives the best results. For the conventional indirect UV mode, case 6, and for case 5 (see Fig. 2B and D) generally negative UV peaks will be obtained. Positive peaks can, however, be obtained applying UV-absorbing counter ions C, case 7 ($K_i/\epsilon = 1 - k_i$), for $m_i > m_A$. Further, it is always favourable to apply both a UV-absorbing counter- and co-ion ($K_i/\epsilon = 1 - 2k_i$) for $m_i < m_A$.

3. Experimental

For all CZE experiments a P/ACE System 2000 HPCE system (Beckman, Palo Alto, CA, USA) was used. All experiments were carried out with a Beckman eCAP capillary tubing (75 μm I.D.) with a total length 46.7 cm and a distance between injection and detection of 40.0 cm. The wavelength of the UV detector was set at 214 nm. All experiments were carried out in the cationic mode (anode at the inlet) and the operating temperature was 25°C. Sample introduction was performed by applying pressure injection, where a 1-s pressure injection represents an injected amount of ca. 6 nl and an injected length of 0.136 cm. Data analysis was performed using the laboratory-written data analysis program CAESAR.

4. Results and discussion

In the theoretical part, the different indirect and direct UV modes have already been pointed out, and assuming an equal molar absorptivity for UV-absorbing components, eight different cases could be distinguished. The K_i/ϵ values in Fig. 2 are a measure of the UV signal. In practice, molar absorptivities are different for the different components, through which both the k_i , determined by the mobilities of all ionic species, and the ϵ values of all ionic species play a role in the size of the UV signal.

For a demonstration of the different effects

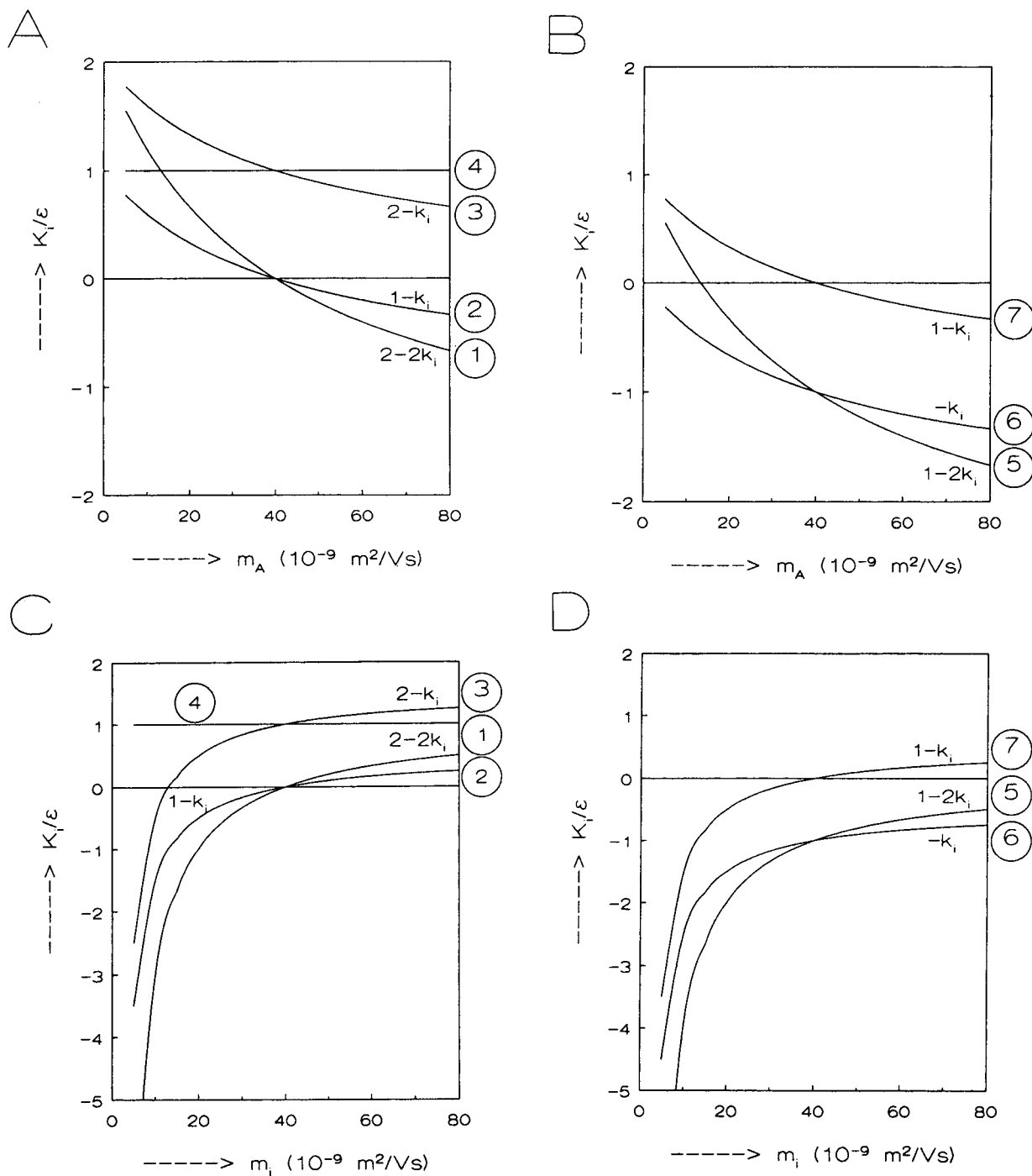


Fig. 2. Calculated values for the parameter K_i/ϵ , assuming an equal molar absorptivity ϵ for all UV-absorbing components, for (A, C) direct UV modes and (B, D) indirect UV modes for various mobilities of the (A, B) co-ions A and of (C, D) the sample ions i . All other mobilities are always taken as $40 \cdot 10^{-9} \text{ m}^2/\text{V} \cdot \text{s}$. The lines are indicated with encircled numbers referring to the cases in Table 1 and with the values of K_i/ϵ . For further information see text and Table 1.

playing a part in the UV detection, an equimolar solution of five UV-transparent cations, potassium, sodium, tetramethylammonium (TMA), tetraethylammonium (TEA) and tetrabutylammonium (TBA), is used, which will be denoted as the MIX. In the electropherograms, peaks for the different components of the MIX are indicated with the numbers 1, 2, 3, 4 and 5 for the ions potassium, sodium, TMA, TEA and TBA, respectively. In Fig. 3 the electropherograms are given for the separation of 5-s pressure injections of $5 \cdot 10^{-4}$ M of the MIX applying BGEs containing UV-absorbing co-ions (case 6) and containing both UV-absorbing counter and co-ions (case 5). The BGEs containing UV-absorbing co-ions consisted of 0.01 M histidine (HiAc) and 0.01 M imidazole (ImAc), respectively, adjusted to pH 4.2 by adding acetic acid. For all BGEs, histidine or imidazole was chosen as the UV-absorbing co-ion because their pK values are ca. 6 and 7, respectively, through which these cat-

ions are protonated for the larger part at the working pH. In the case of HiAc, the mobility of histidine is lower than that of imidazole, the last peaks on the electropherogram are larger and more symmetrical, whereas in the BGE ImAc the first peaks are larger, although the molar absorptivity of imidazole is only about two thirds of that of histidine. This corresponds to the guideline that the mobility of the co-ions of the BGE must be as close as possible to that of the sample component, in order to diminish the effect of electrodispersion. For BGEs with both UV-absorbing counter and co-ions, we adjusted 0.01 M solutions of histidine (HiB) and imidazole (ImB) to pH 4.2 by adding benzoic acid. Although the molar absorptivities of histidine, imidazole and benzoic acid are not equal, so that Fig. 2D is not valid, we can see the effect that by addition of UV-absorbing counter ions to the BGE, all peaks for components with high mobilities are much smaller than those in the corresponding BGE with only UV-absorbing co-ions. This can easily be understood. The transfer ratio is smaller than unity for components with a high mobility through which the total ionic strength increases and therefore also the concentration of the UV-absorbing counter ions increases, counteracting the decrease in UV signal by the lower concentration of the co-ions. For the system HiB the resulting peaks for potassium and sodium are very small. This effect is smaller in the system ImB because of the higher mobility of imidazole.

In Fig. 4 the relationship between calculated K_i/ϵ values and the mobilities of sample components are given for BGEs with UV-absorbing counter ions (case 7), viz., 0.01 M Tris, 0.01 M lithium and 0.01 M potassium ions adjusted to pH 4.2 by adding benzoic acid. In the calculations no corrections are made for activities and relaxation and electrophoretic effect. Because all ionic species are monovalent, changes will be in the same order of attitude for all ionic species. Just as expected according to Fig. 2D, positive peaks can be expected for sample components with $m_i > m_A$. The positions of the components of the MIX are indicated with the dotted lines in Fig. 4.

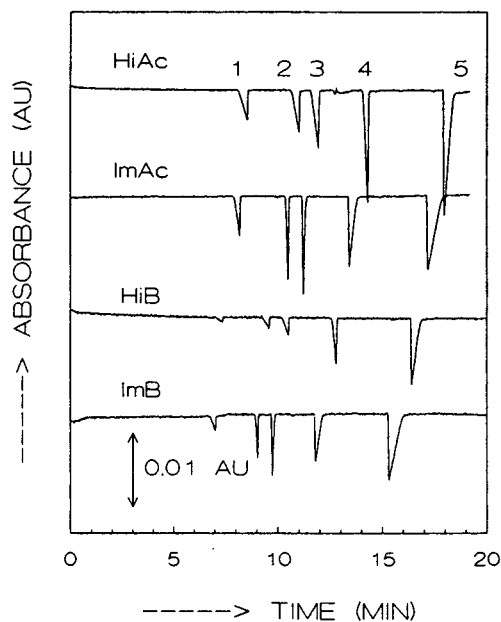


Fig. 3. Electropherograms for the separation of 5-s pressure injections of $5 \cdot 10^{-4}$ M of the MIX applying BGEs of histidine acetate (HiAc), imidazole acetate (ImAc), histidine benzoate (HiB) and imidazole benzoate (ImB). All BGEs consisted of 0.01 M of the cations, adjusted to pH 4.2 by adding the buffering acids. The applied voltage was 5 kV. For further information, see text.

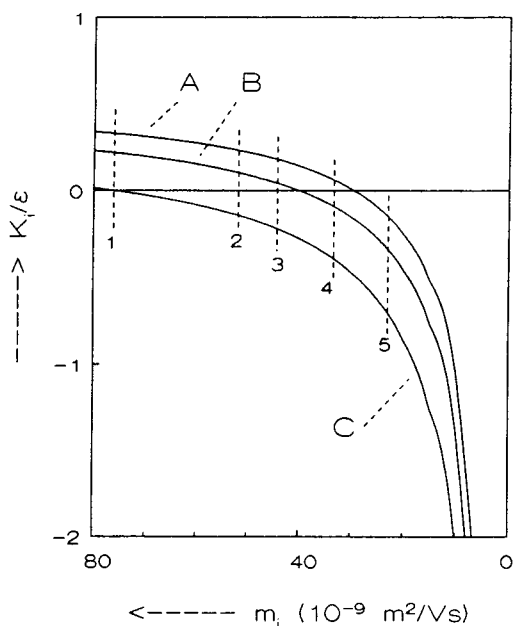


Fig. 4. Relationship between calculated K_i/ϵ values and the mobilities of sample components for BGEs with UV-absorbing counter ions (case 7), (A) 0.01 M Tris-, (B) 0.01 M lithium- and (C) 0.01 M potassium-benzoate at pH 4.2. The dotted lines indicate the values of K_i/ϵ of the cations of the MIX on the curves.

In Fig. 5 the electropherograms are given for the separations of 5-s pressure injections of $5 \cdot 10^{-4}$ M of the MIX applying (A) 0.01 M Tris-benzoate, (B) 0.01 M lithium-benzoate and (C) 0.01 M potassium-benzoate. The applied voltage was 5 kV. According to the theory (see Fig. 4), potassium ions are not visible in system C, whereas all components are dips. In system B the first three components are peaks and the last two are dips, whereas in system A only the last component is a dip, in accordance with the positions indicated in Fig. 4.

4.1. System peaks in CZE

Beckers [11] described that moving boundary zones can originate from discontinuities in the concentration of the co-ions and/or pH of the BGE and showed that injected block-shaped discontinuities in concentration and/or pH of the BGE split up in a migrating part with a mobility

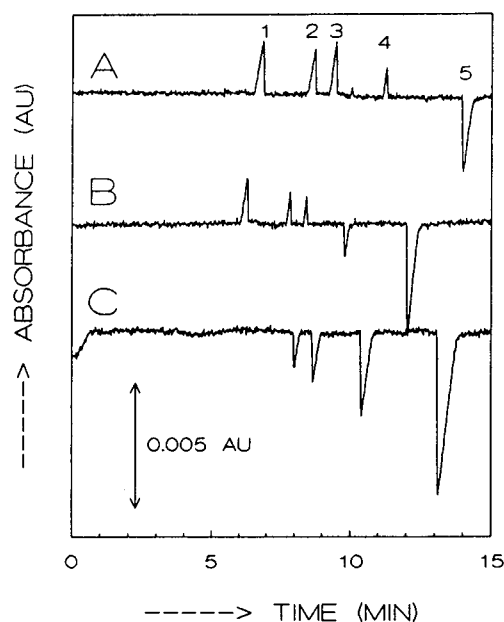


Fig. 5. Electropherograms for the separations of 5-s pressure injections of $5 \cdot 10^{-4}$ M of the MIX applying (A) 0.01 M Tris-benzoate, (B) 0.01 M lithium-benzoate and (C) 0.01 M potassium-benzoate at pH 4.2. Applied voltage, 5 kV.

determined by the composition of the BGE and a part migrating with the velocity of the electroosmotic flow (EOF) at the position of the original disturbance. System peaks are the result. Although the system peak migrating with the velocity of the EOF is at the same position as system peaks described by De Bruin et al. [12], we think that the natures of these system peaks are different. The system peak described by De Bruin et al. are a result of the adaptation to the value of the local Kohlrausch function ω , whereas the system peaks described by Beckers [11] are also dependent on discontinuities in, e.g., pH through which Kohlrausch's regulation function is not constant. The discontinuities are only observable for UV-absorbing BGEs. The concentration of the UV-absorbing co-ions in a system peak can be higher or lower than that of the BGE and we shall denote these system peaks as "positive" or "negative" peaks, respectively. Further, the local electric field strength E_{SP} can be higher or lower than that of the BGE, E_{BGE} , depending on the mobilities and concentrations

of all ionic species concerned. If $E_{SP} < E_{BGE}$ the peaks are diffuse at the front-side and for $E_{SP} > E_{BGE}$, as in ITP, they are sharp at the front-side.

All parameters, such as the mobility of such a system peak, the concentration of all ionic species and the pH in the system peak, can be calculated with a mathematical model [11]. In Fig. 6 the four types of system peak shapes are shown schematically. Positive peaks can be of the type A or C, respectively sharp and diffuse at the front-side, and negative peaks of the type B or D, respectively diffuse and sharp at the front-side. For a smaller system peak, i.e., a system peak with a concentration of the co-ion closer to that of the BGE, the peak shape is given by dotted lines. For a specific BGE composition generally the pairs A–B or C–D are obtained as system peaks. Whether the positive or negative system peak appears depends to the kind of discontinuity introduced.

As an illustration, in Fig. 7 the electropherograms are given for the separation of a 5-s

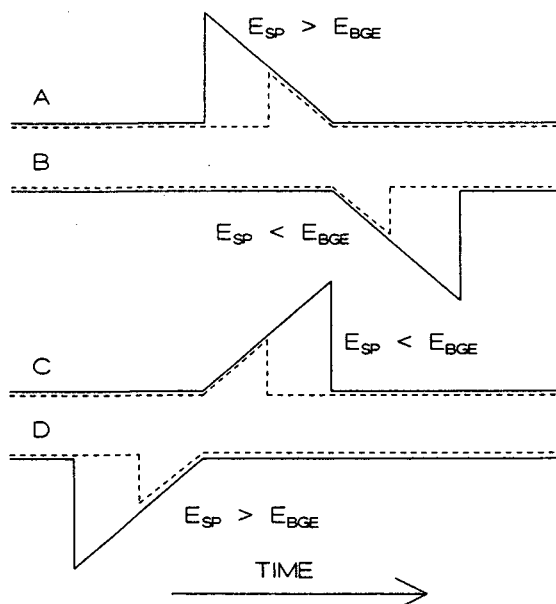


Fig. 6. Schematic representation of four types of system peak (SP) shapes. Positive peaks can be of type A or C, respectively sharp or diffuse at the front-side, and negative peaks of the type B or D, respectively diffuse and sharp at the front-side. For smaller system peaks the peak shape is given as dotted lines. For further information, see text.

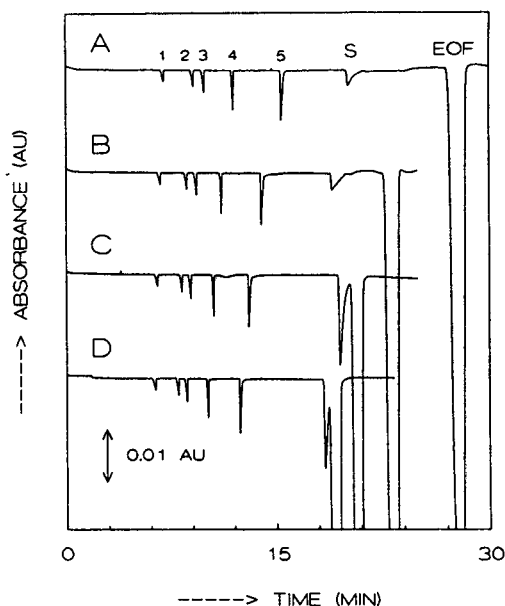


Fig. 7. Electropherograms for the separation of a 5-s pressure injection of 0.0002 M of the MIX on applying BGEs consisting of 0.01 M histidine adjusted to a pH of (A) 4.0 and (B) 4.5 by adding formic acid and (C) 4.5 and (D) 5 by adding acetic acid. The mobilities of the system peaks S are higher for lower system pHs. Applied voltage, 5 kV.

pressure injection of 0.0002 M of the MIX on applying BGEs consisting of 0.01 M histidine adjusted to a pH of (A) 4.0 and (B) 4.5 by adding formic acid and (C) 4.5 and (D) 5 by adding acetic acid. Clearly a system peak of type D can be seen in all instances. The mobility of the system peaks is larger for lower system pHs.

4.2. BGE with two co-ions

Often, BGEs consisting of more than one co-ion are applied. For example, De Bruin et al. [12] added potassium chloride to the BGE to determine the effect of the ionic strength on sensitivity and efficiency. Sometimes two co-ions are used, where one has UV-absorbing properties whereas the other acts as buffer or complexing ions. On applying BGEs with two co-ions, system peaks, with a different character as discussed above (see Fig. 7), often occur. It is remarkable that the mobilities of the sample components determine whether a positive or

negative system peak occurs and the mobilities of the system peaks determine whether a positive or negative component peak is present for the UV-transparent components.

In all our experiments it appears that if the mobility of a component was higher than that of the system peak S, the UV-transparent component gave a positive peak. If the mobility was lower, a negative peak was the result. System peaks belonging to components with a mobility higher than that of the system peak are negative by themselves, otherwise they are positive. As an illustration, in Fig. 8 the electropherograms are given on applying a BGE consisting of 0.004 M histidine and 0.006 M potassium ions adjusted to pH 5 by adding acetic acid for 5-s pressure injections of 0.0005 M solutions of the ions (B)

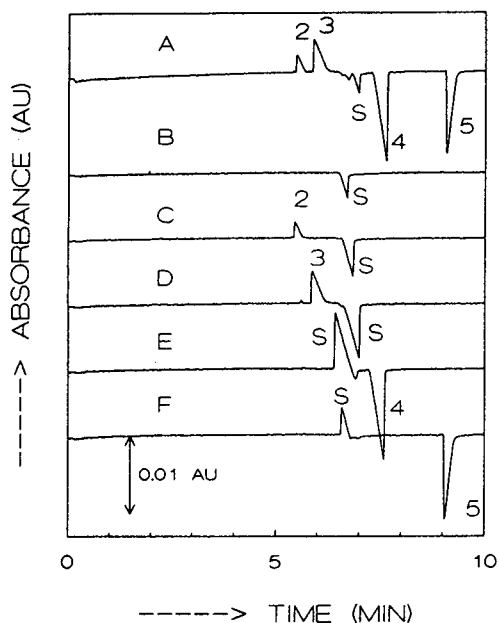


Fig. 8. Electropherograms for the separations of 5-s pressure injections of 0.0005 M solutions of the ions (B) potassium, (C) sodium, (D) TMA, (E) TEA and (F) TBA and (A) a mixture of these components on applying a BGE consisting of a mixture of 0.004 M histidine and 0.006 M potassium ions adjusted to pH 5 by adding acetic acid. The applied voltage was 7 kV. If the mobilities of the sample components are higher than that of the system peak S, the sample components are positive peaks, otherwise they are negative. If the system peak is in the vicinity of a sample component, both peaks are enlarged.

potassium, (C) sodium, (D) TMA, (E) TEA and (F) TBA and (A) a mixture of these components. The applied voltage was 7 kV. Although in all the electropherograms two system peaks were present, the EOF dip and the system peak just before the EOF dip are not shown. In Fig. 8B potassium is not visible, because the BGE contains potassium. As its mobility is higher than that of the system peak, the system peak S is negative. The mobilities of (C) sodium and (D) TMA are higher than that of the system peak S, hence these components show a positive component peak, whereas the system peaks S belonging to them are negative. For (E) TEA and (F) TBA the mobilities are lower than that of the system peak and therefore the component peaks are negative and the system peaks S are positive.

If a system peak and the component peak are close together there seems to be an interaction between the two peaks. Both peaks are enlarged, as if the first peak sucks empty the second peak. Remember that a positive peak means a concentration of UV-absorbing co-ion higher than that in the BGE, whereas in a dip this concentration is lower than that in the BGE. In (A) the electropherogram for the separation of all components is given. Sodium (2) and TMA (3) are positive peaks and TEA (4) and TBA (5) are negative peaks. The resulting system peak S is a negative peak. The type of the system peaks S depends on the mobilities of the sample components injected and are of the A–B type from Fig. 6.

In Fig. 9A the relationship between the measured mobilities of the system peaks S and the concentrations of potassium ions is given for BGEs consisting of the co-ions potassium and histidine at a total cationic concentration of 0.01 M adjusted to a pH of 5 by adding acetic acid. Because the values of the mobilities of system peaks can vary considerably, as this mobility is determined from a large positive peak or negative system peak (see Figs. 6 and 8), we calculated the mobility of the system peak S as the average from a positive and negative system peak. It is remarkable that in Fig. 9 the mobilities of the system peaks seem to vary between

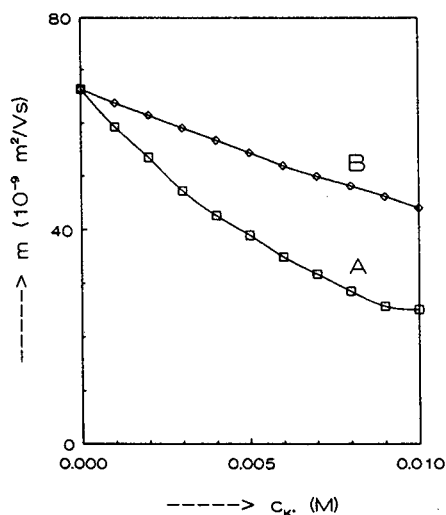


Fig. 9. Relationship between the measured mobilities of the system peaks S and the concentrations of potassium ions for BGEs consisting of the co-ions (A) potassium and histidine and (B) potassium and imidazole at a total cationic concentration of 0.01 M adjusted to pH 5 by adding acetic acid. The mobilities indicated at c_{K^+} values of 0.000 and 0.010 M are the measured mobilities of the potassium and imidazole and histidine ions, respectively.

the mobility of the potassium ions and that of the histidine ions. Therefore, we measured again the mobilities of the system peaks for BGEs consisting of mixtures of potassium and imidazole at a total cationic concentration of 0.01 M and at a pH 5 by adding acetic acid. The results are given in Fig. 9B. Again the mobilities of the system peaks vary between the mobility of imidazole and potassium ions.

To give a complete survey of all the foregoing effects for different compositions of the BGE, in Fig. 10 the electropherograms are given for the separations of 5-s pressure injections of 0.0005 M of the MIX applying BGEs consisting of varying concentrations of potassium and histidine at a total cationic concentration of 0.01 M and adjusted to pH 5 by adding acetic acid. The electropherograms are indicated with a number referring to the concentration of the histidine ion in the BGE. Applying the BGE with 0.01 M histidine, the components potassium (1), sodium (2), TMA (3), TEA (4) and TBA (5) are all visible as negative peaks in the indirect UV

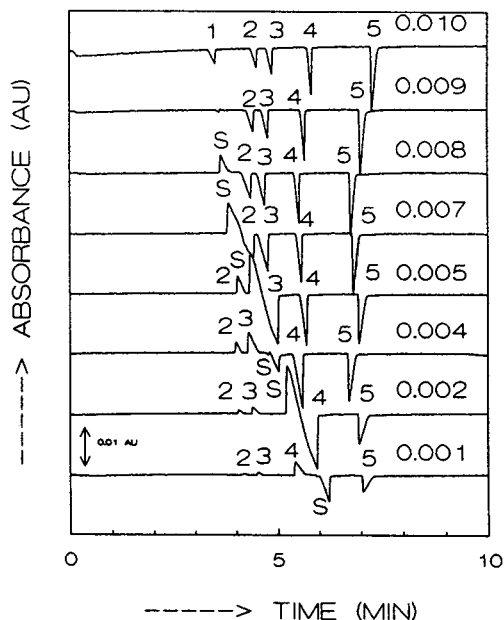


Fig. 10. Electropherograms for the separation of 5-s pressure injections of a mixture of 0.0005 M of the MIX applying BGEs consisting of varying concentrations of potassium and histidine at a total cationic concentration of 0.01 M, adjusted to pH 5 by adding acetic acid. The electropherograms are indicated with a number referring to the concentration of the histidine ions in the BGE. The applied voltage was 7 kV. The mobility of the system peak S varies considerably. Components with mobilities higher than that of the system peaks are peaks and components with lower mobilities are dips.

mode. In the BGE with 0.009 M histidine (and 0.001 M potassium) the potassium peak is not visible because the BGE contains potassium. A small dip marks the position of potassium. In the BGE with 0.008 M histidine a system peak S is present. Because the mobility of the system peak S is higher than that of any sample component, all sample peaks are negative and the system peak is a positive peak. In the BGE with 0.007 M histidine the system peak and the sodium peak are very close, hence these peaks are enlarged. In the BGE with 0.005 M histidine the system peak passed the sodium peak, so sodium is a positive peak. The system peak is still a positive peak and because it is close to the TMA peak, these peaks are enlarged. In the BGE with 0.004 M histidine the system peak passed the TMA peak and lies between TMA and TEA as a

negative peak. Sodium and TMA are positive peaks and TEA and TBA are still negative peaks. In the BGE with 0.002 M histidine the system peak S and TEA are close together and both enlarged. It is not clear which peak is the system peak and TEA. In the BGE with 0.001 M histidine the system peaks passed TEA and is a negative peak between TEA and TBA. Sodium, TMA and TEA are positive peaks, small owing to low concentration of histidine, whereas the system peak S and TBA are negative peaks. In all cases were measured all components separately to identify carefully all peaks, although it is difficult to identify the peaks if a system peak and a component peak are close together.

4.3. Calibration graphs in BGEs with two co-ions

As already indicated, system peaks appear on applying BGEs with two co-ions and their mobilities are between the mobilities of the two co-ions. In all systems measured, components with a mobility higher than that of the system peak are positive peaks whereas the system peaks themselves are negative, and vice versa. Further, if the system peak and component peak are close together, both peaks are enlarged and the quantitative properties seems to be lost.

To study this effect, calibration graphs were measured by injecting 0.0002 M of the MIX for several pressure injection times applying a BGE consisting of 0.005 M histidine and 0.005 M potassium adjusted at pH 5 by adding acetic acid. The applied voltage was 5 kV. As can be seen in Fig. 10, sodium and the system peak are positive, whereas TMA, TEA and TBA are negative peaks. The system peak S and the peak of TMA are close together and enlarged. Compared with several other BGEs the TMA peak is generally smaller than those of the TEA and TBA peaks.

In Fig. 11 the relationship between measured peak area (mAUs) and pressure injection times (s) of 0.0002 M of the MIX is given for all components. As can be seen, there is linear relationship between peak area and pressure injection time for sodium (positive peaks) and

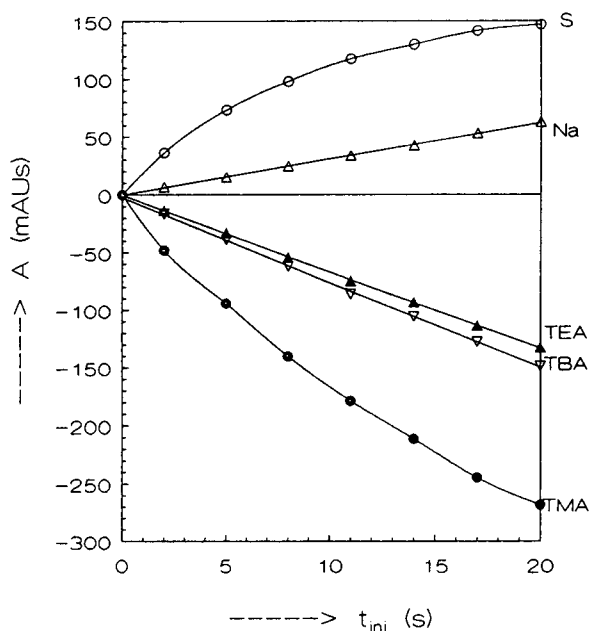


Fig. 11. Relationship between measured peak area A (mAUs) and pressure injection times (s) of 0.0002 M of the MIX applying a BGE of 0.005 M potassium and 0.005 M histidine adjusted to pH 5 by adding acetic acid. The applied voltage was 7 kV. A linear relationship between peak area and pressure injection times is obtained for sodium (positive peaks) and TEA and TBA (negative peaks) with regression correlation coefficients larger than 0.999. For the system peak S and the TMA peak the linear relationship is lost and these peaks are much enlarged.

TEA and TBA (negative peaks) with regression correlation coefficients larger than 0.999. For the system peak S and TMA peak the linear relationship is lost and these peaks are much enlarged.

5. Conclusion

Starting from Kohlrausch's law, derived for fully ionized monovalent ionic constituents, an expression for the response factor can be derived showing that the response factor is small if the mobility of the sample ionic species is higher than that of the co-ion of the BGE. In that case the total ionic strength in the sample zone increases. On applying UV-absorbing counter ions, the total UV absorbance can increase, even

if the sample components are UV transparent. UV-transparent components can show positive peaks in this way. For sample components with very low mobilities the response factor can be very large. If the BGE has UV-absorbing properties, the net UV signal is lower and even UV-absorbing components show dips in such cases. If BGEs are applied with two co-ions, system peaks are the result. This means that the ratio of the concentrations of the two co-ions is not constant in the electrolyte system. The mobility of the system peak is between those of the co-ions and is dependent on the ratio of the concentrations of the co-ions. For BGEs containing potassium and histidine as co-ions, UV-transparent sample components with a mobility higher than that of the system peak appear as peaks, whereas UV-transparent sample components with lower mobilities are dips. Also, the system peaks themselves can be positive peaks or dips. If the sample component is a peak, the system peak is a dip and vice versa. For complex sample mixtures the system peak is a peak or a dip dependent on the sample composition. If the peaks of a system peak and a sample component are close together, they interact, resulting in an enlarged peak and dip, through which quantitative aspects are lost.

Denkert et al. [13] reported that sometimes samples give positive or negative peaks depending on their charge and retention relative to the UV-absorbing ionic component in the mobile phase in reversed-phase ion-pair chromatography, and these phenomena seem to be in accord with phenomena described in this paper for CZE. To answer the question of whether these phenomena in CZE are associated with adsorption phenomena since the UV-absorbing ions are cations that can adsorb on the fused-silica surface producing system peaks just as in chromatography, experiments were carried out to separate anionic species by applying BGEs consisting of mixtures with various concentrations of a UV-absorbing and a UV-transparent anion. Also in the separation of anionic species, system peaks were present and if system peaks and sample components are close together they interact, resulting in enlarged peaks.

In Fig. 12 the electropherograms are given for the separation of 10-s pressure injections of a mixture of $2 \cdot 10^{-4}$ M propionic acid (P) and butyric acid (B) with BGEs consisting of mixtures of phenylacetic acid and acetic acid at various concentrations, (1) 0.01 and 0 M, (2) 0.008 and 0.002 M, (3) 0.004 and 0.006 M and (4) 0.002 and 0.008 M, adjusted to pH 8.1 by adding Tris. In electropherogram (1) applying only the UV-absorbing anion phenylacetic acid, propionic and butyric acids are present as a dip in the indirect UV mode. Applying a BGE with two co-ions a system peak S appears. In electropherogram (2) the mobility of the system peak is higher than that of both anionic species and they are dips. In electropherogram (3) the system peak is in the vicinity of the peak of propionic

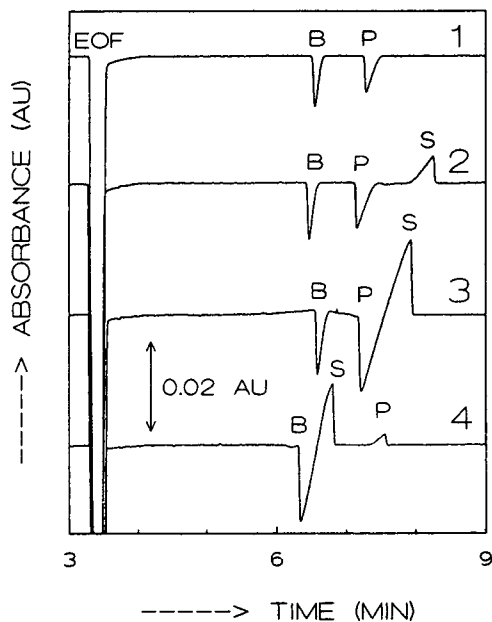


Fig. 12. Electropherograms for the separation of 10-s pressure injections of a mixture of $2 \cdot 10^{-4}$ M (P) propionic acid and (B) butyric acid applying BGEs consisting of mixtures of phenylacetic acid and acetic acid at concentrations of, respectively, (1) 0.01 and 0 M, (2) 0.008 and 0.002 M, (3) 0.004 and 0.006 M and (4) 0.002 and 0.008 M adjusted to pH 8.1 by adding Tris. The applied voltage was 15 kV. Just as for cationic components, sample components with a mobility lower than that of the system peak are dips, whereas sample components with higher mobilities are peaks. For further explanation, see text.

acid and both peaks are enlarged. In electropherogram (4) the system peak has a mobility lower than that of propionate, through which propionate is a peak whereas the butyrate and system peaks are enlarged since they interact together. The mobilities of the system peaks are between those of the anions of the BGE. From Fig. 12, it can be concluded that phenomena as described for cationic components also occur for anionic species, indicating that these phenomena and the presence of system peaks seems not to be associated with adsorption phenomena as in chromatography. The nature of these system peaks is under further investigation.

Acknowledgement

The author expresses his gratitude to Rian Straatman for her very skilful assistance in the experimental work.

References

- [1] E.S. Yeung and W.G. Kuhr, *Anal. Chem.*, 63 (1991) 275A.
- [2] W.G. Kuhr and E.S. Yeung, *Anal. Chem.*, 60 (1988) 1834.
- [3] W.G. Kuhr and E.S. Yeung, *Anal. Chem.*, 60 (1988) 2642.
- [4] T. Wang and R.A. Hartwick, *J. Chromatogr.*, 607 (1992) 119.
- [5] M.W.F. Nielen, *J. Chromatogr.*, 588 (1991) 321.
- [6] F. Foret, S. Fanali, L. Ossicini and P. Bocek, *J. Chromatogr.*, 470 (1989) 299.
- [7] F. Kohlrausch, *Ann. Phys. (Leipzig)*, 62 (1897) 209.
- [8] F.E.P. Mikkers, *Thesis*, University of Technology, Eindhoven, 1980.
- [9] F.E.P. Mikkers, Th.P.M. Verheggen and F.M. Everaerts, *J. Chromatogr.*, 169 (1979) 1.
- [10] M.T. Ackermans, F.M. Everaerts and J.L. Beckers, *J. Chromatogr.*, 549 (1991) 345.
- [11] J.L. Beckers, *J. Chromatogr. A*, 662 (1994) 153.
- [12] G.J.M. de Bruin, A.C. van Asten, X. Xu and H. Poppe, *J. Chromatogr.*, 608 (1992) 97.
- [13] M. Denkert, L. Hackzell, G. Schill and E. Sjögren, *J. Chromatogr.*, 218 (1981) 31.



ELSEVIER

Journal of Chromatography A, 679 (1994) 167-171

JOURNAL OF
CHROMATOGRAPHY A

Spectrophotometric determination of ionization constants by capillary zone electrophoresis

J.A. Cleveland, Jr.^{a,*} C.L. Martin^a, S.J. Gluck^b

^aDiscovery Research, DowElanco, 9410 Zionsville Road, Indianapolis, IN 46268-1053 USA

^bAnalytical Sciences, 1897B Building, Dow Chemical Co., Midland, MI 48667, USA

First received 1 September 1993; revised manuscript received 11 May 1994

Abstract

One of the historical means of determining the ionization constant of a solute relies on the ionized and neutral states of a molecule having different absorption coefficients at an analytical wavelength. An ionic distribution curve can be constructed by directly determining the ratio of neutral species to ionized species in a series of buffer solutions of differing pH. This method is complementary to a recently developed procedure which utilizes electrophoretic mobilities to determine ionization constants. The same data system used to generate mobilities at different pH values also includes information on peak areas, which correlate with the absorbance of a species. Thus, absorbances regressed against pH yields ionization constants which can corroborate those derived from electrophoretic migration.

1. Introduction

Aqueous-phase potentiometric titration, the most widely used method for determining pK_a values requires that the concentration of an analyte be at least 0.1 mM; otherwise, interferences are caused by the presence of dissolved CO_2 . A common alternative for determining the pK_a at low concentrations is UV-Vis spectrophotometric titration, which relies on the neutral and ionic states of a molecule having different absorption coefficients at an analytical wavelength [1]. Recently, capillary electrophoresis (CE) has been introduced as a method for convenient and precise aqueous pK_a determination [2-4]. The method takes advantage of the

relation between electrophoretic mobility and fractional ionization of a compound at different pH values. In this paper we demonstrate that the spectrophotometric method can also be used in conjunction with CE by relating peak areas to absorbance. Moreover, it is possible to determine pK_a by the two methods using the same CE data set, thereby providing an internal check on each method.

2. Theoretical

2.1. Relating pK_a to mobility

The thermodynamic equilibrium constant, K_a^{th} , for the dissociation of a weak acid e.g.

* Corresponding author.



is defined as

$$K^{\text{th}} = \gamma_{\text{Z}^-} \gamma_{\text{H}^+} \cdot \frac{[\text{H}^+][\text{Z}^-]}{[\text{HZ}]} \quad (2)$$

where γ is the activity coefficient and γ_{HZ} is assumed to be 1. Activities can be calculated from Debye-Hückel theory according to the relation

$$-\log \gamma = \frac{0.509z^2\sqrt{\mu}}{1 + 0.328a\sqrt{\mu}}; \quad (3)$$

$$\mu = \frac{1}{2} \cdot \sum_{i=1}^m C_i z_i^2$$

where a is the hydrated diameter of an ion in Å [5], z is the valency of the ion and μ is the ionic strength of the solution. In general, the exact value of the parameter a , which can range from 1-11 Å, will not be known; in this study, the value 5 Å was assumed.

A relation between pH versus electrophoretic mobility plots and titration curves has been known for quite some time [6,7]. Morris and Morris [8] derived an equation for calculating mobilities at different pH values when the pK_a of an acid was known. Similarly, it has recently been shown that the pK_a of an acid/base can be determined when the mobilities are known at different pH values [2-4].

Since $m_e = \alpha m_a$, where m_e is the net electrophoretic mobility, m_a is the electrophoretic mobility of the fully deprotonated species Z^- , and α is the fraction ionized ($0 \leq \alpha \leq 1$), Eq. 2 can be rearranged to give (at 25°C):

$$pK_a^{\text{th}} = \text{pH} - \log \left(\frac{m_e}{m_a - m_e} \right) + \frac{0.509z^2\sqrt{\mu}}{1 + 0.328a\sqrt{\mu}} \quad (\text{acids}) \quad (4)$$

The analogous equation for a base, B, is given as:

$$pK_a^{\text{th}} = \text{pH} + \log \left(\frac{m_e}{m_b - m_e} \right) - \frac{0.509z^2\sqrt{\mu}}{1 + 0.328a\sqrt{\mu}} \quad (\text{bases}) \quad (5)$$

where m_b is the electrophoretic mobility of the fully protonated species, BH^+ .

2.2. Relating pK_a to peak area

Assuming that Beer's law is valid, the absorbance, A , of an acid HZ at some analytical wavelength is the sum of the absorbances of the molecular species, A_m , and the ionized species, A_I [1]:

$$A = A_m + A_I \quad (6)$$

Provided the same total concentration is used for measurements at different pH values, the absorbance at each pH can be expressed in terms of α , A_I and A_m :

$$A = \alpha(A_I - A_m) + A_m \quad \text{for } A_I > A_m \quad (7)$$

$$A = \alpha(A_m - A_I) + A_I \quad \text{for } A_m > A_I \quad (8)$$

From these expressions, it follows directly that

$$\frac{[\text{Z}^-]}{[\text{HZ}]} = \frac{\alpha}{1 - \alpha} = \frac{A - A_m}{A_I - A} \quad \text{for } A_I > A_m \quad (9)$$

$$\frac{[\text{Z}^-]}{[\text{HZ}]} = \frac{\alpha}{1 - \alpha} = \frac{A_m - A}{A - A_I} \quad \text{for } A_m > A_I \quad (10)$$

While in CE it is peak area, A , not absorbance, that is directly measured, these parameters are related through the expression $A \propto A/t$, where t is migration time required for the solute band to travel the distance from the capillary end to the detector [9-11]. Using this relation with Eqs. 9 and 10, Eq. 2 can be rearranged to give:

$$pK_a^{\text{th}} = \text{pH} - \log \left(\frac{\frac{A}{t} - A_m}{A_I - \frac{A}{t}} \right) + \frac{0.509z^2\sqrt{\mu}}{1 + 0.328a\sqrt{\mu}} \quad (\text{acids, } A_I > A_m) \quad (11)$$

$$pK_a^{\text{th}} = \text{pH} - \log \left(\frac{\frac{A}{t} - A_I}{A_m - \frac{A}{t}} \right) + \frac{0.509z^2\sqrt{\mu}}{1 + 0.328a\sqrt{\mu}} \quad (\text{acids, } A_m > A_I) \quad (12)$$

Analogous expressions for bases are as follows:

$$\text{p}K_a^{\text{th}} = \text{pH} + \log \left(\frac{A_I - \frac{A}{t}}{\frac{A}{t} - A_m} \right) - \frac{0.509z^2\sqrt{\mu}}{1 + 0.328a\sqrt{\mu}} \quad (\text{bases, } A_I > A_m) \quad (13)$$

$$\text{p}K_a^{\text{th}} = \text{pH} + \log \left(\frac{\frac{A}{t} - A_I}{A_m - \frac{A}{t}} \right) - \frac{0.509z^2\sqrt{\mu}}{1 + 0.328a\sqrt{\mu}} \quad (\text{bases, } A_m > A_I) \quad (14)$$

3. Experimental

All buffer and sample solutions were prepared in filtered and deionized water. The zwitterionic buffers shown in Table 1 were generated by titrating 20 mM solutions with 1 M NaOH until the desired pH was reached, as determined with an Orion EA 940 pH meter equipped with a

Ross combination electrode. The series was designed so that the maximum gap between data points is 0.6 pH units.

Where applicable, electrophoretic mobilities were calculated according to the relation $m_e = m_{\text{app}} - m_{\text{eof}}$, where m_{app} is the apparent mobility of an analyte and m_{eof} is the electroosmotic mobility. The electroosmotic mobility was determined by monitoring a species added to the sample vial, in this study 200 μM mesityl oxide, which remains neutral throughout the entire pH range.

A SpectraPHORESIS 1000 (Thermo-Separation Products, Fremont, CA, USA) CE instrument was used for all experiments. Instrument parameters included the following: voltage 25 kV, temperature 25°C and hydrodynamic injection time 2 s. Since the hydrodynamic injection rate for this instrument is nominally 6 nl/s for a 70 cm \times 75 μm untreated fused-silica capillary (Polymicro Technology, Phoenix, AZ, USA), approximately 12 nl were loaded onto the column. Absorbance was monitored at 237 nm. The wash cycle performed prior to each run in a sequence consisted of 2.5 min with each of 0.1 M NaOH and deionized water followed by a 5-min rinse with the running buffer.

The buffers given in Table 1 were run in sequence from high to low pH. The Spec-

Table 1
Buffer series spanning pH range 6 to 11

Component	pH	[HZ]	[Z ⁻]	μ	$-\log \gamma^a$
MES, Morpholinoethanesulphonic acid	6.10	0.010	0.010	0.010	0.044
ACES, 2-[(2-amino-2-oxoethyl)amino]ethanesulphonic acid	6.65	0.012	0.008	0.008	0.040
MOPS, 3-(4-morpholino)propanesulphonic acid	7.20	0.010	0.010	0.010	0.044
HEPES, N-(2-hydroxyethyl)piperazine-N'-ethanesulphonic acid	7.65	0.008	0.012	0.012	0.047
HEPPSO, N-(2-hydroxyethyl)piperazine-N'-2-hydroxypropanesulphonic acid	7.90	0.009	0.011	0.011	0.046
Tricine	8.10	0.010	0.010	0.010	0.044
TAPS, N-tris(hydroxymethyl)methyl-3-aminopropanesulfonic acid	8.40	0.010	0.010	0.010	0.044
TAPS	8.70	0.007	0.013	0.013	0.049
AMPSO, 3-[(1,1-dimethyl-2-hydroxyethyl)amino]-2-hydroxypropanesulphonic acid	9.00	0.010	0.010	0.010	0.044
CHES, 2-(N-cyclohexylamino)ethanesulfonic acid	9.30	0.010	0.010	0.010	0.044
CAPSO, 3-(cyclohexylamino)-2-hydroxy-1-propanesulfonic acid	9.60	0.010	0.010	0.010	0.044
CAPSO	10.0	0.006	0.014	0.014	0.050
CAPS, 3-(cyclohexylamino)-1-propanesulfonic acid	10.4	0.010	0.010	0.010	0.044
CAPS	11.0	0.004	0.016	0.016	0.053

^a Sign of correction is + for acids and – for bases.

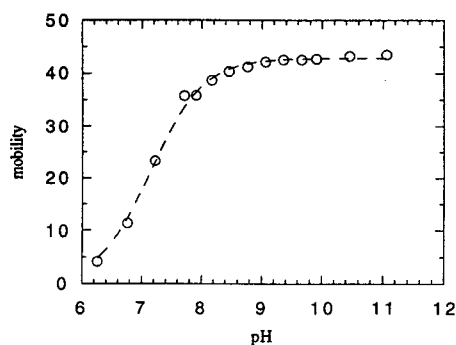


Fig. 1. Plot of net electrophoretic mobility ($m_e, \times 10^5 \text{ cm}^2/\text{V s}$) vs. pH for $200 \mu\text{M}$ *p*-nitrophenol with superimposed curve fit.

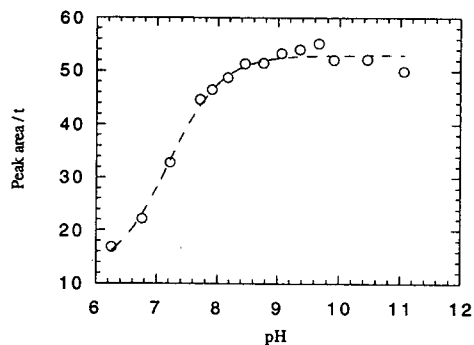


Fig. 2. Plot of peak area divided by migration time (arbitrary units) vs. pH for $200 \mu\text{M}$ *p*-nitrophenol with superimposed curve fit.

traPHORESIS 1000 is equipped with a single reservoir for the buffer at the detector end of the column. This reservoir was filled with 20 mM N-[tris(hydroxymethyl)methyl]glycine (Tricine) at a pH of 8.1. Since each run was 10 min in length, the total analysis time per sample was just under 5 h.

Peak areas and migration times were computed using the SpectraPHORESIS 1000 software package. The nonlinear regression was performed using Kaleidagraph (Synergy Software, Reading, PA, USA).

4. Results

Fig. 1 shows a plot of net electrophoretic mobility vs. pH for $200 \mu\text{M}$ *p*-nitrophenol along with the superimposed curve fit to Eq. 4. Values of $\text{p}K_a$ and m_a as determined from the two-parameter non-linear regression are given in Table 2. For an independent data set acquired using the same sample, Fig. 2 shows a plot of peak area divided by migration time vs. pH with

superimposed curve fit to Eq. 11. The three-parameter non-linear regression yields values of the parameters $\text{p}K_a$, A_1 and A_m given in Table 2. The $\text{p}K_a$ values determined by both methods have precisions of better than 1% and agree with the literature to within experimental error.

5. Discussion

An assumption of the spectroscopic method is that the total concentration of molecular and ionic species of a solute remain constant. As such, the method as described herein is strictly valid only with respect to hydrodynamic injections, where a constant amount of solute can be loaded onto the column in each run by simply specifying the injection period. In an electrokinetic injection, the total amount of an analyte loaded onto a column in a given period of time is not necessarily constant but depends on such factors as the relative ionic strengths and pH values of the sample solutions and running buffers.

Table 2

Comparison of CE-determined $\text{p}K_a$ values with literature value for *p*-nitrophenol at 25°C [1]

Data source	$\text{p}K_a$	m_a ($\times 10^5 \text{ cm}^2/\text{V s}$)	A_1 (arb. units)	A_m (arb. units)
Literature	7.15	—	—	—
Mobility	7.15 ± 0.02	42.8 ± 0.3	—	—
Area	7.19 ± 0.07	—	53.0 ± 0.5	11.9 ± 1.8

Errors are given as standard deviations, where $n = 14$.

The spectroscopic method is not appropriate for an analyte at the solubility limit. Solubility, S'_0 , is described according to the relations [1]:

$$S'_0 = S_i [1 + 10^{(pH - pK_a)}] \quad (\text{acids}) \quad (15)$$

$$S'_0 = S_i [1 + 10^{(pK_a - pH)}] \quad (\text{bases}) \quad (16)$$

where S_i , the intrinsic solubility, is usually determined in 0.01 M HCl for an acid and in 0.01 M NaOH for a base. For a saturated solution of an analyte, the relation between peak area and pH is governed not only by the relative absorption coefficients of the neutral and ionized species, but also by the relative solubilities of these species. Any attempt to apply the spectroscopic analysis to such a system must account for both of these effects.

The limitations of the spectroscopic method characterized above stem directly from the method's reliance on amplitude data. In contrast, mobility-based analysis relies essentially on frequency data and as such is not limited by the above consideration. In addition, mobilities are generally more reproducible than peak areas [12]. All these factors support the conclusion that mobility-based analysis should be more universally applicable and precise than the spectroscopic method when detection limit is not an issue.

Variation in temperature is undoubtedly a source of error for both methods, since mobility varies by 2.7% per °C [13] and buffer pH is temperature-dependent. However, the air-based cooling system of the instrument is quoted as being stable to $< \pm 1^\circ\text{C}$, so that this effect is minimized. It is also possible that the temperature inside the capillary is higher than the surroundings due to the effects of Joule heating. Several studies have recently attempted to examine the magnitude of this difference both experimentally [14–19] and computationally [13]. Because of the low ionic strengths of the buffers used in this study, the current is so low ($< 20 \mu\text{A}$) that internal heating is presumed to be insignificant.

6. Conclusions

In the determination of the ionization constant

of *p*-nitrophenol from electrophoretic mobility, spectroscopic analysis based on peak areas was used as corroborating data. Peak areas divided by migration time versus pH for a constant solute concentration gave an ionic distribution plot which was fit using a non-linear regression. In order to emphasize the independence of the mobility- and spectroscopic-based methods of analysis, each was applied here to a different data set. However, the information required for both methods is supplied in each CE data set. As such, it is possible to perform two independent analyses concurrently, thereby providing an internal check on each method.

References

- [1] A. Albert and E.P. Serjeant, *The Determination of Ionization Constants: A Laboratory Manual*, Chapman & Hall, New York, 3rd ed., 1984.
- [2] J.L. Beckers, F.M. Everaerts and M.T. Ackermans, *J. Chromatogr.*, 537 (1991) 407.
- [3] J. Cai, J.T. Smith and Z. El Rassi, *J. High Resolut. Chromatogr.*, 15 (1992) 30.
- [4] J.A. Cleveland, Jr., M.H. Benko, S.J. Gluck and Y.M. Walbroehl, *J. Chromatogr. A*, 652 (1993) 301.
- [5] J. Kielland, *J. Am. Chem. Soc.*, 59 (1937) 1675.
- [6] H.A. Abramson, *J. Gen. Physiol.*, 15 (1931) 575.
- [7] L.G. Longworth, *Ann. NY Acad. Sci.*, 41 (1941) 267.
- [8] C.J.O.R. Morris and P. Morris, *Separation Methods in Biochemistry*, Pitman Publ., London, 2nd ed., 1976, p. 714.
- [9] D.M. Goodall, S.J. Williams and D.K. Lloyd, *Trends Anal. Chem.*, 10 (1991) 272.
- [10] D. Demoret and J. Dubrow, *J. Chromatogr.*, 559 (1991) 43.
- [11] S. Hjertén, K. Elenbring, F. Kilar, J.-L. Liao, A.J.C. Chress, C.J. Sierbert and M.-D. Zhu, *J. Chromatogr.*, 403 (1987) 47.
- [12] J.A. Lux, H.F. Yin and G. Schomburg, *Chromatographia*, 30 (1990) 7.
- [13] S. Hjertén, *Electrophoresis*, 11 (1990) 665.
- [14] M.S. Bello, M. Chiari, M. Nesi and P.G. Righetti, *J. Chromatogr.*, 625 (1992) 323.
- [15] T.L. Rapp, W.K. Kowalchuk, K.L. Davis, E.A. Todd, K.-L. Liu and M.D. Morris, *Anal. Chem.*, 64 (1992) 2434.
- [16] H. Watzig, *Chromatographia*, 33 (1992) 445.
- [17] S. Hjertén, *Chromatogr. Rev.*, 9 (1967) 122.
- [18] T.T. Lee and E.S. Yeung, *Anal. Chem.*, 63 (1991) 2842.
- [19] M.S. Bello, E.I. Levin and P.G. Righetti, *J. Chromatogr. A*, 652 (1993) 329.

Identification of tryptophan and tyrosine residues in peptides separated by capillary electrophoresis by their second-derivative spectra using diode-array detection

Rudolf Grimm*, Arno Graf, David N. Heiger
Hewlett-Packard, Hewlett-Packard-Strasse, 76337 Waldbronn, Germany

First received 28 April 1994; revised manuscript received 8 June 1994

Abstract

The use of diode-array detection allows the non-destructive identification of tryptophan and tyrosine residues in complex peptide mixtures separated by capillary electrophoresis. Second-order derivative spectra of both amino acids show significant differences while zero-order spectra are overlapping to a great extent. A mixture of peptides containing tryptophan and/or tyrosine residues was used to evaluate this method. Tryptic peptide maps of carbonic anhydrase and of the bacterial chaperonin protein GroEL, and of an autodigest of trypsin were characterized for tryptophan- and tyrosine-containing peptides. Automated spectra library search was performed successfully.

1. Introduction

Diode-array detectors have the major advantage that spectra of eluting or migrating compounds can be stored in a digital form and then manipulated by a variety of algorithms to ascertain, for example, the purity of an eluting peak [1–3]. Such spectral data, in combination with monitoring of the eluate at chosen discrete wavelengths, greatly increases detection specificity over that available from single-channel detectors.

Peptides and proteins exhibit UV-absorption spectra characteristic of their component amino acids [4–6], particularly the aromatic residues tyrosine and tryptophan, and also phenylalanine to a lesser extent. However, analysis of peptides

and proteins for the detection of constituent aromatic residues by UV-Vis spectroscopy poses problems because of overlapping absorption bands of tryptophan and tyrosine. Derivative spectroscopy, in particular second-order derivative spectroscopy which transforms peaks and shoulders into minima, enhances resolution of minor spectral features, thus overcoming some of the problems of similar UV spectra. The great use of diode-array detection in combination with reversed-phase HPLC for the specific identification of aromatic amino acids-containing peptides during their elution under gradient conditions followed by protein sequencing has been shown in detail [7,8].

Application of capillary electrophoresis (CE) for peptide separations and analysis is significantly increasing due to the high resolution of this technique, high speed of analysis and small

* Corresponding author.

amount of sample required. Also fractionation of peptides on CE followed by protein sequencing has been shown already [9]. Hence, the powerful features of two-dimensional UV spectra described above for HPLC are also available for CE and are invaluable for the identification and characterization of peptides.

In this paper we show that the diode-array detector and associated software implemented in the Hewlett-Packard ^{3D}CE system allows to obtain the same valuable information as described for the HPLC system. Automatic evaluation of tyrosine- and tryptophan-containing peptides from peptide maps using spectral library

search functions and second-order derivative spectra are demonstrated.

2. Materials and methods

2.1. Peptides and proteins

All peptides and proteins except the bacterial chaperonin protein GroEL were obtained from Sigma (St. Louis, MO, USA). Peptides were dissolved in water at a concentration of 0.5 mg/ml and proteins in water at a concentration of 3 mg/ml. Purified recombinant GroEL at a con-

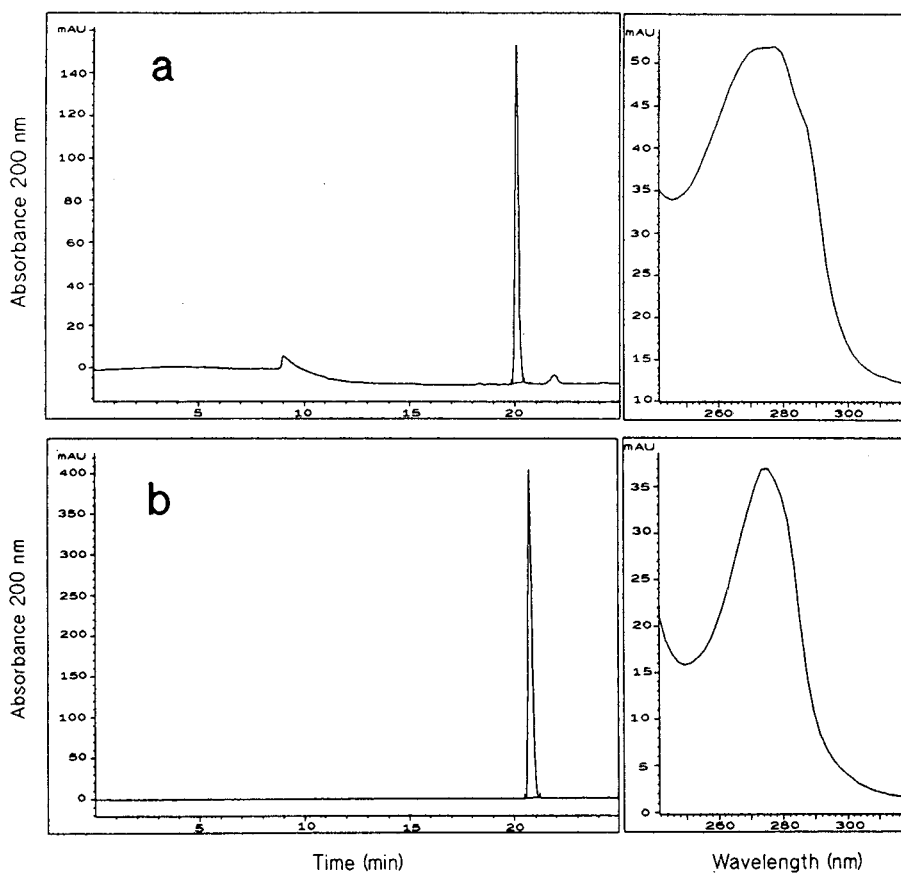


Fig. 1. (a) Electropherogram of tryptophan with recorded zero-order spectrum. (b) Electropherogram of tyrosine with recorded zero-order spectrum.

centration of 4.5 mg/ml was kindly provided by Dr. A.A. Gatenby (DuPont, Wilmington, DE, USA).

2.2. Proteolytic digestion

Carbonic anhydrase and GroEL were incubated with 5% (w/w) trypsin at 37°C for 20 h. An autoprotoleolytic digestion of trypsin was run at 37°C for 20 h.

2.3. CE system and separation

All experiments were carried out on the Hewlett-Packard ^{3D}CE system with built-in diode-array detector. The system was controlled and all data processing and evaluations were performed using an HP ^{3D}CE ChemStation. Peptide separations were performed on 50 μ m and 75 μ m bare-fused-silica capillaries with a 3 \times extended light path for enhanced sensitive detection. Total length of the capillaries was 64.5 cm, effective

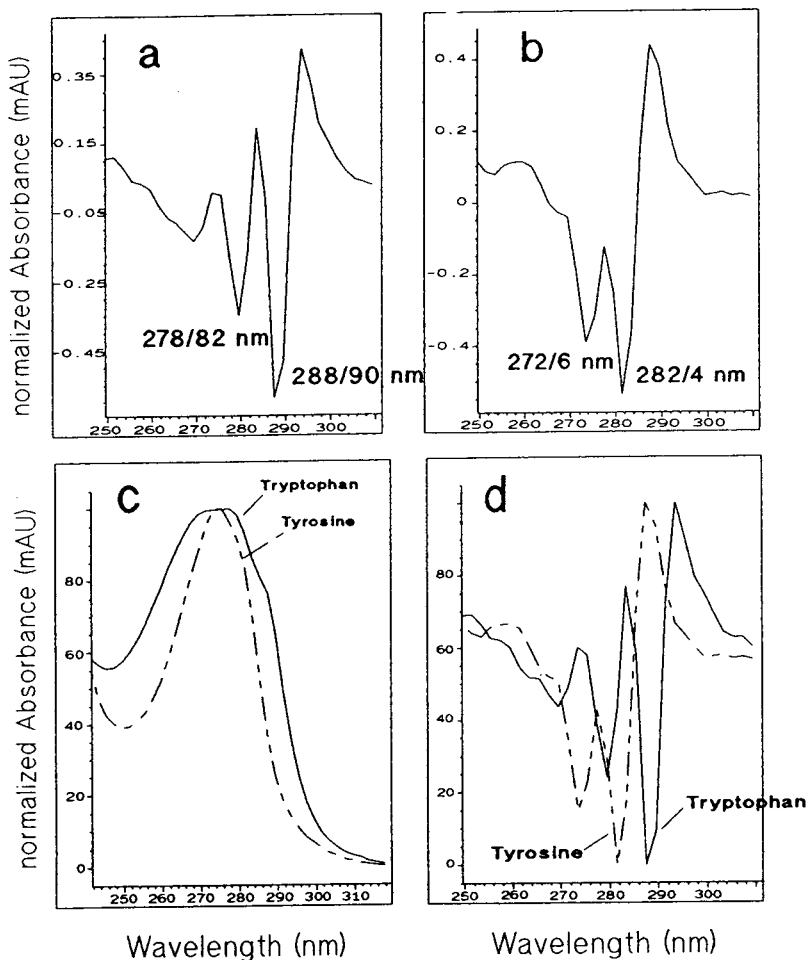


Fig. 2. (a) Second-order derivative spectrum of tryptophan. (b) Second-order derivative spectrum of tyrosine. (c) Overlay of zero-order spectra of tryptophan and tyrosine. (d) Overlay of second-order derivative spectra of tryptophan and tyrosine.

length 56 cm. For the separation of the amino acids and synthetic peptides 20 mM phosphate buffer pH 3.0 was used. Protein digests were separated using 50 mM phosphate buffer pH 2.5. 30 kV was applied to the capillaries resulting in about 25 μ A for the pH 3.0 buffer and about 67 μ A for the pH 2.5 buffer. Separations were run at 25°C. Pressure injection for 200 mbar s was used for sample loading into the capillaries. Other conditions were identical.

2.4. Detection system and second-order derivative spectra

Peptides were monitored with the diode-array detector at both 200 and 280 nm. Simultaneously, all spectra were collected during the runs. Second-order derivative spectra for the range 250–320 nm, which is characteristic for the aromatic amino acid residues tyrosine and tryptophan, were automatically calculated using the standard software of the HP ^{3D}CE ChemStation. A spectra library of the second-derivative spectra of tyrosine and tryptophan was created and automated library search was performed using the same software.

3. Results and discussion

In order to evaluate the potential of this method and to create a library with the second-order derivative spectra of tryptophan and tyrosine both amino acids were electrophoresed and zero-order spectra were recorded using diode-array detection as shown in Fig. 1. Using the standard software of the HP ^{3D}CE ChemStation the algorithm calculating the second-order derivatives was carried out. The resulting second-derivative spectra of tryptophan and tyrosine (Fig. 2a and b) were then used for creating the library for automated search of tryptophan- and tyrosine-containing peptides separated by CE. Whilst the zero-order spectra of tryptophan and tyrosine are overlapping with an absorption maximum of about 278 nm for both amino acids (Fig. 2c), the second-order derivative spectra show significant differences.

Table 1
Synthetic peptides used for method evaluation

Peak 1:	VHLTPVEK
Peak 2:	DRVYIHPF
Peak 3:	SISGLAK
Peak 4:	AGCKNFFWKTFTSC
Peak 5:	ELYENKPRRPWIL
Peak 6:	EGKRPWIL
Peak 7:	WMFDamide
Peak 8:	YGGFL

Tyrosine residues (Y) and tryptophan residues (W) are italicized.

The second-order derivative spectrum of tryptophan shows a main minimum at 290 ± 2 nm and a first side minimum at 280 ± 2 nm while that of tyrosine shows the main minimum at 282 ± 2 nm and the first side minimum at 274 ± 2 nm (Fig. 2d).

For evaluation of the automated second-order derivative spectra library search a mixture of short synthetic peptides of known sequence (Table 1) containing either tryptophan, tyrosine, both of them or none were separated. All peptides were almost baseline separated within

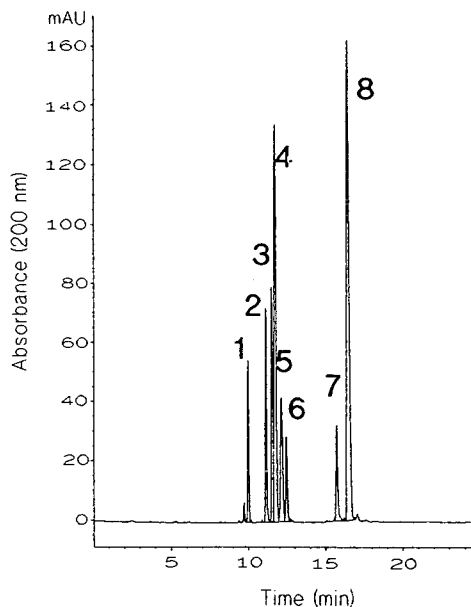


Fig. 3. Electropherogram of 8 synthetic peptides separated by capillary zone electrophoresis (see Table 1 for identification).

17 min (Fig. 3). Peptides containing tryptophan (peaks 4–7) clearly can be identified by their second-order derivative spectrum with the characteristic minimum at 290 ± 2 nm (Fig. 4). The presence of a tyrosine residue besides tryptophan in peptide peak 5 did not affect the identification of tryptophan. Automated library search of those peptides resulted in match factors of about 750–990 for tryptophan and of about 0.02–1.0 for tyrosine. A match factor of 1000 would be the ideal match factor, while matches > 750 indicate undoubtful presence and matches < 100 absence of the search species, respectively.

Similarly, tyrosine-containing peptides can be clearly identified by their characteristic second-order derivative spectral minima around 282 ± 2 nm as shown for peptides in peak 2 and 8 (Fig.

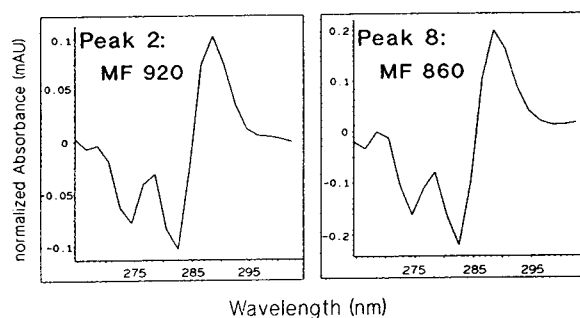


Fig. 5. Second-order derivative spectra of peptides 2 and 8 containing a tyrosine residue.

5). Match factors for tyrosine and tryptophan are in the same range as shown for tryptophan-containing peptides.

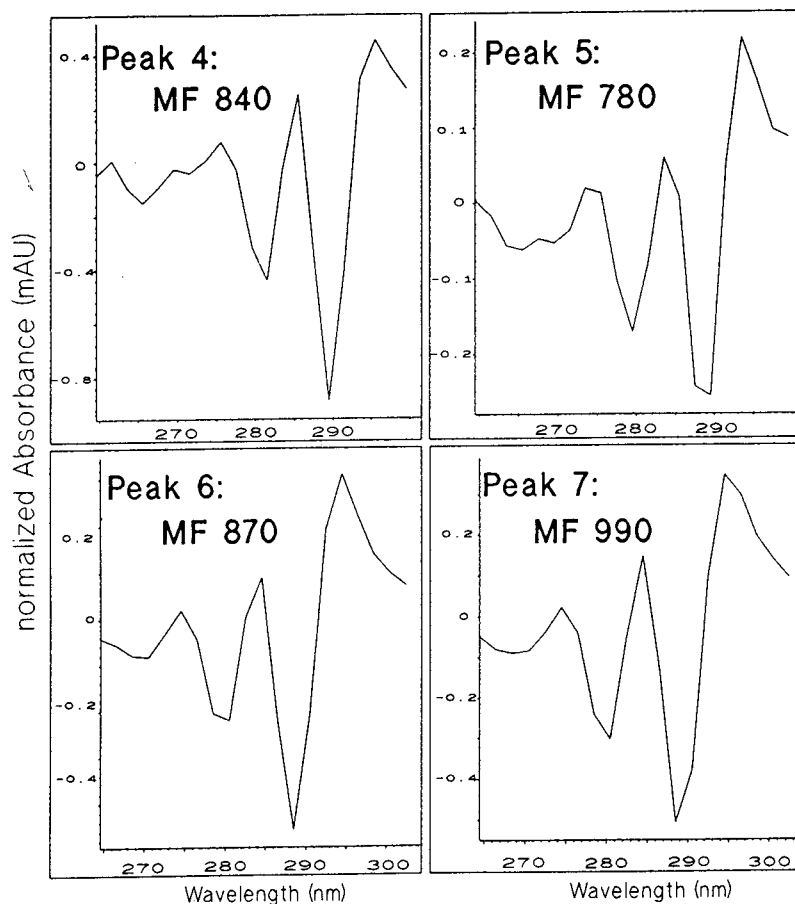


Fig. 4. Second-order derivative spectra of peptides 4–7 containing a tryptophan residue. MF = Match factor.

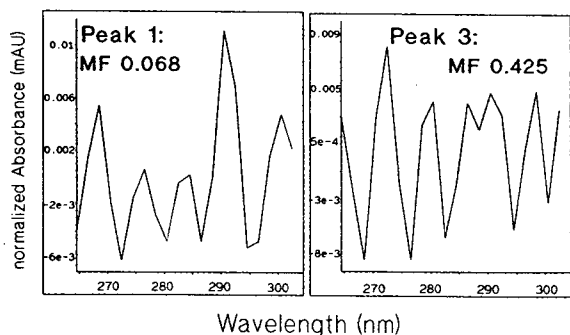


Fig. 6. Second-order derivative spectra of peptides 1 and 3 containing no tyrosine and no tryptophan residue.

As negative control Fig. 6 shows the characteristic second-order derivative spectra of two peptides (peaks 1 and 3) which contain neither tyrosine nor tryptophan residues. No clear minimum can be observed in the wavelength range between 250 and 320 nm and no matches were

found. In this case typically spectra look like "baseline noise".

The peptide containing one tryptophan and one tyrosine residue (peak 5) resulted only in the clear identification of tryptophan with a match factor of 780, but not of tyrosine which resulted only in a match factor of 80 due to the overlap of the major minimum of tyrosine with the side minimum of tryptophan (Fig. 4). This is coincident with the finding of Grego et al. [7] who stated that tyrosine can only be determined in the presence of one tryptophan residue, if three tyrosine residues are present. In this case, the major minimum of tyrosine at around 282 nm will be larger then that of tryptophan at around 290 nm [7].

The method was then applied to tryptic digests of the enzyme carbonic anhydrase, GroEL and the protease itself. Carbonic anhydrase was used due to its high content of tryptophan residues

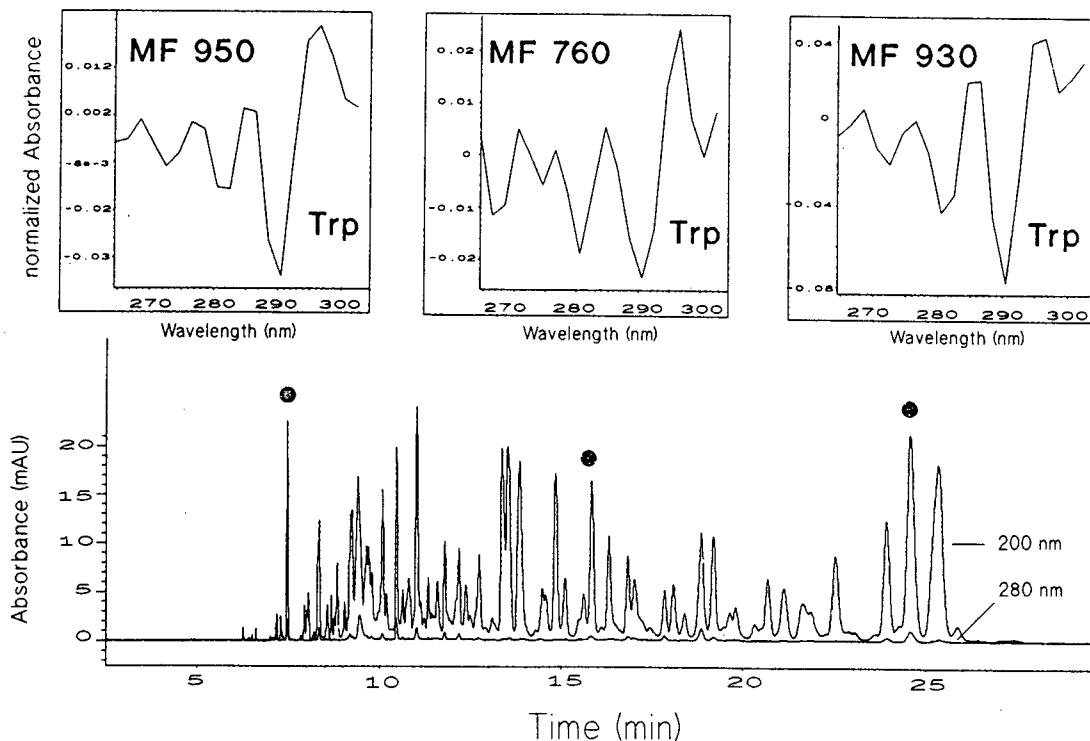


Fig. 7. Electropherogram of the tryptic digest of carbonic anhydrase with three representative second-order derivative spectra of peptides. Electropherogram was recorded at 200 and 280 nm.

while GroEL contains only tyrosine residues and no tryptophan residue. As shown in Figs. 7–9, in the various digests tryptophan- and tyrosine-containing peptides can be easily discriminated and identified by their characteristic second-order derivative spectra. In the electropherograms of Figs. 7 and 9 peptide detection was recorded at 200 nm and in addition at 280 nm to generally identify the aromatic amino acids-containing peptides. In the electropherogram of the tryptic digest of GroEL detection was recorded only at 200 nm. Detection at 280 nm was neglected to show that with diode-array detection and associated software second-order derivative spectra can automatically be calculated and automatic search can be performed allowing unambiguous identification of tyrosine residues in this particular protein digest.

In this paper it was shown that second-order

derivative spectroscopy is a very valuable tool for the unambiguous identification of tryptophan- and tyrosine-containing peptides separated by CE using diode-array detection. In peptides containing both amino acids with the same number only the presence of tryptophan can be clearly identified. The method described will be especially useful for micropreparative isolation of these peptides for further analysis by protein sequencing, similar as previously described for the separations and fraction collection of tryptophan-containing peptides by HPLC [7].

Acknowledgements

We are very grateful to Marzell Herold and Martin Verhoef for critical reading of the manuscript.

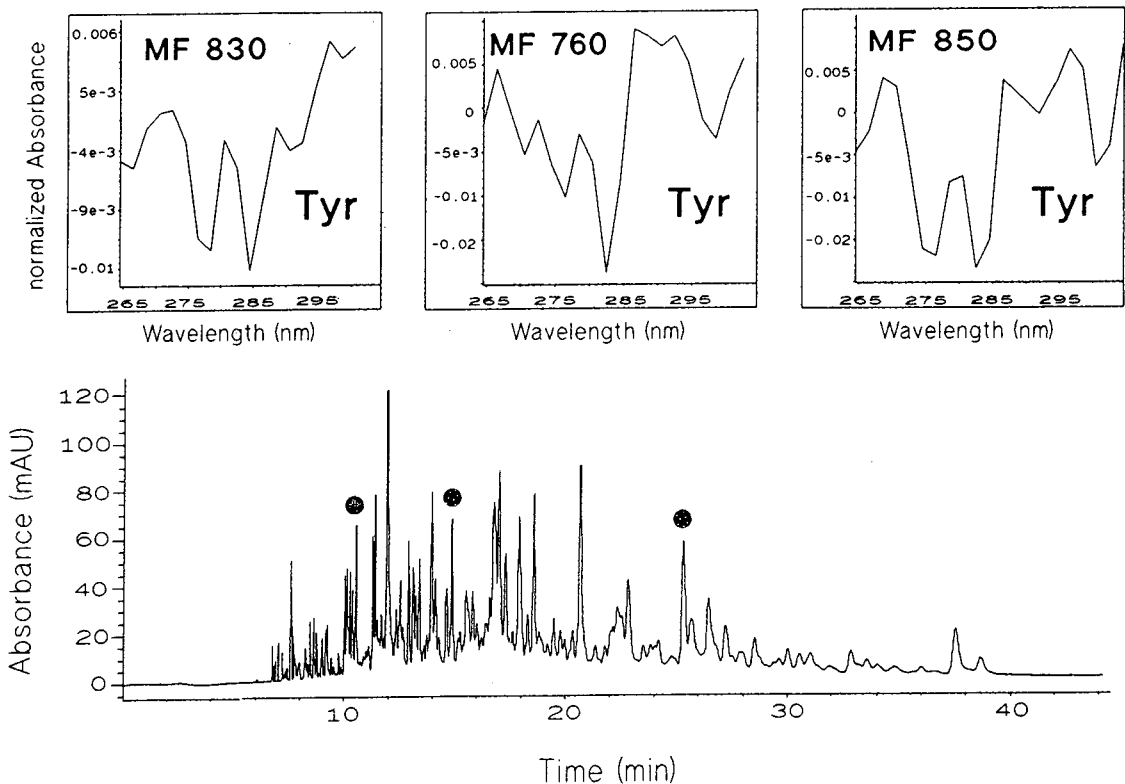


Fig. 8. Electropherogram of the tryptic digest of GroEL with three representative second-order derivative spectra of peptides. Electropherogram was recorded only at 200 nm.

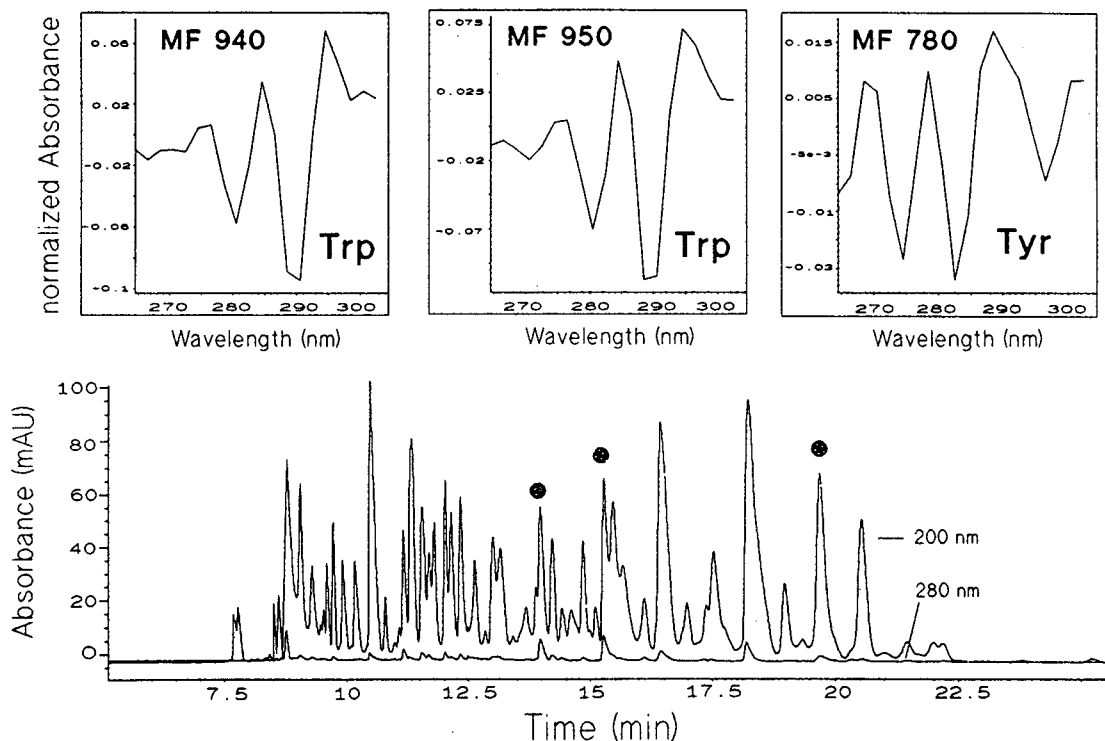


Fig. 9. Electropherogram of the autodigest of trypsin with three representative second-order derivative spectra of peptides. Electropherogram was recorded at 200 and 280 nm.

References

- [1] A.F. Fell, H.P. Scott, R. Gill and A.C. Moffat, *J. Chromatogr.*, 273 (1983) 3–17.
- [2] A.F. Fell, H.P. Scott, R. Gill and A.C. Moffat, *J. Chromatogr.*, 282 (1983) 23–140.
- [3] A.F. Fell, B.J. Clark and H.P. Scott, *J. Chromatogr.*, 297 (1984) 203–214.
- [4] G.H. Beaven, *Adv. Spectros.*, 2 (1961) 331–343.
- [5] D.B. Wetlaufer, *Adv. Protein Chem.*, 17 (1962) 303–390.
- [6] J.W. Donovan, in S.J. Leach (Editor), *Physical Principles and Techniques of Protein Chemistry*, Part A, Academic Press, New York, 1969, p. 101.
- [7] B. Grego, E.C. Nice and R.J. Simpson, *J. Chromatogr.*, 352 (1986) 369–379.
- [8] H. Goetz, *Application Note 12-5954-8920*, Hewlett-Packard, Waldbronn, Germany, 1987.
- [9] T. Bergman, B. Agerberth and H. Jörnvall, *FEBS Lett.*, 283 (1991) 100–103.

Protein microheterogeneity and crystal habits: the case of epidermal growth factor receptor isoforms as isolated in a multicompartment electrolyzer with isoelectric membranes

Wolfgang Weber^{a,*}, Elisabeth Wenisch^{b,c}, Niels Günther^a, Ulf Marnitz^a,
Christian Betzel^d, Pier Giorgio Righetti^b

^a*Institut für Physiologische Chemie, Universitätskrankenhaus Eppendorf, 20246 Hamburg, Germany*

^b*Faculty of Pharmacy and Department of Biomedical Sciences and Technologies, University of Milano, Via Celoria 2, Milan, Italy*

^c*Institute of Applied Microbiology, School of Food and Biotechnology, University of Agriculture and Forestry, Nussdorfer Lände 11, A-1190 Vienna, Austria*

^d*EMBL Outstation, Deutsches Elektronensynchrotron, 22603 Hamburg, Germany*

First received 7 March 1994; revised manuscript received 25 May 1994

Abstract

A purified, soluble form of the epidermal growth factor receptor (sEGFR) was found, by isoelectric focusing in immobilized pH gradients, to consist of three major isoforms (with *pI* values 6.45, 6.71 and 6.96, respectively) and ca. a dozen minor components. This wild-type sEGFR, while producing crystals, has so far defied any attempt at decoding the structure, due to the very poor diffraction pattern. When the wild-type sEGFR was purified in a multicompartment electrolyzer with isoelectric Immobiline membranes, it yielded the three major isoforms as single-*pI* components, collected in three separate chambers of the recycling electrolyzer. The *pI* 6.71 and the *pI* 6.96 isoforms produced large crystals of apparent good quality. However, while the former produced a high-quality diffraction pattern, which may lead to decoding of the three-dimensional structure, the *pI* 6.96 produced crystals which did not diffract at all. It is concluded that, in the case of “tough” proteins (large size, heterogeneous glycosylation, high water content of crystals), purification to single-charge components might be an essential step for growing proper crystals. The unique advantage of purification via isoelectric membranes is that the protein is collected both isoelectric and isoionic, i.e. uncontaminated by soluble buffers (such as the carrier ampholytes used in conventional focusing).

1. Introduction

The epidermal growth factor (EGF) receptor mediates the biological effects of polypeptide mitogens such as EGF and TGF- α , playing an

important role in normal and pathological growth control. The receptor is an M_r 170 000 membrane glycoprotein consisting of three functional domains: an EGF binding cell surface domain which is heavily glycosylated, a short transmembrane region, and a cytoplasmic domain with tyrosine kinase activity (for reviews, see [1] and [2]).

* Corresponding author.

Since overexpression of EGF receptors has been observed in many types of human tumors, structure-based drug design for therapeutic modulation of receptor functions would be of high medical interest. Crystallization of membrane proteins like the EGF receptor, however, is a formidable problem, mainly due to the high extent of glycosylation and to the hydrophobicity of membrane spanning domains. In the case of the EGF receptor one of these problems could be overcome by crystallizing a secreted form of the receptor ("sEGFR") which is produced by a human tumor cell line [3]; it represents the M_r 100 000 external domain of the EGF receptor with functionally intact ligand binding. Crystallization of this hydrophilic receptor ectodomain had been accomplished in the presence of the ligand EGF [4]. Diffraction of these crystals, however, had been only about 10 Å; data collection using these crystals had not been possible so far.

A possible explanation for the poor quality of initial sEGFR crystals may come from the striking charge heterogeneity of the protein: more than 10 components are separated by isoelectric focusing. Since it is known that the presence of several isoforms can induce perturbation of crystal growth, we purified single- pI species of the sEGFR protein by using a multicompartiment electrolyzer with buffering, isoelectric membranes [5,6]. In this system, the protein is always kept in a liquid vein (thus it is not lost by adsorption onto surfaces, as customary in chromatographic procedures) and it is trapped into a chamber delimited by two membranes having pI values encompassing the pI value of the protein being purified. Thus, by a continuous titration process, all other impurities, either non-isoelectric or having different pI values, are forced to leave the chamber, in which the protein of interest will ultimately be present as the sole species, purified from both macromolecular contaminants and buffering and salt ions as well. This technique has been applied to the purification of single EGF receptor isoforms with remarkable results on the quality of the crystals obtained.

2. Experimental

2.1. Materials

Acrylamide, N,N'-methylenebisacrylamide (Bis), N,N,N',N'-tetramethylethylenediamine (TEMED) and ammonium persulphate (APS) were from Bio-Rad, Hercules, CA, USA. The following Immobiline species: pK 3.6, pK 4.6, pK 6.2, pK 7.0 and pK 8.5 were from Pharmacia-LKB Biotechnology, Uppsala, Sweden. N-(2-Hydroxyethyl)piperazine-N'-(2-ethanesulphonic acid) (HEPES) and L-histidine (free base) were from Sigma, St. Louis, MO, USA.

2.2. Biologicals

EGF ligand was prepared from adult mouse submaxillary glands [7]. A monoclonal anti-sEGFR E30 antibody was developed using immunoaffinity purified protein as antigen [8] (this antibody is now commercially available from E. Merck, Darmstadt, Germany). Monoclonal antibody E30 recognizes a non-carbohydrate epitope located between residues 332 and 589 of the EGF receptor in its native as well as in its denatured conformation.

2.3. Preparation of de-sialo sEGFR

Serum-free medium (Dulbecco's modified Eagle's medium + Ham's F12 medium, mixed 1:1) was conditioned by confluent cultures of a special A431 variant cell line selected for maximal biosynthesis of EGF receptor; supernatants were freed from cellular debris, stabilized with 1 mM EDTA, 100 U/ml Trasylol (Bayer) and concentrated by ultrafiltration prior to immunoaffinity chromatography [9]. sEGFR was eluted from the immuno adsorbent with 0.1 M acetic acid, 0.05 M sodium chloride and immediately neutralized with trisodium phosphate. Purified sEGFR (30 mg, 8 ml) was then dialyzed against 50 mM sodium acetate pH 5.5, in presence of 4 mM calcium chloride, and digested for 3 days at room temperature with 1 unit of neuraminidase (1 mg/ml, from *Vibrio cholerae*; Boehringer

Mannheim) immobilized on 0.3 ml of tresyl chloride-activated agarose (Pharmacia). Dialysis against 10 mM Tris acetate buffer, pH 7.4, added with 15% glycerol represented the final step prior to the immobilized pH gradient (IPG) separation.

2.4. Preparation of analytical IPG gels

These gels were of 25 × 10 cm size and 0.5 mm thick. An IPG pH 5.0–8.0 was set in a 5% T, 4% C polyacrylamide matrix¹ (the recipe can be found in Ref. 10). Note that, after preparing the two limiting, acidic and basic mixtures, they are titrated (with a weak acid and a weak base) to pH values close to neutrality. This is important in order to ensure uniform polymerization and efficient monomer conversion throughout the preformed pH gradient. Upon gel washing (4 × 30 min) in distilled water, all added titrants (as well as catalysts and ungrafted monomers) are efficiently removed. The gels are then equilibrated for 30 min in 2% glycerol solution, dried in air and reswollen in 15% (v/v) glycerol solutions. The protein samples (ca. 50 μg in 20 μl) are usually applied in surface wells both close to the anode and to the cathode. Focusing is continued (at 5000 V after an initial 1 h period at 500 V) for 6 h at 10°C. Staining is carried out in Coomassie Brilliant Blue R-250 in presence of Cu²⁺ according to Righetti and Drysdale [11].

2.5. Preparation of isoelectric immobiline membranes

After determining, in the above analytical pH 5.0–8.0 gels, the precise *pI* values of the sEGFR isoforms, seven isoelectric membranes are made having the following *pI* values: 5.90, 6.34, 6.63, 6.76, 6.92, 7.05 and 7.35. The first and last membranes, being adjacent to the anolyte and catholyte compartments, respectively, are made in a 10% T, 5% C matrix, whereas the other five are polymerized in a 5% T, 4% C polyacrylamide. The membranes have a diameter of

4.7 cm and a thickness* of ca. 1 mm. Note that the membranes are supported by glass fibre filters (see Ref. [5] for a detailed description of their properties). After washing and equilibrating the membranes in 15% (v/v) glycerol, the multicompartament apparatus is assembled and the entire protein amount (40 mg) equally distributed into the two sample chambers closer to the anodic reservoir. In order to avoid sample dilution, no reservoirs have been connected to the six recycling chambers, so that the total sample volume has been limited to 39 ml total (6.5 ml per chamber). After an initial, low-voltage run (500 V) for eliminating excess salt in the sample, purification has been achieved at 2500 V (over a 12 cm electrode distance) in less than 10 h. The anolyte was 52 mM HEPES (pH 5.27, conductivity: 9.1 μS) and the catholyte 14 mM L-histidine (pH 7.56; conductivity 11.5 μS). The supporting solution in all chambers was 15% (v/v) glycerol. No circulating coolant was utilized and joule heat was dissipated in air in a cold room (5°C). Under the above conditions, the temperature rise in the liquid in the electrolyzer, at steady state, was only 3°C.

2.6. Crystallization and X-ray investigation

Crystals were grown at a controlled temperature of 20°C by the hanging as well as sitting drop vapour diffusion technique [12]; droplets of 20 μl sEGFR (15 mg/ml) complexed with equimolar amounts of EGF were mixed with 7 μl precipitant (1.95 M ammonium sulphate or sodium phosphate, pH 7.5) and exposed to 5 ml reservoir solutions (same as precipitant); crystals grew within variable time spans (>1 week). Crystals were analyzed on the X11 synchrotron beam-line in the EMBL Outstation at DESY (Deutsches Elektronen-Synchrotron, Hamburg, Germany). The storage ring was operated in main user mode with 4.465 GeV and 20–45 mA. Rotation images were recorded on a MAR 300 mm image plate scanner at room temperature. Exposure times were set to about 6 min for 1° rotation images using a wavelength of 0.92 and a crystal-to-plate distance of 500 mm. Images were

¹ T = (g acrylamide + g Bis)/100 ml solution; C = g Bis/%T.

processed with a version of the XDS integration package [13]. Some crystals were analyzed using a GX21 rotating anode generator (Nonius, Delft, Netherlands) operating at 40 kV and 75 mA (we acknowledge the assistance of Drs. R. Hilgenfeld and H. Bertchold for these experiments).

3. Results

Affinity-purified EGF receptor ectodomain (sEGFR) exhibits one single band in electrophoresis on sodium dodecyl sulphate gels; however, > 25 bands can be separated by isoelectric focusing (not shown). Since the charge heterogeneity is mainly caused by variable presence of terminal sialic acid residues on numerous oligosaccharide side chains (11 N-glycosylation sites), the receptor protein was extensively digested with neuraminidase. Desialylation resulted in an increment of *pI* values by ca. 0.5 pH units and a reduction of microheterogeneity, but not on its elimination. Fig. 1 shows the results of an analytical Immobiline gel (pH 5–8) of de-sialo sEGFR: three major isoforms are well separated (with *pI* values of 6.45, 6.71 and 6.96) together with about a dozen minor components. In order to ascertain the origin of these bands, they were blotted and stained with monoclonal anti-sEGFR antibodies (alkaline phosphatase detection). It is seen that all the different bands are isoforms of the sEGFR.

Fig. 2 shows the results of a preparative run in the multicompartiment electrolyzer (mounted with six sample chambers plus the two electrodic reservoirs) for the purification of sEGFR. It is seen that the unfractionated sample is composed of three major isoforms and a number (> 6) of minor components. Upon purification, we could collect, as single bands, six isoforms, with the three major components collecting in chambers 2, 3 and 5 (*pI* values 6.45, 6.71 and 6.96, respectively).

As the *pI* 6.71 and 6.96 isoforms represented the most abundant components, and were in a state of high purity, attempts were made at crystallizing them. Fig. 3A shows a crystal of the *pI* 6.71 isoform. This crystal could be grown to

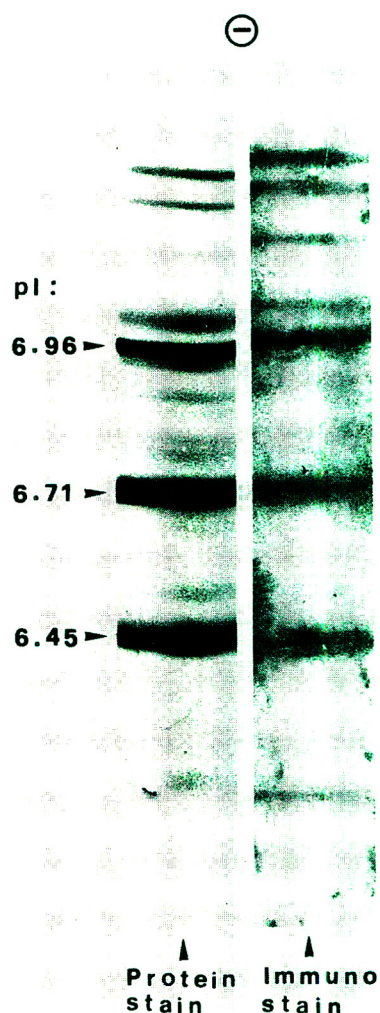


Fig. 1. Analytical isoelectric focusing gel of affinity-purified sEGFR. The gel contained an immobilized pH gradient (IPG, pH 5–8) grafted on a 5% T, 4% C matrix. The protein samples (ca. 50 μg in 20 μl) were applied in surface wells at the cathode. Focusing was at 10°C for 6 h at 5000 V. Staining with Coomassie Brilliant Blue in presence of Cu^{2+} (left gel strip). The right strip is a blot on cellulose nitrate followed by immuno fixation with monoclonal anti-sEGFR antibodies and alkaline phosphatase detection.

the remarkable size of $1.3 \times 0.5 \times 0.3 \text{ mm}^3$. The *pI* 6.71 isoform exhibited the best diffraction ever achieved with this protein (see Fig. 3B). It allowed data collection up to 6 Å for the first 10 images; then diffraction patterns decreased to 10 Å during the following 10 exposures because of increasing radiation damage. A number of 2942

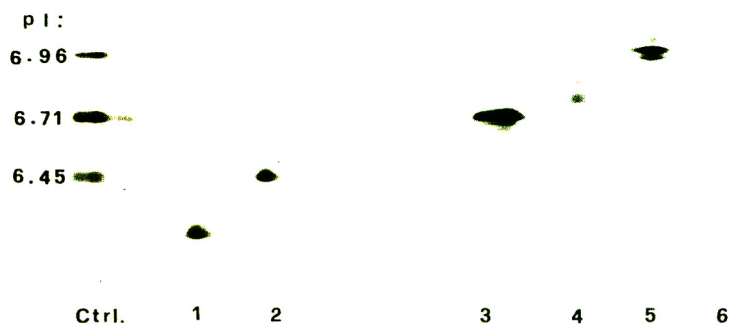


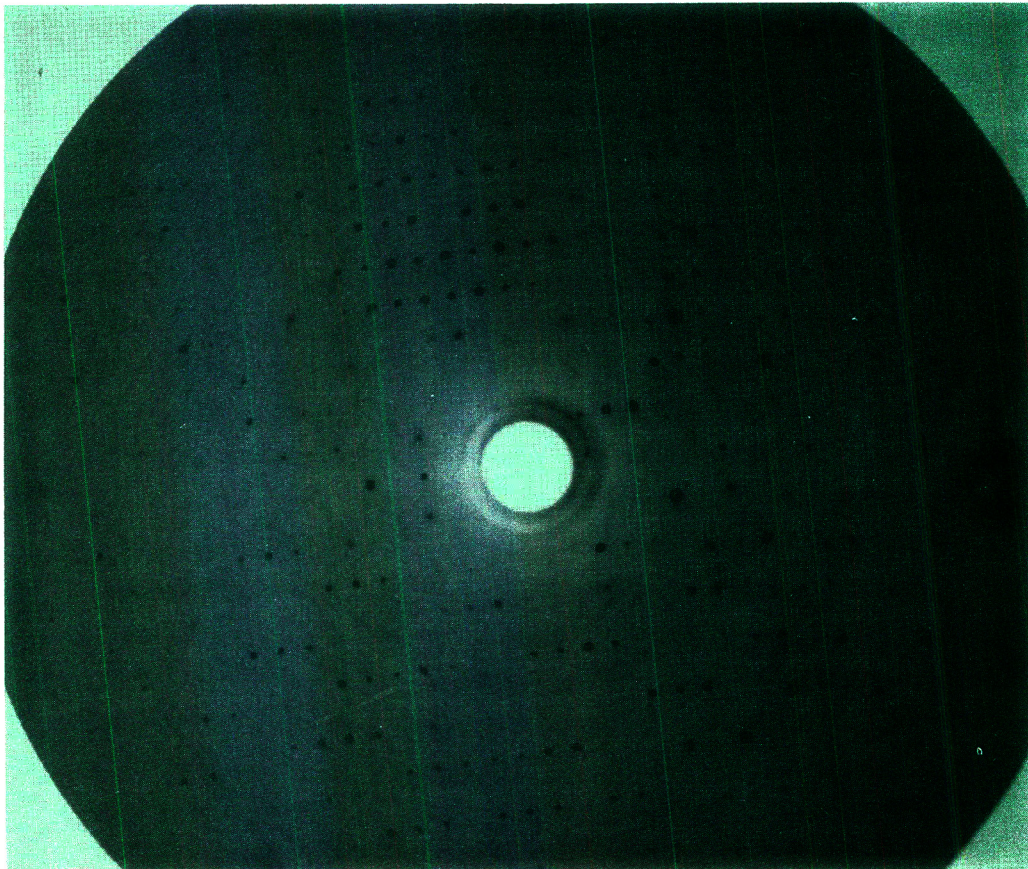
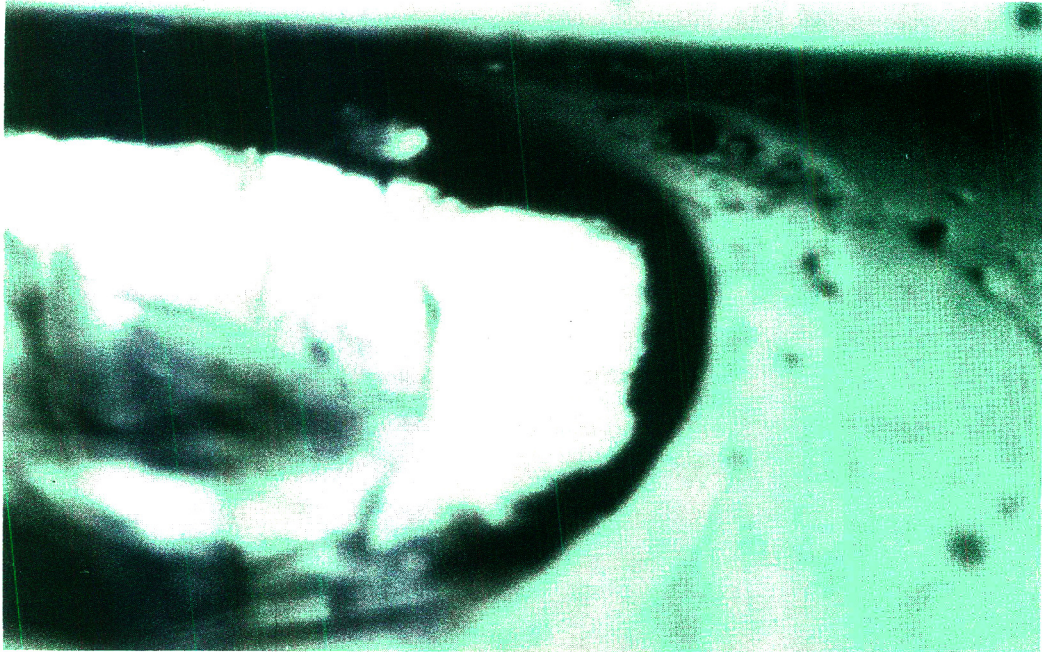
Fig. 2. Analytical IPG run (pH 5–8) of the content of the multicompart ment electrolyzer. Lanes 1–6: content of each of the six chambers of the electrolyzer assembled with seven isoelectric membranes with *pI* values as given in the Experimental section. All other conditions as in Fig. 1. Ctrl. = control, unfractionated sEGFR. The *pI* values of the three major isoforms are given on the left side. Note the high purity of each isoform.

reflections was merged to yield a reliability factor (*R*, symm) of 5.4%. The reduced data set showed a completeness of 26%. The space group was assigned to be orthorhombic $P2_122$ or $P2_12_12$ with pseudo-tetragonal unit cell parameters of $a = 116.3 \text{ \AA}$, $b = 119.5 \text{ \AA}$ and $c = 204.5 \text{ \AA}$. These values yield a unit cell volume of $2.8 \cdot 10^6 \text{ \AA}^3$ and a packing parameter V_M of $3.58 \text{ \AA}^3/\text{u}$ assuming two molecules each of receptor and ligand in the asymmetric unit. The fractional volume occupied by solvent was calculated to be 65% which is higher than found in most other proteins (40–60%) but observed also for virus crystals. This fact indicates a loose arrangement of the molecules in the crystal lattice and may explain the fast radiation decay. Additional crystals of the *pI* 6.71 isoform could be grown from a different sEGFR protein batch. These crystals of 1.2 mm diameter were used to test whether the crystal quality would allow data collection with a conventional X-ray source (as opposed to synchrotron radiation). Even under these far-from-optimal conditions, using a rotating anode generator, data collection was possible to about 7 \AA , thus helping in refining the cell dimensions. Interestingly, several crystals could be grown also from the *pI* 6.96-sEGFR isoform (Fig. 4) and were analyzed by synchrotron radiation; although these crystals had a comparably well-shaped morphology and remarkable size, they did not diffract at all (in Fig. 4 the diffraction pattern is substituted by a question mark).

4. Discussion

4.1. Protein isoforms and crystal habits

Our data clearly prove that the crystal quality of protein isoforms may differ significantly. In our particular case, we could grow crystals from both isoforms, highly purified in the multicompart ment apparatus. However, while the crystals produced by the *pI* 6.71 isoform gave a good diffraction pattern, the crystals of the *pI* 6.96 band did not diffract at all. This might explain the failure at decoding the structure of such crystals so far, since they were up to the present time grown from the entire spectrum of different isoelectric forms. The *pI* 6.71 crystal allowed, for the first time, collection of a partial diffraction data set. The present crystal quality, therefore, is sufficient, in combination with cryotechniques, to search heavy atom derivatives (it should be noted that at the same time a sEGFR crystal of comparable quality was grown also from the wild-type protein during a space shuttle flight; apparently the microgravity conditions could compensate for the negative influence of charge heterogeneity of the protein which—in this study—is eliminated by preparative isoelectric focusing). Purified receptor isoforms tend to form crystals with sharper edges (as opposed to the more roundish forms of the wild-type protein, i.e. the protein still containing all the different isoforms). But—most important—they



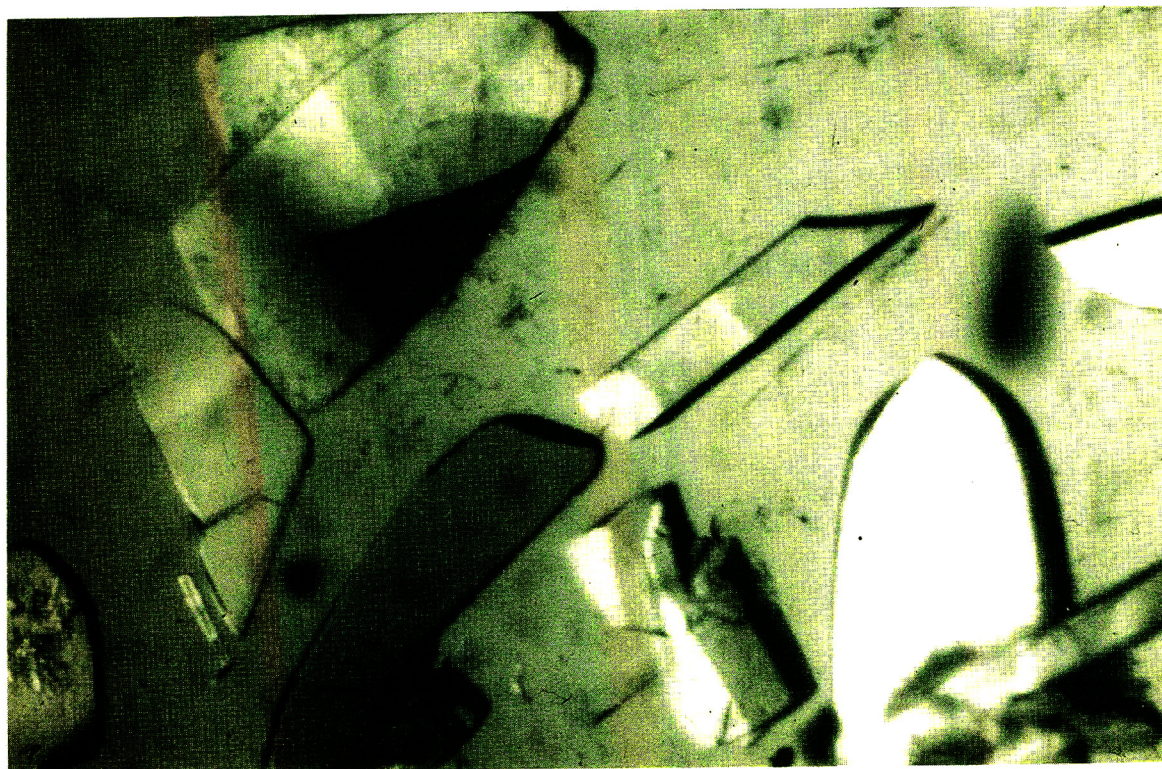


Fig. 4. Picture of some crystals of the *pI* 6.96 isoform as recovered from chamber 5 of the multicompartiment electrolyzer. Also this isoform gave large-size crystals, but no one of them produced a diffraction pattern (as indicated by the question mark in the lower part of the figure). Scale: 1.2 cm corresponds to 0.1 mm.

tend to grow to a larger size. The *pI* 6.71 crystal had the surprising size of $1.3 \times 0.5 \times 0.3 \text{ mm}^3$, which had never been obtained before. For the crystallography of such “tough” glycoproteins like EGFR with their high solvent content and

loose crystal lattice the crystal volume can be regarded as the limiting parameter. Therefore, since the higher homogeneity achieved by isoform separation seems to favour growth to a large crystal volume, the isoelectric focusing in

Fig. 3. (Top) Picture of the crystal of the *pI* 6.71 isoform as recovered from chamber 3 of the multicompartiment electrolyzer. The crystal has a size of $1.3 \times 0.5 \times 0.3 \text{ mm}^3$ and is shown mounted in the glass capillary of the synchrotron beam line. (Bottom) Picture of the diffraction pattern, showing the high quality of the diffracting crystal. Scale: 1.7 cm corresponds to 0.1 mm.

the multicompartiment electrolyzer reveals to represent an ideal or even an essential step in crystallographic projects.

4.2. Chromatography vs. electrophoresis

The fact that chromatography so far has had the lion share in down-stream protein processing is well-documented in the literature [14,15]. Boschetti [16] has recently reviewed advanced sorbents for protein separation, while Narayanan [17] has covered preparative affinity chromatography of proteins. Yet, there are hints that we are witnessing a revival of electrophoretic techniques as well. With our multicompartiment electrolyzer, based on the Immobiline technology, we have now purified a number of r-DNA proteins, including superoxide dismutase [18], human growth hormone [19], monoclonal antibodies against the gp41 of AIDS virus [6], eglin C [20], glucoamylase [21] and sEGFR [22]. This technique is in general very mild to proteins and allows full recovery of enzyme activities coupled to high yields (typically >80%). The other unique advantage of our recycling technique is that the protein is recovered both isoelectric and isoionic, i.e. uncontaminated by any kind of soluble buffer or counterion. Conversely, in conventional isoelectric focusing in soluble, amphoteric buffers, the protein is always contaminated by the amphoteric ions cofocusing in the same (and neighbouring) region. It has been reported quite often that these amphoteric buffers, at the isoelectric state, have a tendency to adhere to the protein surface, thus paradoxically, hampering crystallization even of species purified to single-pI isoforms. With the Immobiline technology this situation can never occur, since the isoelectric membranes are thoroughly washed free of any leachable contaminant. Other electrophoretic techniques are emerging as well. Thus, Bier's group is now offering simple buffers for their recycling isoelectric focusing unit, instead of the ill-defined carrier ampholyte mixture [23,24]. Also preparative isotachopheresis in agarose gels [25], in sucrose density gradients [26] and in the recycling free-flow mode [27] is

being evaluated and discussed with increasing frequency [28]. Additionally, a new wave of interest is rising on protein purification by continuous-flow electrophoresis (CFE; the "Han-nig" technique) [29]. CFE has never become quite popular, due to a number of problems connected with sample stream deformation (sedimentation, thermal convection, electroosmosis and, most deleterious of them all, electrohydrodynamic distortion) [30]. There are now hints that the latter problem could be cured by superimposing onto the a.c. field responsible for the separation a d.c. field transverse to it and to the flow direction, with an appropriate frequency, and an effective strength equal to that of the d.c. field [31]. As operative problems in preparative electrophoresis are solved with increasing frequency, it will be of interest to see how these different modes of protein purification will develop and grow in the years ahead.

Acknowledgements

Supported in part by the Deutsche Forschungsgemeinschaft, Sonderforschungsbereich 232 to W.W. and by a grant from Agenzia Spaziale Italiana (Rome, Italy) and from the Radius in Biotechnology (ESA, Paris, France) to P.G.R. E.W. is the winner of the first Luigi Napolitano Fellowship from ESA (Paris, France).

References

- [1] G. Carpenter, *Annu. Rev. Biochem.*, 56 (1987) 881–914.
- [2] Y. Yarden and A. Ullrich, *Annu. Rev. Biochem.*, 57 (1988) 443–478.
- [3] W. Weber, G.N. Gill and J. Spiess, *Science*, 224 (1984) 294–297.
- [4] N. Guenther, C. Betzel and W. Weber, *J. Biol. Chem.*, 265 (1990) 22082–5.
- [5] P.G. Righetti, E. Wenisch and M. Faupel, *J. Chromatogr.*, 475 (1989) 293–309.
- [6] P.G. Righetti, E. Wenisch, A. Jungbauer, H. Katinger and M. Faupel, *J. Chromatogr.*, 500 (1990) 681–696.
- [7] C.R. Savage, Jr. and S. Cohen, *J. Biol. Chem.*, 247 (1976) 7609–7611.

- [8] W. Weber and P. Nobis, unpublished results.
- [9] G.N. Gill and W. Weber, *Methods Enzymol.*, 146 (1987) 82–88.
- [10] P.G. Righetti, *Immobilized pH Gradients: Theory and Methodology*. Elsevier, Amsterdam, 1990.
- [11] P.G. Righetti and J.W. Drysdale, *J. Chromatogr.*, 98 (1974) 271–321.
- [12] A. Hampel, M. Labananskas, P.G. Connors, L. Kirkegard, U.L. Raj Bandari, P.B. Sigler and R.M. Bock, *Science*, 162 (1968) 1384–1387.
- [13] W. Kapsch, *J. Appl. Cryst.*, 21 (1988) 916–924.
- [14] V.B. Lawlis and H. Heinsohn, *LC·GC Int.*, 6 (1993) 684–688.
- [15] R.E. Majors, *LC·GC Int.*, 6 (1993) 276–288.
- [16] E. Boschetti, *J. Chromatogr. A*, 658 (1994) 207–236.
- [17] S.N. Narayanan, *J. Chromatogr. A*, 658 (1994) 237–258.
- [18] E. Wenisch, K. Vorauer, A. Jungbauer, H. Katinger and P.G. Righetti, *Electrophoresis*, 15 (1994) 647–653.
- [19] C. Etori, P.G. Righetti, C. Chiesa, F. Frigerio, G. Galli and G. Grandi, *J. Biotechnol.*, 25 (1992) 307–318.
- [20] P.G. Righetti, E. Wenisch and M. Faupel, *Adv. Electr.*, 5 (1992) 159–200.
- [21] E. Wenisch, P. Schneider, S.A. Hansen, R. Rezzonico and P.G. Righetti, *J. Biochem. Biophys. Methods*, 27 (1993) 199–213.
- [22] E. Wenisch, P.G. Righetti and W. Weber, *Electrophoresis*, 13 (1992) 668–673.
- [23] M. Bier and T. Long, *J. Chromatogr.*, 604 (1992) 73–83.
- [24] M. Bier, J. Ostrem and R.B. Marquez, *Electrophoresis*, 14 (1993) 1011–1018.
- [25] F. Acevedo, *J. Chromatogr.*, 470 (1989) 407–414.
- [26] F. Acevedo, *Electrophoresis*, 14 (1993) 1019–1022.
- [27] M. Bier, G.E. Twitty and J.E. Sloan, *J. Chromatogr.*, 470 (1989) 369–376.
- [28] T. Hirokawa and Y. Kiso, *J. Chromatogr. A*, 658 (1994) 343–354.
- [29] K. Hannig, *Electrophoresis*, 3 (1982) 235–243.
- [30] M.J. Clifton, *Electrophoresis*, 14 (1993) 1284–1291.
- [31] C. Heller, L. Limat, P. Sergot and J.L. Viovy, *Electrophoresis*, 14 (1993) 1278–1283.

Short communication
**Antibody against branched epitope as an affinity ligand to
separate the parent protein**

Z.J. Yao^{a,*}, M.C.C. Kao^a, K.C. Loh^a, M.C.M. Chung^{a,b}

^a*Bioprocessing Technology Unit, National University of Singapore, 10 Kent Ridge Crescent, Singapore 0511, Singapore*

^b*Department of Biochemistry, National University of Singapore, 10 Kent Ridge Crescent, Singapore 0511, Singapore*

First received 30 March 1994; revised manuscript received 9 June 1994

Abstract

A peptide that contained one of the continuous epitopes of recombinant human lymphotoxin (rhLT) (amino acid residues 139–154) has been located by epitope mapping. The branched form of this peptide was synthesized by the multiple antigen peptide procedure with an octameric branched resin and was subsequently used to elicit anti-epitope antibody in rabbits. The resulting anti-epitope was then used as an immunoaffinity ligand in affinity chromatography to purify the parent protein, rhLT, from the host cell lysate directly.

It is suggested that this approach would be a general way to create novel biospecific ligands for affinity separations.

1. Introduction

Immunopurification is one of most selective and powerful methods of protein purification [1]. Antibodies, for example, can readily distinguish between very similar antigens and therefore can overcome many of the separation problems that no other method can resolve. Both polyclonal and monoclonal antibodies can be used as the affinity ligand for this method of purification, but both have their unique advantages and limitations.

Polyclonal antibodies can be conveniently produced by injecting a purified antigen into a suitable animal and then harvesting the antibodies after 1–2 months time. However, since the resolution of separation is based on the

specificity of an antibody, which in turn is mainly dependent on the purity of an antigen, an elaborate and often time-consuming purification protocol for the antigen usually has to be developed in advance. On the other hand, monoclonal antibodies are more specific in their interaction as they can recognize the epitope of a protein, but elicitation of monoclonal antibodies needs additional expertise and facilities for cell fusion. Therefore, it is thought that when the epitope(s) of an antigen is/are known (e.g., through epitope mapping), anti-epitope antibodies would be useful alternative affinity ligands for separation.

Several continuous epitopes of recombinant human lymphotoxin (rhLT or TNF- β) have been located and their topographies studied in our laboratory [2]. In this communication we wish to report on a branched epitope-carrying peptide that has been used as immunogen to elicit anti-

* Corresponding author.

epitope antibody; the resulting antibody subsequently worked as an affinity ligand of chromatography to purify the parent protein (rhLT) efficiently. Because a branched peptide can be chemically synthesized with an automatic peptide synthesizer and its immunogenic property was reported to be stronger than the linear peptide, the branched peptide might be a common way to produce anti-epitope antibodies that exhibit similar specificity as a monoclonal antibodies, but which can be produced as conveniently as for a polyclonal antibody.

2. Materials and methods

2.1. Materials

Escherichia coli cell lysate containing rhLT was obtained from recombinant HB101 host cells [3]. Purified rhLT, which was used as a standard in sodium dodecyl sulfate–polyacrylamide gel electrophoresis (SDS-PAGE), Western blotting and for coating enzyme-linked immunosorbent assay (ELISA) plates, was purified from this cell lysate [4].

Freund's adjuvants and keyhole limpet hemocyanin were purchased from Sigma. Glutaraldehyde was obtained from Fluka. CNBr-activated Sepharose and SDS-PAGE molecular markers were from Pharmacia. Nitrocellulose membrane was purchased from Schleicher & Schuell while ELISA plates were from Nunc. Other chemicals and reagents not specifically mentioned were obtained from standard commercial sources.

2.2. Methods

Peptide synthesis

Peptides were synthesized with an ABI 431A peptide synthesizer using 9-fluorenylmethoxycarbonyl (Fmoc) chemistry. A Fmoc 8-branched multiple antigen peptide (MAP) [5] resin was used to synthesize the peptide based on the recommended procedure of the manufacturer [6]. Amino acids and other synthesis chemicals

were purchased from Applied Biosystems (Foster City, USA).

Conjugation of peptide

The epitope-carrying peptide was coupled to hemocyanin using a two-step glutaraldehyde method [7].

Immunization

Emulsion solutions were prepared by mixing equal volumes of complete Freund's adjuvant with either branched peptide, peptide conjugated to hemocyanin or pure peptide separately. Two to three rabbits were used for immunization in each group. Complete Freund's adjuvant was used in the first injection, whereas incomplete adjuvant was used in subsequent booster injections. Rabbits were injected subcutaneously (at multiple points in the back region) at a dose of 0.5 mg peptide per animal. Booster injections were carried out at 2, 4 and 6 weeks after the first injection.

A polyclonal anti-rhLT antibody was similarly elicited by using purified rhLT as the immunogen.

ELISA

An indirect antibody ELISA method was used to measure the specificity of antibodies to rhLT. ELISA plates (96 wells) were first coated with purified rhLT (in 0.05 M carbonate–hydrogen-carbonate buffer, pH 9.5) at 1 μ g/well, followed by blocking with 1% (w/v) albumin. Antibodies diluted in 5% (w/v) skimmed milk solution were added to the wells and incubated overnight at 4°C, washing four times with washing buffer (0.05% Tween 20 in phosphate buffered saline, pH 7.4), then reacted with anti-rabbit immunoglobulin–horseradish peroxidase conjugate for 1 h at 37°C. Finally, after washing phenylenediamine dihydrochloride (OPD) was added as substrate and the absorbance was measured at 492 nm.

Affinity chromatography

Sera were bled on the 68th day from rabbits immunized by the branched peptide. The immunoglobulin was purified from pooled sera by

DEAE-cellulose ion-exchange chromatography [8]. Affinity separation was performed on a column prepared by coupling the purified immunoglobulin to CNBr-activated Sepharose (8×1 cm). The column was pre-equilibrated with 10 mM Tris buffer, pH 7.5. After removing the unbound fraction, the bound fraction was eluted with 100 mM triethylamine, pH 11.5. These collected fractions were neutralized with 0.5 M HCl immediately.

Protein estimation

Protein estimation was performed according to the method of Bradford [9] using the reagents purchased from Bio-Rad Labs.

SDS-PAGE and Western blotting

SDS-PAGE was carried out based on Laemmli's procedure [10] and the separated proteins were visualized by Coomassie Brilliant Blue or silver staining. Western blotting was performed at room temperature and 30 V overnight using a mini-transblot cell (Bio-Rad Labs.). The blotting membrane was blocked with 5% (w/v) skimmed milk powder before being incubated with anti-rhLT antibody overnight at 4°C. This was followed by incubation with anti-rabbit antibody-

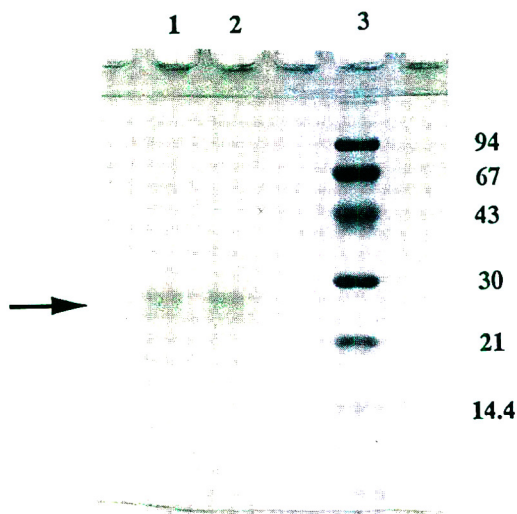


Fig. 1. The apparent molecular mass of branched epitope on SDS-PAGE. Lanes: 1, 2 = branched epitope; 3 = molecular mass markers (M_r indicated in kilodalton).

horseradish peroxidase conjugate (Silenus Labs.) for 1 h at room temperature. The membrane was finally developed with 4-chloro-1-naphthol.

3. Results and discussion

3.1. Multiple antigen peptide of human lymphotoxin epitope

Peptide mapping studies of rhLT showed that the peptide with the sequence FQLTQGDQLSTHTDGI (residues 139–154, molecular mass 1761) displayed the strongest antigenicity when cross-reacted with anti-hLT antibodies among the rhLT fragments investigated. This peptide was subsequently shown to contain an epitope, FQLTQGDQL, residues 139–147 of this cytokine [2]. This 16 amino acid residue peptide FQLTQGDQLSTHTDGI was synthesized as an 8-branched MAP to elicit anti-peptide antibodies. The branched peptide displayed a single broad peak on reversed-phase HPLC and gave the expected amino acid composition (data not shown). SDS-PAGE analysis showed that it had a higher apparent molecular mass of approximately 26 000 (Fig. 1) as compared to the expected value of 14 100

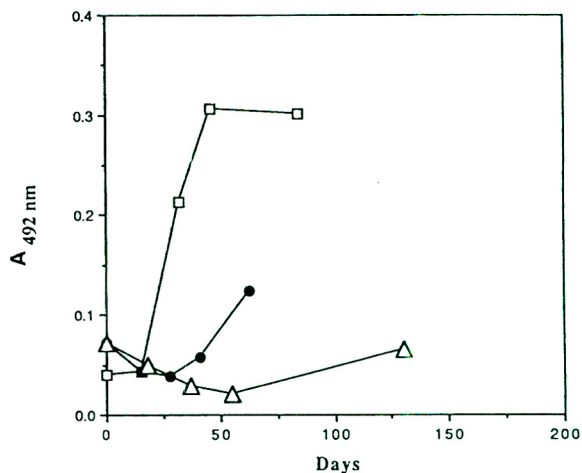


Fig. 2. Specific binding of antibodies to parent protein, rhLT. □ = antibody vs. branched epitope; ● = antibody vs. conjugate of epitope-hemocyanin; △ = antibody vs. the linear peptide-carrying peptide.

(FQLTQGDQLSTHTDGI $\times 8 = 1761 \times 8$). This could be due to the extensive branching of the MAP which may have in some way retarded the mobility of the peptide and/or reduced the expected stoichiometric binding of SDS (1.4 g SDS/g protein) to the peptide.

3.2. Anti-peptide titre and specificity of rabbit antibody

For comparison, the immunogenicity of the branched peptide was compared with that of two other immunogenic methods: peptide coupled to

hemocyanin and the linear peptide itself being used as the immunogens. The results showed that significant antibody titres were obtained in the branched peptide and peptide–hemocyanin groups after 6–8 weeks, whereas there was little response being observed in the linear peptide group after the same period of time.

ELISA was carried out to evaluate the specific binding of the antibodies to rhLT. Although both antibodies from the branched peptide and the peptide–hemocyanin conjugate displayed specific binding to rhLT, the antibody from the branched one exhibited a stronger response (Fig.

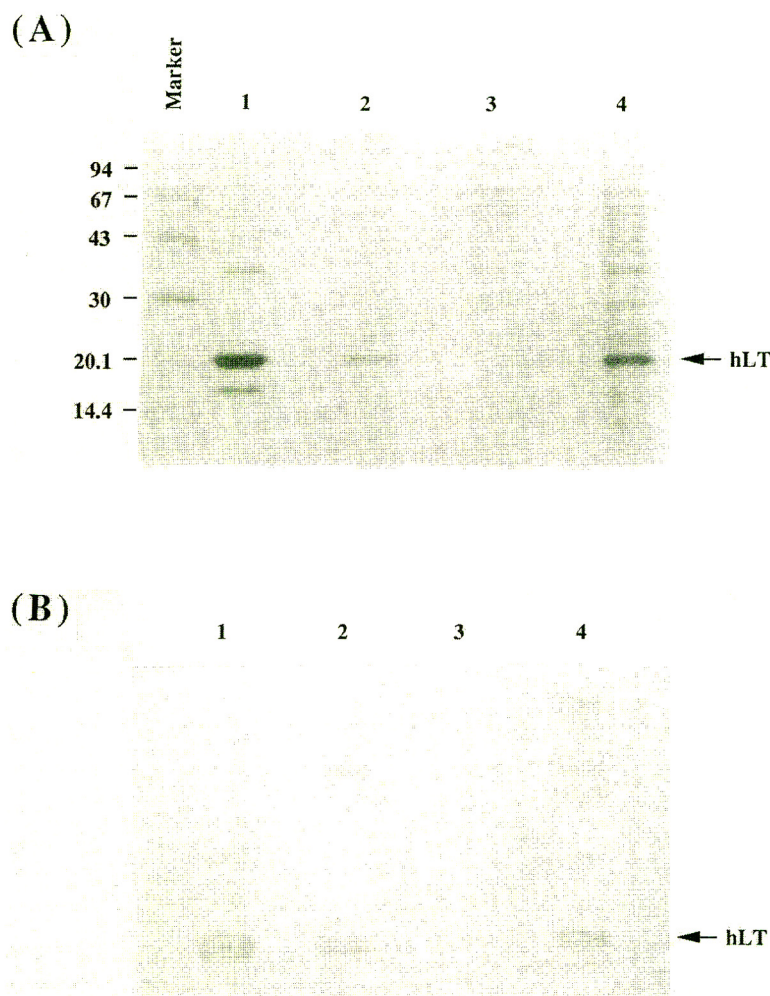


Fig. 3. SDS-PAGE (A) and Western blot (B) of the fractions derived from affinity chromatography. Lanes: 1 = purified rhLT (as standard); 2 = bound fraction; 3 = unbound fraction; 4 = cell lysate before separation. M_r indicated in kilodalton.

2). These results seemed to confirm that branched epitope are better immunogens in producing anti-peptide antibodies [11,12].

3.3. Immunoaffinity chromatography

When purified rhLT was applied to the affinity gel column (prepared by coupling purified immunoglobulin against the branched peptide to activated Sepharose 4B), the parent protein, rhLT, was adsorbed to the column quantitatively and the capacity of the affinity gel was proportional to the amount of antibody coupled to the gel matrices (data not shown).

When the cell lysate containing rhLT obtained from recombinant *E. coli* HB101 cells was loaded directly onto the affinity column without any pretreatment, the rhLT was also specifically retained. The bound fraction could be easily recovered by applying elution buffer. Fig. 3 shows the SDS-PAGE (A) and corresponding Western blot (B) profiles of the bound and unbound fractions obtained from this chromatographic separation step. It clearly demonstrated that rhLT was separated from most of the *E. coli* proteins in a single step. These separations were highly reproducible and more than 100 runs were performed in the same column without any decrease in efficiency.

The results reported here demonstrated that a protein epitope synthesized as a branched peptide is a valuable alternative for eliciting anti-peptide antibodies as affinity ligands for protein purification. Although it was reported that some synthetic linear peptides might be good immunogens [13], other peptides, such as the peptide used in this study (residues 139–154 of hLT), was unable to induce antibody production efficiently. Some procedures, such as coupling of the pure peptide to a carrier protein or by peptide cyclization, were used to overcome this problem [14], but these methods often need additional chemical manipulations and exhibit variable efficiency on a case to case basis. On the other hand, a branched epitope peptide can enhance the immunogenicity without introducing extra foreign sequences. Moreover, the branched

peptide can be synthesized automatically on a peptide synthesizer.

Recently several more rapid epitope mapping methods have been developed [15]. Some of these methods are based on the so-called random peptide library approach in which epitope mapping is performed without any prior knowledge of the protein sequence [16,17]. As the branched epitope procedure can be readily linked with epitope mapping to produce biospecific ligands for affinity chromatography, this may lead to a wider application of anti-epitope antibodies for protein purification in the future.

References

- [1] P. Bailon and S.K. Roy, in M.R. Ladisch, R.C. Willson, C.C. Painton and S.E. Builder (Editors), *Protein Purification, from Molecular Mechanisms to Large-Scale Processes*, American Chemical Society, Washington, DC, 1990, p. 150.
- [2] Z.J. Yao, M.C.C. Kao, K.C. Loh and M.C.M. Chung, *Biochem. Mol. Biol. Int.*, 32 (1994) 951.
- [3] H.F. Seow, C.R. Goh, L. Krishnan and A.G. Porter, *Bio/Technology*, 7 (1989) 363.
- [4] K.C. Loh, Z.J. Yao, M.G.S. Yap and M.C. M. Chung, *Protein Expression Purif.*, 5 (1994) 70.
- [5] P.J. Tam, *Proc. Natl. Acad. Sci. U.S.A.*, 85 (1988) 5409.
- [6] *User Bulletin No. 34*, Applied Biosystems, Foster City, CA, 1992.
- [7] M. Reichlin, *Methods Enzymol.*, 70 (1980) 159.
- [8] C.J. van Oss, in M.Z. Atassi, C.J. van Oss and D.R. Absolom (Editors), *Molecular Immunology*, Marcel Dekker, New York, Basel, 1984, p. 284.
- [9] M.M. Bradford, *Anal. Biochem.*, 72 (1976) 248.
- [10] U.K. Laemmli, *Nature*, 227 (1970) 680.
- [11] J.P. Tam, *Methods Enzymol.*, 168 (1989) 7.
- [12] G.W. McLean, A.M. Owsianka, J.H. Subak-Sharpe and H.S. Marsden, *J. Immunol. Methods*, 137 (1991) 149.
- [13] H.L. Niman, R.A. Houghten, L.E. Walker, R.A. Reisfeld, I.A. Wilson, J.M. Hogle and R.A. Lerner, *Proc. Natl. Acad. Sci. U.S.A.*, 80 (1983) 4949.
- [14] S. Muller, in M.H.V. Van Regenmortel, J.P. Briand, S. Muller and S. Plaeue (Editors), *Synthetic Polypeptides as Antigen*, Elsevier, Amsterdam, 1988, p. 131.
- [15] S. Birnbaum and K. Mosbach, *Current Opinion Biotechnol.*, 3 (1992) 49.
- [16] J.K. Scott and G.P. Smith, *Science*, 249 (1990) 386.
- [17] K.S. Lam, S.E. Salmon, E.M. Hersh, V.J. Hruby, W.M. Kazmierski and R.J. Knapp, *Nature*, 354 (1991) 82.



ELSEVIER

Journal of Chromatography A, 679 (1994) 195–200

JOURNAL OF
CHROMATOGRAPHY A

Short communication

Determination of purine bases and nucleosides by conventional and microbore high-performance liquid chromatography and gas chromatography with an ion-trap detector

Petr Šimek^{a,*}, Alexandr Jegorov^b, František Dusbábek^c

^a*Institute of Entomology, Laboratory of Analytical Chemistry, Academy of Sciences of the Czech Republic, Branišovská 31, 370 05 České Budějovice, Czech Republic*

^b*Research Unit, Galena Co., Branišovská 31, 370 05 České Budějovice, Czech Republic*

^c*Institute of Parasitology, Academy of Sciences of the Czech Republic, Branišovská 31, 370 05 České Budějovice, Czech Republic*

First received 15 April 1994; revised manuscript received 20 June 1994

Abstract

A reversed-phase high-performance liquid chromatographic method has been developed for the analysis of purine and pyrimidine bases, uric acid and nucleosides largely relating to the purine synthetic and degradation metabolic pathways, with particular attention to the separation of hypoxanthine, xanthine and guanine. Complete separation and quantitation of the purines has been accomplished in the nanogram–microgram scale on conventional 4.6 mm I.D. columns with a standard gradient HPLC instrumentation as well as on 1 mm I.D. microbore columns with a dedicated isocratic micro-HPLC system using a dioxane–sodium acetate buffer. For the definite identification of components in excreta of ticks a GC–MS method has been described involving formation and GC of the trimethylsilyl derivatives on a 25-m DB-5 column directly coupled with an ion trap detector. The methods are demonstrated on the analysis of the purine metabolites having an assembly pheromone effect on argasid ticks.

1. Introduction

Blood-feeding arthropods living on high protein diet, such as ticks, excrete relatively high amounts of nitrogenous metabolites into the environment, in particular hematin and purine bases [1–4]. An interest in products of the purine metabolism has recently been stimulated by the finding that certain purine compositions excreted by argasid ticks represent their assembly pheromones which induce ticks' clustering in natural habitat [5–7].

Since ticks obtain food in variable long-term intervals, the concentration of individual purines in physiological fluids, excretory organs and waste material varies with their physiological stage. As a result, assembly efficacy of the pheromone composed of guanine (Gua), hypoxanthine (Hyp) and xanthine (Xan) is also affected and there is a need of reliable monitoring of large-range purine levels in the excretory products of various arthropods by a sophisticated analytical method [6].

* Corresponding author.

With the advent of high-performance liquid chromatography (HPLC) accurate and sensitive analysis of small nucleic acid constituents in physiological samples has become a routine technique. A number of studies has appeared on this subject including those dealing with the separation of intermediates of purine metabolism (see, e.g. reviews [8,9]). The experimental knowledge accumulated in recent years shows that reversed-phase (RP) HPLC is particularly suited for the separation of purine metabolites. Generally, octadecylsilica packing materials and 0.001–0.1 M potassium dihydrogenphosphate or sodium acetate buffers with a methanol gradient as a mobile phase have been most widely used for the analysis of this class of compounds [8–15].

Searching a suitable analytical method for the determination of purines in our samples of tick excretory products we encountered that guanine, xanthine and hypoxanthine are eluted very close together on the RP-HPLC columns [11–14] so that their separation is difficult, particularly if one component predominates. The present investigation was therefore undertaken to develop a RP-HPLC method with emphasis on the separation of the three purines in a large range of concentrations. We also examined 1 mm I.D. microbore columns and a micro-HPLC dedicated instrumentation to this subject. As a complementary method, identity of individual components in the excretory samples was confirmed by gas chromatography (GC)–mass spectrometry (MS) using an ion-trap detector.

2. Experimental

2.1. Chemicals

Purine and pyrimidine bases, uric acid and nucleosides were obtained from: guanine (Loba Chemie, Fischamend, Austria), uric acid, hypoxanthine, adenosine, xanthosine, inosine, guanosine, thymidine, cytidine, uridine, cytosine, thymine, uracil (Merck, Darmstadt, Germany), guanine hydrochloride, xanthine, adenine (Lachema, Brno, Czech Republic). Sol-

vents and other chemicals were purchased from: acetonitrile (Fluka, Buchs, Switzerland), pyridine (Loba Chemie), methanol, dichloromethane, *n*-butanol, *n*-hexane, sodium acetate, phosphoric acid, hydrochloric acid (Lachema), bis(trimethylsilyl)trifluoroacetamide (BSTFA) (Supelco, Gland, Switzerland). Water, organic solvents and buffer solutions used in HPLC were filtered through a 0.22- μ m Durapore membrane (Millipore, Bedford, MA, USA). Pyridine and acetonitrile were dried and distilled before to use.

2.2. Sample treatment

Sample collection and bioassays have been described elsewhere [6]. Collected waste excreta of ticks (about 3 mg) were dissolved in 10% H_3PO_4 and further diluted to the final 1% H_3PO_4 . After centrifugation, 10 μ l or 0.5 μ l (micro-HPLC) aliquots were injected into the HPLC devices. Physiological fluids (coxal fluid, haemolymph) were analysed directly without dissolution in H_3PO_4 . In order to study mutual ratios of purines on the surface of spherulic excrements, distilled water and 1% NaCl solution were utilized as extraction reagents instead of H_3PO_4 .

2.3. HPLC instrumentation

HPLC system I

Studies with conventional packed columns were carried out on a Varian Vista 5500 apparatus (Varian, Walnut Creek, CA, USA) equipped with a 10- μ l injection valve (Rheodyne 7126); a UV-200 variable-wavelength detector set at 254 nm and a DS-604 data station. The column was a Hypersil ODS; 5 μ m, 250 mm \times 4.6 mm I.D. (Keystone Scientific, Bellefonte, PA, USA); placed in an oven thermostatted to 30°C. Solvent A was 0.004 M sodium acetate pH 4.5, solvent B was distilled water, solvent C was acetonitrile–water (80:20). Isocratic elution was with a mixture A–B (10:90) for 10 min, then a 15-min linear gradient to C–B (10:90) was used.

A constant flow of 1.00 ml/min was maintained during the analysis.

HPLC system II

The micro-HPLC system used in this work was a Carlo Erba Instruments System 20 (Carlo Erba, Milan, Italy) consisting of a single micro-processor-controlled syringe pump (Phoenix 20), a 0.5- μ l injection valve (Rheodyne 7520); a variable-wavelength UV-visible detector (Micro UVIS 204) set at 254 nm and a SP 4270 integrator (Spectra-Physics, Darmstadt, Germany). An Alltech C₁₈ (P.N. 8005) column was used, packed with the Carbosieve C₁₈ HS 5V; 5 μ m, 250 mm \times 1 mm I.D. (Alltech, Deerfield, IL, USA), held at room temperature. The analyses were performed in the isocratic mode using a 0.8% solution of dioxane in 0.5 mM sodium acetate, pH 5.5. The flow-rate was 25 μ l/min.

2.4. Derivatization procedure for GC-MS analysis

About 0.25 mg of the ticks' excrements were placed in 2-ml Micro reaction vials (Supelco) and dried at 80°C for 1 h. A freshly prepared mixture of BSTFA-pyridine (1:1, v/v) was added (150 μ l). The vials were capped with PTFE-lined caps and heated in an oil bath at 150°C for 30 min. After cooling, 1- μ l aliquots were analysed.

2.5. GC-MS

GC-MS was carried out on a Varian 3400 gas chromatograph (Varian, USA) directly coupled to an ion-trap detector ITD 800 (Finnigan-MAT, San Jose, CA, USA). Compounds were separated on a 25 m \times 0.25 mm I.D. DB-5 fused-silica capillary column (J&W Scientific, Folsom, CA, USA). The operation conditions were: injector temperature 260°C, split 20:1; helium carrier gas velocity about 1 ml/min; column temperature programme, typically: 1 min hold at 90°C, then 10°C/min to 260°C, 15 min hold; transfer line temperature 260°C on average. The ITD 800 was operated under the automated gain control; the mass range 70–650 u was scanned every 1 s.

3. Results and discussion

3.1. HPLC separation of hypoxanthine, xanthine and guanine

The complete separation of the Hyp/Xan/Gua trio was accomplished by the isocratic RP-HPLC system I on a carefully selected 4.6 mm I.D. octadecylsilica column as shown in Fig. 1a and c. Separation of bases together with nucleosides was performed using a methanol-sodium acetate buffer gradient elution (Fig. 2). The column must be thermostatted in order to obtain reproducible retention of components, particularly nucleosides.

Preliminary experiments revealed that resolution of purines is largely influenced by the ionic strength and pH of buffer, organic modifier and also the performance of the manufactured column. The desired resolution of the components was only achieved by means of diluted buffers below the concentration of 5 mM. The capacity factors of the purines decrease with increasing pH and, under the condition used, optimal resolution was reached either at pH 5.1 (Fig. 1c) or below pH 4.5 (Fig. 1a).

Having tested various columns in our laboratory, we ascertained that optimization of the ion strength and pH failed in most cases, e.g., also with our microbore column. Fortunately, res-

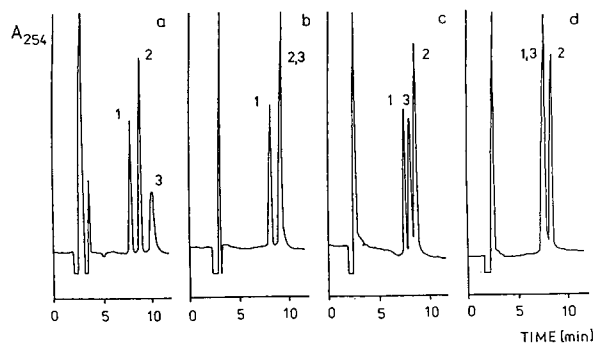


Fig. 1. Elution profile of Hyp (1), Xan (2) and Gua (3). HPLC system I; ODS Hypersil (250 \times 4.6 mm I.D., 5 μ m) column, isocratic elution with water-4 mM sodium acetate (9:1, v/v), pH: (a) 4.2, (b) 4.8, (c) 5.1, (d) 7.4; flow 1.0 ml/min, detection at 254 nm. Amounts injected: 7.8 (1), 18.2 (2) and 24.5 (3) ng.

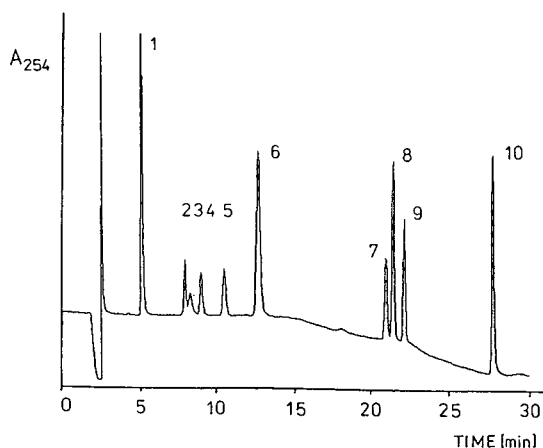


Fig. 2. Elution profile of bases and nucleosides. HPLC system I; ODS Hypersil (250×4.6 mm I.D., $5 \mu\text{m}$) column, gradient elution, for conditions, see Experimental. Peaks: 1 = uracil; 2 = Hyp; 3 = Gua; 4 = Xan; 5 = uridine; 6 = thymine; 7 = xanthosine; 8 = inosine; 9 = guanosine; 10 = adenosine.

olution can further be increased by using an organic modifier.

We experimented with the dioxane–sodium acetate mobile phase, since retention of guanine on the reversed-phase packing materials is selectively affected by interaction with this solvent [11]. As an example, the complete separation of the Hyp/Xan/Gua trio using the isocratic sodium acetate–dioxane elution on a 1 mm I.D. octadecylsilica RP-HPLC column (micro-HPLC system II) is shown in Fig. 3a.

Detection limits were estimated to be about 1–2 ng for purine bases with HPLC system I. The use of buffers with low pH values (below pH 4.5) caused the increase of the guanine tailing (Fig. 2) and thus the decrease of its detection limit to 4 ng. The relationship between the concentration and the peak area of these compounds was linear from 10 ng to $100 \mu\text{g}$. Detection limits for adenine and nucleosides were about 2 ng and 0.7–1 ng, respectively. With the micro-HPLC system II the detection limits were somewhat lower; about 200 pg for the particular purine ($S/N=2$). The standard curves were linear over three orders of magnitude from 1 ng to $50 \mu\text{g}$ of each purine with a correlation coefficient of 0.998.

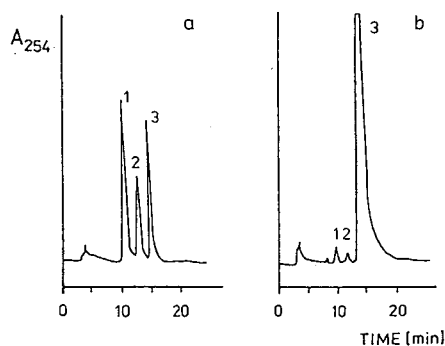


Fig. 3. Separation of the purine triplet Hyp/Xan/Gua on a 1 mm I.D. microbore column. Micro-HPLC system II; Alltech C_{18} (250×1 mm I.D., $5 \mu\text{m}$) column, isocratic elution with 0.5 mM sodium acetate pH 5.5 containing 0.8% (v/v) dioxane; flow $25 \mu\text{l}/\text{min}$, detection at 254 nm. (a) Standard solution: 1 = Hyp, 2 = Xan, 3 = Gua; amounts injected 3.1, 2.9 and 2.6 ng, respectively. (b) Real sample of tick excreta of *Argas persicus*, Hyp (1), Xan (2), Gua (3).

3.2. Analysis of tick excretory products

Because of the poor solubility of guanine in water, aqueous acids were used for complete solubilization of the excreta. Since uric acid was found in excreta in low concentrations which are readily dissolved in 10% H_3PO_4 , its quantitation is also possible. At higher concentrations, uric acid can be determined by a HPLC method using alkaline buffers [16]. Since guanine predominates in the excreta of ticks, the buffer with a pH below 4.2 (Fig. 1a) could only be used for simultaneous quantitation of Xan, Hyp and Gua due to the unfavourable resolution of the components with the increase of its concentration. However, if the dioxane–acetate buffer is employed, the desired resolution of purines can be accomplished at pH 5.5 as documented in Fig. 3b on the analysis of the excrements of the tick *Argas persicus*.

Mutual ratios of the purines in the excreted spherules produced by *Argas persicus* were found to be about 2% for Hyp and 1–10% with respect to the total amount of Gua (as 100%) found as the principle component of the assembly pheromone [5]. The composition of tick excreta varied slightly with their aging; the concentration of xanthine increased particularly

on the surface of excreted spherules, which was accompanied with the decrease of their pheromonal activity. Some species of ticks were found to have similar purine contents in waste excreta (*Ornithodoros moubata*, *O. tartakovskyi*) or slightly different in concentration of Hyp and Xan (*Argas reflexus*, *A. polonicus*) [6,7]. Thus, assembly effect of purine pheromones is poorly specific for different tick genera or species. Using the gradient method with HPLC system I, guanosine was found in the excreta of ticks in some cases in the quantity not exceeding about 0.1% with respect to the total amount of Gua. The excretion of energetically rich nucleosides is unusual and, to our knowledge, has not been reported so far.

Identity of the compounds in the tick waste material was further established by a GC–MS method after trimethylsilylation. GC–MS analysis of the standard mixture of nucleic acid constituents of interest and a representative sample of the ticks' waste excreta is shown in Fig. 4 and 5, respectively. All glassware used must be presilylated to avoid adsorption of purines on the surfaces. Since most trimethylsilyl derivatives of purines (with the exception of uric acid) tend to react with active sites in capillary columns, the column must be carefully selected, as in the case of the HPLC method. A short, 10–12-m fused-silica capillary column coated with SE-54 was recommended for analyses of DNA bases [17]. We used a longer, 25-m DB-5 fused-silica column in order to achieve complete separation of the closely eluting uric acid and guanine peaks.

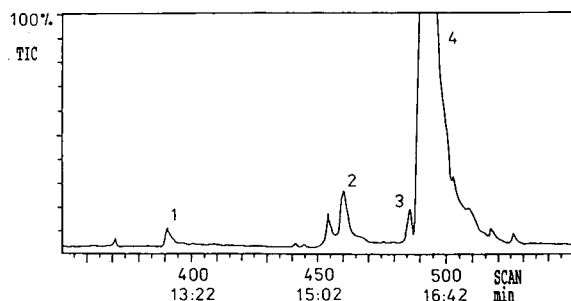


Fig. 5. Representative GC–MS TIC chromatogram obtained from the analysis of the waste excreta of the tick *Argas persicus*. Peaks: 1 = Hyp; 2 = Xan; 3 = uric acid; 4 = Gua. Temperature programme: 90°C, 1 min hold, 10°C/min, 170°C, 6°C/min, 260°C.

Under such conditions some purine exhibited slight tailing. Nevertheless, peak area ratios of the found purines were in fairly good accordance with the results obtained by RP–HPLC. The detection limit for the GC–MS method was estimated to be about 100 pg per each purine injected by measuring the peak area representing the characteristic M^{+} or $(M - 15)^{+}$ ions. Due to the high sensitivity of the ion-trap detector in the full scan mode identification can be easily obtained in the low nanogram range by matching characteristic electron impact mass spectra of the components with the standard mass spectral libraries such as the US National Bureau of Standards library (the ITD 800 standard option). Thus, the presence of Hyp, Xan, Gua and uric acid was unequivocally proved in the waste excreta of argasid ticks [6].

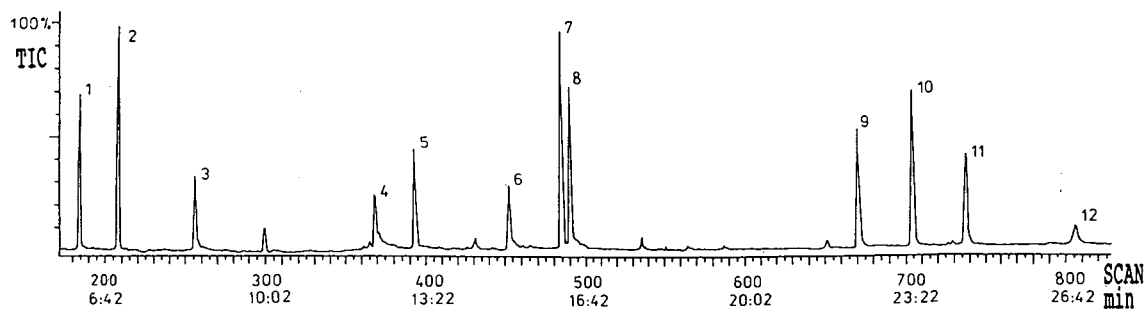


Fig. 4. GC–MS total ion current (TIC) chromatogram of bases, uric acid and nucleosides as trimethylsilyl derivatives. Peaks: 1 = uracil; 2 = thymine; 3 = cytidine; 4 = Hyp; 5 = adenine; 6 = Xan; 7 = uric acid; 8 = Gua; 9 = inosine; 10 = adenosine; 11 = xanthosine; 12 = guanosine. Capillary column DB-5, 25 m. A 20-ng amount of each component was injected. Split injection 20:1.

4. Conclusions

RP-HPLC separation of hypoxanthine, xanthine and guanine is largely dependent on the octadecylsilica sorbent used for the column packing. Using a suitable batch of reversed-phase material, simultaneous separation of the purines and related nucleosides has been accomplished. However, in a large range of concentrations, e.g. if one purine component predominates in sample as it is in the case of the ticks' excretory products, the use of dioxane modifier can further enhance the resolution of the components required for quantitation. The method has been proved valuable in the determination of the purine trio in excretory products showing an assembly pheromone effect on the family of argasid ticks.

Acknowledgements

This work was supported by grant No. 508-94-0052 of the Grant Agency of the Czech Republic. The authors also thank Erba Science, Schottenfeldgasse 79, A-1072 Vienna, Austria, for the provision of the micro-HPLC chromatograph.

References

- [1] L.B. Coons, R. Rosell-Davis and B.I. Tarnowski, in J.R. Sauer and A. Hair (Editors), *Morphology, Physiology, and Behavioural Biology of Ticks*, Ellis Horwood, Chichester, 1985, p. 248.
- [2] G.O. Evans, *Principles of Acarology*, C.A.B. International, Wallingford, 1992, p.563.
- [3] B.H. Hamdy, *J. Med. Entomol.*, 10 (1973) 53.
- [4] B.H. Hamdy, *J. Med. Entomol.*, 14 (1977) 15.
- [5] D.A. Otieno, A. Hassanali, F.D. Obenchain, A. Sternberg and R. Galun, *Insect Sci. Appl.*, 6 (1985), 667.
- [6] F. Dusbábek, P. Šimek, A. Jegorov and J. Triska, *Exp. Appl. Acarol.*, 11 (1991) 307.
- [7] F. Dusbábek, A. Jegorov and P. Šimek, in F. Dusbábek and V. Bukva (Editors), *Modern Acarology*, Vol. 1, Academia, Prague and SPB Acad. Publ., The Hague, 1991, p.59.
- [8] R.C. Simpson and P.R. Brown, *J. Chromatogr.*, 379 (1986) 269.
- [9] K. Nakano, *Adv. Chromatogr.*, 25 (1986) 245.
- [10] R. Boulieu and C. Bory, *J. Chromatogr.*, 339 (1985) 380.
- [11] M. Ryba, *J. Chromatogr.*, 219 (1981) 245.
- [12] R.A. Hartwick and P.R. Brown, *J. Chromatogr.*, 126 (1976) 679.
- [13] P.R. Brown and E. Grushka, *Anal. Chem.*, 52 (1980) 1210.
- [14] R.J. Simmond and R.A. Harkness, *J. Chromatogr.*, 226 (1981) 369.
- [15] G. Liu, *Chromatographia*, 28 (1989) 493.
- [16] B. Pekič, B. Slavica and Z. Zekovič, *Chromatographia*, 27 (1989) 493.
- [17] M. Dizdaroglu, *J. Chromatogr.*, 295 (1984) 103.

Short communication
Size-exclusion chromatography of nylons in methylene
chloride–dichloroacetic acid

T.H. Mourey*, T.G. Bryan

*Analytical Technology Division, Manufacturing Research and Engineering Organization B-82, Eastman Kodak Company,
Rochester, NY 14650-2136, USA*

Received 12 April 1994

Abstract

Methylene chloride–dichloroacetic acid (80:20, v/v) is used as a room-temperature size-exclusion chromatography eluent for a variety of nylons. The eluent was previously shown to be suitable for poly(ethylene terephthalate), and this application shows its utility for other polymer classes that are difficult to solubilize. Absolute molecular masses are measured by low-angle light-scattering detection, and a means is provided for generating narrow-standard calibration curves from polystyrene standards.

1. Introduction

Four approaches have been taken in the characterization of nylons by size-exclusion chromatography (SEC):

(1) High-temperature SEC in phenolic solvents [1–3], benzyl alcohol [4–6] or hexamethylphosphoramide [7–9].

(2) SEC in common solvents such as tetrahydrofuran after solubilization by trifluoroacetylation [10–16].

(3) SEC in fluorinated alcohols such as trifluoroethanol [17–22] and 1,1,1,3,3,3-hexafluoroisopropanol (HFIP) [9,23–25].

(4) SEC at room temperature in mixed solvents such as *m*-cresol–chlorobenzene [3] or HFIP–toluene [26].

Each approach has advantages and disadvantages

discussed in most of the papers referenced above. Methylene chloride–dichloroacetic acid (DCAA) (80:20, v/v), containing 0.01 *M* tetrabutylammonium acetate (TBAA) is an alternative for room-temperature SEC of crystalline polyesters such as poly(ethylene terephthalate) (PET) [27]. The solvent pair is nearly isorefractive, allowing the use of light-scattering detection. It does not significantly degrade PET, polystyrene standards are suitable for calibration, it is used at room temperature, and it is comparatively inexpensive. Application to nylons is a logical and practical extension of its use; some of these polyamides are soluble only in solvents that dissolve PET. The intent of this study is to evaluate this eluent originally developed for PET, without modification, with the practical objective of using the same solvent and SEC system for both crystalline polyesters and polyamides.

* Corresponding author.

2. Experimental

2.1. Sample preparation

Narrow molecular mass distribution polystyrenes were obtained from Polymer Labs. (Amherst, MA, USA). Nylon 6,6, 46K and 32K standards were obtained from American Polymer Standards (Mentor, OH, USA). All other nylon samples were obtained from Scientific Polymer Products (Ontario, NY, USA). Typically, 25 mg of nylon were dissolved at room temperature in the SEC eluent containing 0.01% 1-chloro-2,4-dinitrobenzene as a flow marker.

2.2. Size-exclusion chromatography

The SEC was similar to that described for PET [27]. Eluent was methylene chloride–DCAA (80:20, v/v) containing 0.01 M TBAA. The nominal flow-rate was 1.0 ml/min, and sample injection volumes were 100 μ l. A Spectroflow 757 UV detector operating at 310 nm, an LDC Analytical KMX-6 low-angle laser-light-scattering (LALLS) photometer, and a Waters Model 401 differential refractive index (DRI) detector were connected in series after the columns. The SEC columns and DRI detector were thermostated to 30.0°C. The UV and LALLS detectors were operated at room temperature. All light-scattering intensities were measured at 6–7° with an aperture of 0.15 mm. Flow-rates were corrected using the UV chromatogram and the retention volume of the 1,2-chloro-2,4-dinitrobenzene flow marker.

3. Results and discussion

3.1. Dissolution and solution properties

Nylon pellets dissolve in the methylene chloride–DCAA (80:20) eluent at room temperature in less than 1 h at a concentration of 2.5 mg/ml. There is no evidence for phase separation at this polymer concentration, even after several days in solution. Dilute solution viscosity is adequately fitted by the conventional relationships of

specific, η_{sp} , and reduced, η_r , viscosity with concentration, c :

$$\eta_{sp} = [\eta]c + k'[\eta]^2c^2 \quad (1)$$

$$\ln \eta_r = [\eta]c + k''[\eta]^2c^2 \quad (2)$$

The intrinsic viscosity $[\eta]$ of a nylon 6 sample with weight-average molecular mass of 24 800 is 0.643 dl/g, $k' = 0.39$ and $k'' = -0.13$. It is possible to use less DCAA acid for SEC; nylon 6, 6/6, 6/9, 6/10, and 6/12 are soluble at a concentration of 2.5 mg/ml in dichloromethane containing 5% (v/v) DCAA. Nylon 11 and nylon 12 require a minimum of approximately 10% dichloroacetic acid. SEC results in these eluent compositions have not been investigated extensively; instead, our objective is to show the general utility of a single solvent system (methylene chloride–DCAA, 80:20) for both crystalline polyesters and nylons.

3.2. Chromatography

Typical LALLS and DRI chromatograms of nylon 6,6 are shown in Fig. 1. A small peak in the DRI chromatogram from TBAA appears near the solvent peaks. This salt eliminates polyelectrolyte effects in polar solvents and is necessary for reproducible elution of PET. Its necessity for nylons has not been established. The salt does not absorb above 300 nm and the interference is not observed with a UV detector

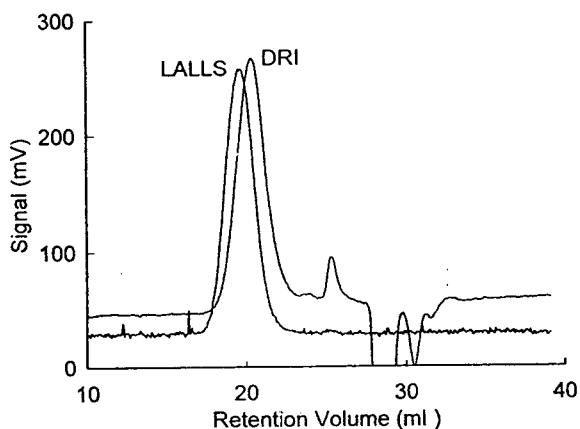


Fig. 1. LALLS and DRI chromatograms of nylon 6,6 46K.

for PET and nylon 6T. However, UV detection cannot be used with this solvent for aliphatic nylons, and the low-molecular-mass information (e.g., number-average molecular mass) obtained from the DRI is limited if the salt is present. A similar problem exists with SEC of aliphatic nylons in HFIP with sodium trifluoroacetate [9].

Previous experience with PET suggests that sample degradation is most likely at high temperatures, with water concentrations greater than 1% (v/v), and with standing in the eluent for greater than four days. Degradation or transamidation is also a concern for nylons in an acidic eluent. There is no discernible difference in the normalized chromatograms of nylon 6 samples that sat for 48 h in the eluent at room temperature. Unlike PET, there is also no change in nylon 6 after exposure for 48 h to eluent containing 4% water. Stability at high temperatures is not an issue since all nylon samples are dissolved and analyzed at room temperature. The results show that sample degradation in the eluent is less important for nylons than for PET.

3.3. Specific refractive index increment

The specific refractive index increment of nylon samples is estimated from the differential refractometer response by the method of Berkowitz [28]. This method was successfully applied to PET in this eluent [27]. We note that the

differential refractometer used in the previous study (Waters Model 410) developed leaks around the inlet fittings after approximately nine months of continuous use. The older and simpler Waters Model 401 has fewer inlet fittings and is a sturdier substitute with this eluent, which is corrosive to some stainless-steel ferrules. Specific refractive index increments of nylons are given in Table 1.

3.4. Light-scattering detection

Absolute molecular masses are calculated from the excess Rayleigh scattering, $R_{\theta,i}$ and the signal from a concentration detector (either UV or DRI) c_i at each eluting slice i ,

$$\frac{Kc_i}{R_{\theta,i}} = \frac{1}{M_{w,i}P(\theta)_i} + 2A_2c_i + 3A_3c_i^2 + \dots \quad (3)$$

where K is the light-scattering optical constant, $P(\theta)_i$ is the particle scattering function and A_2 and A_3 are virial coefficients. The weight-average molecular mass (M_w) of the whole polymer (values reported in Table 1) is obtained from either the light-scattering signal alone (no DRI) or from summation of the molecular masses and concentrations at each slice i of the chromatogram, as described in Ref. 27. Results reported in Table 1 are from integration of the light-scattering chromatograms (no DRI). Precision is comparable to that obtained for PET. There is

Table 1
SEC-LALLS of nylons

Sample	No. of samples	dn/dc ^a (ml/g)	M_w ^b	β_1	β_2
Nylon 6	10	0.180 ± 0.006	24 800 ± 1000	-0.372	1.005
Nylon 6,6 46K	10	0.188 ± 0.008	41 400 ± 1300	-0.758	1.067
Nylon 6,6 32K	10	0.194 ± 0.007	31 100 ± 900	-0.379	1.001
Nylon 6,6	8	0.182 ± 0.012	33 000 ± 1300	-0.657	1.053
Nylon 6,9	10	0.163 ± 0.002	30 500 ± 1200	-0.678	1.082
Nylon 6,10	4	0.163 ± 0.002	33 700 ± 450	-0.703	1.094
Nylon 6,12	10	0.149 ± 0.002	25 700 ± 700	-0.128	0.963
Nylon 11	6	0.133 ± 0.002	26 000 ± 900	-1.339	1.197
Nylon 12	6	0.133 ± 0.004	28 200 ± 900	-0.460	1.009
Nylon 6T	8	0.201 ± 0.003	36 800 ± 400	-0.403	1.021

^a Specific refractive index increment.

^b Weight-average molecular mass from SEC-LALLS.

reasonable agreement with vendor values for nylon 6,6 with weight-average molecular masses of 46 000 (46K) and 32 000 (32K).

3.5. Calibration curves from light-scattering detection

Size-exclusion calibration curves can be established from the relationship between nylon molecular mass, M_2 , and standard molecular mass, M_1 ;

$$\log M_2 = \beta_1 + \beta_2 \log M_1 \quad (4)$$

The constants β_1 and β_2 are obtained by plotting the polystyrene $\log M$ -retention volume calibration curve versus the $\log M$ -retention volume curve for nylon measured by light-scattering detection [29]. A similar approach has been used to convert poly (methylmethacrylate) (PMMA) equivalent molecular masses to nylon molecular masses in HFIP with supporting electrolyte [30]. Viscosity measurements and direct application of universal calibration are not required. Calibration curves for nylons are obtained by calibrating the column set with narrow molecular mass distribution polystyrene stan-

dards. Polystyrene molecular masses are converted to nylon molecular weights using Eq. 4 and the constants provided in Table 1. A typical nylon 6,6 calibration curve is compared to polystyrene in Fig. 2. This calibration curve allows calculation of absolute molecular mass distributions from a concentration detector only.

4. Discussion

The eluent composition is optimized for PET and related crystalline polyesters and may not be optimized for nylons. As evaluated, the eluent is compared with the four other approaches for the SEC of nylons:

(1) Operation at room temperature is desirable. There is also no evidence for polymer degradation; this is a concern in phenolic solvents at high temperatures.

(2) There is no derivatization step. In the case of trifluoroacetylation, some workers have cited differences in results depending on the degree of acetylation and complications in the calculation of molecular masses by universal calibration [12,14]. Trifluoroacetyl derivatives are also sensitive to moisture and the eluents must be carefully dried.

(3) The solvent is less expensive than fluorinated solvents. However, it causes skin burns and it is corrosive to stainless steel after long-term use. Typically, connecting tube fittings (especially ferrules) and pump parts will require replacement after 6–9 months of continuous use. We have been unsuccessful using viscometry detection because of flow fluctuations that develop from minor leaks in and about viscometer detectors. It is noted, however, that fluorinated solvents such as HFIP also pose significant safety hazards, particularly to the eyes.

(4) Criticism of mixed solvents, including sensitivity to changes in eluent composition, selective solvation and complications with light-scattering detection and DRI baseline stability are minimized with methylene chloride–DCAA. There is little difference in chromatograms obtained at 20% and 10% DCAA [27], and the solvent pair is nearly isorefractive, making it

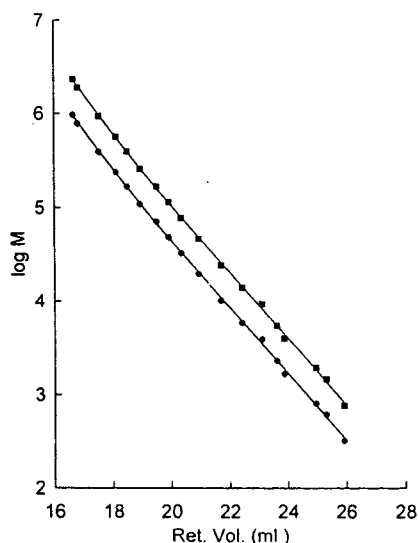


Fig. 2. Narrow standard calibration curves for (□) polystyrene and (●) nylon 6,6.

suitable for light-scattering. Acceptable DRI baselines are easily established and remain stable. Specific refractive index increments in this eluent are lower than in fluorinated solvents such as HFIP, thereby reducing the sensitivity of light-scattering detectors. However, it is relatively easy to obtain low scattering background with the higher solvent refractive index and LALLS cell windows require infrequent cleaning.

5. Conclusions

The methylene chloride–DCAA eluent used for crystalline polyesters such as PET can also be used for the SEC of nylons at room temperature. There is no evidence for degradation of nylons in this solvent, and absolute molecular masses are obtained from light-scattering detection. To its disadvantage, the low-molecular-mass region is difficult to quantitate in aliphatic nylons because of interference from TBAA.

References

- [1] M.A. Dudley, *J. Appl. Polym. Sci.*, 16 (1972) 493.
- [2] Z. Tuzar, P. Kratochvíl and M. Bohdaneck, *Adv. Polym. Sci.*, 30 (1979) 117.
- [3] P.S. Ede, *J. Chromatogr. Sci.*, 9 (1971) 275.
- [4] G. Pastuska and U. Just, *Angew. Makromol. Chem.*, 81 (1979) 11.
- [5] G. Pastuska, U. Just and H. August, *Angew. Makromol. Chem.*, 107 (1982) 173.
- [6] G. Marot and J. Lesec, *J. Liq. Chromatogr.*, 11 (1988) 3305.
- [7] D. Petit, R. Jerome and Ph. Teyssie, *J. Polym. Sci., Polym. Chem. Ed.*, 17 (1979) 2903.
- [8] R. Panaris and G. Pallas, *J. Polym. Sci., Polym. Lett.*, 8 (1970) 441.
- [9] D.J. Goedhart, J.B. Hussem and B.P.M. Smeets, in J. Cazes (Editor), *Liquid Chromatography of Polymers and Related Materials (Chromatographic Sciences Series, Vol. 13)*, Marcel Dekker, New York, 1977, p. 203.
- [10] H. Schuttenberg and R.C. Schulz, *Angew. Chem.*, 88 (1976) 848.
- [11] E. Jacobi, H. Schuttenberg and R.C. Schulz, *Makromol. Chem. Rapid Commun.*, 1 (1980) 397.
- [12] E. Biagini, E. Gattiglia, E. Pedemonte and S. Russo, *Makromol. Chem.*, 184 (1983) 1213.
- [13] K. Weiskopf and G. Meyerhoff, *Polymer*, 24 (1983) 72.
- [14] K. Weiskopf, *Polymer*, 26 (1985) 1187.
- [15] T. Ogawa and M. Sakai, *J. Liq. Chromatogr.*, 8 (1985) 1025.
- [16] T. Ogawa and M. Sakai, *J. Polym. Sci.: Part A: Polym. Chem. Ed.*, 26 (1988) 3141.
- [17] G. Costa and S. Russo, *J. Makromol. Sci., Chem. Ed.*, A18 (1982) 299.
- [18] T. Provder, J.C. Woodbrey and J.H. Clark, *Sep. Sci.*, 6 (1971) 101.
- [19] T. Provder, J.C. Woodbrey, J.H. Clark and E.E. Drott, *Adv. Chem. Ser.*, 125 (1973) 117.
- [20] M. Matzner, L.M. Robeson, R.J. Gref and J.E. McGrath, *Angew. Makromol. Chem.*, 26 (1972) 137.
- [21] P.J. Wang and R.J. Rivard, *J. Liq. Chromatogr.*, 10 (1987) 3059.
- [22] C.A. Veith and R.E. Cohen, *Polymer*, 30 (1989) 942.
- [23] E.E. Drott, in J. Cazes (Editor), *Liquid Chromatography of Polymers and Related Materials (Chromatographic Sciences Series, Vol. 13)*, Marcel Dekker, New York, 1977, p.41.
- [24] H. Schorn, R. Kosfeld and M. Hess, *J. Chromatogr.*, 282 (1983) 579.
- [25] S.R. Samanta, *J. Appl. Polym. Sci.*, 45 (1992) 1635.
- [26] T. Ogawa, M. Sakai and W. Ishitobi, *J. Polym. Sci.: Part A: Polym. Chem. Ed.*, 24 (1985) 109.
- [27] T.H. Mourey, T.G. Bryan and J. Greener, *J. Chromatogr. A*, 657 (1993) 377.
- [28] S.A. Berkowitz, *J. Liq. Chromatogr.*, 6 (1983) 1359.
- [29] T.H. Mourey and S.T. Balke, *J. Appl. Polym. Sci.*, submitted for publication.
- [30] S. Mori and Y. Nishimura, *J. Liq. Chromatogr.*, 16 (1993) 3359.



ELSEVIER

Journal of Chromatography A, 679 (1994) 206–211

JOURNAL OF
CHROMATOGRAPHY A

Short communication

Determination of trace impurities of peptides and alkaloids by capillary electrophoresis–ion spray mass spectrometry

Frank Y.L. Hsieh^{*}, Jianyi Cai, Jack Henion^{*}

Analytical Toxicology, Diagnostic Laboratory, Cornell University, 927 Warren Drive, Ithaca, NY 14850, USA

First received 6 April 1994; revised manuscript received 15 June 1994

Abstract

Two different mixtures have been analyzed by CE–UV–MS using selected ion monitoring (SIM) conditions to evaluate whether this technique can detect trace impurities in such mixtures. The first mixture consisted of two bioactive peptide analogues which included Lys–bradykinin (kallidin) and Met–Lys–bradykinin. The presence of 0.1% Lys–bradykinin was detected by SIM CE–MS but not by CE–UV at the 0.1% level as it migrated from the capillary column prior to the major component, Met–Lys–bradykinin. The second mixture consisted of two antibacterial alkaloids, berberine and palmatine. The presence of 0.15% palmatine was detected by CE–UV and SIM CE–MS at the 0.15% level as it migrated from the capillary column following the major component, berberine. These results suggest that SIM CE–MS offers the necessary separation efficiencies and sensitivity to provide a complementary analytical determination of trace components in such sample mixtures.

1. Introduction

Capillary electrophoresis–mass spectrometry (CE–MS) offers a promising technique for biomedical and biochemical studies to characterize biomolecules and other compounds of interest [1–7]. In the chemical, pharmaceutical and biotechnology industries there frequently is a need for the characterization of trace impurities in products or product formulations. To deal with these needs reports have appeared from several bioanalytical investigators who have attempted to characterize the impurities in peptides as well as drugs and drug products. These include a

report of the determination of a 0.1% impurity in a synthetic peptide [8], a 0.075% impurity in a nifedipine drug substance [9], a 0.1% drug steroid impurity [10] and a 1% anticancer drug minor impurity [11]. A recent report using CE–MS described the determination of an impurity in biological matrices where the synthetic peptide impurity was identified and quantitated at the 0.7% level [12]. This report prompted us to further explore the analytical utility of CE–MS for the determination of trace level impurities in biological samples.

In this CE–MS investigation, two bioactive peptide analogues, Lys–bradykinin (kallidin) and Met–Lys–bradykinin, which are important compounds for dealing with pain as well as inflammation, were detected by CE–UV–MS under selected ion monitoring (SIM) conditions.

^{*} Corresponding author.

^{*} Present address: PerSeptive Biosystems, Inc., 38 Sidney Street, Cambridge, MA 02139, USA.

Moreover, SIM CE-MS was also used to monitor trace levels of one antibacterial isoquinoline alkaloid, palmatine, in the presence of the other, berberine. These compounds are found at low levels in the bark of *Phellodendron chinese Schneid.* [13,14]. Comparisons of different relative levels of Lys-bradykinin and Met-Lys-bradykinin as well as berberine and palmatine were explored by CE-UV-MS to evaluate the potential of CE-MS to detect a trace impurity in such sample mixtures.

2. Material and methods

2.1. Chemicals

Bradykinin (Arg-Pro-Pro-Gly-Phe-Ser-Pro-Phe-Arg, $M_r = 1060.2$), Lys-bradykinin ($M_r = 1188.4$), Met-Lys-bradykinin ($M_r = 1319.6$), Ile-Ser-bradykinin ($M_r = 1260.5$), berberine ($M_r = 336.4$) and palmatine ($M_r = 352.4$) were purchased from Sigma (St. Louis, MO, USA). All solvents, buffers and common chemicals were reagent grade or better and purchased from Fisher Scientific (Rochester, NY, USA).

2.2. Conditions for ion spray mass spectrometry

A Sciex TAGA 6000E atmospheric pressure ionization (API) triple quadrupole mass spectrometer (Thornhill, Canada) updated to an API-III with a scan range from m/z 10–2400 was used for all experiments. The ion spray sprayer was positioned approximately 1 cm off-axis and 1 cm away from the ion-sampling orifice and maintained at 4.5 kV with a flow of liquid nitrogen blow-off nebulizing gas maintained at 45 p.s.i. (1 p.s.i. = 6894.76 Pa). Polypropylene glycol in acetonitrile-water (80:20) (3 mM NH_4OAc) was used for tuning and mass-axis calibration for each mass-resolving quadrupole (Q1 and Q3). Electropherograms for peptides and alkaloids were acquired at a declustering energy of 60 V and 30 V, respectively. All CE-MS experiments were carried out in the SIM mode using the standard PE-Sciex Macintosh-based software.

2.3. Conditions for CE-MS

A high-performance CE system (Model P/ACE 2050, Beckman Instruments, Palo Alto, CA, USA) was used in this study. Separation was performed on an uncoated 120 cm \times 50 μm I.D. fused-silica capillary (Polymicro Technologies, Phoenix, AZ, USA).

On-line UV detection (200 nm for the peptides and 254 nm for the alkaloids) occurred approximately 17 cm from the inlet of the CE capillary. The in-house ion spray interface shown in Fig. 1 consists of three concentric capillaries for introducing a sheath liquid flow and nebulizing gas. The sheath liquid flow was comprised of 80% CH_3CN and 20% 5 mM NH_4OAc at pH 3.5 and was delivered at 2 $\mu\text{l}/\text{min}$ by an infusion pump (Harvard Apparatus, South Natick, MA, USA). The three concentric capillaries are coupled with the two stainless-steel Tee's [SGE, 1/32 in. (1 in. = 2.54 cm), see Fig. 1] for separate but simultaneous introduction of the sheath liquid flow and the nitrogen nebulizing gas. This device affords a robust CE-MS combination coupled with the ion spray interface. When the concentric capillaries are appropriately positioned at the tip as shown in Fig. 1 and the flow of sheath liquid and nitrogen nebulizing gas are optimized, the described experiments may be routinely performed.

The CE separation was accomplished by applying 30 kV at the anode end while 4.5 kV was applied to the cathode via the ion spray interface high-voltage supply resulting in a potential difference across the CE capillary of 25.5 kV. Samples were loaded into the anode end of the capillary via either a 5-s pressure injection or a 10-s electrokinetic injection at 10 kV. The pressure injection technique was used for 1 mg/ml samples of the peptides, while the electrokinetic injection technique was used for the $\mu\text{g}/\text{ml}$ samples of the alkaloids.

All the solutions including the 25 mM NH_4OAc at pH 3.5 for peptides and 100 mM NH_4OAc at pH 4.5 for alkaloids were prepared fresh daily and filtered through 0.2- μm nylon HPLC syringe filters (Krackler Scientific, Albany, NY, USA) before use.

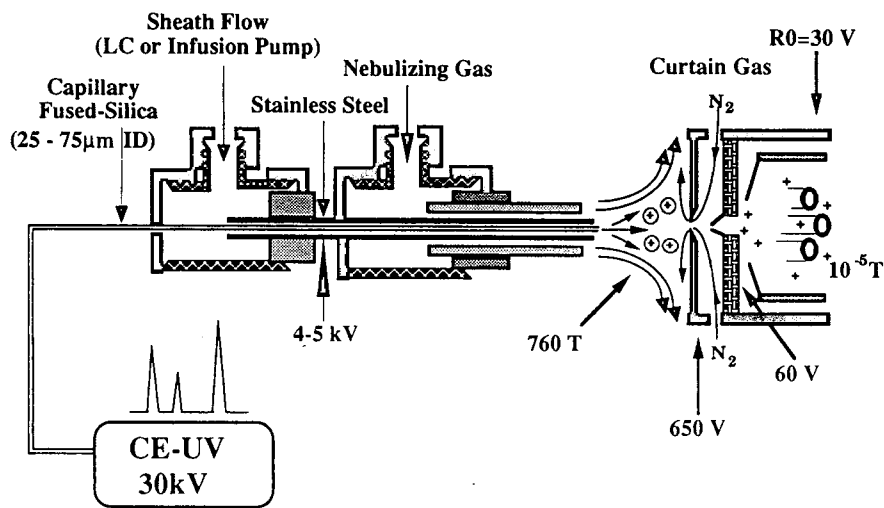


Fig. 1. Ion spray CE-MS interface equipped with a coaxial sheath-flow of liquid.

3. Results and discussion

The goal of this work was to determine the practical CE-UV-MS detection limits for representative minor components in simple synthetic mixtures. Two synthetic mixtures were prepared for study. One was a binary peptide mixture where the faster migrating peptide's concentration was systematically reduced relative to the other. This example was chosen to represent an impurity determination where the minor component migrates from the capillary exit before the major component. The second synthetic mixture was prepared containing berberine and palmatine with reduced amounts of the latter, longer-migration-time component. The minor component was monitored by CE-UV-MS as the concentration of this component was reduced in stages to 0.15% that of the major component. In each case CE-MS was conducted under SIM conditions where the abundant protonated molecule ion was monitored.

The corresponding doubly charged ions for the two peptides chosen for this study, Lys-bradykinin and Met-Lys-bradykinin (m/z 595 and 661, respectively) were monitored by SIM following their separation on an uncoated 50 μm I.D. capillary fused-silica capillary column (Fig. 2). Lys-bradykinin and Met-Lys-bradykinin

were selected as a two-component mixture with lower levels of the former in the presence of the other. Lys-bradykinin was used as the "impurity" or diminutive component in the presence of higher levels of Met-Lys-bradykinin. Fig. 2 shows the CE-UV-MS comparison UV and SIM electropherograms for Lys-bradykinin and Met-Lys-bradykinin at ratios of 35, 5 and 0.1% by on-line CE-UV-MS. The Lys-bradykinin component present at the 35 and 5% levels in the binary mixture was readily detected by both UV and MS detection (see Fig. 2A and B). Although the peak heights in Fig. 2A appear comparable, the peak areas are indicative of the 35% level of the Lys-bradykinin component. It is interesting to note, however, that the 0.1% level of Lys-bradykinin is not observed in the CE-UV electropherogram (Fig. 2C, inset) although it is readily detected in the corresponding CE-MS electropherogram (Fig. 2C). This is in part due to the improved separation afforded in the case of CE-MS detection where the mixture components transit the entire 120 cm of the separation capillary prior to detection (see above). These results demonstrate that CE-MS can be a complimentary technique to UV for detecting the presence of trace levels of selected components. By CE-MS, however, one has an increased level of specificity due to the ability to

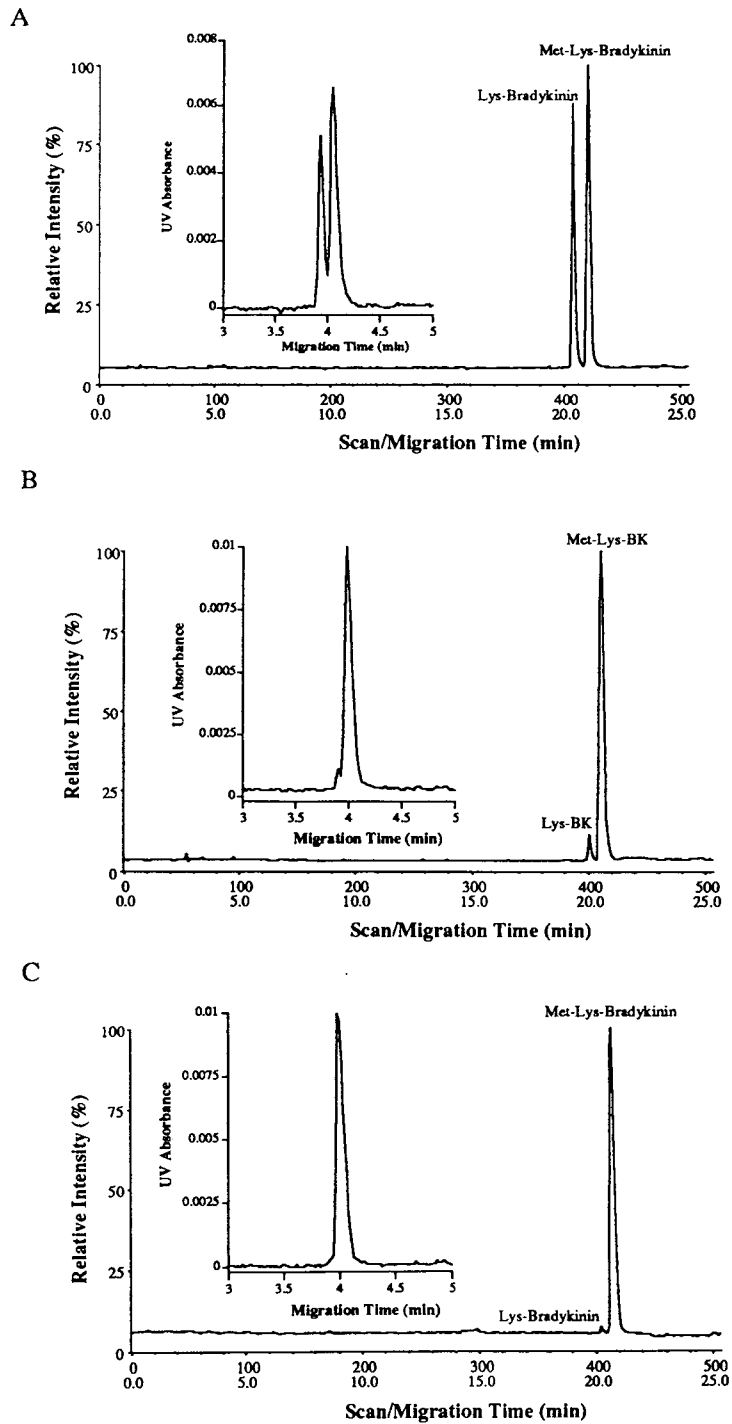
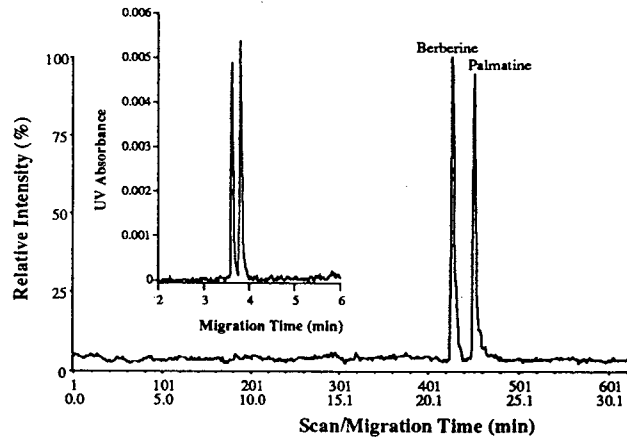
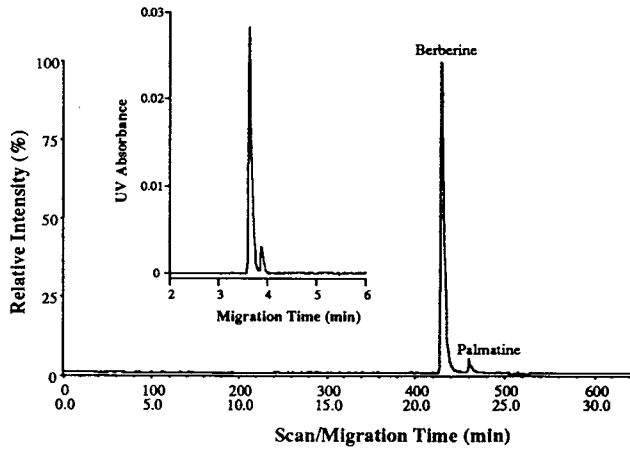


Fig. 2. SIM CE-MS electropherograms for a synthetic mixture containing Lys-bradykinin and Met-Lys-bradykinin with (A) 35%, (B) 5% and (C) 0.1% Lys-bradykinin in the presence of Met-Lys-bradykinin. BK = Bradykinin.

A



B



C

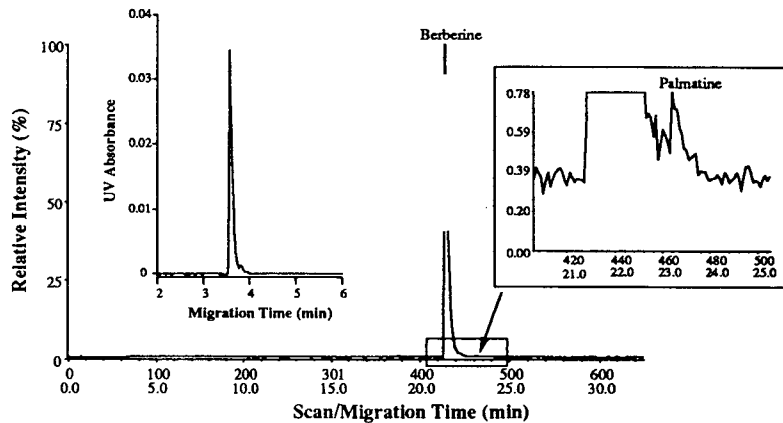


Fig. 3. SIM CE-MS electropherograms for a synthetic mixture containing palmatine and berberine with (A) 50%, (B) 4% and (C) 0.15% of palmatine in the presence of berberine.

monitor one or more ions characteristic of the target analyte(s). Of course if one has sufficient sensitivity it may be possible to acquire the full-scan mass spectrum for an impurity to facilitate its characterization in the event that it is an unknown compound.

The second example of combined CE–UV–MS determination of impurities is shown in Fig. 3. In this case the longer-migration-time component was chosen as the “impurity” in a binary mixture composed of berberine and palmatine. The percentages of palmatine in berberine in Fig. 3 were 50, 4 and 0.15%. It should be noted that both the UV and SIM electropherograms in these experiments reveal the presence of the trace component at each level. CE–MS detection of the minor component at the 0.15% level may be facilitated by amplification in the y -direction of the appropriate region in the electropherogram (Fig. 3C). As indicated above the added specificity benefits of CE–MS include monitoring ions that are characteristic of the target impurity. Full-scan mass spectra should also be especially helpful for characterizing unknown impurities in mixtures.

In conclusion, the combination of high sensitivity and specificity afforded by CE–MS demonstrated by these studies may provide complementary information for detecting and characterizing diminutive components in synthetic drug mixtures, drug metabolism profiles, byproducts of manufacturing and enantiomeric drug products. Recent results from this laboratory suggest that the determination of chiral mixtures by CE–MS may provide a new approach to validating the purity of enantiomeric drugs. Results from these studies will be published subsequently.

Acknowledgement

This research was supported in part by the National Institutes of Health (GM 47931). The

authors also thank Beckman Instruments for providing the P/ACE 2050 CE system used in this work.

References

- [1] J.A. Olivares, N.T. Nguyen, C.R. Yonker and R.D. Smith, *Anal. Chem.*, 59 (1987) 1232.
- [2] E.D. Lee, W. Muck, J.D. Henion and T.R. Covey, *J. Chromatogr.*, 458 (1988) 313.
- [3] M.A. Mosely, L.J. Detering, K.B. Tomer and J.W. Jorgenson, *Rapid Commun. Mass Spectrom.*, 3 (1989) 87.
- [4] R.W. Hallen, C.B. Shumate, W.F. Siems, T. Tsuda and H.H. Hill, Jr., *J. Chromatogr.*, 480 (1989) 233.
- [5] R.D. Smith, J.H. Wahl, D.R. Goodlett and S.A. Hofstadler, *Anal. Chem.*, 65 (1993) 574.
- [6] H.R. Udseth, J.A. Loo and R.D. Smith, *Anal. Chem.*, 61 (1989) 228.
- [7] W. Nichols, J. Zweigenbaum, F. Garcia, M. Johansson and J.D. Henion, *LC·GC*, 10 (1992) 676.
- [8] D.J. Burinsky, R. Dunphy, A.R. Oyler, C.J. Shaw and M.L. Cotter, *J. Pharm. Sci.*, 81 (1992) 597.
- [9] M.B. Maurin, R.D. Vickery, P. Ma, J. Manalo and M.A. Hussain, *Pharm. Res.*, 9 (1992) 1518.
- [10] J.L. Bernal, M.J. Del Nozal and G.A. Garcia Buj, *J. Chromatogr.*, 607 (1992) 175.
- [11] D.O. O’Keefe, A.L. Lee and S. Yamazaki, *J. Chromatogr.*, 627 (1992) 127.
- [12] K.J. Rosnack and J.G. Stroh, presented at the 41st ASMS Conference on Mass Spectrometry and Allied Topics, San Francisco, CA, May 31–June 4, 1993, abstracts, p. 1056a.
- [13] W.N. Wu, L.A. Mitscher and J.L. Beal, *Lloydia*, 39 (1976) 249.
- [14] C.P. Rosnack, *Chinese Herbal Medicine: A Publication of the John E. Fogarty International Center for Advanced Study in the Health Sciences; DHEW Publication No. (NIH) 75-732*, U.S. Superintendent of Documents, Washington, D.C., 1974, p. 81.



ELSEVIER

Journal of Chromatography A, 679 (1994) 212

JOURNAL OF
CHROMATOGRAPHY A

Book Review

Practical High-Performance Liquid Chromatography, by V.R. Meyer, Wiley, Chichester, New York, 1993, XIV + 376 pp., price £49.60 (hardbound), £24.95 (paperback), ISBN 0-471-94132-8.

Veronika Meyer's book on *Practical High-Performance Liquid Chromatography* appeared in the original German language in the 7th edition. The present English version is an updated translation of the last German edition. These books give a practical introduction to the principles of HPLC theory and practice. There are no theoretical discussions, and moreover the few equations required are exemplified and discussed with real figures and calculations of the important parameters to demonstrate what the use of a theory for the practitioner can be. However, these "Problems" and their solutions sometimes block the reading of the text, especially when they apply too simple algebra in too much space (Problems 22 and 23 may serve as negative examples). On the other hand, some "Problems" are summarized in an Appendix.

The introduction to the practice of HPLC is described via instructive examples. The fundamentals are given in a very condensed and straightforward manner. For those desiring to go into further detail, supplementary references to

original and review articles are given. Also included is an extensive summary of review papers for the separation of individual groups of components. In more than 40 pages the various commercially available stationary phases and columns for dedicated applications are summarized.

There are minor criticisms on this book. One is related to the process of preparing consecutive editions. Some subjects, still important 15 years ago (e.g., Fresnel refractometer), are now out of use, whereas the very important diode-array detectors are not discussed together with common UV detectors, but some pages later in the chapter on "Analytical HPLC".

Despite these minor deficiencies, the book can be recommended to every starter in HPLC, because it gives a good practical introduction to HPLC with only the important and necessary theoretical discussions.

Saarbrücken, Germany

H. Engelhardt

PUBLICATION SCHEDULE FOR THE 1994 SUBSCRIPTION

Journal of Chromatography A and Journal of Chromatography B: Biomedical Applications

MONTH	1993	J-J	J	A	S	O	
Journal of Chromatography A	652-657	Vols. 658-672	673/1 673/2 674/1 + 2 675/1 + 2 676/1	676/2 677/1 677/2 678/1	678/2 679/1 679/2 680/1	680/2	The publication schedule for further issues will be published later.
Bibliography Section		Vol. 681			682/1		
Journal of Chromatography B: Biomedical Applications		Vols. 652-656	657/1 657/2	658/1 658/2	659	660/1 660/2	

INFORMATION FOR AUTHORS

(Detailed *Instructions to Authors* were published in *J. Chromatogr. A*, Vol. 657, pp. 463-469. A free reprint can be obtained by application to the publisher, Elsevier Science B.V., P.O. Box 330, 1000 AH Amsterdam, Netherlands.)

Types of Contributions. The following types of papers are published: Regular research papers (full-length papers), Review articles, Short Communications and Discussions. Short Communications are usually descriptions of short investigations, or they can report minor technical improvements of previously published procedures; they reflect the same quality of research as full-length papers, but should preferably not exceed five printed pages. Discussions (one or two pages) should explain, amplify, correct or otherwise comment substantively upon an article recently published in the journal. For Review articles, see inside front cover under Submission of Papers.

Submission. Every paper must be accompanied by a letter from the senior author, stating that he/she is submitting the paper for publication in the *Journal of Chromatography A or B*.

Manuscripts. Manuscripts should be typed in **double spacing** on consecutively numbered pages of uniform size. The manuscript should be preceded by a sheet of manuscript paper carrying the title of the paper and the name and full postal address of the person to whom the proofs are to be sent. As a rule, papers should be divided into sections, headed by a caption (e.g., Abstract, Introduction, Experimental, Results, Discussion, etc.). All illustrations, photographs, tables, etc., should be on separate sheets.

Abstract. All articles should have an abstract of 50-100 words which clearly and briefly indicates what is new, different and significant. No references should be given.

Introduction. Every paper must have a concise introduction mentioning what has been done before on the topic described, and stating clearly what is new in the paper now submitted.

Experimental conditions should preferably be given on a *separate* sheet, headed "Conditions". These conditions will, if appropriate, be printed in a block, directly following the heading "Experimental".

Illustrations. The figures should be submitted in a form suitable for reproduction, drawn in Indian ink on drawing or tracing paper. Each illustration should have a caption, all the *captions* being typed (with double spacing) together on a *separate sheet*. If structures are given in the text, the original drawings should be provided. Coloured illustrations are reproduced at the author's expense, the cost being determined by the number of pages and by the number of colours needed. The written permission of the author and publisher must be obtained for the use of any figure already published. Its source must be indicated in the legend.

References. References should be numbered in the order in which they are cited in the text, and listed in numerical sequence on a separate sheet at the end of the article. Please check a recent issue for the layout of the reference list. Abbreviations for the titles of journals should follow the system used by *Chemical Abstracts*. Articles not yet published should be given as "in press" (journal should be specified), "submitted for publication" (journal should be specified), "in preparation" or "personal communication".

Vols. 1-651 of the *Journal of Chromatography*; *Journal of Chromatography, Biomedical Applications* and *Journal of Chromatography, Symposium Volumes* should be cited as *J. Chromatogr.* From Vol. 652 on, *Journal of Chromatography A* (incl. Symposium Volumes) should be cited as *J. Chromatogr. A* and *Journal of Chromatography B: Biomedical Applications* as *J. Chromatogr. B*.

Dispatch. Before sending the manuscript to the Editor please check that the envelope contains four copies of the paper complete with references, captions and figures. One of the sets of figures must be the originals suitable for direct reproduction. Please also ensure that permission to publish has been obtained from your institute.

Proofs. One set of proofs will be sent to the author to be carefully checked for printer's errors. Corrections must be restricted to instances in which the proof is at variance with the manuscript.

Reprints. Fifty reprints will be supplied free of charge. Additional reprints can be ordered by the authors. An order form containing price quotations will be sent to the authors together with the proofs of their article.

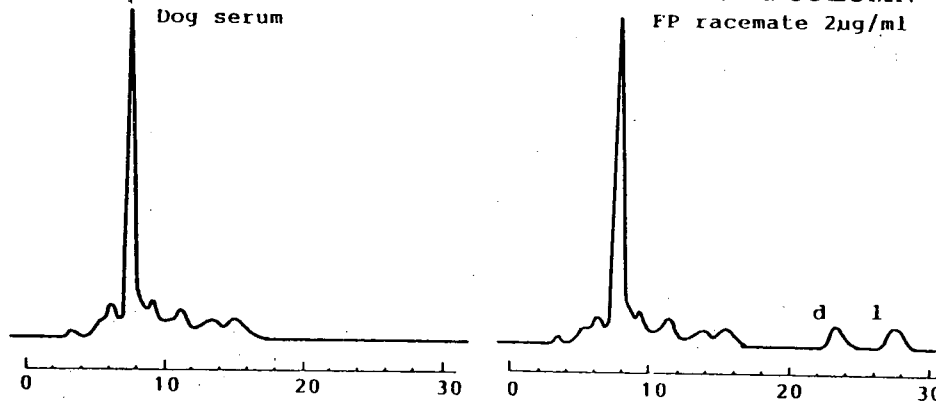
Advertisements. The Editors of the journal accept no responsibility for the contents of the advertisements. Advertisement rates are available on request. Advertising orders and enquiries can be sent to the Advertising Manager, Elsevier Science B.V., Advertising Department, P.O. Box 211, 1000 AE Amsterdam, Netherlands; courier shipments to: Van de Sande Bakhuyzenstraat 4, 1061 AG Amsterdam, Netherlands; Tel. (+31-20) 515 3220/515 3222. Telefax (+31-20) 6833 041, Telex 16479 els vi nl. UK: T.G. Scott & Son Ltd., Tim Blake, Portland House, 21 Narborough Road, Cosby, Leics. LE9 5TA, UK; Tel. (+44-533) 753 333, Telefax (+44-533) 750 522. USA and Canada: Weston Media Associates, Daniel S. Lipner, P.O. Box 1110, Greens Farms, CT 06436-1110, USA; Tel. (+1-203) 261 2500, Telefax (+1-203) 261 0101.

ULTRON ES-OVM

Narrow-Bore Column (2.0 I.D. x 150 mm) for Trace Analyses
Analytical Column (4.6 I.D., 6.0 I.D. x 150 mm) for Regular Analyses
Semi-Preparative Column (20.0 I.D. x 250 mm) for Preparative Separation

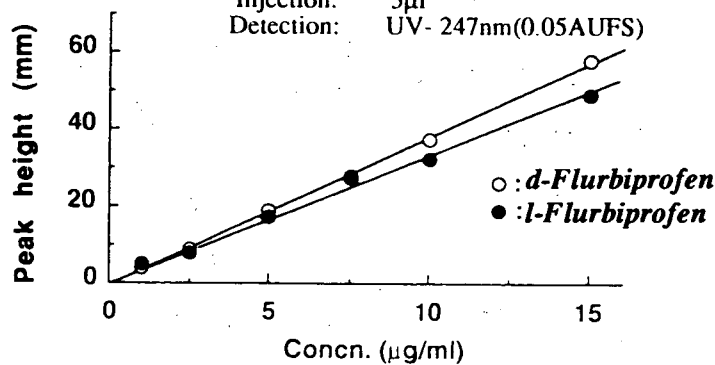
Analysis of Trace FLURBIPROFEN in Metabolite

with NARROW-BORE COLUMN



Conditions

Column: ULTRON ES-OVM(2.0I.D. x 150mm)
Mobile Phase: 20mM Phosphate Buffer(pH=3.0)/CH₃CN
=100/15
Flow Rate: 0.1ml/min
Temperature: 25°C
Injection: 5µl
Detection: UV- 247nm(0.05AUFS)



Calibration Curve for Each Enantiomer of Flurbiprofen

SHINWA CHEMICAL INDUSTRIES, LTD.

50 Kagekatsu-cho, Fushimi-ku, Kyoto 612, JAPAN
Phone: +81-75-621-2360 Fax: +81-75-602-2660

In the United States and Europe, please contact:

Rockland Technologies, Inc.

538 First State Boulevard, Newport, DE 19804, U.S.A.

Phone: 302-633-5880 Fax: 302-633-5893

This product is licenced by Eisai Co., Ltd.



0021-9673(19940909)679:1;1-F